ı" University of Timisoara, ROMANIA
Electrical Engineering
ıt of Electrical Machines and Drives

New Contributions to the Matrix Converter Technology

PhD Dissertation

by Christian KLUMPNER

Supervisor: Professor Ion BOLDEA

December 2000

Contents

Preface

This thesis was started in 1996, at "Politehnica" University of Timisoara, Faculty of Electrical Engineering, under the supervision of professor Ion Boldea, having a general focus on bi-directional power flow converters for AC drives. In April 1997 the topic was more accurate established on matrix converter drives. The first period of studying the matrix converters was spent reading literature and simulating the converter that helped me to understand the basic principle of operation. Next, during the first visit at Institute of Energy Technology, Aalborg University, Denmark (1 August 1998 – 30 November 1998), i have built a prototype and i have carried out some of the experimental work, preparing two papers for publication. After i returned home, i had the possibility to evaluate the domains where contributions could be added to this technology. During my second visit at Institute of Energy Technology (1 July 1999 – 30 April 2000) i performed the experiments to validate these ideas, designing and building a 4 kW integrated motor drive based on a matrix converter topology. As a result of this work, other four papers have been published.

Many people have contributed to the development of my PhD thesis. First, i wish to express my gratitude to my supervisor, professor Ion Boldea, for giving me the chance to work in a very interesting topic and for guidance during this PhD program. Then, i wish to express my gratitude for the financial support offered by the Institute of Energy Technology and by the Danfoss Professor Programme. Special thanks for professor Frede Blåbjerg from Institute of Energy Technology for providing me the necessary support at Institute for Energy Technology to complete my work and to Peter Nielsen from Danfoss Drives A/S, for guidance and support in the matrix converter field. Also, i wish to thank to the supervisory group from Danfoss Drives A/S of the Matrix Converter-Motor project: Paul Thøgersen, Ulrik Jens Jæger, Michael Sachmann and Ejgil Petersen for giving me good advises and technical support in solving the issues of industrial drives implementation.

I wish to express my gratitude to my colleagues from Bee Speed Automatizari Timisoara, for giving me the opportunity to improve my skills and to gain more field experience to apply the AC frequency converter technology in various industrial applications. I wish to thank to my professors and colleagues at "Politehnica" University of Timisoara and to my former professors at "Eftimie Murgu" University of Resita, for good discussions and guidance in the field of electrical engineering.

Christian Klumpner
M.App.Sc in Electrical Engineering

December 2000, Timisoara, ROMANIA

Index of symbols

3 ~	Three–phase load
3∅/1∅	Three-phase to single-phase
3∅/3∅	Three-phase to three-phase
a, b, c	symbols used for the input of the matrix converter (lowercase)
A, B, C	symbols used for the output of the matrix converter (uppercase)
AC	Alternate Current
ASD	Adjustable Speed Drive
B6	Three-phase bridge topology of a rectifier/inverter
CC	Common Collector: bi-directional switch topology of anti-paralleled IGBT's
CE	Common Emitter: bi-directional switch topology of anti-paralleled IGBT's
CPU	Central Processing Unit
CSR	Current Source Rectifier
CSI	Current Source Inverter
DC	Direct Current
DFC	Direct Frequency Converter
DTC	Direct Torque Control
di/dt	Rising current slope, characteristic for current waveforms produced by force-switched converters
dv/dt	Rising voltage slope, characteristic for voltage waveforms produced by force-switched converters
ESR	Equivalent Series Resistance: datasheet parameter specific for capacitors
EMC	Electro Magnetic Compatibility
EMF	Electro-Magnetic Force
FCM	Frequency Converter Motor – trademark for An integrated motor drive (Danfoss)
FFT	Fast Fourier Transformation
f_{in}	Frequency of the voltage on the converter input (grid side)

f_{out}	Frequency of the voltage on the converter output (load side)
f_{sw}	Switching frequency of the converter
FRD	Fast Recovery Diode
GTO	Gate Turn-Off: A type of thyristor
$\boldsymbol{I}$	Inversion stage matrix (bold)
IEC	refereeing a standard issued by International Electrotechnical Commission
IEEE	refereeing a standard issued by Institute of Electrical and Electronic Engineers
IGBT	Insulated-Gate Bipolar Transistor
$\boldsymbol{I}_{in}$	Input phase current matrix (bold)
IM	Induction Motor
IPM	Intelligent Power Module
$\boldsymbol{I}_{out}$	Output phase current matrix (bold)
I_{out}	Output phase current
JTAG	Communication protocol for programmable logic devices
MC	Matrix Converter
MCM	Matrix Converter - Motor
MCT	MOS Controlled Thyristor
m_I	rectification stage modulation index
m_{ij}	duty cycles of a switch connecting an input i to an output j
m_U	inversion stage modulation index
p.u.	per unit
p	Pole pair (specific for AC machines)
PCB	Printed Circuit Board
PEBB	Power Electronic Building Block
PEC	Peripheral Event Controller
PF	Power Factor
PLD	Programmable Logic Device
PWM	Pulse-Width Modulation
$\boldsymbol{R}$	Rectification stage matrix (bold)
RFI	Radio Frequency Interference
RIGBT	Reverse blocking IGBT

R_k	Critical resistance (Eq. 4.1, pp. 59): defines the transient of an R-L-C series circuit
RMS	Root Mean Square value
RS232	Communication serial protocol
SM	Synchronous Motor
SMPS	Switch-Mode PowerSupply
SVM	Space Vector Modulation
S_{xy}	Bi-directional switch connecting an input line x, to an output line y
$\boldsymbol{T}$	Transfer matrix (bold)
T_A	Adapting transformer (Fig. 1.8)
THD	Total Harmonic Distortion factor: $THD = \frac{\sqrt{RMS^2 - H_1^2}}{H_1} \times 100$ [%]
T_{sw}	Switching period
TTL	Family of logic circuits, characterizeb by certain signal logic level
u_d	Momentary DC-link voltage in a Voltage Source Converter
U_{DC}	Measured DC-link voltage
U_{DCref}	Reference DC-link voltage
U_{dc}	DC-link voltage
U_{dc+}	Positive DC-link voltage of a split capacitor bank
U_{dc-}	Negative DC-link voltage of a split capacitor bank
u_{dl}	Momentary line side DC-link voltage in a Current Source Converter (Fig. 1.7)
U_{dlim}	Limit for DC-link voltage, where the rectifier operation changes (Rectification/Inversion)
u_{dm}	Momentary motor side DC-link voltage in a Current Source Converter (Fig. 1.7)
$\boldsymbol{U_{in}}$	Input phase voltage matrix
$\boldsymbol{U_{out}}$	Output line-to-line voltage matrix
U_{pn}	Momentary virtual DC-link voltage for the matrix converter
V_{RRM}	Maximum Reverse Repetitive Voltage (for diodes)
VSI	Voltage Source Inverter

Romanian résumé - Rezumatul în limba română

Convertorul matricial a atras atenţia multor cercetători în domeniul electronicii de putere, datorită avantajelor pe care această solutie integrală cu elemente semiconductoare le oferă: transferul necondiţionat şi bidirecţional de putere, formă de undă sinusoidală, atât la intrare (curent), cât şi la ieşirea convertorului (tensiune), defazaj controlabil al curentului de intrare şi înalt potenţial de integrare ce vizează în special reducerea gabaritului. Câteva dezavantaje majore însoţesc acest tip de convertor. Coeficientul subunitar de transfer al tensiunii dintre ieşire şi intrare determină imposibilitatea atingerii fluxului nominal la o maşină de curent alternativ, normal dimensionată din punct de vedere a tensiunii de alimentare. Lipsa elementelor de stocare a energiei în circuitul de forţă determină o mare sensibilitate la perturbaţii ale reţelei de alimentare şi deci imposibilitatea de traversare a golurilor de tensiune.
Multe lucrări prezintă doar simulări, deoarece acestă topologie de convertor de frecvenţă, considerată exotică, implică un volum mare de muncă şi resurse pentru construcţia unui prototip într-o gamă reprezentativă de putere, pentru efectuarea de experimente.

SUMARUL TEZEI

Teza este structurată pe opt capitole principale şi unul de concluzii. Capitolul 1 prezintă situaţia existentă în domeniul acţionărilor de curent alternativ cu circulaţie bidirecţională de putere. Sunt prezentate pe scurt topologia diverselor convertoare de frecvenţă care permit aceasta. În categoria conversiei directe de energie se prezintă cicloconvertorul cu elemente de comutaţie naturală şi convertorul matricial, care în fapt este un cicloconvertor care utilizează elemente comutatoare ce permit blocarea forţată. În categoria conversiei indirecte, se enumeră convertorul cu circuit intermediar de curent şi convertoarele cu circuit intermediar de tensiune. În cadrul celei din urmă categorii sunt enumerate posibilitatea de utilizare a unui redresor cu circulaţie bidirecţională construit prin dispunerea în paralel a două punţi complet comandate cu tiristoare, redresorul trifazat cu comutaţie forţată cu IGBT-uri dar şi varianta economică de acţionare cu circulaţie bidirecţională cu redresor monofazat şi invertor de tensiune bifazar. O configuraţie de acţionare ce oferă recuperarea energiei de frânare, prin redistribuire către celelalte acţionări, este configuraţia cu acţionări multiple (multidrive). Aceasta constă în alimentarea mai multor invertoare de tensiune dintr-un circuit intermediar comun, alimentat de un redresor comun. Ultimul tip de acţionare, interesant din punct de vedere al nivelului puterii instalate in convertorul bidirecţional, inferior puterii motorului, este reprezentat de maşina asincronă dublu alimentată, cu convertor de frecvenţă cu circulaţie bidirecţională de putere montat în circuitul rotoric.
În concluzie se arată că, în concordanţă cu tendinţele actuale, care pun mult mai mult accent pe creşterea eficienţei conversiei de energie şi a întregii acţionări, pe realizarea unei interfeţe performante cu reţeaua de alimentare prin îmbunătăţirea formei de undă şi a defazajului curentului şi nu în ultimul rând, pe reducerea dimensiunilor, convertorul matricial de frecvenţă poate oferi un mare potenţial de aplicare în viitorul apropiat, în ciuda multor aspecte rămase nerezolvate încă, dar care motivează continuarea muncii de cercetare în acest domeniu, prin posibilitatea de a aduce reale contribuţii în această tehnologie.

Capitolul 2 prezintă elementele de bază pentru abordarea teoretică şi practică a acestui tip de convertor de frecvenţă. Sunt prezentate contribuţiile importante în acest domeniu din ultimii 20 de

ani: prezentarea unei scheme pentru implementare practică, posibilitatea implementării elementelor de comutație care să permită circulația bidirecțională de curent cu elemente comutatoare unidirecționale, metode specifice pentru comutația acestor elemente, diferite strategii de modulare care să permită operarea cu undă sinusoidală atât la ieşire (tensiune), cât şi la intrare (curent), cât şi controlul defazajului curentului de intrare. Alte contribuții majore în domeniul convertoarelor matriciale sunt prezentate: diverse strategii de compensare a dezechilibrului rețelei de alimentare şi strategii de control inteligent al mişcării.

Capitolul 3 prezintă detalii de implementare a unui prototip de 8.5 kVA, construit pentru realizarea de experimente în laborator. Sunt prezentate criteriile de dimensionare a elementelor reactive din filtrul de intrare şi din circuitul de protecție. Felul în care criteriile de dimensionare cunoscute afectează volumului total al filtrului de intrare este demonstrată matematic. De asemenea, caracteristicile tehnice pentru elementele reactive sunt determinate matematic, arătându-se că solicitarea provocată asupra condensatorului din circuitul de protecție este redusă, nefiind necesară folosirea unui tip cu du/dt mare, specializat pentru circuite tip snubber.
Capitolul 4 propune câteva îmbunătățiri ale structurilor, respectiv a configurației fizice a convertorului matricial. Este tratată influența valorilor elementelor reactive din filtrul de intrare şi din circuitul de protecție, pentru reducerea riscului de supratensiuni, cauzate de posibile goluri de tensiune. Este arătat că există o dependența a nivelului supratensiunii de comportarea rezistiv-inductivă a circuitului de intrare ce include rețeaua de alimentare, dar şi o strânsă dependență de valorile condensatoarelor din cele două circuite pentru prevenirea supratensiunilor. Prin simulări este demonstrat efectul benefic al circuitului de protecție (clamp circuit) în prevenirea supratensiunilor. Este propus un circuit pentru asigurarea punerii sub tensiune fără risc de defectare datorită supratensiunilor. Acesta elimină regimul tranzitoriu, specific filtrului de intrare ce are o configurație de circuit L-C serie, prin introducerea în circuit a unor rezistențe, care produc dispariția (rezistențe înseriate cu inductanțele) sau doar atenuarea la nivele admisibile (rezistențe în paralel cu inductivitățile) a posibilelor supratensiuni. Sunt prezentate simulări în ambele situații, iar pentru reducerea numărului de elemnte de circuit, sunt prezentate şi două soluții ce necesită un număr redus de elemente de circuit, montate doar în două din fazele filtrului de intrare. Efectul saturației în inductanțele din filtrul de intrare asupra supracurenților ce apar la punerea sub tensiune arată că prin alegerea corespunzătoare a curbei de magnetizare, vârful de curent se reduce.
Sunt analizate cele mai avantajoase moduri pentru construirea unor elemente de comutație bidirecționale, utilizând elemente de comutație unidirecționale (diode ultrarapide şi tranzistoare IGBT), din punct de vedere al numărului de elemente de forță, a randamentului de conversie, al gamei de putere pentru care integrarea în module de forță ar fi cea mai avantajoasă, ca şi a consumului de componente auxiliare (optocuploare, surse cu izolare galvanică) pentru realizarea fizică a unui prototip. Se arată că topologia de element bidirecțional cu colector comun (CC) prezintă avantaje în gama de puteri mici, în timp ce topologia de element bidirecțional cu emitor comun (CE) prezintă avantaje când este utilizat în gama de puteri mari.
În domeniul gamei reduse de puteri sunt propuse două soluții care permit reducerea costurilor. O nouă topologie de convertor matricial, utilizând ambele configurații de elemente comutatoare bidirecționale, CE şi CC, şi bazându-se pe tehnica surselor de alimentare cu masă flotantă (boostrap supply) este propusă, permițând reducerea de la şase la trei, a numărului surselor de tensiune cu izolare galvanică utilizate la alimentarea circuitelor de comandă a IGBT-urilor. De asemenea, o nouă topologie a filtrului de intrare este propusă, implementând fizic principiul

transformării de coordonate de la sistemul trifazat (a-b-c) la sistemul bifazat (α-β). Această propunere este însoțită şi de rezultate experimentale. În acest fel se reduce numărul de miezuri feromagnetice utilizate la construcția bobinelor din circuitul de intrare, de la trei la două, ceea ce permite reducerea gabaritului şi a costului pentru întregul ansamblu. Rezultatele experimentale includ forme de undă ale tensiunii şi curentului de intrare, hodograful curentului de intrare şi transformatele rapide Fourier (FFT) ale curenților de intrare pentru ambele configurații de filtru de intrare iar evaluarea calitativă include măsurători ale parametrilor de intrare cu un analizor trifazat de putere.

Capitolul 5 tratează modalități de reducere a riplului de înaltă frecvență din curentul de intrare. Sunt investigați factorii care pot influența riplul de curent. Se arată prin simulări că acesta se datorează în special componentei active din curentul de sarcină al convertorului. Prin analiza stărilor convertorului din timpul perioadei de comutație, se observă că frecvența de comutație vazută dinspre filtrul de intrare depinde de numărul de vectori zero. Astfel, în cazul prezenței distinct a doi vectori zero în succesiunea de stări, frecvența de comutație văzută dinspre intrări se dublează, ceea ce are ca efect reducerea drastică a riplului de curent. Această soluție presupune însă un număr sporit de comutații, ceea ce, la aceeaşi perioadă de comutație, provoaca pierderi de comutație mai mari şi deci o solicitare sporită a elementelor de comutație. Pentru a asigura condiții de testare similare a acestei propuneri, două succesini de stări sunt considerate, cu unul respectiv cu doi vectori zero, la diferite frecvențe de comutație a convertorului, în aşa fel încât frecvența de comutație raportată pe elementul de comutație să fie identică. Un nou model de modulator SVM pentru convertoare matriciale este propus, care să permită o mai bună rezoluție a pulsurilor generate, ca şi posibilitatea de a asigura riplu minim de curent în tot domeniul de reglaj, prin selecția în domeniul inferior de frecvență (factor de modulare) a unei succesiuni cu doi vectori zero, iar în gama de frecvență (factor de modulare) ridicat, a unui singur vector zero. Evaluarea experimentală validează propunerea făcută, în condiții de stres echivalent al elementelor semiconductoare, pe un motor asincron de 4 kW. La 15 Hz, oscilograma formelor de undă de curent, ca şi transformata rapidă Fourier (FFT), arată o reducere a riplului, în timp ce factorul de distorsiuni armonice (THD), măsurat cu un analizor de putere monofazat, confirmă reducerea de la 21 % la 15 %.

Capitolul 6 prezintă posibilitatea de a utiliza un convertor matricial în încărcarea artificială a motoarelor de inducție. Încărcarea artificială este o aplicație care, pentru a produce curent şi cuplu în maşină apropiat de valoarea nominală, se bazează pe schimbarea rapidă a regimului de funcționare din motor în generator şi viceversa. O trecere în revistă a modalităților de a testa cu succes maşinile de inducție, fără a le cupla mecanic cu o altă maşină de încărcare, prin utilizarea unor echipamente speciale bazate pe electronică de putere, arată deficiențele care apar în utilizarea unei configurații standard de convertor de frecvență cu circulație unidirecțională de putere: posibilitatea apariției de supratensiuni în timpul funcționării în regim de generator, cu efect în oprirea repetată a testării. Concluzia este că un convertor cu circulație bidirecțională de putere înlătură aceste neajunsuri, iar configurațiile vizate sunt: convertorul matricial şi invertoare de tensiune cuplate în circuitul intermediar (back-to-back VSI). O comparație a celor două topologii arată că, deşi convertorul matricial necesită mai multe elemente de comutație, consumul în elemente reactive, dar şi de traductori este mai redus. Principalul inconvenient al convertorului matricial, factorul subunitar de transfer al tensiunii, este propus a se compensa fie prin utilizarea unui autotrasformator cu putere instalată de 15 % din puterea convertorului, care să înlocuiască bobinele din filtrul de intrare, fie prin conectarea motorului de testat în conexiune delta - 220 V. O

metodă de control a convertorului este propusă, constând în modificarea rapidă a frecvenței instantanee a fluxului statoric, a carui amplitudine este păstrată constantă, între două limite fixe determinate de frecvența nominală statorică şi alunecarea nominală (± s_N), pentru a asigura că alunecarea rotorică nu depăşeşte alunecarea nominală. Teste pe un motor de 1,1 kW arată clar validitatea propunerii, fiind atinsă încărcarea de 100 % în curent, ca şi o încărcare în cuplu electromagnetic estimat de aproximativ 64 %. Prin conectarea maşinii de inducție în conexiune delta-220 V, a fost depăşită limitarea în tensinea de ieşire. Este remarcat că metoda propusă pentru încărcarea artificială necesită un factor de modulare mai scăzut (0.6-0.62), față de metoda celor două frecvențe (0.7-0.75) şi o utilizare mai bună a convertorului de frecvență prin obținerea unui raport mai bun între vârful de curent şi curent mediu din motor, de 2.2 față de 2.34.

În capitolul 7 este propusă o nouă metodă pentru a permite traversarea golurilor de tensiune de durată limitată, pentru convertoarele directe de frecvență, şi în special pentru convertorul matricial. Strategia de traversare a golurilor de tensiune utilizează fluxul rotoric al motorului asincron, care variază încet descrescător, datorită constantei de timp rotorice de ordinul a zeci-sute de milisecunde, poate facilita conversia de energie, stocată în rotorul motorului, aflat încă în mişcare. Energia este acumulată în inductivitatea de dispersie a maşinii, prin aplicarea unui vector zero, care practic scurcircuitează pentru un timp foarte scurt maşina, forțând curenții statorici să crească. Prin deschiderea tuturor elementelor de comutație, energia este forțată să treacă în condensatorul circuitului de protecție, montat înspre motor. În cazul în care sursa în comutație ce alimentează circuitele de comandă şi control ale convertorului este conectată la acest condensator, se permite recuperarea de energie necesară funcționării convertorului, timp de sute de milisecunde, chiar dacă acționarea nu este capabilă să dezvolte cuplu motor sau să controleze descreşterea fluxului în maşină. Testarea acestei strategii arată că este posibilă recuperarea unei cantități suficiente de energie. De asemenea este propusă o metodă pentru estimarea turației motorului şi a poziției inițiale a fazorului tensiune de ieşire, în timpul acestui regim, pentru a permite o repornire rapidă, fără şocuri de curent. Această strategie a fost testată cu succes pe un motor de 4 kW, alimentat de la un convertor de frecvență cu circuit intermediar de tensiune, dar care în timpul unui presupus gol de tensiune, cu durata de 300 de milisecunde, utilizează doar stări de comutație permise unui convertor matricial. Sunt prezentate teste atât cu cuplu de sarcină zero, cât şi cu 10 % cuplu de sarcină. De asemenea, este prezentat un test efectuat cu un flux inițial în motor mai scăzut, cauzat de tensiunea redusă din circuitul intermediar cu care s-au efectuat testările. Toate aceste experimente demonstrează că este recuperată energie din rotorul motorului şi că acțiunea de repornire a motorului este efectuată cu succes, în condiții nenule de turație şi flux remanent, fără a produce supracurenți deoarece vârful de curent în timpul repornirii este egal cu amplitudinea curentului nominal al motorului.

Capitolul 8 demonstrează viabilitatea aplicării convertorului de tip matricial în obținerea unei acționări integrate, motor-convertor de frecvență, care permite obținerea atât a circulației bidirecționale de putere, a curentului de intrare sinusoidal şi a unui factor de putere unitar. Principalul dezavantaj al convertorului matricial, factorul subunitar de transfer al tensiunii, este depăşit aici de utilizarea unui motor asincron, cu tensiunea nominală corespunzătoare factorului maxim de transfer al convertorului, lucru posibil deoarece motorul şi convertorul reprezintă un tot unitar. Sunt expuse cerințele generale pentru realizarea unei acționări de uz industrial. Sunt descrise topologia convertorului, criteriile de dimensionare a circuitelor de forță şi performanțele acestora, ca şi caracteristicile tehnice ale prototipului. Este construit practic un prototip de 4 kW al unui motor asincron cu convertor matricial integrat, ce conține toate circuitele necesare controlului

şi funcţionării în condiţii de autonomie, care să permită o evaluare corectă a acestei soluţii. Sunt descrise în detaliu, funcţionarea software-ului ce controlează intern convertorul dar şi funcţionarea acţionării. Descrierea este însoţită de fotografii ce ilustrează munca de implementare practică, ca şi manevrele necesare operării cu acest prototip. O comparaţie în ce priveşte volumul ocupat de elementele reactive, dintre un convertor industrial utilizând o topologie clasică cu circuit de tensiune continuă şi redresor cu diode şi acest convertor matricial, la aceeaşi putere de 4 kW, arată ca acestea sunt apropiate, dar că este posibilă reducerea în viitor a volumului în cazul convertor matricial ca urmare a optimizării ulterioare a filtrului de intrare, ca şi a alegerii a unor elemente reactive mult mai compacte.
Evaluarea experimentală este realizată la tensiune nominală de intrare şi cuprinde testarea protecţiei la supracurent, testarea acţionării la 30 Hz şi 50 % cuplu nominal la arbore ca şi un test dinamic de accelerare a maşinii de la 5 Hz la 30 Hz, în timpul cărora convertorul debitează curentul maxim de 14 Amperi. Evaluarea calitativă cuprinde parametrii dinspre reţea, măsuraţi în cadrul testului static, în condiţiile descrise anterior, în două ipostaze: reţea de alimentare în condiţii normale, cu nivel de distorsiune de cca. 2.8 % şi sursă de alimentare de laborator, cu parametrii reglabili. Deşi sunt înregistrate nivele superioare de distorsiuni în curent (17.5 % în primul caz şi 16 % în cel de-al doilea caz), acestea se datorează în principal frecvenţelor de ordin superior (> 1 kHz), care sunt înregistrate de analizorul de putere. Nivelul armonicilor de curent de joasă frecvenţă, ordinul 5 – 19, fiind scăzute.

CONTRIBUŢIILE TEZEI DE DOCTORAT

Capitolele 4-8 prezintă contribuţiile acestei teze, reprezentând material original, publicate anterior în şase lucrări ştiinţifice, care îl au ca prim autor pe autorul acestei teze de doctorat. Aceste lucrări au fost prezentate în reviste şi conferinţe internaţionale în anul 2000. Contribuţiile principale ale tezei de doctorat sunt:

- © A fost demonstrată prin simulări necesitatea folosirii unui circuit pentru punerea sub tensiune fără risc a convertorului matricial. Au fost arătate precauţiile care trebuie luate pentru alegerea componentelor reactive din filtrul de intrare şi circuitul de protecţie pentru a minimiza riscul apariţiei de supratensiuni, în cazul golurilor de tensiune. A fost arătată influenţa saturaţiei asupra regimului tranzitoriu a filtrului de intrare. (capitolul 4)

- © Au fost analizate configuraţiile optime de elemente comutatoare bidirecţionale, prin prisma gamei de putere, arătându-se că un tip (CC) implică minimul de componente în gama de puteri mici, în timp ce celălalt tip (CE) aduce maximul de performanţă, necesar în gama de puteri mari. Sunt propuse câteva soluţii de a reduce cerinţele hard pentru configuraţii de convertor matricial destinate din gamei de puteri mici. Este propusă o nouă topologie de modul de putere, care necesită numai trei surse de tensiune cu izolare galvanică. Pentru reducerea dimensiunilor, este propusă şi experimentată o configuraţie de filtru de intrare ce foloseşte principiul transformării de coordonate, reducând la două numărul de miezuri feromagnetice. Rezultatele experimentale arată comparativ cu situaţia unui filtru de intrare standard, că perfomanţele calitative nu sunt afectate major. Aceasta include forme de undă de tensiune şi curenţi de intrare, transformate rapide Fourier ale undei de curent şi monitorizarea mărimilor electrice dinspre reţeaua de alimentare cu un analizor trifazat de putere. (capitolul 4)

- © A fost propusă o nouă metodă de reducere a riplului de curent. Se arată că numărul de vectori zero aplicați distinct în succesiunea de stări dictează frecvența de comutație văzută de filtrul de intrare. Deoarece în literatură s-au mai făcut evaluări de strategii de modulare la frecvențe de comutație identică, dar la număr diferit de stări pe perioada de comutație, se propune ca analiza comparativă să se facă în condiții comparabile de stres al elementelor semiconductoare. Deşi folosirea a doi vectori zero implică o frecvență de comutație mai redusă, se dovedeşte experimental că riplul de curent se reduce simțitor. (capitolul 5)
- © Este investigată utilizarea convertorului matricial în încărcarea artificială a motorului asincron. Se arată că utilizarea unui convertor de frecvență cu circulație bidirecțională de putere înlătură dezavantajul capacității limitate de frânare a convertoarelor cu circulație unidirecțională. Se propune o metodă de control a convertorului matricial, pentru încărcarea artificială a motorului de inducție, permițând echivalarea pierderilor mecanice, a pierderilor în fier statorice a pierderilor şi a pierderilor în înfăşurări. Rezultatele experimentale evidențiază atingerea curentului nominal în maşină şi o încărcare apreciabilă în cuplul electromagnetic. Comparativ cu metoda celor două frecvențe, această metodă permite funcționarea cu un factor mai redus de modulare şi o utilizare mai eficientă a convertorului de frecvență. (capitolul 6)
- © Este propusă o metodă originală de traversare a golurilor de tensiune, pentru acționările cu convertoare directe de frecvență. Metoda utilizează fluxul remanent din maşina asincronă, care descreşte lent datorită constantei de timp rotorice de ordinul a zeci-sute de milisecunde şi energia mecanică înmagazinate în rotorul în mişcare al maşinii pentru a recupera energie pentru alimentarea electronicii de comandă, chiar dacă metoda nu facilitează menținerea fluxului şi nici producerea de cuplu motor. Conversia se face în doi paşi: în primul pas, aplicarea unui vector zero forțează creşterea curenților statorici şi deci transferul energiei mecanice în energie magnetică a inductanțelor de dispersie ale maşinii asincrone, iar în al doilea pas, prin deschiderea tuturor elementelor de comutație, energia magnetică este transferată în condensatorul circuitului de protecție. Aceasta permite pe lângă recuperarea de energie, controlul variației curenților maşinii şi estimarea condițiilor de restart: viteză şi unghi al vectorului spațial de tensiune. Teste experimentale validează metoda, simulând unui gol de tensiune de 200 ms şi repornind acționarea din condiții nenule de flux şi turație la arbore. (capitolul 7)
- © Este realizat primul prototip de acționare integrată motor-convertor de frecvență, care permite circulația bi-direcțională de putere, având la bază o configurație de convertor matricial. Implementarea vizează construirea fizică a prototipului într-o carcasă existentă de convertor integrat, cu limitări drastice în ce priveşte spațiul util, obținându-se o reducere substanțială a volumului ocupat față de prototipul de laborator. Ca şi cerință de proiectare, este asigurată operarea autonomă cu comandă de la distanță, prin manevrarea a trei butoane şi un potențiometru. Sunt proiectate şi realizate plăcile electronice care să permită controlul motorului. Programul de microcontroller asigură sinteza pulsurilor şi comanda motorului, în concordanță cu tensiunile la borne şi a comenzii, asigurând undă sinusoidală a curentului de intrare în fază cu tensiunea. Rezultatele experimentale confirmă cerințele de proiectare, prin prezentarea formelor de undă ale tensiunii şi curenților de intrare, cât şi a curentului de ieşire, în timpul unui test static la 30 Hz şi 50% cuplu de sarcină, dar şi în timpul unui test dinamic de accelerare de la 5 Hz la 30 Hz. De

asemenea, indicii calitativi spre intrare sunt monitorizaţi, utilizând un analizor trifazat de putere. (capitolul 8)

PERSPECTIVE

Chiar dacă perspectivele acestei tehnologii sunt mari, rămâne dificilă satisfacerea cerinţelor tehnice la nivelul condiţiilor de exploatare pe care convertoarele de frecvenţă în configuraţie standard le îndeplinesc. Coeficientul limitat de transfer al tensiunii reprezintă o limitare serioasă în concurarea unei topologii de convertor cu circuit intermediar de tensiune continuă. O posibilă cale de a ocoli aceste impedimente o reprezintă utilizarea convertorului matricial în obţinerea unei acţionări integrate motor-convertor cu circulaţie bi-direcţională de putere, în gama redusă de puteri, pentru instalaţii de ridicare. Pentru aceasta este necesară o evaluare completă a soluţiei pentru aplicaţii industriale. De asemenea, este neceasară definirea de către producătorul de instalaţii de ridicat a unui set de cerinţe minime pentru această acţionare, în special în cazurile cele mai defavorabile ce pot apărea în timpul exploatării: reţea de alimentare dezechilibrată sau satisfacerea unui anumit scenariu în timpul golurilor de tensiune. Este necesar a se stabili dacă acest convertor de frecvenţă este capabil să îndeplinească aceste condiţii.
Pentru scăderea în continuare a dimensiunilor fizice ale acestui convertor, este necesară creşterea frecvenţei de comutaţie, ceea ce necesită utilizarea unor sisteme de control mai performante, capabile să sintetizeze cu mai mare rezoluţie pulsurile de comandă. De asemenea, dezvoltarea de noi serii de elemente reactive, care să ofere o densitate mai mare de energie, va facilita reducerea de gabarit.
În final trebuie menţionat că pentru a investiga multiplele aspecte de implementare ale convertorului matricial, volumul de muncă din cercetare trebuie să crească. Aceasta se poate face doar prin atragerea mai multor cercetători în acest domeniu, care să participe la acest efort. Primul pas care trebuie facut este facilitarea accesului pe scară largă la un prototip performant de convertor matricial, care să fie produs în serie de către o firmă specializată, sub forma unui kit hardware, care să ofere o operare sigură şi să ofere o demarare rapidă a activităţii de cercetare, prin includerea de documentaţie completă de exploatare şi a unei interfeţe performante cu un sistem de control, bazat pe un sistem comercial cu DSP.

Chapter 1

Bi-directional Power Flow AC Drives: state-of-the-art

This chapter presents the state-of-the-art in the bi-directional power-flow AC drives technology, pointing out that future trends in power electronics will lead the research effort toward the most convenient converter technology. Increasing the reliability, minimizing the cost and the physical size of the drive and increasing the overall efficiency of the drive system are only a few of these trends [1.1]-[1.12].
A special class of applications, where important increase of the overall efficiency is achieved, involves frequent regenerative operation. Friendly interaction with the grid becomes an important issue, while various standards as IEC 555, IEC 61000-3, IEEE 519 have been issued and compliance to them will become soon obligatory. These aspects lead to a conclusion that modern topologies of bi-directional power-flow converters, as the active front-end or the matrix converters, will become interesting for industrial implementation.
Investigations in possible application areas for bi-directional power flow converters have a great role in defining the requirements, which leads to a correct comparison of the converter topologies. An introduction in bi-directional power-flow converters presents each topology and points out on the most significant advantages and drawbacks. The matrix converter topology offers an attractive solution, but still, due to many other unresolved implementation aspects, is far from becoming a commercial solution and therefore, offers an ideal field for working to a PhD thesis.

1.1. OVERVIEW OF TODAYS AC DRIVES TECHNOLOGY

Today, AC drive technology is based mainly on the diode-bridge Voltage Source Inverter (VSI) topology feeding a three-phase AC motor, which depends on the specific of the application. The topology is shown in Fig. 1.1. A single or a three-phase diode rectifier feeds the DC-link filter, which consists of a choke and a large capacitor, to provide a stiff DC-link voltage. There are two version of the choke: using only a single (or two) DC choke connected on the DC side, or using three AC chokes connected on the AC side of the diode rectifier. The choke decreases di/dt for the

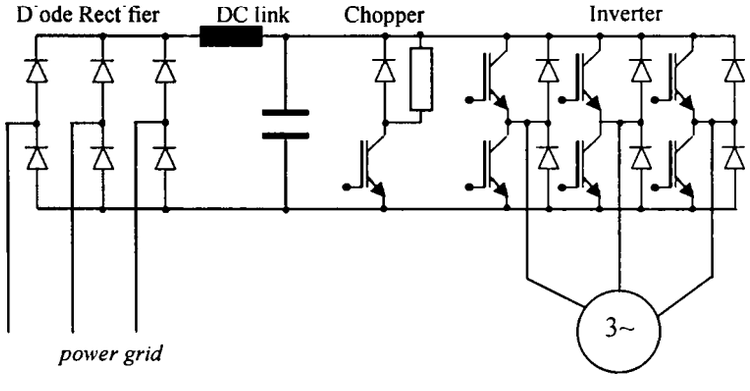

Fig. 1.1 The topology of the diode rectifier VSI

diodes and extends the conduction period for the rectifier and therefore reduce the current peak and improves significantly the input current THD, from about 80 % down-to 40 %.
Optionally, based on these chokes, RFI filters are easily to implement providing the necessary EMC compatibility. A three-phase PWM-VSI feeds the AC motor. In case regenerative operation of the motor is desired, a braking chopper is connected in the DC-link, to dissipate the energy and to keep the DC-link voltage below the protection limit, while the overall efficiency of the drive is low. This topology became so popular and widely employed in industry, due to the following reasons:

- higher performance of AC motors, compared to DC motors, as higher efficiency and reliability, lower production and maintenance cost;
- the development of high performance AC motor control strategies, based on vector control theory, allows for de-coupled control of the AC motor flux and torque and provides similar performance to a DC motor drive [1.13]-[1.17];
- strong support in theory for high-performance modulators, as Pulse Width Modulation (PWM), to provide a higher efficiency of the converter in synthesizing desired waveforms, similar to class D power amplifiers [1.13]-[1.17];
- the development of power switches for a wide power range, as the Insulated Gate Bipolar Transistor (IGBT), providing good switching capabilities as: gate controlled by voltage type signals, high ratings for the current and the voltage, low switching losses allowing for snubberless operation of the inverters [1.18]-[1.19];
- the rapid developing of high density-high voltage electrolytic capacitors, to provide a stiff DC-link voltage, required by VSIs [1.20];

Drawbacks of this technology has been reported in the literature [1.7]-[1.12], [1.21]-[1.22] as:

- higher input current THD (>40 %), due to a diode bridge rectifier interface to the grid;
- higher stress in the motor windings due to higher dv/dt of the output voltage waveforms, generated by a PWM-VSI;
- the drive is tripping during motor deceleration, caused by the increase of the DC-link voltage during regeneration, when a breaking chopper is not used;
- reduced lifetime and high sensitivity to the environment temperature, which are specific to the electrolytic capacitors, as it is shown in Fig. 1.1;

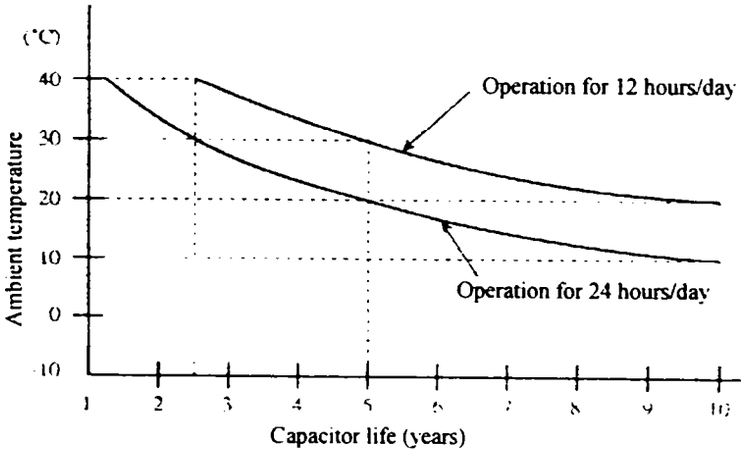

Fig. 1.2: Capacitor life-time expectation depending on the ambient temperature in a low-power industrial diode-bridge VSI (reprinted from [1.23], pp. A-19, Appendix 5)

1.2. APPLICATION AREAS FOR BI-DIRECTIONAL POWER FLOW AC DRIVES

As a component of an AC drive, the AC motor is an inherent bi-directional power flow electromechanical system. The frequency converter is the limiting component in the circulation of the energy from the motor to the mains, due to the diode bridge rectifier. However, short-term regenerative operation of the drive is allowed due to a limited energy storage capability of the DC-link capacitor bank, which in most of the cases satisfy the requirements of any general application. The main reason to employ a bi-directional power flow converter is the energy savings, which reduces the payback time of the investment. The other possible benefit of a bi-directional power flow converter, the friendly interface with the grid, improves the power quality due to sinusoidal and balanced input currents, but could not justify the cost, as long as no penalty is applied to electrical customers with distorted and unbalanced loads. Therefore, specific application areas have to be identified and then, analysis of the optimal bi-directional power flow topology for that application has to be carried out.
Bi-directional power-flow converters are suited in applications where:

- a higher duty-cycle for the AC drive working in regenerative operation, makes attractive to recover the braking energy, when frequent speed reversals or rapid decelerations are involved, or in hoisting applications, as elevators and cranes;
- for equipments used to test induction motors by using the artificial loading method;
- for special environment conditions (corrosive), where the cost required to dissipate the heat produced during the regenerative operation is prohibitive;
- special AC drive topologies, as the doubly-fed induction motor, which requires a smaller installed power in the converter, but requires bi-directional power flow;

1.3. TOPOLOGIES OF BI-DIRECTIONAL POWER FLOW AC DRIVES

Implementation of variable-speed bi-directional power-flow drives has evolved during the last century, led by evolutions in the electrical machine technology and in the power electronics technology. At the beginnings, power electronics were not existent and variable speed drives have been implemented by adding extra-windings (e.g amplidyne) or a mechanical frequency changer (e.g. DC motor with brushes used in Ward-Leonard drives) [1.3], [1.6]. However, variation of the voltage in the main circuits was required, and mainly achieved by introducing variable resistors, which causes higher losses, or by employing a motor-generator assembly, which occupies space, makes noise, has a low efficiency and a low flexibility.
When high efficiency power electronics devices, capable to change the electrical parameters of the power grid according to desired command signals, start to develop, the reduction in size and in installed power of the electrical machinery and the improvement in efficiency was achieved. Two solutions to change the fixed voltage and frequency of the power grid are possible:

- Direct (AC/AC) single-stage frequency conversion, shown in Fig. 1.3a. This has the advantage that the frequency converter uses a single stage transformation, with reduced energy storage components, but dependent on the power grid quality. There are two typical configurations: the cycloconverter and the matrix converter;
- DC-link (AC/DC/AC) two-stage frequency conversion, shown in Fig. 1.3b and Fig. 1.3c. This uses a DC intermediary stage in order to de-couple the influence between the two different frequency electrical systems. This has the advantage to reduce influence to disturbances, but employs large energy storage reactive components. These types of

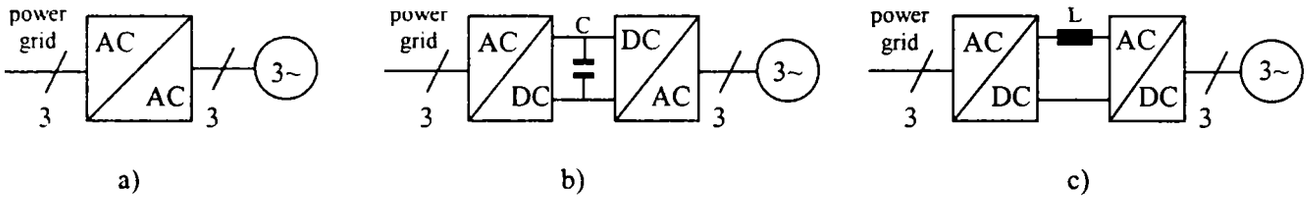

Fig. 1.3: Categories of frequency converters
a) single stage AC/AC conversion; b) DC-link back-to-back VSI; c) DC-link back-to-back CSI;

converters are divided in two categories, depending on the type of the DC-link used to decouple the input and output sides. One type is the voltage source DC-link, shown in Fig. 1.3b, where the main element is a large DC capacitor. The other type is the current source DC-link, shown in Fig. 1.3c, where the main element is a large DC choke.

Depending on the modulation, there are two types of converters: with natural commutation and with forced (PWM) commutation. By analysing the topologies of two-stage bi-directional power-flow converter, it is concluded that a mixture of modulation types may be used, to reduce cost and complexity and to fulfil the requirements, as well. In the following subsections, a brief description of possible bi-directional power-flow two-stage topologies, emphasising the specific advantages and disadvantages, is shown.

1.3.1 Cycloconverter fed synchronous motor drive

The cycloconverter is a direct frequency converter and consists of three four-quadrant three-phase-to-one-phase phase-shift controlled converters, using natural commutated elements as thyristors, disposed in a configuration shown in Fig. 1.4.

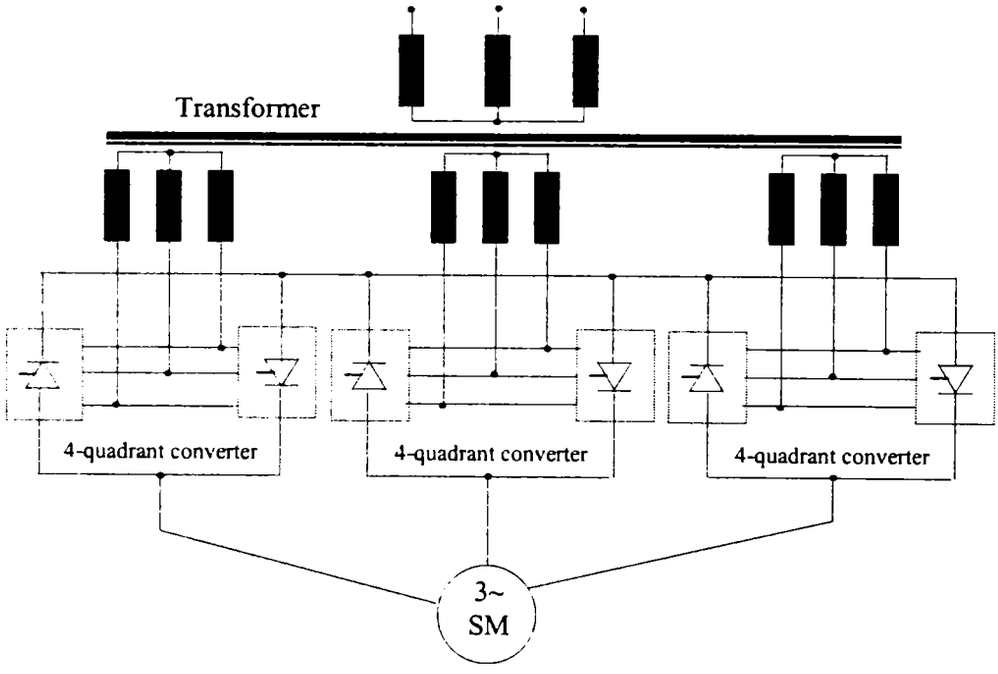

Fig. 1.4: Scheme of a cycloconverter fed synchronous motor drive

A transformer with three insulated three-phase secondary windings is necessary in order to adapt the voltage level and to allow star connection of the three four-quadrant converters. [1.3], [1.13]-[1.17]. Due to natural commutation, the maximum obtainable output frequency is low (0.3-0.6 f_{in}) in order to synthesise a voltage waveform with a reasonable THD. In Fig. 1.5 waveforms of output

phase voltage produced from the input phase voltages is shown (upper side), as well as the current, filtered by an inductive load and the operation mode of the two anti-paralleled thyristor bridges of the same output line is explained. This class of bi-directional power flow drive has limited application, especially in the low-speed high-power range of synchronous motors.

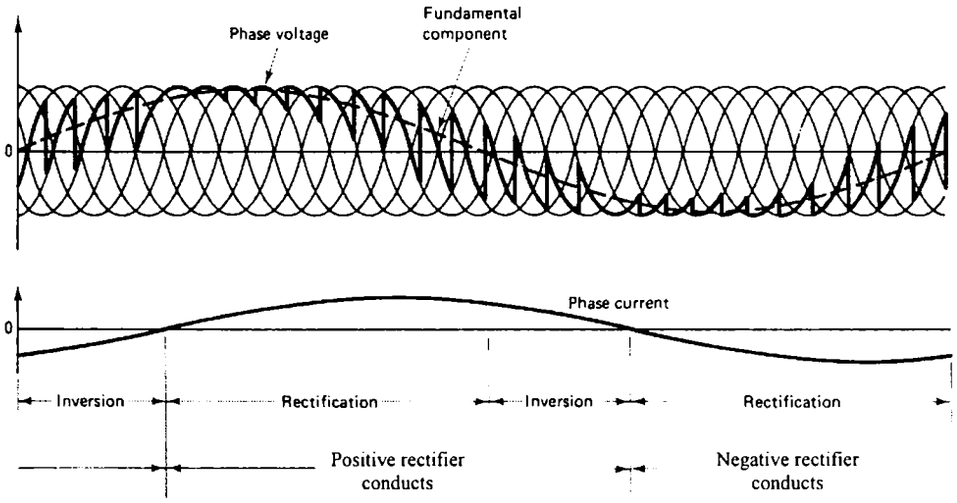

Fig. 1.5: Generation of the output voltage, the load current and the regime of the 4-quadrant converters in a cycloconverter drive (Reprinted from [1.3], pp. 1313, Fig. 17)

The cycloconverter is usually used to drive in low-speed (5 Hz), large synchronous and induction motors. However, auxiliary circuits to reduce the harmonic content in the input current, caused by the low "switching frequency", are necessary. Filtering becomes more complicated, as the harmonic content is dependent on the modulation conditions: output frequency and voltage transfer ratio.

1.3.2 Matrix converter fed induction motor drive

Working at higher switching frequency (2-20 kHz) with forced commutation, it is possible to improve the waveforms synthesised by a classical cycloconverter, to achieve sine-wave in, sine-wave out operation, independent control of the input current displacement angle and inherent bi-directional power flow [1.24]-[1.26]. Therefore, the need of low-order bulky filters disappears and the topology presents a great potential for volume reduction, as the size of the input filter depends on the switching frequency. The scheme of a practical matrix converter drive is shown in Fig. 1.6.

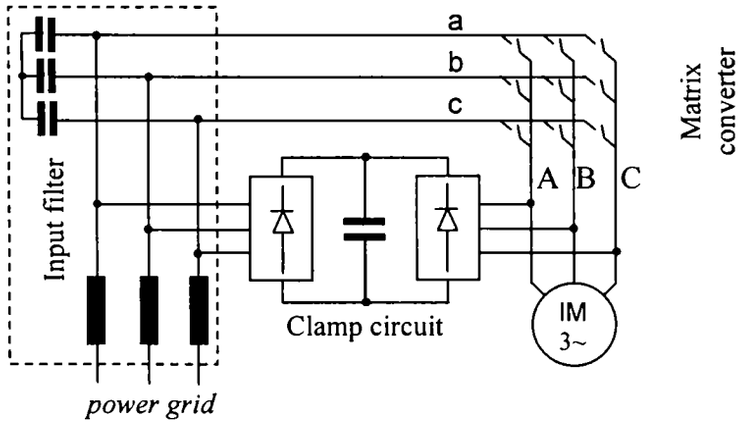

Fig. 1.6: The practical scheme of a matrix converter drive

This consists of an input filter, a matrix of 3x3 bi-directional switches capable to control current and to withstand voltage of both polarities and a clamp circuit, for protection purpose. However, additional aspects of implementing the topology in industry have not been totally resolved, which makes the research work a real challenge. Industrial implementation is seen by many visionary authors to come in the near future [1.1]-[1.12], as for the tomorrows frequency converters increasing the efficiency, reducing the physical size, friendly interaction with the grid and bi-directional power flow become the important issues.

1.3.3 Current source inverter fed induction motor drive

This type of bi-directional power flow converter was developed in the 70's, based on the characteristic of the thyristors: unidirectional current switch with reverse blocking voltage capability. In this way, the implementation of a bi-directional power flow converter, based on a back-to-back CSI topology required only 12 thyristor devices and compared with the back-to-back VSI topology, which requires 12 IGBT's and 12 FRD's, offers a more economical solution [1.27], [1.28]. The general topology is shown in Fig. 1.7.

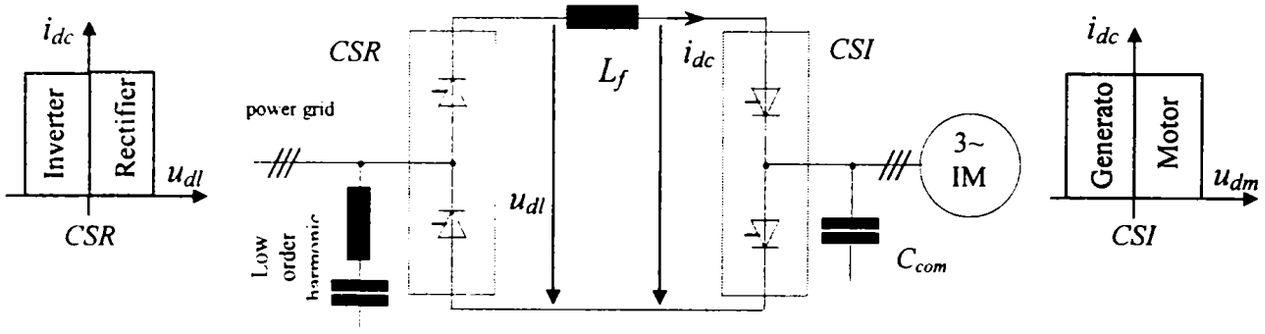

Fig. 1.7: Bi-directional current source converter fed induction motor

When phase-shifted controlled thyristors are employed, only a six-pulse waveform could be synthesised with high distortion level. Extra circuits employing capacitors mounted between output lines and diodes for separation are used for commutation (turn-off) purpose, because these devices have no turn-off capability. Implementation difficulties, as discontinuous current operation at low-load and instabilities of the motor feed by a current source supply appears.
For high-performance, forced commutated devices as GTO thyristors or IGBT's in series with diodes to achieve reverse blocking have to be used. The higher switching frequency produces higher resolution of the waveforms. The capacitors on the output side are used only to avoid overvoltages during commutations, because the device has turn-off switching capability. Even though this solution was widely employed in AC drives at the beginnings, now it is used only in the high power range, tens of MW drives. Another advantage is a good output current and voltage waveforms, with low dv/dt in the output voltage, which reduces the stress in the motor windings and improves the EMC compatibility.

1.3.4 Thyristor rectifiers VSI fed induction motor drive

As the VSI based on an IGBT power stage is considered ideal to feed the AC motors in a wide power range, only the diode bridge (B6) is susceptible for changes in order to provide bi-directional power flow. Therefore, industrial implementation of regenerative rectifiers has followed a few intermediary steps, in order to improve the performance of the rectifier stage, first by employing two anti-paralleled thyristor-bridges [1.29]-[1.31].

As this type of line side converters have been widely used to feed DC motors, allowing for bi-directional power flow, all the implementation issues were already known and solved before.
The operation of the thyristor rectifier is explained in Fig. 1.8. Two thyristor four-quadrant bridges are anti-paralleled, one for each regime: rectification or inversion. In case the DC-link voltage U_d is below a certain level U_{dlim}, the bridge allowing for rectification receives firing signals on gates (30° lagging). During regenerative operation of the motor, energy flows back in the DC-link causing the voltage to rise. When the DC-link voltage exceeds the limit U_{dlim}, the firing signals for the rectification bridge stops. When all the thyristors are turned off, the control logic activates the inversion-bridge (150° lagging). It is noticed that the firing angle does not vary in a certain range, therefore only constant DC-link voltage is achieved.

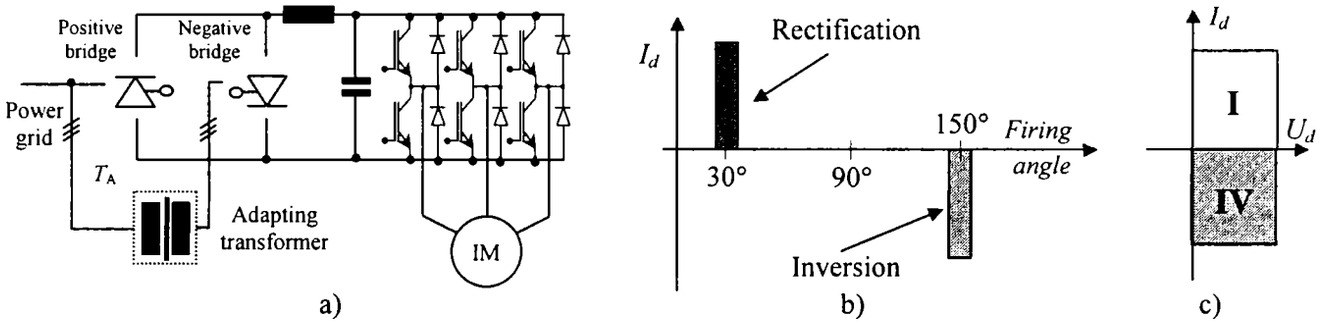

Fig. 1.8: Thyristor rectifier with bi-directional power flow VSI fed induction motor: a) principle diagram b) firing angle; c) operation quadrants;

Large chokes or adapting transformers for the inversion-bridge are necessary in the input side of the thyristor bridge to avoid commutation failures, which occurs usually when the input stage starts working in regenerative operation, causing the input fuses to blow. This was reported in [1.31].

1.3.5 Three-phase PWM rectifier with three-phase VSI fed induction motor drive

This topology consists of two PWM-VSI's, connected in a back-to-back configuration [1.32]-[1.34], at a common DC-link capacitor, as is shown in Fig. 1.9.

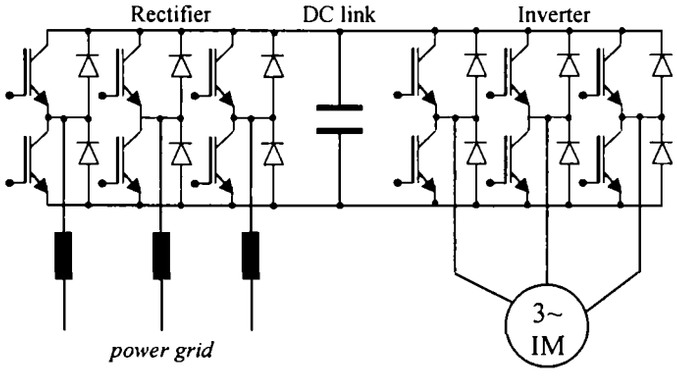

Fig. 1.9: The topology of the back to back VSI

Benefits of this solution is to regulate accuratly the DC-link voltage at a voltage level higher than the amplitude of the input line-to-line voltage and to synthetise sinusoidal and balanced input currents, even for unbalanced supply conditions. Large AC chokes (5-15 %.) are required in the

input side to improve the ripple in the input current. In order to comply with EMC requirements, an RFI filter has to be employed in the input side, whith an L-C-L configuration, which furthermore increase the size of the reactive elements. In the last 3 years this solution had become comercial. Because this topology could be assembled by connecting back to back two standard frequency converters, some companies reccomand to use a standard converter with a different control software for rectification and a three-phase AC choke in the input side, to achieve bi-directional power flow [1.32].
The control of a PWM voltage source rectifier is illustrated in Fig. 1.10. The control loop has to maintain the DC-link voltage at a certain level: U_{DCref}. A measurement of the DC-link voltage is used to determine the error, which is introduced in a PI controller. The result is a continous variable, which represents the magnitude of the voltage to be sinthetized by the PWM rectifier. To produce sinusoidal input currents, a multiplication by a function similar to the input voltage has to be performed. Therefore, the input current I_A becomes a result of appliying the result of two two voltage vectors substraction V_{An} - E_A to the input choke L_{in}.

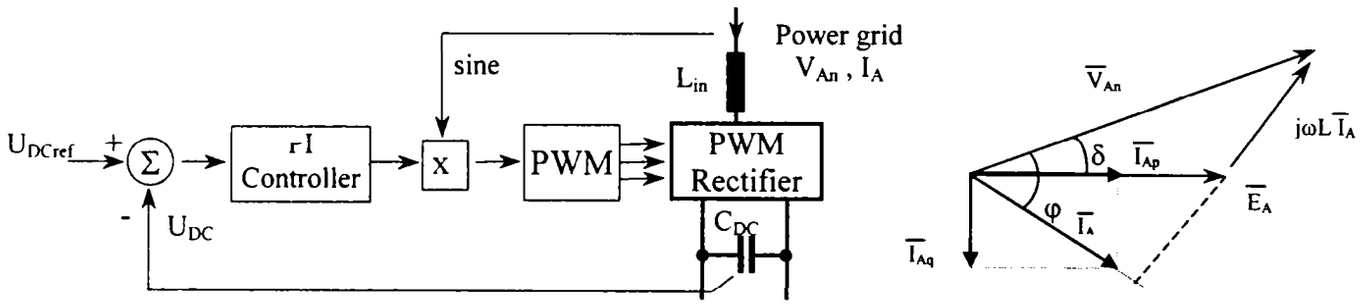

Fig. 1.10: Single-phase PWM rectifier: a) control scheme; and b) vector diagram;

By varying the displacement angle between the two voltages δ, the displacement angle of the input current φ is controlled, while by varying the reference DC-link volatge U_{DCref}, the magnitude of the active power is changed.

1.3.6 Single phase PWM rectifier with two-phase VSI fed induction motor drive

This version of a regenerative AC drive was proposed as an economical solution in the low power range, for domestic applications. The topology is shown in Fig. 1.11 and employ three VSI legs, one for the PWM active rectifier to provide for bi-directional power flow, sinusoidal input current, unitary power factor and the other two to form a two-phase VSI, to feed the two-phase induction motor, or even a single phase induction motor with auxiliary winding, as was proposed in [1.35].
The substantial savings in the power switches count is considered as a main advantage of this topology, in conjunction with the possibility to use a standard power module for three-phase VSI's. The drawback, as in any asimetrical configuration, is that the power devices in the rectifier leg and in the inverter leg have different ratings, which is worse in case of a single-phase induction motor, with the auxiliary phase rated at different voltage and current.. This requires to oversize the DC-link capacitors, compared to a similar three-phase topology, in order to minimise the voltage ripple, because of the AC currents, mixture of the input and output frequency harmonics, which flows through. Another disadvantage is that employing a two-phase PWM inverter, makes impossible to apply zero-vectors to the motor, causing higher ripple in the output current and in the electromagnetic torque. Therefore, in order to obtain similar results, a higher switching frequency has to be used.

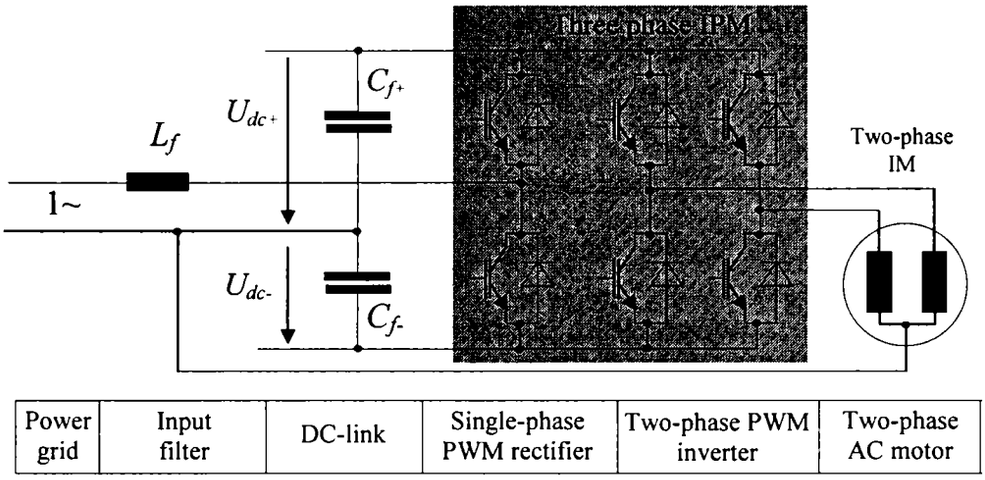

Fig. 1.11: Low cost solution for a bi-directional power flow drive in the low power range

1.3.7 Multidrive application with bi-directional power flow rectifier

In the situation of an electromechanical system, requiring many bi-directional drives which work independent, but are fed from a common supply, it is more convenient to use a multidrive topology of DC/AC inverters, supplied from a common rectifier [1.36]. The topology is presented in Fig. 1.12. A bi-directional power flow rectifier, using anti-paralleled phase-shift controlled supply units (with thyristors), or a PWM rectifier (with IGBT's), produces a stiff DC-link voltage. The operation mode is controlled by the DC-link voltage error. Each inverter unit $I_1...I_n$ is connected to the common DC-link through high-speed fuses, to protect and interrupt fast a possible hardware failure in any of the inverter units.

The necessity of using a bi-directional rectifier results from sizing the electromechanical system and studying the working cycles. In case one large drive is working only in motoring mode, it is possible to use all the energy fed back by the other drives working in regenerative mode. In this situation, there is no need for bi-directional power flow and a standard supply unit fulfils the requirements. In case the power flow has different levels for each direction and a phase-shift controlled supply unit is employed, using anti-paralleled thyristor bridges, it is possible to chose different ratings for the rectifier and for the inverter bridges, and therefore to minimise the cost.

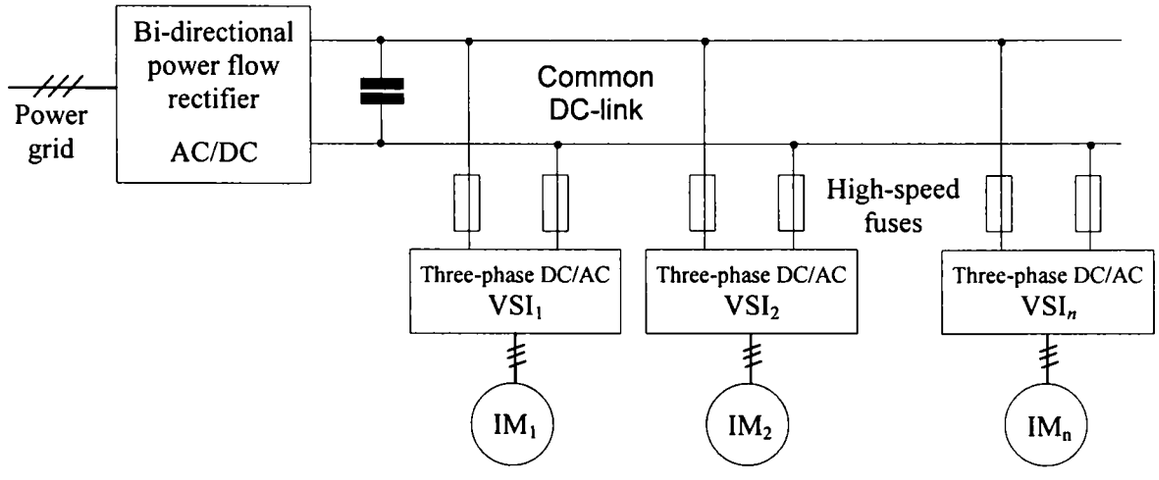

Fig. 1.12: Multidrive topology with bi-directional power flow rectifier

1.3.8 Doubly-fed slip-ring induction motor with bi-directional power flow converter

An interesting application of a bi-directional power flow converter is in doubly-fed slip-ring induction machines [1.37]-[1.40], with regard to the ratio of the drive power and the power installed in the converter, which in this case is dependent on the maximum slip.

$$S_{conv}[\text{kVA}] = s_{max} \cdot P_{drive} \tag{1.1}$$

This solution is suitable for applications where the necessary variable speed range is limited around the synchronous speed (e.g. ± 20%), in the high-speed range. In this situation the speed range is 0.8-1.2 of the synchronous speed, giving a continuous variable speed range of 1.5:1. This is useful especially in variable torque applications as high-power pumps and fans, where below a certain speed, the load torque becomes insignificant. This drive requires only a fraction of the motor power installed in the bi-directional power flow converter. The configuration of the drive is shown in Fig. 1.12 in two situations: two mechanical line-contactors for both direction of rotation and three star-up resistors connected in the rotor circuit (a) and a five-phase-shift static contactor for both directions of rotation and to provide soft-start for the motor (b).

In the first situation presented in Fig. 1.13a, the stator of the slip-ring induction motor ASM is fed from the fixed frequency power grid by a group of two line contactors, one for each direction of rotation if needed, to reverse direction of the magnetic field. A circuit breaker provides the necessary short-circuit and overload protection. In the rotor circuit of the motor, three resistors and a contactor is needed to start-up the drive, until the shaft speed reaches the range of variable speed operation, and the voltage induced in the rotor decreases below the maximum limit of the bi-directional power flow converter. Then, the resistors are disconnected from the rotor circuit and the bi-directional power flow converter is connected in the circuit. An adapting transformer may be needed in order to adapt the voltage level for the converter, according to the variable speed range, in order to minimise the installed power of the converter (kVA).

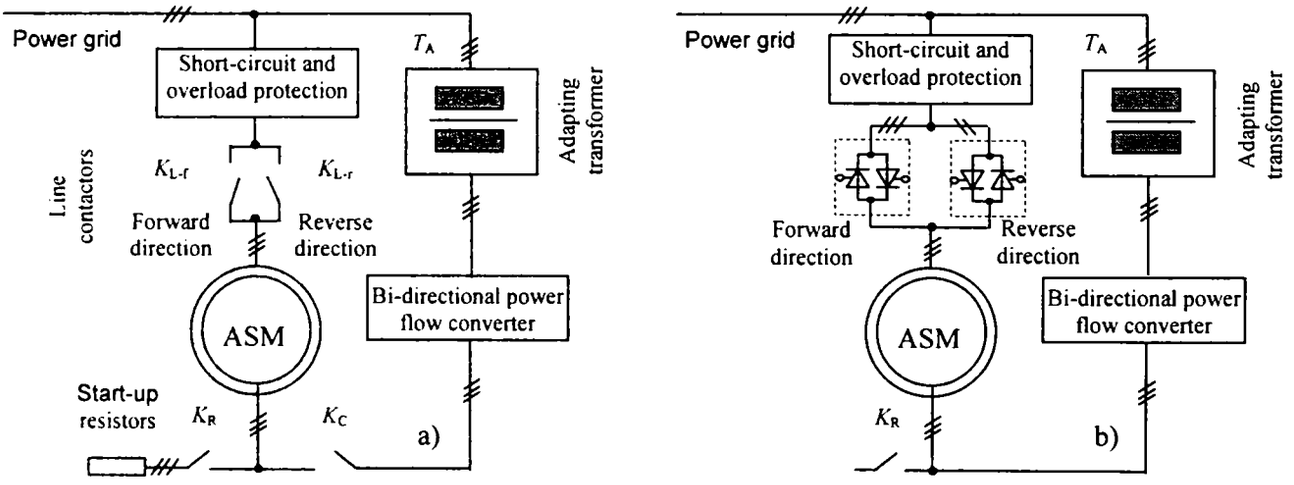

Fig. 1.13: Double-fed slip-ring induction motor with bi-directional power flow converter in the rotor: a) principle diagram with mechanical contactors and star-up resistors; b) principle diagram with static contactors providing soft-start;

It is possible to simplify the scheme by employing a five bi-directional phase-shift single-phase switches to provide soft-start and to allow for direction reversal of the stator flux, while the resistors in the rotor circuit are removed. This is shown in Fig. 1.13b. Only one mechanical contactor is required to short-circuit the rotor circuit, while the speed is outside the variable speed

operation domain and the voltage on the rotor rings is above the admissible level. When the speed reaches the variable speed domain of the drive, the contactor is opened and the bi-directional power flow converter is connected in the circuit.
Fig. 1.14a shows the four-quadrant mechanical characteristic of the drive. The contactors in the motor stator change the succession of the voltage system, enabling the operation of the drive in quadrant **I** (motoring, forward direction) and **IV** (generating, forward direction) and respectively **II** (generating, reverse direction) and **III** (motoring, reverse direction). It is noticed that quick torque reversal is possible, while to perform a speed reversal, is necessary first to decelerate down-to-zero speed outside the continuous variable speed range and then to perform the change of the succession of the voltage system, which limits the drive dynamics.

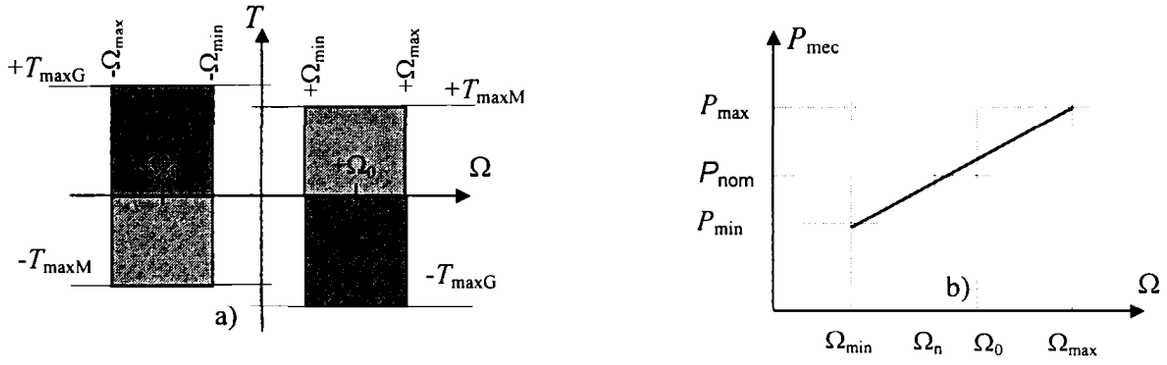

Fig. 1.14: Double-fed slip-ring induction motor drive with bi-directional power flow converter in the rotor: a) torque dependence and b) power dependence on the shaft speed;

Fig. 1.14b shows the variation of the mechanical power with the shaft speed. There is a linear dependence of the power with speed, given by limitation of the torque, until the region where the voltage induced in the rotor exceeds the maximum level of the bi-directional power flow converter.

MOTIVATION FOR CHOOSING THIS TOPIC FOR THE THESIS

During the last 15 years, almost all the topologies presented in this chapter have been implemented in industrial applications. Based on advances in the power switch technology, on control circuits technology, the AC drives have evolved slowly, making small steps towards high performance, low volume and low cost. The trend in industry was to improve the technology step by step, instead of introducing new technologies and making major changes. The main reason to do this has always been dictated by a conservative market, much more than by the research and development teams.
If in the last decade, the effort was oriented to reduce the active power switches count. Now, improvements in the overall efficiency of drives, reducing the physical size and improving the interaction with the grid are desired.
The matrix converter represents now a great challenge, recognised by many visionary authors, due to the advantages offered: lack of bulky and limited lifetime reactive elements, instantaneous and inherent bi-directional power flow transfer. But these advantages are shaded by a few disadvantages as a limited voltage transfer ration, a major dependence of the grid unbalance conditions and the lack of ride-through capability as well. Intense activity in the research field in the last 20 years proves that real advance in this technology was made and concludes that the

moment of industrial implementation is close. This motivates that choosing this field for developing a Ph.D thesis is a good opportunity to contribute to bring the next generation of frequency converters closer to industrial implementation.

REFERENCES

[1.1] R.J. Kerkman, T.M. Rowan, "*Voltage controlled current regulated PWM inverters*", Proc. of IAS Annual Meeting, vol. 1, pp. 381-387, 1988.

[1.2] T.A. Lipo, "*Recent progress in the development in solid-state AC motor drives*", IEEE Trans. on Power Electronics, vol. 32, pp. 105 –117, 1988.

[1.3] B.K. Bose, "*Power Electronics – A technology review*", Proc. of IEEE, vol. 80, no. 8, pp. 1303-1334, 1992.

[1.4] W. Drury, D. Grant, "*Variable-speed drives-the future*", Power Engineering Journal, vol. 81, pp. 27 –34, 1994.

[1.5] S. Williamson, D.C. Jackson, "*Integrated drives for industrial applications*", Proc. of PCIM'99, Intelligent motion, pp. 9-13, 1999.

[1.6] T.M. Jahns, E.L. Owen, "*AC adjustable-speed drives at the millennium: how did we get here?*", Proc. of APEC'00, paper 1.3 (plenary session), CD-ROM version, 2000.

[1.7] P. Thoegersen, P. Nielsen, F. Abrahamsen, "*Impact on energy savings by variable speed drives from motor and converter technology*", Proc. of PCIM'99, Intelligent motion, pp. 1-7, 1999.

[1.8] J.D. van Wyk, F.C. Lee, "*Power electronics technology at the dawn of the new millennium – status and future*", Proc. of PESC'99, paper 1.1 (plenary session), CD-ROM version, 1999.

[1.9] R. Kerkman, G.L. Skibinski, D.W. Schengel, "*AC drives: Year 2000 (Y2K) and beyond*", Proc. of APEC'99, vol. 1, pp. 28-39, 1999.

[1.10] P. Thoegersen, F. Blaabjerg, "*Adjustable speed drives in the next decade. The next step in industry and academia*", Proc. of PCIM'00, Intelligent motion, pp.95-104, 2000.

[1.11] R.D. Lorentz, "*The future of electric drives: where are we headed?*", Proc. of PEVD'00, pp. 1-6, 2000.

[1.12] K. Phillips, "*Power electronics: Will our current technical vision take us to the next level of AC drive product performance?*", Proc. of IAS Annual Meeting, paper 1.1 (plenary session), CD-ROM version, 2000.

[1.13] L. Gyugyi, B.R. Pelly, "*Static power frequency changers. Theory, performance and application*", ISBN 0-471-67800-7, 442 pages, John Willey&Sons, USA, 1976.

[1.14] N. Mohan, T.M. Undeland, W.P. Robbins, "*Power electronics. Converters, applications and design*", ISBN 0-471-30576-6, 802 pages, John Wiley&Sons, Inc., USA, 1995.

[1.15] B.K. Bose (editor), "*Power electronics and variable speed drives. Technology and applications*", ISBN 0-7803-1061-6, 640 pages, IEEE Press, USA, 1997.

[1.16] G. K. Dubey, "*Power semiconductor controlled drives*", ISBN 0-13-686890-8, 495 pages, Prentice Hall, Englewood Cliffs, New Jersey 07632, USA, 1989.

[1.17] I. Boldea, S.A. Nasar, "*Electric drives*", ISBN 0-8493-2521-8, 411 pages, CRC Press, US, 1999.

[1.18] F. Blaabjerg, J.K. Pedersen, "*Optimal design of a complete three-phase PWM-VS Inverter*" IEEE Trans. on Power Electronics, vol. 12, no. 3, pp. 567-577, 1997.

[1.19] F. Blaabjerg, J.K. Pedersen, U. Jaeger, "*Evaluation of modern IGBT-modules for hard-switched AC/DC/AC converters*", Proc. of IAS Annual Meeting, vol. 2, pp. 997-1005, 1995.

[1.20] M. Bramoulle, "*Electrolytic of film capacitors?*", Proc. of IAS Annual Meeting, paper 25.3, CD-ROM version, 1998.

[1.21] S. Hansen, P. Nielsen, F. Blaabjerg "*Harmonic cancellation by mixing non-linear single- phase and three-phase loads*", IEEE Trans. on Industry Applications, vol. 36, no. 1, pp. 152-159, 2000.

[1.22] D. Rendusara, P. Enjeti, "*A method to reduce common mode & differential mode dv/dt at the motor terminals in PWM rectifiers/PWM inverter type adjustable speed drive system*", Proc. of APEC'98, paper 22.2 , CD-ROM version, 1998.

[1.23] *Hitachi Inverter - J100 SERIES, Instruction manual*, appendix 5, pp. A-19, Hitachi Ltd., Tokyo, Japan.

[1.24] C.L. Neft, C.D.Shauder, "*Theory and design of a 30-hp matrix converter*", IEEE Trans. on Industry Applications, vol. 28, no. 3, pp. 546-551, 1992.

[1.25] L. Huber, D. Borojevic, "*Space vector modulated three-phase to three-phase matrix converter with input power factor correction*", IEEE Trans. on Industry Applications, vol. 31, no. 6, pp. 1234- 1246, 1995.

[1.26] P. Nielsen, "*The matrix converter for an induction motor drive*", Industrial PhD Project EF493, ISBN 87-89179-14-5, 296 pages, Aalborg University, Denmark, 1996.

[1.27] B. Wu, G.R. Slemon, S.B. Dewan, "*PWM-CSI induction motor drive with phase angle control*", Proc. of IAS Annual Meeting, vol. 1, pp. 675-679, 1989.

[1.28] T. Halkosaari, H. Tuusa, "*The comparison of the efficiency in a current and a voltage source inverter supplied from a controlled rectifier*", Proc. of PCIM'99, Intelligent motion, pp. 217-222, 1999.

[1.29] ABB, "*ACS600 Multidrive. Commissioning of SAFUT thyristor braking unit*", Student Binder, ABB Industry Oy, Helsinki, Finland, 1997.

[1.30] I.G. Park, S. I. Kim, "*A new thyristor phase-controlled voltage source converter with bidirectional power flow capability*", Proc. of IAS Annual Meeting, vol. 2, pp. 1368-1375, 1997.

[1.31] J. Rodriguez, J. Pontt, A. Weinstein, "*Regenerative drives in the megawatt range for high performance downhill belt conveyors*", Proc. of IAS Annual Meeting, paper 50.2, CD-ROM version, 2000.

[1.32] "*Vacon starts new era for frequency converters. Active input bridge enhances performance of Vacon frequency converters*", http://www.vacon.com/what/newera.html, april 2000.

[1.33] T. Noguchi, H. Tomiki, "*Direct power control of PWM converters without power source voltage sensors*", IEEE Trans. on Industry Applications, vol. 34, no. 3, pp. 473-478, 1998.

[1.34] M. Malinowski, M.P. Kazmierkowski, S. Hansen, F. Blaabjerg, G. Marques, "*Virtual flux based direct power control of three-phase PWM rectifiers*", Proc. of IAS Annual Meeting, paper 53.6, CD-ROM version, 2000.

[1.35] M.F. Rahman, L. Zhong, S.Y. Hui, "*A single-phase, regenerative, variable speed induction motor drive with sinusoidal input current*", Proc. of EPE'95, vol. 3, pp. 3.777-3.780, 1995.

[1.36] ABB, "*ACS 600 MultiDrive Modules. Product catalogue*" 3BFE 64104268 R0125, ABB Industry Oy, Helsinki, Finland, 1999.

[1.37] S. Tnani, S. Diop, S.R. Jones, A. Berthon, "*Novel control strategy of doubly-fed induction machines*", Proc. of EPE'95, vol. 1, pp. 1.553-1.558, 1995.

[1.38] L. Xu, W. Cheng, "*Torque and reactive power control of a doubly fed induction machine by position sensorless scheme*", IEEE Trans. on Industry Applications, vol. 31, no. 3, pp. 636-642, 1995.

[1.39] P. Poure, S. Saadate, B. Davat, "*Double fed rotor controlled machine used for dynamic compensation of mains harmonics*", Proc. of E.M&D'96, IEEE London, pp. 84-89, 1996.

[1.40] L. Zhang, C. Watthanasarn, "*A matrix converter excited doubly-fed induction machine as a wind power generator*", Proc. of PEVD'98, pp. 532-537, 1998.

Chapter 2

Fundamentals of the Matrix Converter Technology

This chapter presents the state-of-the-art in the matrix converter technology, at the time this thesis was in the final stage. New contributions reported in this PhD thesis, which will be presented in the following chapters, have been excepted. The introduction presents the basic diagrams and the permitted switching states of the converter and the transfer functions of the output voltage and input current. Because this converter employs bi-directional switches, the specific bi-directional switch commutation techniques are presented. Different modulation strategies, advanced control strategies applied to matrix converters and protection issues, proposed in literature, are briefly presented. Unresolved issues, which have delayed the implementation of the matrix converters in industry applications, are pointed out in the chapter summary.

2.1 INTRODUCTION

A matrix converter consists of nine bi-directional switches, arranged in three groups of three, each group being associated with an output line. This arrangement of bi-directional switches connects any of the input line *a*, *b* or *c* to any of the output line *A*, *B* or *C*, as is shown in Fig. 2.1a. A bi-directional switch is able to control the current and to block the voltage in both directions. If the input and the output three-phase systems are orthogonal disposed, the converter diagram becomes similar to a matrix, with the rows consisting of the three input lines (*a*, *b*, *c*), the columns consisting of the three output lines (*A*, *B*, *C*) and bi-directional switches connecting each row to each column, which in Fig. 2.1b are symbolised with circles. There are 512 possible combinations of switches in a three-phase to three-phase matrix converter. In order to provide safe operation of the converter, when operating with bi-directional switches, two basic rules have to be followed:

- DO NOT connect two different input lines to the same output line (short-circuit of the mains, which causes overcurrents);
- DO NOT disconnect the output line circuits (interrupt inductive loads, which causes overvoltages);

Therefore, an output line has to be all the time connected to a single input line. This allows to be symbolise the state of the matrix converter by using a group of three letters, which gives the input lines connected to the output lines in the following order: *A-B-C*. E.g. "*acc*" means that the output lines *A*, *B*, and *C* are respectively connected to input lines *a*, *c* and *c*.

If the basic rules mentioned before applies, the maximum number of permitted switching states of the matrix converter is reduced to 27, and these are shown in Fig. 2.2. Six switching states provide a direct connection of each output line to a different input line, producing a rotating voltage vector with amplitude and frequency similar to the input voltage system and direction dependent on the sequence: synchronous or inverse. Other eighteen switching states produce active vectors, of variable amplitude, depending on the selected line-to-line voltage, but of stationary position. The last three switching states produce a zero-vector, by connecting all the output lines to the same input line.

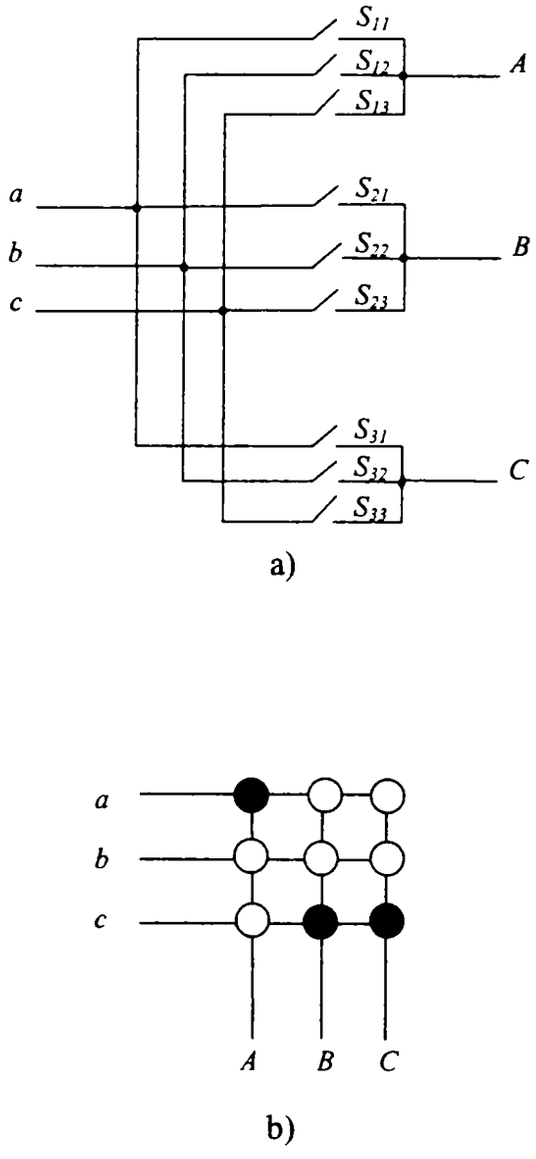

Fig. 2.1: Basic topology of a matrix converter: a) electric scheme; b) symbol

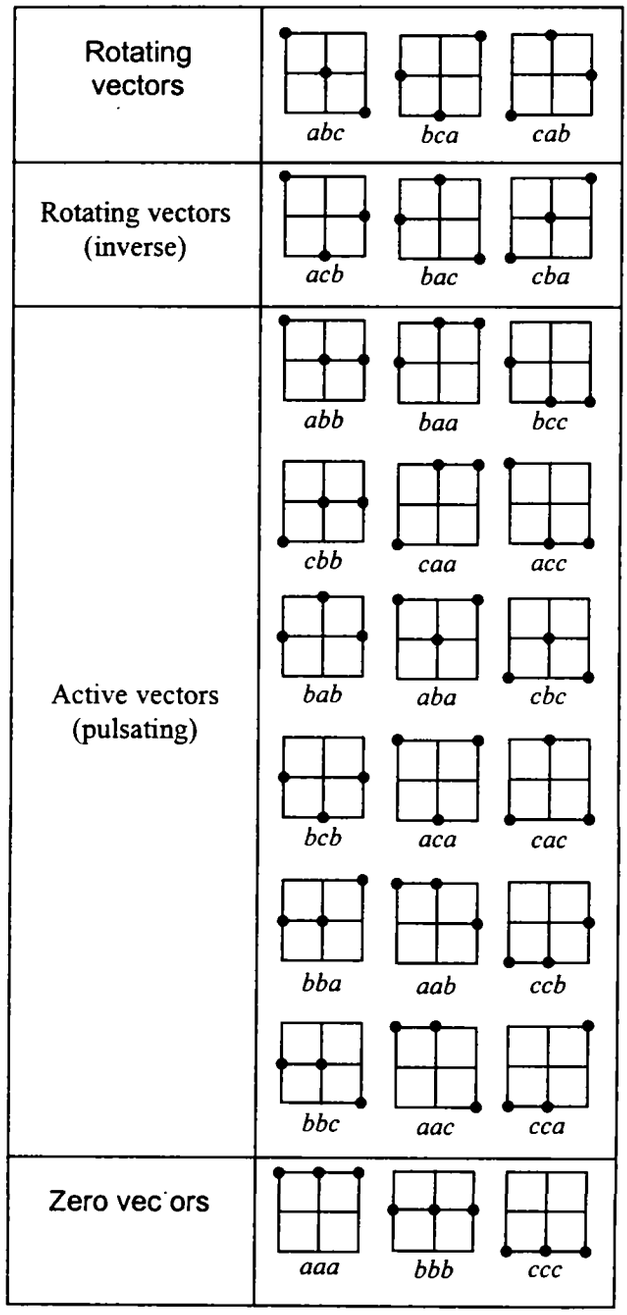

Fig. 2.2: Permitted switching states (27) in a three-phase to three-phase matrix converter

The transfer matrix T usually represents the state of the converter switches:

$$T = \begin{bmatrix} T_{11} & T_{12} & T_{13} \\ T_{21} & T_{22} & T_{23} \\ T_{31} & T_{32} & T_{33} \end{bmatrix} \tag{2.1}$$

where: $T_{ij} = \{-1, 0, 1\}$ are the possible conduction states of the bi-directional switches. Each row shows the state of the switches connected on the same input line and each column shows the state of the switches connected on the same output line. Due to the instantaneous power transfer of the matrix converter, the electrical parameters (voltage, current) in one side may be reconstructed from the corresponding parameters in the other side, at any instant. The input phase

voltages are given, because the matrix converter is connected to the grid. Therefore, by applying the direct transformation for the input phase voltages $U_{a,b,c}$, the output line-to-line voltages $U_{AB,\ BC,\ CA}$ are found:

$$\begin{bmatrix} U_{AB} \\ U_{BC} \\ U_{CA} \end{bmatrix} = \begin{bmatrix} T_{11} & T_{12} & T_{13} \\ T_{21} & T_{22} & T_{23} \\ T_{31} & T_{32} & T_{33} \end{bmatrix} \cdot \begin{bmatrix} U_a \\ U_b \\ U_c \end{bmatrix} \qquad \text{or} \qquad \boldsymbol{U}_{out} = \boldsymbol{T} \times \boldsymbol{U}_{in} \tag{2.2}$$

The output currents are a result of applying the previously determined output voltages to a given load. By applying the inverse transformation for the output currents $I_{A,B,C}$, the input currents $I_{a,b,c}$ are found:

$$\begin{bmatrix} I_a \\ I_b \\ I_c \end{bmatrix} = \begin{bmatrix} T_{11} & T_{21} & T_{31} \\ T_{12} & T_{22} & T_{32} \\ T_{13} & T_{23} & T_{33} \end{bmatrix} \cdot \begin{bmatrix} I_A \\ I_B \\ I_C \end{bmatrix} \qquad \text{or} \qquad \boldsymbol{I}_{in} = \boldsymbol{T}^T \times \boldsymbol{I}_{out} \tag{2.3}$$

Therefore, by knowing the load parameters, the input voltages and the switching states, given by a proper modulation strategy, the output voltages and the input current are found. This is a simple method of solving a matrix converter drive system in a simulation program.

2.2 ANALYSIS OF BI-DIRECTIONAL SWITCH TOPOLOGIES

In a synthesis paper written in 1988 [2.1], one of the first presenting the expectations from future development in AC drives, the matrix converter was credited with great perspectives. This was before important advances in this technology have been achieves, as reaching the highest limit of the voltage transfer ratio (0.86), proposing space vector modulation for matrix converters and proposing the semi-soft commutation strategy of bi-directional switches. At that time, it was considered that MCT's will evolve towards a reverse blocking capability and will provide the "ideal" switch for matrix converters. Later, due to the soft-commutation advantage, it has been shown that higher efficiency compared to standard VSI may be reached at higher switching frequency, of more that 10 kHz. As the MCT is a slow device, the solution to implement a bi-directional switch remains the IGBT device. Other synthesis papers published later [2.2] – [2.6] give the same credit to the matrix converter technology, as the trend now is towards improving the interaction with the power grid, providing bi-directional power flow, increasing the efficiency of the drive while operating at higher switching frequency, decreasing the drive size, integrating more complex silicon structures in power modules.

After attempts have been reported in the literature [2.7], a patent was issued [2.8], proposing a new power device for matrix converter applications: the reverse blocking IGBT (RIGBT), which decreases at one, the number of devices per phase. This will create conditions to increase the efficiency of the matrix converters above the diode-bridge VSI, because the conduction losses will be produced only by a single RIGBT per phase. Lately, in year 2000 [2.9], the first commercial RIGBT device has been reported to be available on the market.

The industrial development of the matrix converter has been obstructed by the lack of a true force-commutated bi-directional switch. Using unidirectional devices available on the market, there are three ways to obtain a bi-directional switch: the diode embedded unidirectional switch (Fig. 2.3a), the two common-collector unidirectional switches (CC) (Fig. 2.3b) or the two common-emitter (CE) unidirectional switches (Fig. 2.3c).

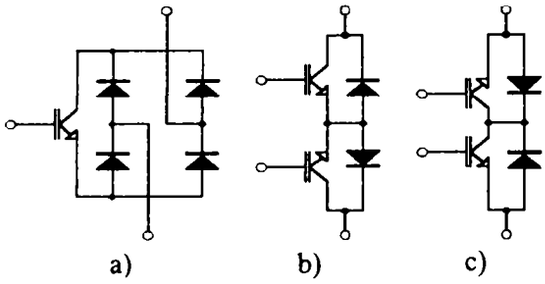

Fig. 2.3: Bi-directional switch topologies using unidirectional switches: a) diode embedded switch; b) common emitter switch (CE); c) common collector switch (CC);

The embedded switch requires only one gate driver and one active switch, which is more convenient for implementation than the other two configurations. A comprehensive analysis [2.7] [2.10]-[2.12] shows that the embedded switch topology causes higher conduction losses because the current path consists of two FRDs and one IGBT and higher switching losses because all commutations are hard switched. The two topologies based on anti-paralleled connection of two unidirectional switches (CE and CC) allow for lower conduction losses because the current path consist only of one FRD and one IGBT and for semi-soft switching (half soft-switching and half hard-switching), as it will be presented in the following section.

2.3 BI-DIRECTIONAL SWITCH COMMUTATION TECHNIQUES

Similar to VSI, where dead-time commutation is necessary to eliminate the risk of shoot-through (short-circuit of the DC-link capacitors through an inverter leg) caused by non-ideal commutation characteristic, specific commutation techniques are necessary to be implemented when bi-directional switches are operated. Fig. 2.4a shows the basic circuit and Fig. 2.4b shows the ideal command signals when the output line *out* is switched from one input line x, to the other input line y, by operating two bi-directional switches S_x and S_y. The commutation technique depends on the type of bi-directional switches employed in the matrix converter hardware.

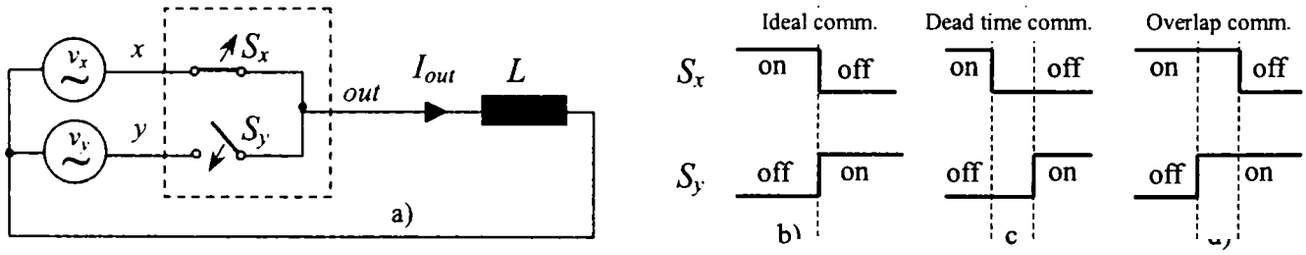

Fig. 2.4: Commutation of the output phase out from input phase x to input phase y: a) principle diagram; b) ideal commutation; c) dead-time commutation; d) overlap commutation;

In case of ideal true four-quadrant switches, there are two methods to perform the commutation:

- the dead-time current commutation, referred as "break before make" is shown in Fig. 2.4c. This method consist in turning off the off-going switch, while the on-coming switch is still disconnected, to avoid short-circuit of the inputs, in order to eliminate the overcurrent risk. This will cause overvoltage on the output side, therefore a clamp circuit connected to the output to provide continuity of the load current is necessary, but will cause high switching losses.
- the overlap current commutation, referred as "make before break" is shown in Fig. 2.4d. This method consist in turning on the on-coming switch, while the off-going switch

is still conducting, to provide continuity for the output line circuit, in order to eliminate the risk of overvoltage. This will cause high circulating currents between input phases, which has to be limited during the commutation, by adding extra chokes in the inputs to decrease d*i*/d*t*.

Both methods require extra reactive elements and produce high losses. Due to the practical implementation reasons, a bi-directional switch uses anti-paralleled unidirectional switches, which provide independent control for each direction of the current. Therefore, other commutation strategies have been proposed [2.13]-[2.18]. Basically, the operation principle consists in a two or four-step commutation technique. Depending on the direction of the output current or on the magnitude of the input voltages involved in the commutation process, the first action is to disable the current path for circulating currents and the second is to apply overlapping for the on-coming switch with the off-going switch. Therefore the risk of short-circuit on the input side is eliminated, and semi-soft commutation, which means that half of the switch commutations is performed naturally, is achieved.

2.3.1 Four-step commutation strategy [2.13]-[2.16]

This strategy operate the switches in a way that after the commutation is completed, the switch acts as a four-quadrant bi-directional switch, so that the load current could reverse freely direction. The commutation takes place in four steps:

- *1st step*: turn-off the off-going non-conducting switch. This way, current direction is not able to change sign.
- *2nd step*: turn-on the on-coming conducting switch. Now, there is unidirectional connection between input lines, but no circulating current may occur. In case there are condition for a natural commutation (from smaller voltage to higher voltage) between the off-going switch and on-coming switch, this starts at this moment.
- *3rd step*: turn-off the off-going conducting switch. At this time, in case of a hard commutation, the current is forced to switch from the off-going switch to the on-coming switch.
- *4th step*: turn-on the on-coming non-conducting switch. This is a passive step, with purpose to re-establish the 4-quadrant characteristic of the AC switch, so the currents can change sign naturally.

This is shown in Fig. 2.5 where the commutation scheme takes into account the current sign and also the possibility to switch from one steady switching state to the other steady switching state.

In Fig. 2.6 the possible path for the output current allowed by the four-step commutation strategy is illustrated for both current signs. The duration of the "passive" commutation steps (1 and 4) is not critical, because it is supposed that the device which are switched are or will not conduct, therefore it may change state faster. Duration of the "active" commutation (2 and 3) is critical and should be chosen in agreement with the switching characteristics of the devices employed in the anti-parallel topology. A complicate solution to adapt the duration of this "active" commutation has been proposed in [2.16], which modifies the period of the commutation clock in respect with the output current magnitude, but imply complicated hardware.

However, by adjusting the commutation clock period according to the maximum current magnitude, safe and low-loss commutation is achieved and for smaller output currents, the commutation will take place faster than the clock period, which does not cause any problem.

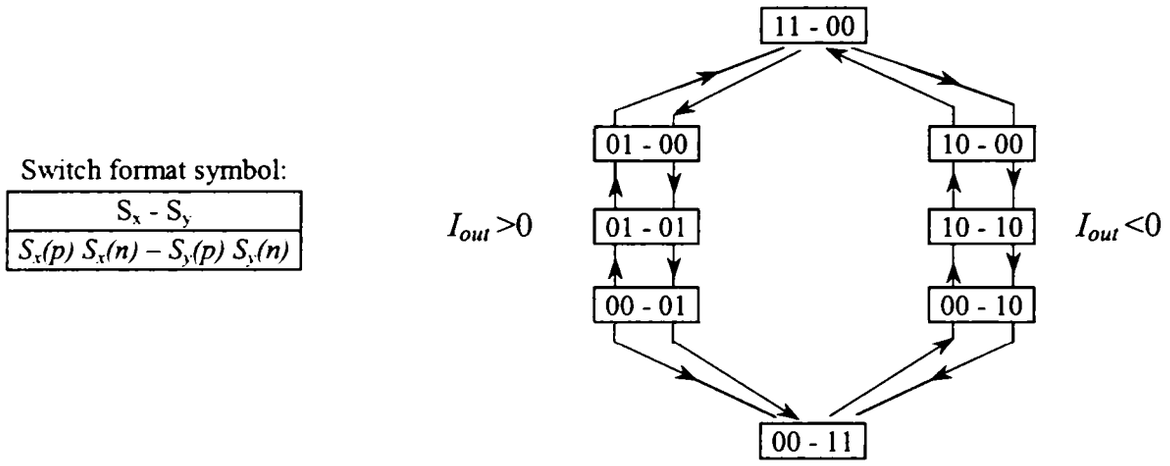

Fig. 2.5: Four-step commutation scheme depending on the current sign

The variation of the duty-cycle duration caused by the load current, according to real commutation situation, may be satisfactory compensated in the processor control program in the same way as for VSI, as a function of the load current which is measured and the device parameters which may be given.

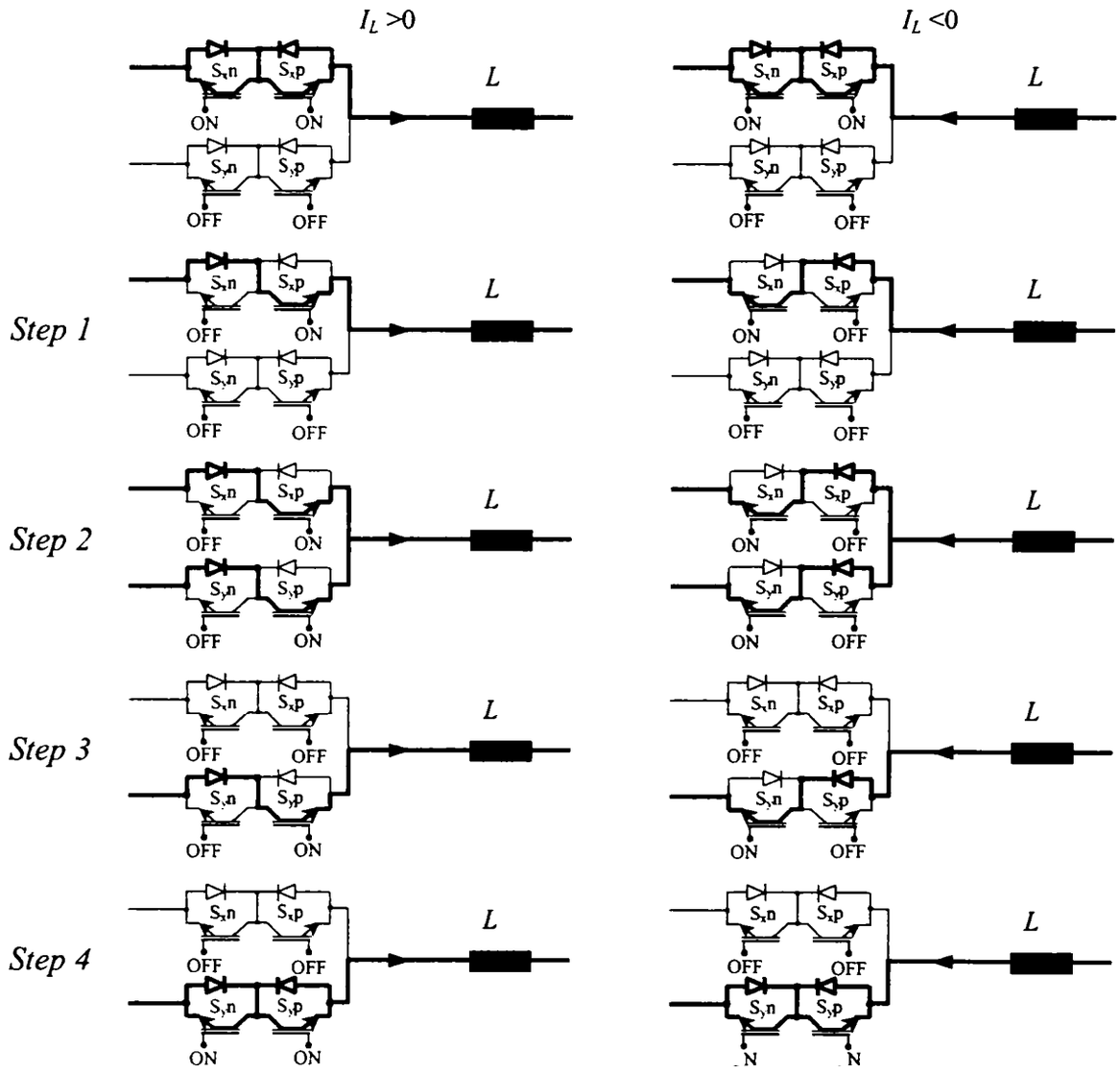

Fig. 2.6: Illustration of current path allowed during the four-step commutation

An another problem is commutation near to zero output current, where errors in the current sign may cause dead-time commutation. However, the energy in the leakage inductance of the load, at very low current level susceptible to cause offset errors, should not cause dangerous overvoltage, which may not be handled by the clamp circuit, without additional increase in the commutation losses.

2.3.2 Two-step commutation strategy [2.17]-[2.18]

This strategy has been developed in order to reduce the number of steps and the complexity of the commutation control unit. To perform the commutation in only two steps, the bi-directional current path of the switch in the turn-on steady-state is normally disabled but the strategy performs similar to the four-step commutation, while steady-states of bi-directional switches corresponds to step 1, respectively step 3, presented in Fig. 2.6. At low current levels where the current transducer may be affected by offset, it has been proposed to enable bi-directional current path of the on-state switch. In order to avoid the risk of a short-circuit of the input lines during the commutations, a true dead-time current commutation has to be used.

2.3.3 Current sign detection methods

In order to control properly the bi-directional switch commutation, current transducers as Hall transducers or shunts have been used. Also, a few other methods which claim not to be susceptible to offset error and exploiting the characteristic of the bi-directional switch topology have been reported in the literature:

- comparing the magnitude of the voltage across the unidirectional switches in a CE bi-directional topology [2.17]. This method has the advantage that does not require any transducer and provides good precision, but require components to handle the peak line-to-line voltage, which appears across non-conducting unidirectional switches

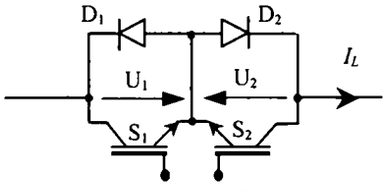

If $I_L > 0$ then S_1 and D_2 are conducting, D_1 and S_2 are reverse biased
$U_1 = +1.5$ V, $U_2 = -0.7$ V
If $I_L < 0$ then D_1 and S_2 are conducting, S_1 and D_2 are reverse biased
$U_1 = -0.7$ V, $U_2 = +1.5$ V

Fig. 2.7: Logic algorithm based on the voltage drop to detect the current direction [2.17]

(IGBT+FRD);

- measuring the voltage drop across two anti-parallel diodes connected on the output line [2.19]. This method is very simple, but causes voltage drop on the output side, in an application where the voltage transfer ratio is a sensitive issue. However, for a normal (slow) diode, which cause a 0.7-1 V voltage drop, the decrease of the voltage transfer ratio is only 0.2-0.3 %.

2.4 MODULATION TECHNIQUES FOR MATRIX CONVERTERS

The first modulator proposed for matrix converters, known as the Venturini modulation, used a complicated scalar model that gave a maximum voltage transfer ratio of 0.5 [2.20], [2.21]. An injection of a third harmonic of input and output voltage (2.4) was proposed in order to fit the reference output voltage in the input voltage system envelope and the voltage transfer ratio reached a maximum value of 0.86 [2.22]-[2.26]. This is shown in Fig. 2.8.

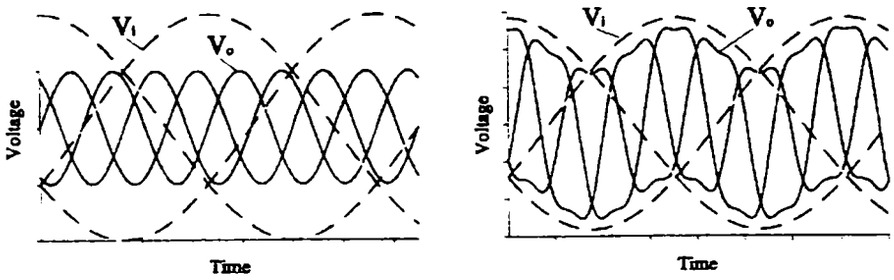

Fig. 2.8: Output voltage reference waveforms fitting in the input voltage system a) sinusoidal (V_{out}/V_{in} = max 0.5); b) injection of third harmonics (V_{out}/V_{in} = max 0.86) (reprinted from [2.10], Fig. 3.3, pp. 36)

$$v_{ref} = v_{out} \cdot \sin(\omega_{out} \cdot t) - \frac{v_{out}}{6} \cdot \sin(3 \cdot \omega_{out} \cdot t) + \frac{v_{in}}{4} \cdot \sin(3 \cdot \omega_{in} \cdot t) \tag{2.4}$$

Next, the indirect modulation was proposed [2.27]-[2.29]. This approach simplified the modulator model by making possible to implement classical PWM modulation strategies in matrix converters [2.27]. Modulation models using Space Vectors (SVM) [2.30]-[2.34] or the Direct Torque Control (DTC) [2.35] simplified the modulator model, making easier to control the converter under unbalanced and distorted power supply condition or to implement high-performance control of the induction motors. A few modulation techniques are briefly presented, while more details are given for the Space Vector Modulation, as all the experimental work in this thesis was made using this modulation technique.

2.4.1 Venturini modulation [2.11]

In order to provide balance for the output voltages and also for the input currents it is necessary that the modulation strategy to use equally the input voltages when producing the output voltages. The Venturini modulation method establish independent relations for each output, by sampling and distributing slides of input voltages in such a way that the average result follows the reference output phase voltage. Therefore [2.11], (2.2) and (2.3), which define relations between output and input at any instant, in order to provide balance during the switching period becomes:

$$\begin{bmatrix} V_A \\ V_B \\ V_C \end{bmatrix} = \begin{bmatrix} m_{11}(k) & m_{12}(k) & m_{13}(k) \\ m_{21}(k) & m_{22}(k) & m_{23}(k) \\ m_{31}(k) & m_{32}(k) & m_{33}(k) \end{bmatrix} \cdot \begin{bmatrix} V_a \\ V_b \\ V_c \end{bmatrix} \tag{2.5}$$

$$\begin{bmatrix} I_a \\ I_b \\ I_c \end{bmatrix} = \begin{bmatrix} m_{11}(k) & m_{21}(k) & m_{31}(k) \\ m_{12}(k) & m_{22}(k) & m_{32}(k) \\ m_{13}(k) & m_{23}(k) & m_{33}(k) \end{bmatrix} \cdot \begin{bmatrix} I_A \\ I_B \\ I_C \end{bmatrix} \tag{2.6}$$

where $m_{ij}(k)$ represents the duty-cycles of a switch connecting output line i to input line j in the k switching period.

The input phase voltages and the output current are considered constant during the switching period. At any time, $0 \leq m_{ij}(k) \leq 1$, and also, because the output phase circuit should not remain disconnected from an input phase (rule no. 2):

$$\sum_{j=1}^{3} m_{ij}(k) = 1 \tag{2.7}$$

In order to provide maximum voltage transfer ratio, injection of third harmonics is needed (2.4) and the reference output voltage becomes:

$$\begin{bmatrix} V_A(t) \\ V_B(t) \\ V_C(t) \end{bmatrix} = \sqrt{2} \cdot V_O \cdot \begin{bmatrix} \cos(\omega_O \cdot t) \\ \cos(\omega_O \cdot t - 2\pi/3) \\ \cos(\omega_O \cdot t - 4\pi/3) \end{bmatrix} - \sqrt{2} \cdot \frac{V_O}{6} \cdot \begin{bmatrix} \cos(3\omega_O \cdot t) \\ \cos(3\omega_O \cdot t) \\ \cos(3\omega_O \cdot t) \end{bmatrix} + \sqrt{2} \cdot \frac{V_I}{4} \cdot \begin{bmatrix} \cos(3\omega_I \cdot t) \\ \cos(3\omega_I \cdot t) \\ \cos(3\omega_I \cdot t) \end{bmatrix} \tag{2.8}$$

where V_O and V_I are the RMS value of the output voltage system, ω_O and ω_I are the angular frequencies of the output and input voltage systems.

If the reference voltage vector, given in (2.8), is replaced in the transfer function of the output voltages depending on the duty-cycles and the input voltages (2.5), a complicated model results. However, if a simplification is introduced, as zero angle displacement between the input current and voltage, the duty-cycles [2.11] are given by:

$$\begin{aligned} m_{ij} = \frac{1}{3} \cdot \Bigg\{ & 1 + 2 \cdot \frac{V_O}{V_I} \cdot \cos\left(\omega_I t - 2 \cdot (j-1)\frac{\pi}{3}\right) \cdot \\ & \left[\cos\left(\omega_O t - 2 \cdot (i-1)\frac{\pi}{3}\right) - \frac{1}{6} \cdot \cos(3\omega_O t) + \frac{1}{2\sqrt{3}} \cdot \cos(3\omega_I t)\right] - \\ & - \frac{2}{3\sqrt{3}} \cdot \frac{V_O}{V_I} \cdot \left[\cos\left(4\omega_I t - 2 \cdot (j-1)\frac{\pi}{3}\right) - \cos\left(2\omega_I t - 2 \cdot (1-j)\frac{\pi}{3}\right)\right] \Bigg\} \end{aligned} \tag{2.9}$$

Due to the complexity of the duty-cycles computation, this algorithm is time consuming and requires nine commutations in the switching period. It is possible to reduce the number of sequences inside the switching period, if the three zero-vectors (*aaa*, *bbb*, *ccc*) theoretically generated separately by the Venturini method, are compressed in a single sequence and this is placed at the beginning of the switching pattern [2.11]. Due to the fact that the modulation is scalar, the switching state for each output phase is established independently, both type of vectors, rotating and active, are inherent generated. Other modulator models have been derived by employing only one type of the switching state vectors, which simplified the mathematical models, as the space vector modulation by using only active vectors [2.30]-[2.35], or by using only rotating vectors [2.36]-[2.38].

2.4.2 Modulation with rotating vectors

In this situation only rotating vectors of both, direct and inverse sequence, are used, in conjunction with zero vector, in order to vary smoothly the amplitude and the instantaneous frequency of the output voltage [2.36]-[2.38]. The situation when direct rotation vectors with zero vectors are used is shown in Fig. 2.9a, while in Fig. 2.9b inverse rotating vectors and zero vectors are used. The construction of the resulting motor flux is shown in both situations, presenting similar results. Both papers which present this modulation method have reported that is necessary to mix the two type of rotating vectors in order to gain independence for the displacement of the input current vector.

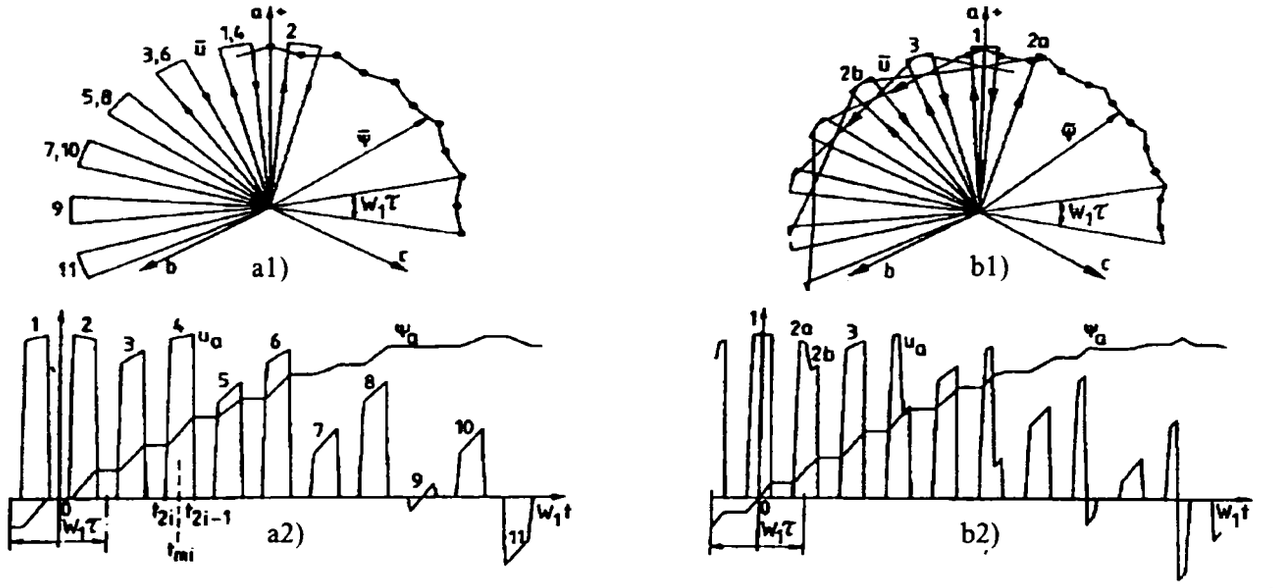

Fig. 2.9: Modulation with rotating vectors direct rotating (left side) and inverse rotating (right side); selected rotating voltage vectors (upper side) and construction of the motor flux (lower side); (reprinted from [2.37], Fig. 2 in the left side and Fig. 3 in the right side)

2.4.3 Indirect modulation

The indirect modulation model uses only active (pulsating) vectors. The main idea of the indirect modulation technique is to consider the matrix converter as a two stage transformation converter: a rectification stage to provide a constant imaginary DC-link voltage during the switching period and an inverter stage to produce the three output voltages [2.27]-[2.29]. Fig. 2.10 shows the converter model when the indirect modulation technique is used.

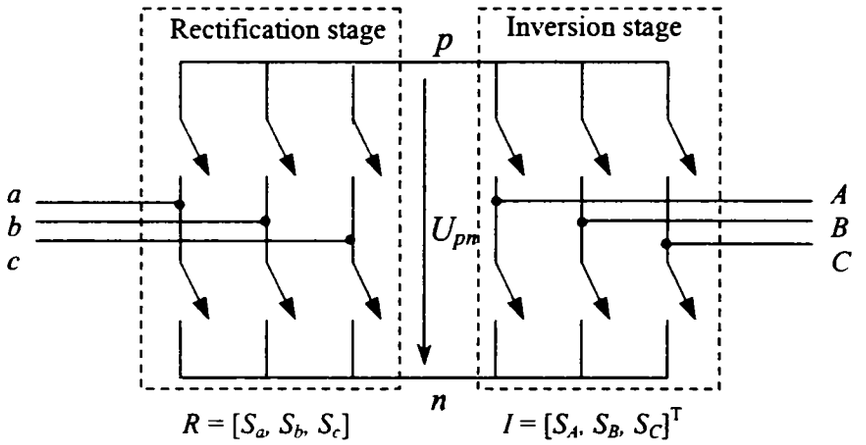

Fig. 2.10: The matrix converter model when an indirect modulation technique is used

By multiplying the rectification stage matrix R to the inversion stage matrix I, the converter transfer matrix T is obtained:

$$T = I \cdot R \tag{2.10}$$

$$\begin{bmatrix} T_{11} & T_{12} & T_{13} \\ T_{21} & T_{22} & T_{23} \\ T_{31} & T_{32} & T_{33} \end{bmatrix} = \begin{bmatrix} I_1 \\ I_2 \\ I_3 \end{bmatrix} \cdot \begin{bmatrix} R_1 & R_2 & R_3 \end{bmatrix} \tag{2.11}$$

where R_i = {-1, 0, 1} are the switch states of the rectification stage and I_j = {0, 1} are the switch states of the inversion stage.

In this way it is possible to implement known PWM strategies in both the rectifier and the inverter stage. The first implementation of the indirect modulation, reported in [2.27], is illustrated in Fig. 2.11.

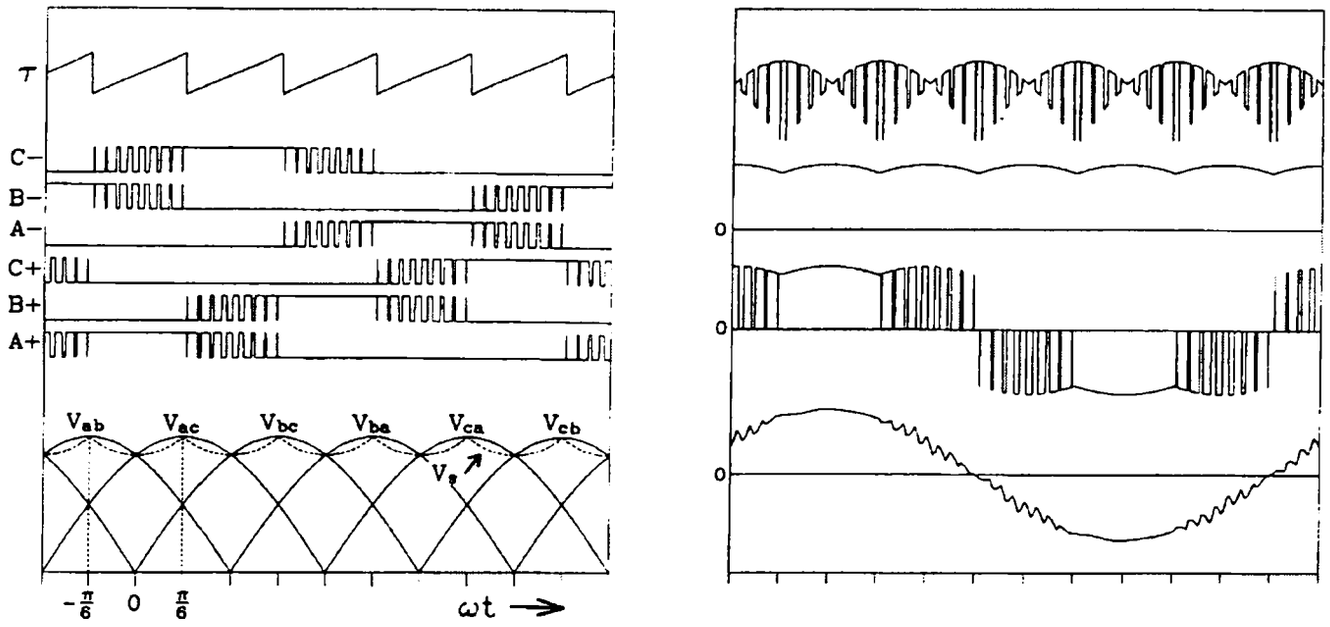

Fig. 2.11: Indirect modulation: a) modulation function; b) rectifier control function; c) source voltage derivation d) dc-link voltage; e) dc-link current; f) filtered line current; (reprinted from [2.27] Fig. 2 in the left side and Fig. 4 in the right side)

A modulation function τ (0...1) in order to combine the two line-to-line input voltages of the highest magnitude, provides virtual constant DC-link voltage and sinusoidal sharing of the virtual DC-link current in the unfiltered input currents. The command switching signals, corresponding to this virtual rectifying stage are sent to the corresponding row of matrix converter switches, while the signal for the columns are generated by a scalar PWM, according to the motor control requirements. By combining the signals for the rows and columns with AND-logic gates, the gate signals for each bi-directional switch are generated.

2.4.4 Indirect Space Vector Modulation (SVM)

A method to generate the desired PWM pattern is to use the Space Vector Modulation (SVM) technique [2.30]-[2.34]. The principle of Space Vector Modulation theory is presented in general papers about modulation, [2.39] and therefore it won't be explained here.

This technique uses a combination of the two adjacent vectors and a zero-vector to produce the reference vector. The proportion between the two adjacent vectors gives the direction and the zero-vector duty-cycle determines the magnitude of the reference vector. The input current vector I_{in} that corresponds to the rectification stage (Fig. 2.12a) and the output voltage vector U_{out} that corresponds to the inversion stage (Fig. 2.12b) are the reference vectors.

In order to implement the SVM, it is necessary to determine the position of the two reference vectors. The input reference current vector I_{in} is given by the input voltage vector in case instantaneous unitary power factor is desired, or is given by a custom strategy to compensate for

unbalanced and distorted input voltage system. The output reference voltage vector U_{out} may be produced with a classical V/Hz dependence or may be a result of a vector control scheme.

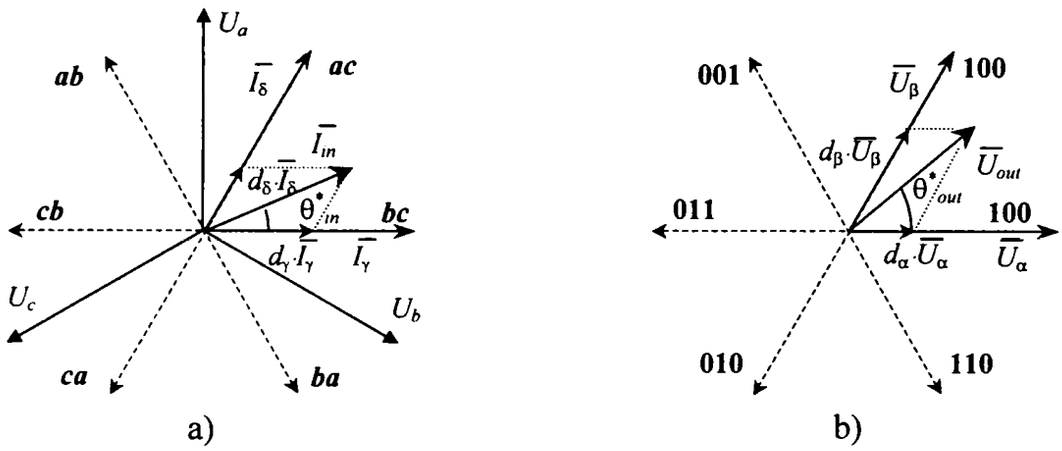

Fig. 2.12: Generation of the reference vectors using SVM

When the absolute position of the two reference vectors θ_{in} and θ_{out} are known, the relative position inside the corresponding sector θ^*_{in} and θ^*_{out}, as well as the sectors of the reference vectors are determined:

$$in\_\sec = trunc\left(\frac{\theta_{in}}{\pi/3}\right) \qquad \theta^*_{in} = \theta_{in} - \pi/3 \cdot in\_\sec \tag{2.12}$$

$$out\_\sec = trunc\left(\frac{\theta_{out}}{\pi/3}\right) \qquad \theta^*_{out} = \theta_{out} - \pi/3 \cdot out\_\sec \tag{2.13}$$

The duty-cycles of the active switching vectors are calculated for the rectification stage by using (2.14) and (2.15):

$$d_\gamma = m_I \cdot \sin\left(\frac{\pi}{3} - \theta^*_{in}\right) \tag{2.14}$$

$$d_\delta = m_I \cdot \sin\left(\theta^*_{in}\right) \tag{2.15.}$$

and for the inversion stage by using (2.16) and (2.17):

$$d_\alpha = m_U \cdot \sin\left(\frac{\pi}{3} - \theta^*_{out}\right) \tag{2.16}$$

$$d_\beta = m_U \cdot \sin\left(\theta^*_{out}\right) \tag{2.17}$$

where: m_I and m_U are the rectification and inversion stage modulation indexes, θ^*_{in} and θ^*_{out} are the angles within their respective switching hexagon of the input current and output voltage reference vectors. Usually:

$$m_I = 1 \qquad \text{and} \qquad m_U = U_{out}/U_{pn} \tag{2.18}$$

In ideal sinusoidal and balance input voltages:

$$U_{pn} = d_\gamma \cdot U_{line\text{-}\gamma} + d_\delta \cdot U_{line\text{-}\delta} = 0.86 \cdot \sqrt{2} \cdot U_{line} \tag{2.19}$$

To obtain a correct balance of the input currents and the output voltages, the modulation pattern should be a combination of all the rectification and inversion duty-cycles (αγ-αδ-βδ-βγ-0). The duty-cycle of each sequence is determined as a product of the corresponding duty-cycles:

$$d_{\alpha\gamma} = d_\alpha \cdot d_\gamma;\ d_{\alpha\delta} = d_\alpha \cdot d_\delta;\ \ d_{\beta\delta} = d_\beta \cdot d_\delta;\ \ d_{\beta\gamma} = d_\beta \cdot d_\gamma; \tag{2.20}$$

The duration of the zero-vector is calculated by:

$$d_0 = 1 - (d_{\alpha\gamma} + d_{\alpha\delta} + d_{\beta\delta} + d_{\beta\gamma}) \tag{2.21}$$

Finally, the duration of each sequence is calculated by multiplying the corresponding duty-cycle to the switching period. It is possible to optimise the switching pattern by changing the position of sequences inside the pattern, the number of switchings could be reduced in order to provide a single commutation per switch, proposed in [2.33]. The commutation pattern corresponds to a double-sided SVM, but unlike the classic SVM there is only one zero per switching period. In this way the number of commutations can be reduced from 10 to 8 and the switching loses can be reduced.

2.4.5 Optimised double-sided SVM switching pattern

This idea was proposed in [2.33] to avoid multiple switch commutations, inherently caused by combining a fixed rectifier switching sequence γ-δ-0 to produce the input current reference vector, with a fixed inversion switching pattern α-β-β-α-0 to produce the output voltage reference vector. In Fig. 2.13 is shown the result in the switching states in two situations of the input sector and the output sector. While in the first situation (*in_sec* = I, *out_sec* = I), an 8 branch-switch-over pattern is generated, in the second situation (*in_sec* = I, *out_sec* = II), the same combination of sequences generate a 10 branch-switch-over pattern. This situation occurs only when the sum of the input sector and the output sector is odd. The proposed solution was to change the switching sequence in the inversion stage in β-α-α-β-0, when this sum is odd. Also, when the input sector is even, the output zero vector must be 000, otherwise is 111. It has been showed that it is possible to implement the switching pattern in a look-up table, to provide minimised number of commutation.

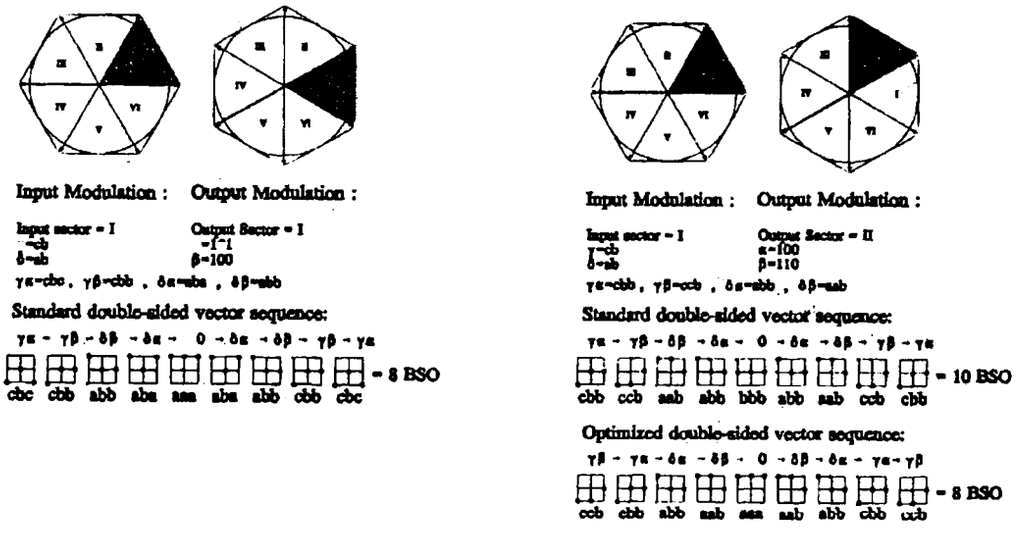

Fig. 2.13: Generation of the double-sided switching pattern in two situations showing how the reduction of the number of commutation is achieved (reprinted form [2.33], Fig. 5 in the left side and Fig. 6 in the right side)

2.5 DTC APPLIED TO A MATRIX CONVERTER FED INDUCTION MOTOR DRIVE

In [2.35] was proposed an extended application of the DTC principle to a matrix converter fed induction motor drive. Additional to the classical DTC model, based on a commutation table with two entries to select the inverter stage vector, depending on the flux and torque error signals, a new entry was added to select the rectifying stage vector: the error of the angle of the input current vector. The diagram of the estimator for the motor flux and torque and for the converter input current angle sine is presented in Fig. 2.14a. The control scheme of the matrix converter is presented in Fig. 2.14b.

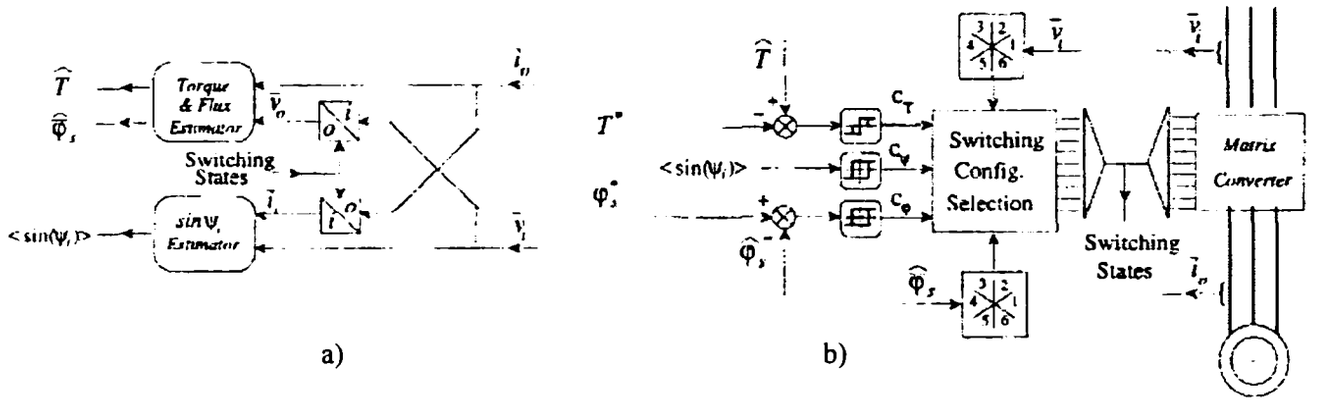

Fig. 2.14: DTC of induction motor using a matrix converter: a) Motor torque and flux estimator and displacement angle estimator; b) The control scheme; (reprinted from [2.35] Fig. 8)

The control uses the input voltages and the output currents information, as well as the matrix converter switching state, in order to reconstitute the output voltages and the input currents, due to the instantaneous power transfer characteristic. The output voltage and current are used to estimate the induction motor flux by using the voltage model and the torque. The input current is software filtered to eliminate the ripple. The input current vector is compared with the input voltage vector to establish the displacement sine angle. It may be concluded that this scheme uses indirect modulation scheme, as the displacement sine angle selects which line-to-line voltage will be chosen as a "DC-link voltage", giving the rectification stage vector. After that, the classical DTC applies, the flux and torque error selects the appropriate inversion stage vector. Combining the two vectors, the matrix converter switching state is determined.
The authors claim that this DTC scheme gives good performance in the high speed range, proven with simulations, but no investigation has been made to determine how the limit of the voltage transfer ratio is affected. Also, a control strategy to improve performance in the overmodulation range, by restricting the freedom of selecting a low line-to-line voltage, in the control of the rectification stage ($\sin(\psi_i)$ in Fig. 2.14) has to be considered.

2.6 STRATEGIES TO COMPENSATE UNBALANCED AND DISTORTED INPUT VOLTAGES

Due to the fact that the conversion uses instantaneous power transfer, the matrix converter performance is affected by unbalance and distortion of the input voltage system. In case of input voltage unbalance, the distortion of the output voltages is caused, which produces distorted output currents. Due to the backward transformation of the output currents to the input currents, distorted

input currents are produces. The overall effect is that distorted input voltage causes distorted and unbalanced input current. Therefore, research work has been directed to investigate different modulation strategies, to compensate these effects [2.33]-[2.34]. As a general remark, all these methods are effective only if the locus of the output voltage vector could be fit inside the input voltage locus. Considering the indirect modulation model, there are two possibilities to compensate the overall influence of unbalance and low-order harmonics supply for a matrix converter drive:

- by correcting the reference angle of the input current, to reduce the harmonics content in the input currents;
- by correcting the modulation index in the inversion stage, in respect to the virtual DC-link voltage, to provide constant magnitude of the output voltage vector;

In order to improve the motor side performance, it is possible to compensate the influence of unbalanced and distorted input voltages, which causes the virtual DC-link voltage to fluctuate. This method is similar to the DC-link ripple compensation in standard converters and was already presented in [2.33]. However, distortion of the input current is inherently caused.
Three strategies to modulate the input current vector reference for unbalance conditions have been reported in [2.34] in case of unbalanced supply conditions and are presented in Fig. 2.15, where * denotes the complex conjugate. In case of ideal sinusoidal and balanced supply condition, all three modulation methods give identical performance. The detection of the positive e_p and negative e_n sequence is therefore necessary. Because real supply condition implies also low-order harmonics, the compensation process becomes more complicated.

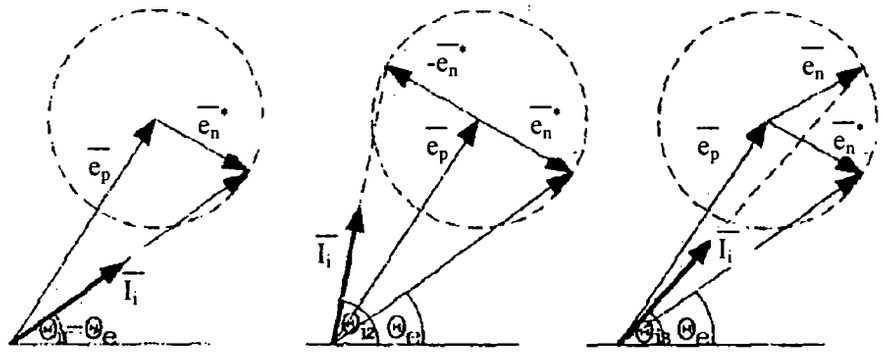

Method 1: $\theta_{i1} = arg(\overline{e_p} + \overline{e_n}^*) = \theta_e$

Method 2: $\theta_{i2} = arg(\overline{e_p} - \overline{e_n}^*)$

Method 3: $\theta_{i3} = arg(\overline{e_p} + \overline{e_n}^*)$

Fig. 2.15: Detection of the input current reference angle in unbalanced supply condition (reprinted from [2.34], Fig. 1)

First compensation method is equivalent to the instantaneous power factor and is easy to implement, but causes the highest THD, while harmonics of positive sequence are produced. The second compensation method, with no physical meaning, removes completely harmonics in the input current spectrum, but causes positive and negative sequence of the fundamental (unbalance). The third compensation method requires to rotate with constant velocity the input reference current vector, easily to implement by incrementing a counter, while the reset of the counter is synchronised with the zero crossing of input phase-to-neutral voltage on input line *a*. This causes current harmonics of both, positive and negative sequence, but with half amplitude than first compensation method.

2.7 PROTECTION ISSUES IN MATRIX CONVERTERS

Similar to standard diode bridge VSI, the matrix converter topology needs to be protected against overvoltage and overcurrent. Furthermore, due to the lack of an energy storage element in the DC-link, capable to suppress disturbances from both line and motor sides, this topology is more sensitive to disturbances and therefore more susceptible to failures. Disturbances, which may cause hardware failures, are:

- faulty inter-switch commutations, as internal short-circuit of the mains or discontinuing the circuit of the motor currents;
- shutdown of the matrix converter during an overcurrent situation, in the motor side;
- possible overvoltage on the input side caused by the converter power-up or by voltage sags;

Protection issues of matrix converters has commanded attention, in order to build a reliable prototype. A solution to solve some of the problems consists of connecting a clamp circuit on the output side [2.27], [2.40], one patent being issued for the necessity of clamping the output lines [2.28], [2.29]. The clamp circuit consists of a B6 fast recovery diodes rectifier and a capacitor to store the energy accumulated in the leakage inductance of the load, caused by the output currents. The worst case regarding the energy level stored in the leakage inductance occurs when the output current reaches the overcurent protection level, causing a converter shutdown. The design of the clamp capacitor to provide safe-shutdown during an overcurrent situation will be presented in Chapter 3, where implementation details of the laboratory prototype will be presented.
The protection method presented before requires extra semiconductor devices (6 pcs), with similar ratings as the power devices in the main circuit, and a capacitor, which has a similar level of reactive energy, as the input filter. An interesting method to clamp the reactive energy of the inductive load without the need of a clamp circuit, was proposed in [2.25], and experimentally proven in [2.41]. This uses the voltage on the input lines to clamp the energy from the output side. This is performed by creating an unidirectional freewheeling path for the motor currents, depending on the potential on the input lines, forcing the currents to decrease fast to zero and not being able to reverse direction. Therefore, there is no need for reactive elements which are not normally used, but extra-circuits have to be employed in the commutation control. During the clamping operation, the negative potential of the mains becomes negative pole of the clamp capacitor, while the input line with the positive potential becomes the positive pole of the clamp capacitor. It is necessary to use information of output currents magnitude to detect the faulty situation, output current signs to control the bi-directional switch commutation and the freewheeling operation, and information of the input voltages sign and magnitude to establish the input phase used control the freewheeling operation. An another disadvantage, which has not been pointed out, was that the inductance of the input filter slows down the process, and in case the capacitance is not sufficient, dangerous overvoltages could appear. Also, in case of momentary power interruptions or accidental short-circuit of the input lines, the freewheeling operation cause higher currents, which may destroy the converter.

SUMMARY

Since 1980, when the first mathematical model to provide sine wave in – sine wave out operation of the matrix converter was proposed, starting the research in a new area of power electronics, many advances of this technology towards industrial implementation has been added, as:

- building of few prototypes, which have experimentally proved the high-performance operation of this single stage converter topology, as sinusoidal input current and bi-directional power flow, but also pointed out of a few implementation problems;
- identifying and proposing protection circuits for matrix converters;
- proposing criterions to design the reactive elements of the input filter;
- developing new switch commutation techniques to provide semi-soft commutation;
- developing switches with reverse blocking capability, to reduce the number of semiconductor devices and the conduction losses of the matrix converter;
- developing integrated power modules with bi-directional switches for matrix converters;
- developing new modulation strategies which simplified the mathematical model and improved the performance;
- developing control strategies to compensate for unbalanced and distorted input voltage conditions;
- implementation of smart control strategies for induction motors;

However, other aspects remained unresolved as:

- the lack of applications well suited for the matrix converter topology, which may accelerate the industrial implementation;
- the lack of ride-through capability, characteristic for direct frequency converters;
- the direct power-up is critical, as an LC filter is employed between grid and the power devices;
- the development of a true prototype of a matrix converter drive for realistic evaluation in industry applications, with all necessary circuits built-in;

For some of these unresolved aspects, solutions will be proposed in the following chapters of this thesis.

REFERENCES

[2.1] T.A. Lipo, "*Recent progress in the development in solid-state AC motor drives*", IEEE Trans. on Power Electronics, vol. 32, pp. 105 –117, 1988.

[2.2] B.K. Bose, "*Power Electronics – A technology review*", Proc. of IEEE, vol. 80, no. 8, pp. 1303-1334, 1992.

[2.3] R. Kerkman, G.L. Skibinski, D.W. Schengel, "*AC drives: Year 2000 (Y2K) and beyond*", Proc. of APEC'99, vol. 1, pp. 28-39, 1999.

[2.4] P. Thoegersen, F. Blaabjerg, "*Adjustable speed drives in the next decade. The next step in industry and academia*", Proc. of PCIM'00, Intelligent motion, pp.95-104, 2000.

[2.5] R.D. Lorentz, "*The future of electric drives: where are we headed?*", Proc. of PEVD'00, pp. 1-6, 2000.

[2.6] K. Phillips, "*Power Electronics: Will our current technical vision take us to the next level of AC drive product performance?*", Proc. of IAS Annual Meeting, Plenary session.1, CD-ROM version, 2000.

[2.7] S. Bernet, T. Matsuo, T.A. Lipo, "*A matrix converter using reverse blocking NPN-IGBT's and optimized pulse patterns*", Proc. of PESC'96, vol. 1, pp. 107-113, 1996.

[2.8] H-H. P. Li, "*Bidirectional lateral insulated gate bipolar transistor having increased voltage blocking capability*", US Patent (1997) 5977569, 1999.

[2.9] IXYS, "IXRH 50N60, IXRH 50N120: *High voltage RBIGBT. Forward and reverse blocking IGBT*", Advanced technical information, http://www.ixys.net/l400.pdf, 2000.

[2.10] P. Nielsen, "*The matrix converter for an induction motor drive*", Industrial Ph.D. Fellowship EF 493, ISBN 87-89179-14-5, Aalborg University, Denmark, August 1996.

[2.11] L. Zhang, C. Watthanasarn, W. Shepherd, "*Analysis and comparison of control techniques for AC-AC matrix converters*", IEE Proc.-Electr. Power App., vol. 145, no. 4, pp. 284-294, 1998.

[2.12] S. Sunter, H. Altun, "*A method for calculating semiconductor losses in the matrix converter*", Proc. of MELECON'98, vol. 2, pp. 1260 –1264, 1998.

[2.13] N. Burany, "*Safe control of 4quadrant switches*", Proc. of IAS Annual Meeting, vol. 2, pp. 1190-1194, 1989.

[2.14] J.H. Youm, B.-H. Kwon, "*Switching technique for current-controlled AC-to-AC converters*", IEEE Trans. on Industrial Electronics, vol. 46, no. 2, pp. 309-318, 1999.

[2.15] A. Christensson, "*Switch-effective modulation strategy for matrix converters*", Proc. of EPE'97, pp. 4.193-4.198, 1997.

[2.16] J. Chang, "*Adaptive overlapping commutation control of modular AC-AC converter and integration with device module of multiple AC-AC switches*", US Patent (1997) 5892677, 1999.

[2.17] L. Empringham, P. Wheeler, J.C. Clare, "*Intelligent commutation of matrix converter bi-directional switch cells using novel gate drive techniques*", Proc. of PESC'98, pp. 707-713.

[2.18] M. Ziegler, W. Hofmann, "*Semi natural two steps commutation strategy for matrix converters*", Proc. of PESC'98, pp. 727-731, 1998.

[2.19] K.G. Kerris, P.W. Wheeler, F. Clare, L. Empringham, "*Implementation of a matrix converter using P-channel MOS-controlled thyristors*", Proc. of PEVD'00, pp. 35-39, 2000.

[2.20] M. Venturini, "*A new sine wave in, sine wave out conversion technique eliminates reactive elements*", Proc. of Powercon7, E3_1-E3-15, 1980.

[2.21] M. Venturini, A. Alesina, "*The generalised transformer: a new bi-directional sinusoidal waveform frequency converter with continuously adjustable input power factor*", Proc. of PESC'80, pp. 242-252, 1980.

[2.22] M. Venturini, A. Alesina, "*Analysis and design of optimum-amplitude nine-switch direct AC-AC converters*", IEEE Trans. on Power Electronics, vol. 4, no. 1, pp 101-112, 1989.

[2.23] D.G. Holmes, T.A. Lipo, "*Implementation of a controlled rectifier using AC-AC matrix converter theory*", Proceed. of PESC'89, pp. 353-359, 1989.

[2.24] G. Roy, G.E. April, "*Cycloconverter operation under a new scalar control algorithm*", Proc. of PESC'89, vol. 1, pp. 368-375, 1989.

[2.25] R. R. Beasant, W.C. Beattie, A. Refsum, "*An approach to realisation of a high-power Venturini converter*", Proc. of PESC'90, pp. 291-297, 1990.

[2.26] P.W. Wheeler, D.A. Grant, "*A low loss matrix converter for AC variable-speed drives*", Proc. of EPE'93, pp. 27-32, 1993.

[2.27] C.L. Neft, C.D. Shauder, "*Theory and design of a 30-hp matrix converter*", IEEE Trans. on Industrial Applications, vol. 28, No. 3, pp. 546-551, 1992.

[2.28] C.L. Neft, "*AC power supplied static switching apparatus having energy recovery capability*", US Patent (1996) 4697230, 1987.

[2.29] C.D. Schauder, "*Matrix converter circuit and commutation method*", US Patent (1994) 5594636, 1997.

[2.30] L. Huber, D. Borojevic, "*Space vector modulator forced commutated cyclo-converters*", Proc. of PESC'89, pp. 871-8761, 1989.

[2.31] L. Huber, D. Borojevic, "*Space vector modulated three-phase to three-phase matrix converter with input power factor correction*", IEEE Trans. on Industry Applications, vol. 31, no. 6, pp. 1234-1245, 1995.

[2.32] E.P. Wiechmann, J.R. Espinoza, L.D. Salazar, J.R. Rodriguez, "*A direct frequency converter controlled by space vectors*", Proceedings of PESC'93, pp. 314-317, 1993

[2.33] P. Nielsen, F. Blaabjerg, J.K. Pedersen, "*Space vector modulated matrix converter with minimized number of switchings and feedforward compensation of input voltage unbalance*", Proc. of PEDES'96, vol.2, pp. 833-839, 1996.

[2.34] P. Nielsen, D. Casadei, G. Serra, A. Tani, "*Evaluation of the input current quality by three different modulation strategies for SVM controlled matrix converters with input voltage unbalance*", Proc. of PEDES'96, vol. 2, pp. 794 –800, 1996.

[2.35] D. Casadei, G. Serra, A. Tani, "*The use of matrix converter in direct torque control of induction machines*", Proc.. of IECON'98, pp. 744-749, 1998.

[2.36] S. Halasz, I. Schmidt, T. Molnar, "*Matrix converter for induction motor drive*", Proc. of EPE'95, vol. 2, pp. 2-664-2.669, 1995.

[2.37] S. Halasz, I. Schmidt, T. Molnar, "*Induction motor drive with matrix converter*", Proc. of PEDS'95, vol. 1, pp. 104-109, 1995.

[2.38] M. Milanovic, B. Dobaj, "*A novel unity power factor correction principle in direct AC to AC matrix converters*", Proc. of PESC'98, pp. 746-752, 1998.

[2.39] J. Holtz, "*Pulsewidth modulation for electronic power conversion*", IEEE Trans. on Industry Applications, vol. 82, no. 8, pp. 1194-1214, 1994.

[2.40] P. Nielsen, F. Blaabjerg, J.K. Pedersen, "*Novel solution for protection of matrix converter to three phase induction machine*", Proc. of IAS Annual Meeting, vol. 2, pp. 1447-1454, 1997.

[2.41] A. Schuster, "*A matrix converter without reactive clamp elements for an induction motor drive system*" Proc. of PESC'98, pp. 714-720, 1998.

Chapter 3

Matrix Converter Prototype: Design and Implementation

This chapter presents implementation details of a matrix converter prototype built for laboratory test purpose. The design of the power stage was first proposed and built as a part of an industrial PhD Thesis at Aalborg University, in 1996 [3.1]. Now, improvements have been added to enhance the prototype performance by increasing the computational capability of the control system, by integrating the commutation control unit in a single PLD chip and by investigating the real requirements of the passive components, to be able to minimize the drive cost and volume. This prototype will be used to perform the experiments presented in Chapter 4, 5 and 6 [3.2]-[3.7]. Furthermore, this prototype is used to validate several solutions for developing another compact and high performance integrated motor drive prototype, which will be presented in Chapter 8: the Matrix Converter Motor [3.8].

3.1 THE POWER STAGE OF THE LABORATORY PROTOTYPE

It was already presented in the previous chapter that the matrix of bi-directional switches needs a few reactive elements in order to run properly. An input filter, which consists of an L-C low pass filter (second order), is employed in the front side to reduce the high frequency ripple from the input current. A clamp circuit, which consists of a capacitor and B6 diode bridges connected to the input and output lines of the converter, is required to protect against overvoltages in both sides. The topology of a practical matrix converter drive is shown in Fig. 3.1.

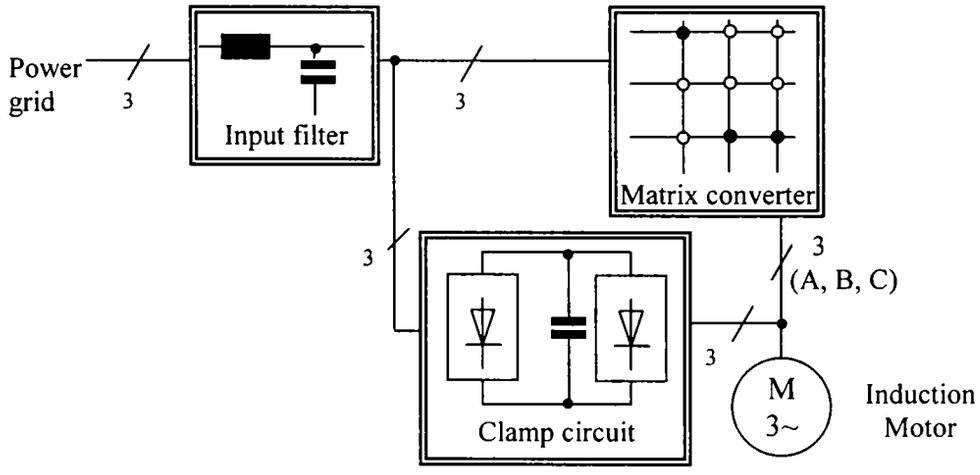

Fig. 3.1: Block scheme of the matrix converter prototype

In order to achieve high performance and reliability when building a matrix converter prototype, a few aspects have to be taken into account. The power stage has to provide safe operation of the prototype, especially in possible faulty situations as: shutdown of the converter due to an overcurrent situation on the motor side, loosing the gate signal for one of the IGBT's or noise on the command signals. The stray inductance caused by connections between the power switches

has to be minimised, in order to keep overvoltages caused by commutation low. Therefore, integration of bi-directional switches in power modules is the necessary step towards increasing the reliability of the matrix converter and also to make a real evaluation of this solution for industry applications.
The control of bi-directional switch commutation has to be reliable and independent from the processor system, preferable implemented with programmable logic devices (PLD). For the motor and the line-side control, a powerful DSP board should be used, to allow for high computational capability, expanding the test possibilities for the drive system, providing a wide range for varying the switching frequency or implementing advanced motor-side or line-side control strategies.

3.1.1 Technical specification for the power module with bi-directional switches

In the previous chapter it has been show that an important drawback of building a matrix converter prototype is the lack of power semiconductor bi-directional switches, eventually integrated in power modules, to provide lower leakage inductance on the main current path. When such devices are developed in a reduced number for research purpose, these are more expensive than regular devices at equivalent ratings, which means that it is very expensive to start building custom designed devices for a wide power range. Therefore, when the research is started in a new application field, a realistic target for power of the prototype should be defined, which would make the results representative. In this case it has been decided to build a type of three-phase to one-phase power modules with bi-directional switches based on 1200V/25A IGBT's. Details about the first generation of power modules designed for use in matrix converter applications are presented in Fig. 3.2.

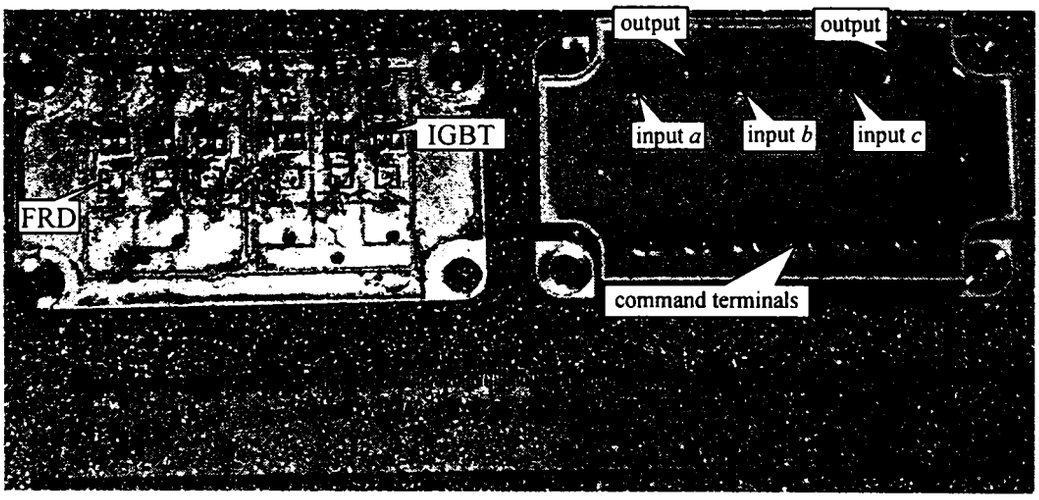

Fig. 3.2: 1200 V/25 A three-phase-to-one-phase power module for matrix converters: (left side: internal structure; right side: power module case)

Because the overcurrent protection level is usually established at 80% of the rated IGBT current, a maximum current of 20 A will result for this prototype. The input voltage of the prototype is rated at 400 V, according to the 1200 V IGBT's class. Therefore, the installed power of the prototype may be calculated, considering the maximum (theoretical) voltage transfer ratio of 0.86, as follows:

$$S = \sqrt{3} \cdot m_{U\max} \cdot U_{line} \cdot \frac{I_{\lim}}{\sqrt{2}} = 8.48 \text{ kVA} \qquad (3.1)$$

In order to determine the mechanical power of an induction motor, suitable to be loaded at full power using this prototype, typical values for the efficiency ($\eta_N \cong 0.8$) and for the displacement power factor ($\cos \varphi_N \cong 0.8$) of a motor in this power range must be taken into account. A coefficient to save a margin from the output current capability of the converter for dynamic operation ($k_d = 0.8$) must be taken into account, as well:

$$P_N = S_{inv} \cdot \eta_N \cdot \cos\varphi_N \cdot k_d = 4.34 \text{ kW} \tag{3.2}$$

Considering the closest standard power level to the previous value, it is concluded that the laboratory prototype is suitable for driving a 4 kW induction motor.

3.1.2 The input filter

The cut-off frequency ω_0 of the second order L-C filter is chosen to give a certain attenuation of the current ripple, at the switching frequency. Then dependence between the input filter elements C_{in}, L_{in} is given by:

$$L_{in} \cdot C_{in} = \frac{1}{\omega_0^2} \tag{3.3}$$

Choosing a higher capacitance in the filter will smooth the ripple in the choke current, with effect in reducing the ripple in the input voltage, but at low level of active power drawn from the mains the displacement power factor becomes unsatisfactory. On the contrary, at high level of active power, the inductance value should not increase the voltage drop at the fundamental frequency:

$$\frac{\Delta U}{U_n} = 1 - \sqrt{1 - (\omega_n \cdot L_{in})^2 \cdot \left(\frac{I_n}{U_n}\right)^2} = 1 - \sqrt{1 - l_{in}^2} \tag{3.4}$$

where $\omega_n = 2 \cdot \pi \cdot f_{in}$ is the fundamental input frequency, I_n and U_n are the rated input phase current and voltage, L_{in} is the filter inductance and l_{in} is the inductance in p.u.

A methodology to design the input filter was proposed in [3.1], [3.9], which limits the reactive component of the current generated by the capacitors in the input filter at a certain level of the output power. It was proposed a minimum displacement factor of $\cos \varphi_{min} \cong 0.9$ (cap) to be achieved at 10 % active power transferred through the filter. Considering the three line chokes are sized for the nominal current I_n and three star-connected capacitors are sized for the nominal input phase voltage U_n, a relation between the reactive power installed in the input filter components for one phase is determined, as follows:

$$S_L = \omega_n \cdot L_{in} \cdot I_n^2 \text{ (choke)} \qquad S_C = \omega_n \cdot C_{in} \cdot U_n^2 \text{ (capacitor)} \tag{3.5}$$

$$\frac{S_L}{S_C} = \frac{1}{\left(3 \cdot \omega_0 \cdot U_n^2\right)^2} \cdot \left(\frac{P_n}{C_{in}}\right)^2 \tag{3.6}$$

$$\text{where } P_n = 3 \cdot U_n \cdot I_n \text{ and } \omega_0 = 2 \cdot \pi \cdot f_0 = (L_{in} \cdot C_{in})^{-1/2} \tag{3.7}$$

Also, in case the value of the input filter capacitors is given from a restrictive design criteria, as a minimum displacement factor ($\cos \varphi_{min}$) corresponding to a minimum active power ($k_{min} \cdot P_n$):

$$\frac{C_{in}}{P_n} = k_{\min} \cdot tg\varphi_{\min-in} \frac{1}{3 \cdot \omega_n \cdot U_n^2} \tag{3.8}$$

$$\frac{S_L}{S_C} = \frac{f_n}{f_0} \cdot \frac{1}{k_{\min} \cdot \eta_{mot} \cdot tg\varphi_{\min-in}} \tag{3.9}$$

In Appendix 3.1 the characteristics of the input filter are presented. To evaluate (3.9) for the laboratory prototype, the following values were used: $k_{min} = 0.1$; $\cos \varphi_{min\text{-}in} = 0.877$; $f_n = 50$ Hz, $f_0 = 1876$ Hz; $\eta_{mot} = 0.8$. This gives:

$$S_L/S_C = 0.608 \tag{3.10}$$

More important is that considering the specific weight density (VAr/kg) or volume density (VAr/m^3) for the choke and the film capacitors, an optimisation design loop of the input filter mass or volume may be done to minimise the size in an industrial converter. For this prototype, by considering the data of the choke and the capacitors from [3.14]:

$$(L/C)_{weight} = 6.9 \quad \text{and} \quad (L/C)_{volume} = 1.7 \tag{3.11}$$

Even though the installed power is higher in the capacitors, both, weight and volume is higher for the filter choke, because of higher specific density of the capacitors.

The value of the input filter capacitors 3x6 μF/250 V_{ac}, X2 class, star connected. Due to the fact that the matrix converter acts as a current source inverter in the input side, it is necessary to decouple the input line inductance. Therefore, the capacitors in the input filter are mounted as close as possible to each power module input. The solution is to split the 6 μF capacitance in three groups of 2 μF per each phase, to decouple the lines at each power module input. In order to decrease the stray inductance of the power bus, a two-layers PCB was used. The physical design is shown in Fig. 3.3.

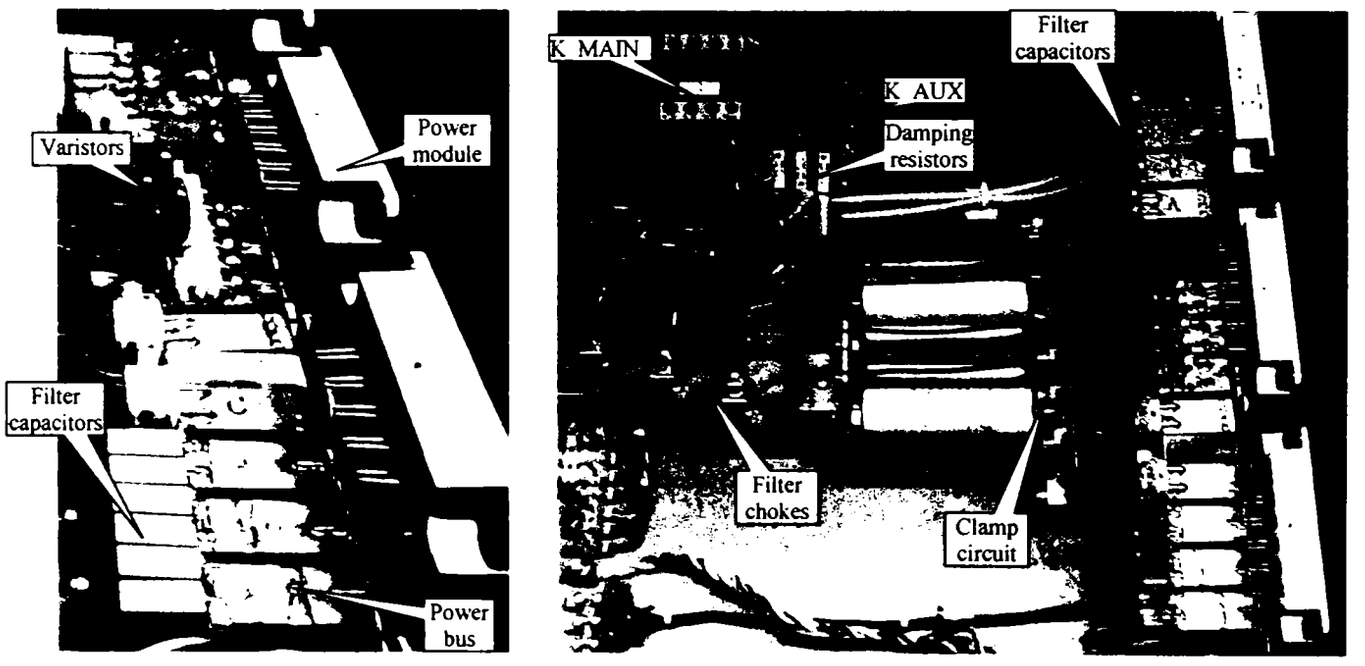

Fig. 3.3: Power stage of the laboratory prototype - physical design
(left side: decoupling of the power terminals; right side: overview of the power stage)

3.1.3 The clamp circuit

This circuit has to protect against overvoltage, when the matrix converter is turned off due to an overcurrent fault [3.1], [3.10], [3.11]. Transferring safely the energy from the leakage inductance in the clamp capacitor gives the design criteria for choosing the value of the capacitance:

$$\frac{3}{4}\cdot i_{\max}{}^{2}\cdot\left(L_{\delta S}+L_{\delta R}\right)=\frac{1}{2}\cdot C_{clamp}\cdot\left(U_{\max}{}^{2}-565^{2}\right) \tag{3.12}$$

where i_{max} is the current level which triggers the overcurrent protection, $L_{\delta S}$+$L_{\delta R}$ is the overall leakage inductance of the induction motor, C_{clamp} is the value of the clamp capacitor and U_{max} is the maximum allowable overvoltage.

An analysis of the phenomenon that takes place when the matrix converter, which is feeding an induction motor, is shutdown may reveal the real requirements for the clamp circuit components: the fast recovery diodes and the capacitor. This has never been shown, and the general perception is that expensive components are required, as snubber type capacitors with high du/dt.

During the clamping mode, the matrix converter is shutdown. Therefore, the equivalent circuit includes the leakage inductance of the induction motor, the clamp diodes and the clamp capacitor. The leakage inductance and the clamp capacitor create an L-C oscillating circuit. Initial conditions for the transients are:

- the initial voltage in the capacitor is the peak value of the line-to-line input voltage;
- the initial current in the leakage inductance is the overcurrent limit of the converter;

The oscillatory mode starts in these initial conditions and ends when the motor currents decrease to zero, because the clamp diodes do not allow the current to reverse direction. When all motor currents reach zero, all the energy from the leakage inductance has been transferred into the clamp capacitor. It is possible to simulate the transient by using the R-L-C circuit theory, but is necessary to transform the clamp capacitor in three-phase star-connected capacitors, as shown in Fig. 3.4.

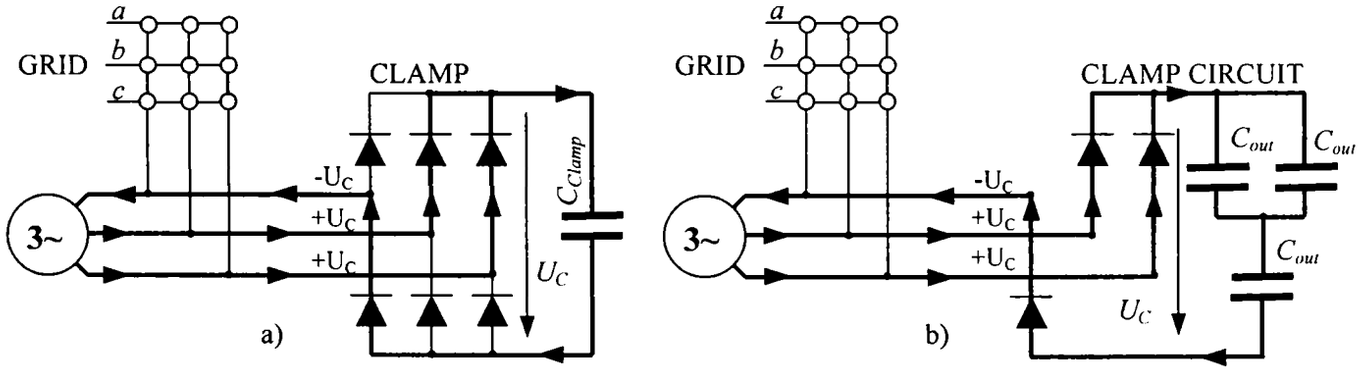

Fig. 3.4: Freewheeling of motor currents during a converter shutdown: a) scheme with clamp circuit; b) equivalent scheme with capacitors on each phase;

When the clamp circuit is taking over the motor current conduction, two lines of the load with the same current sign are connected together through the clamp diodes, as presented in Fig. 3.4a. Therefore, an equivalent scheme with capacitors star connected may be draw, as shown in Fig. 3.4b, in order to reduce the three-phase circuit to a single-phase circuit. The equivalent capacitance per motor phase C_{out} is given for identical value of capacitance in the clamp circuit:

$$C_{out} = 1.5\ C_{clamp} \tag{3.13}$$

The resonance (cut-off) frequency of each phase L-C circuit becomes:

$$f_{out} = \frac{1}{2\pi\sqrt{1.5 \cdot C_{clamp} \cdot (L_{\sigma S} + L_{\sigma R})}} \tag{3.14}$$

Considering C_{clamp} = 10 μF and $L_{s,r}$ = 12 mH (typical for a 4kW motor), results f_{out} = 460 Hz. The capacitor stress to voltage variation may be determined:

$$\begin{aligned}(dU/dt)_{\max} &= \left.\frac{d(\sqrt{2}U_f \sin(2\cdot\pi\cdot f_{out}\cdot t))}{dt}\right|_{t=0} \\ &= 2\sqrt{2}\cdot U_f \cdot \pi \cdot f_{out} \cdot \left.\frac{d(\sin(2\cdot\pi\cdot f_{out}\cdot t))}{d(2\cdot\pi\cdot f_{out}\cdot t)}\right|_{t=0} = 8.86\cdot U_f \cdot f_{out}\end{aligned} \tag{3.15}$$

For parameters considered in the example, with U_f = 220 V, and f_{out} = 460 Hz, results du/dt = 0.9 V/μs, which is low, resulting that no special requirement for the capacitor type is needed. However, the capacitor has to be able to handle the peak value of the faulty current and to provide a low ESR and a low inductance. The stray inductance and the resistance of clamp circuit have to be low in order to provide fast transfer of the faulty current from the matrix converter switches to the clamp diodes and capacitor, without producing dangerous overvoltages. According to these recommendations, the specification for the clamp circuit elements is given:

Diodes:

- fast recovery type;
- $V_{RRM} \geq U_{max}$ (1000 V); $I_{F(RMS)} \geq I_{lim}$ ($20A_{peak}$);

Clamp capacitor:

- type: non-electrolytic type, preferred metallized polypropylene capacitor;
- $I_{max} \geq I_{lim}$; dU/dt ≥ 10 V/μs;

In Appendix 3.2 the characteristics of the clamp circuit are presented.

3.2 THE AUXILIARY CIRCUITS OF THE LABORATORY PROTOTYPE

This category contains the safe power-up circuit, the current transducer unit, with overcurrent and sign detection features, and the bi-directional switch commutation control unit.

3.2.1 The Safe Power-up Circuit

The purpose of this circuit is to provide a fast and safe direct-on-line power-up of the prototype, by eliminating the transients with higher overvoltage levels, characteristic for L-C series circuits. The principle of eliminating the overvoltage during power-up will be presented in Chapter 4.

The diagram scheme of the *Safe Power-up Circuit* is presented in Fig. 3.5. The auxiliary contactor $K\__{AUX}$ introduces in the circuit, first the damping resistors $R\__1$, $R\__2$, $R\__3$, when the *ON* button is pressed. The main contactor $K\__{MAIN}$ is energised by the auxiliary contactor and bypasses the damping resistors. Therefore, it has to be able to handle continuously the converter current. The delay between the two contactors depends on the mechanical inertia, and in this case was of about 10 ms, enough that no transient occurs. By feeding the transformers T_1...T_6 for the IGBT gate-driver power supplies from the same supply as the two contactor coils, the power-up procedure takes place only if the gate drivers are already fed, which ensures that no hazardous command signals may damage the power switches.

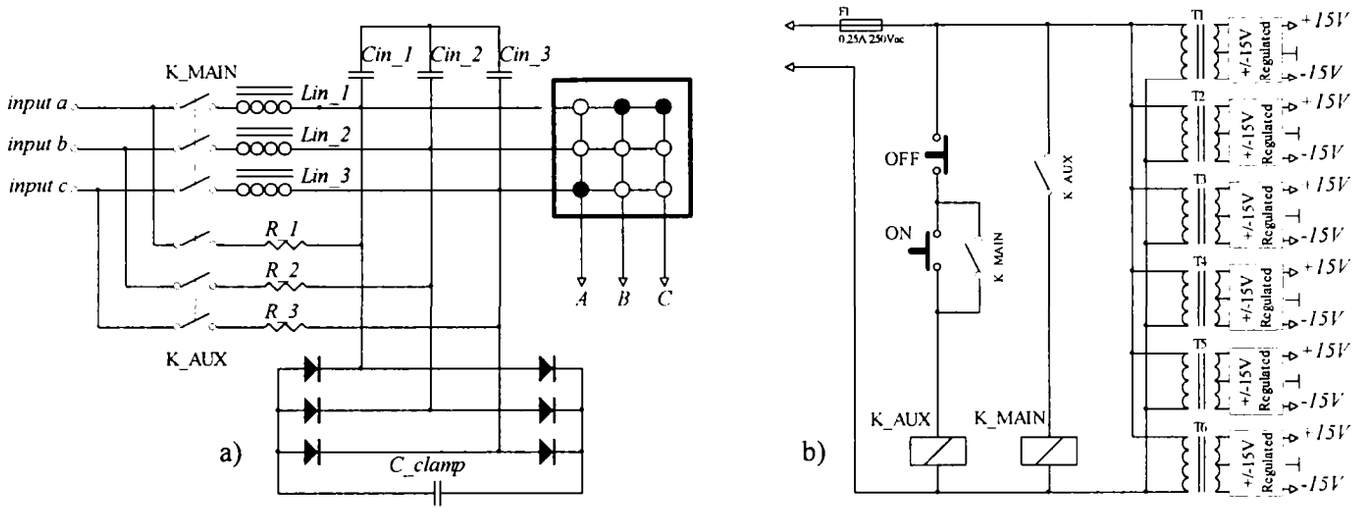

Fig. 3.5: Safe power-up circuit for the matrix converter prototype: a) diagram of the power stage; b) diagram of the control circuits;

3.2.2 The Current Transducer Unit

The current detection is based on Hall transducers, on each of the matrix converter output lines, providing quick response and the necessary safety insulation from the motor circuits. The scheme diagram of the current transducer unit is shown in Fig. 3.6.

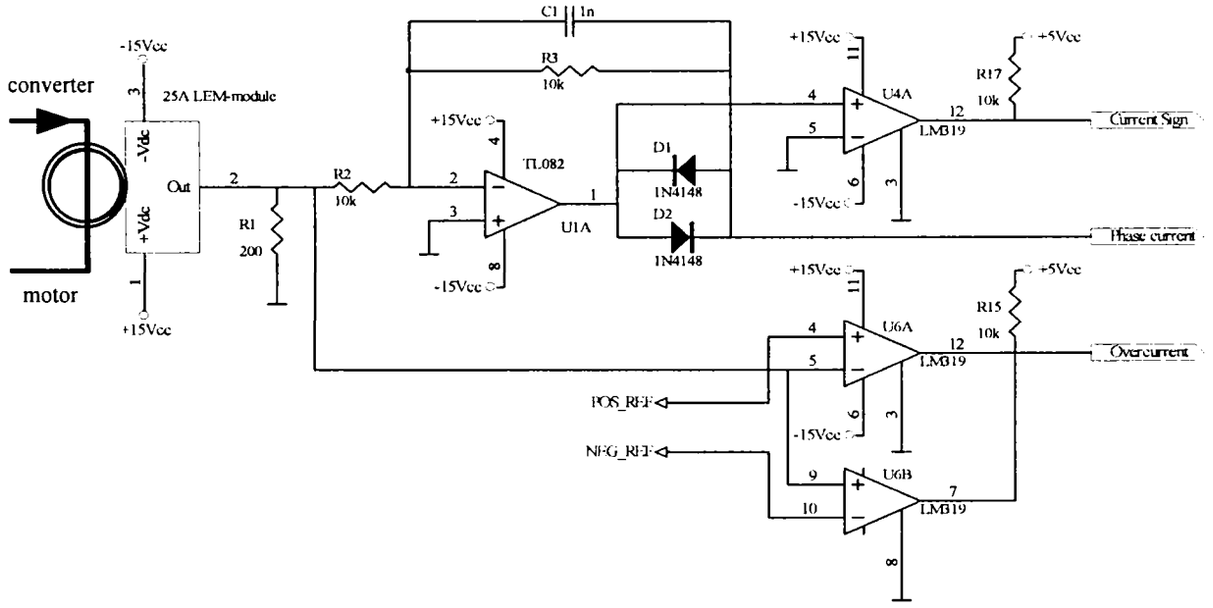

Fig. 3.6: The scheme diagram of the current transducer unit

The current transducer (LA25-NP) [3.16] has a rated current of 25 Amps, while at the output produces a 25 mA current, which gives a scale of k_{transd} = 1 A/mA. It requires a regulated differential supply of ± 15V_{dc}, and a recommended load resistance of 200 Ω. Therefore, the scale of the transducer is modified to 5 A/V. This signal feeds directly the overcurrent detector, which uses two high-speed comparators (LM319) in a configuration for window detection. The two voltage references "*POS_REF*" and "*NEG_REF*" are tuned in such a way that a signal produced

by the current transducer, with magnitude above the hardware protection level, which is set at 20 Amps, will force the "Overcurrent" signal to toggle in "LOW" state.

$$REF = \frac{I_{\lim}}{k_{transd}} \cdot R_{load} = \frac{20A}{25A/25mA} \cdot 200\Omega = 4\ \text{V} \tag{3.16}$$

As the comparators have an open collector output stage, all three overcurrent signals may be summed, to produce a single "*Overcurrent*" signal. This goes into the commutation control unit where is memorised, disabling the gate signals for the IGBT's.
The same signal from the current transducer feeds an operational amplifier (TL082) configured as a low-pass filter with unitary gain, which removes the high frequency noise (>20 kHz), producing a signal for ordinary measurement purpose. In the output side, two anti-paralleled diodes (1N4148) are connected in order to magnify the zero crossing of the output current signal. The feedback loop closes after the diodes group, so the signal "*Phase current*" follows the motor current shape with good precision and provide a scale of ±25 A/±5 V, for the AD converters. The signal, which is magnifies at zero-crossings, feeds a comparator (LM319) that produces the signal "*Current_sign*". This signal is used to control the four-step commutation, in the *Commutation Control Unit*.

3.2.3 The bi-directional switches Commutation Control Unit

The bi-directional switch commutation strategy implemented in this matrix converter prototype uses a four-step commutation proposed in [3.12]. The implementation of the four-step commutation strategy was proposed in [3.1]. The commutation logic for a bi-directional switch is implemented in a cell, which uses logic circuits, D flip-flops and logic gates (AND, OR). This cell has four input signals: control (*CTRL*), clock (*CLK*), current sign (*CRT_SIGN*) and error (*ERROR*). The clock signal has a frequency of 2.5 MHz, giving a timing of 400 ns for each commutation step. The first commutation step is executed instantly, by turning off the non-conducting outgoing switch, while the other three steps are delayed with the constant clock resolution of 400 ns. All the commutation control cells for a 3-phase-to-3-phase matrix converter has been integrated in a single complex PLD chip (type XC95108) [3.17]. The interconnection scheme for programming the PLD chip was developed using specific software (Xilinx Foundation Series©) developed by the manufacturer (XILINX). The scheme diagram is presented in Fig. 3.7.
The bi-directional switch commutation cell, which is the core of the Commutation Control Unit, was implemented in a macro named *MATRIX*, and all the scheme is built around nine of these macro-cells. In order to minimise the number of inputs, but also to avoid the risk of receiving a faulty command from the microcontroller due to noise or malfunction, the switching state was 2-bit/4 states coded. Three decoders, using logic gates are necessary to decode the command signal for each bi-directional switch, but in the Fig. 3.7, only one decoder was shown, for simplicity.
Distinct inputs in the PLD are: the clock-signal (*Clock*), the signs of the output currents (*sign_I_A*, *sign_I_B*, *sign_I_C*), the switching states 2-bit encoded (*cmd_A0*, *cmd_A1*, *cmd_B0*, *cmd_B1*, *cmd_C0*, *cmd_C1*), the fault signal (*Fault*), produced as a result of an overcurrent situation, memorised by the logic control. The outputs are only the command signals for the gate drivers (a_p, a_n, b_p, b_n, c_p, c_n), for each output phase groups (A, B, C).

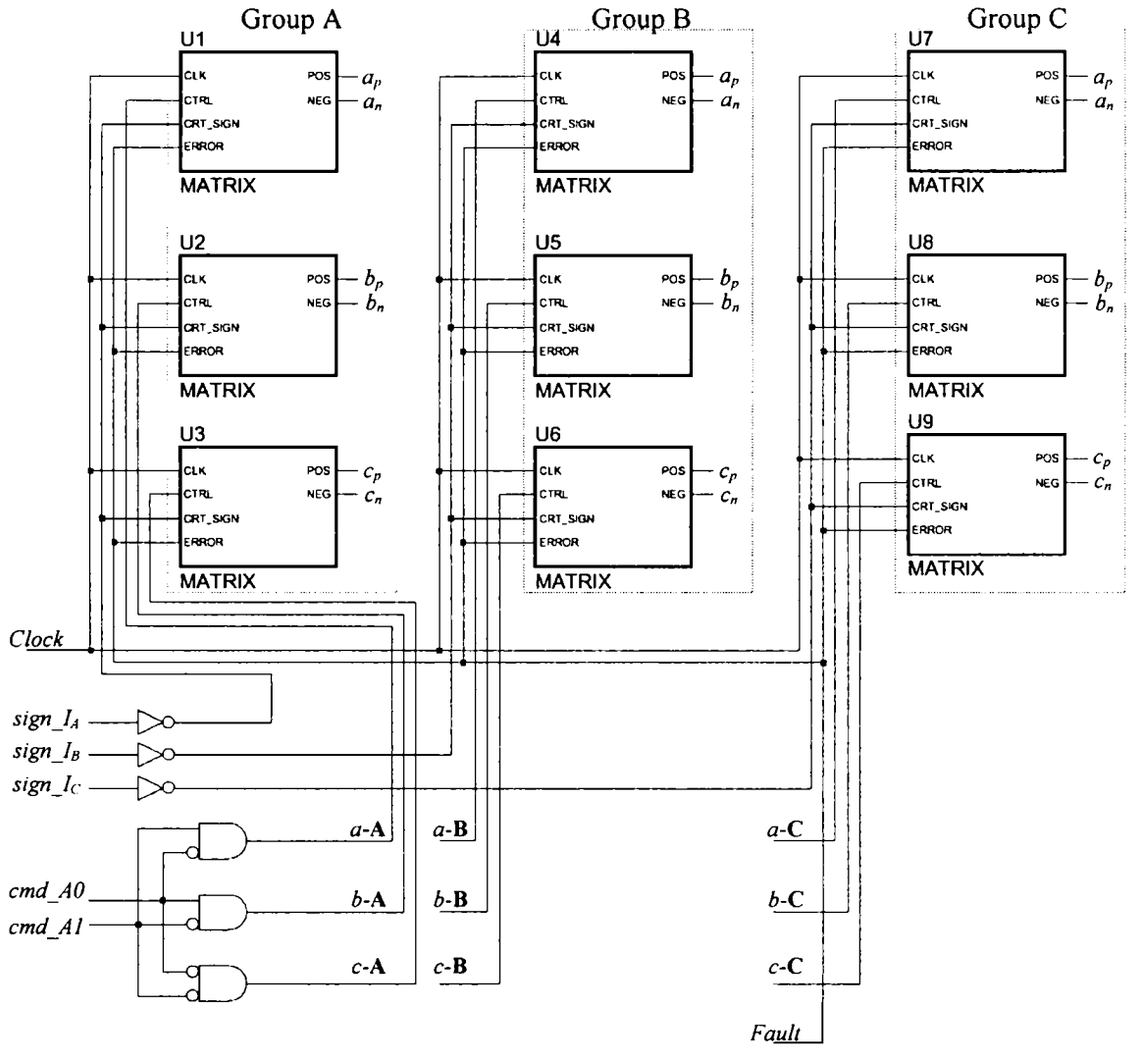

Fig. 3.7: Logic diagram of the Commutation Control Unit

During the first start-up, attention should be paid to match the current sign given by the *Current Transducer Unit* with the IGBT's gate signals which allows the conduction of the current in the same direction. It is possible to test if all the four-step commutation works by feeding the matrix converter with a reduced input voltage (20-30 V_{ac}), while at the output a high-impedance inductive load is connected. The clamp circuit has to be permanently connected on both sides, to protect against overvolatges. A load resistor has to be connected in the clamp circuit to dissipate the energy caused eventually by a faulty dead-time current commutation.
This method has been applied during first tests in the laboratory to check the functionality of the prototype. On the output side, a small induction motor (1.1 kW) has been connected. The motor has been driven at reduced modulation index, which produced a current of about 0.5 Amps. For the wrong direction of the current signs, a voltage level of 200-300 V_{dc} was reached in the clamp circuit, while for the correct direction of the current signs, no substantial increase of the voltage was noticed (50-70 V_{dc}).

3.3 THE CONTROL SYSTEM OF THE LABORATORY PROTOTYPE

In order to provide high performance results, the control strategy of the matrix converter was implemented in a 32-bit floating point Digital Signal Processor (DSP) with 2 Mbytes internal RAM, produced by Analog Devices (ADSP 21062) [3.18], [3.19]. A board based on this DSP is mounted inside of a PC host, to provide high-speed communication and high capacity for data storage. Acquisitions are performed using a fast 8-channel 12-bit AD converter board, mounted on an external board. A microcontroller board based on SAB 80C167 (Siemens) [3.20] is used to perform the timing of the system, due to special built-in timing functions. The block diagram of the system is shown in Fig. 3.8.

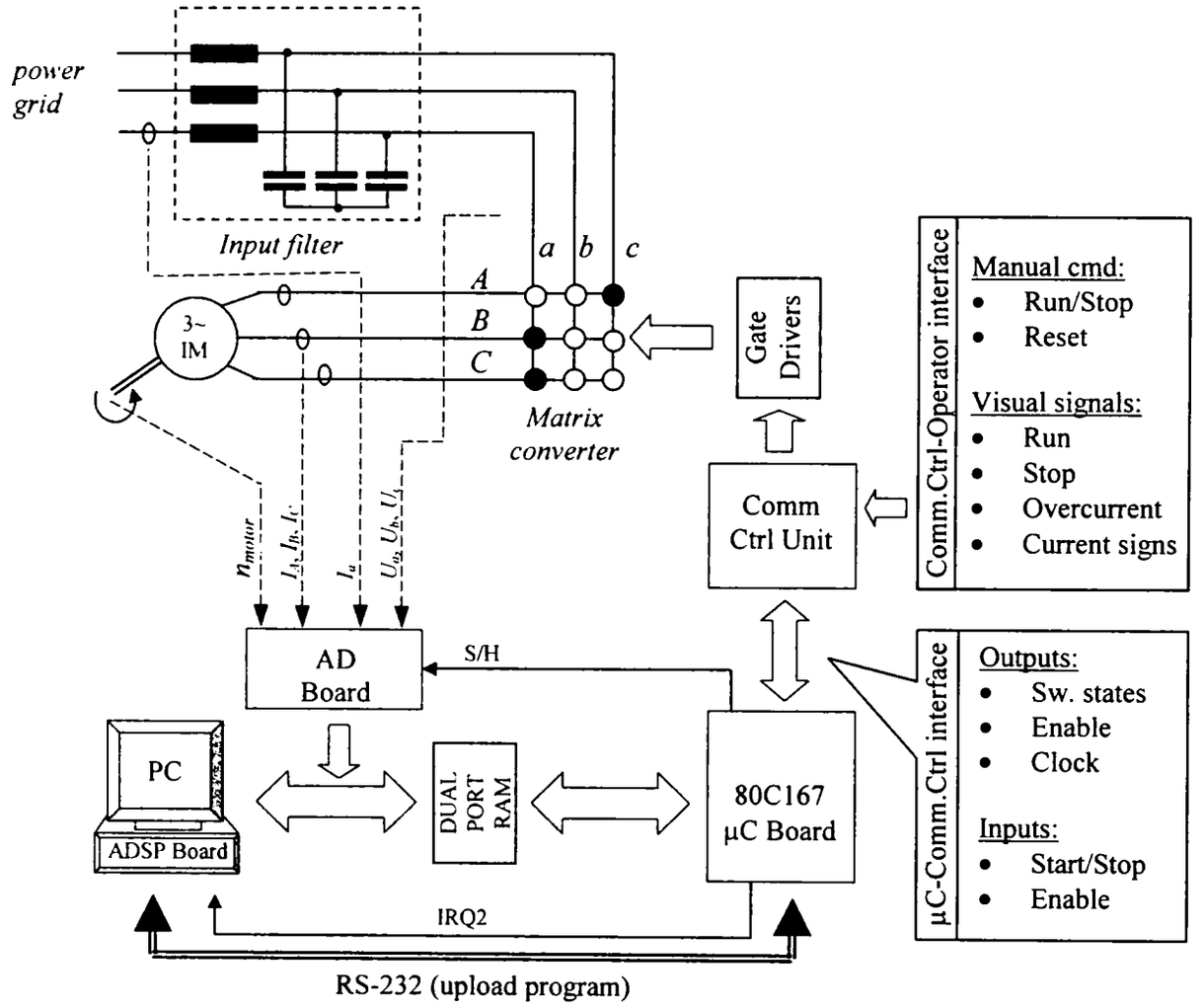

Fig. 3.8: Block diagram of the matrix converter control system

Table 3.1 shows the cyclic task operation of the control system. The core of the system is the microcontroller, which produces all signals necessary for the control. Timer T0 runs in the automatic reload mode, counting for the switching period until overflow. A few system signals (hardware and software) are generated in order to control the matrix converter switches, the AD board and the DSP board:

- *CC0...7* are capture-compare units, configured to trigger a PEC (Peripheral Event Controller) transfer from memory to an output port (P2) the current switching state, when the value stored in the CCx registers (sequence duration) matches with timer T0;

- *S/H* (sample and hold), which controls the sample and hold circuits of the AD board in order to provide simultaneous acquisition of all the 8 A/D channels;
- *IRQ2* starts an interrupt routine in the DSP, which contains the matrix converter SVM control algorithm, at the beginning of the switching period, during a zero-vector;
- *write DPRAM* starts the DSP procedure of writing data in the dual RAM port, which later are read by the microcontroller board;
- *read DPRAM* starts the microcontroller procedure of reading data from dual-port RAM and loading the new switching states and the corresponding duty-cycles (in CCx);

Table 3.1
Control system task management of the matrix converter prototype

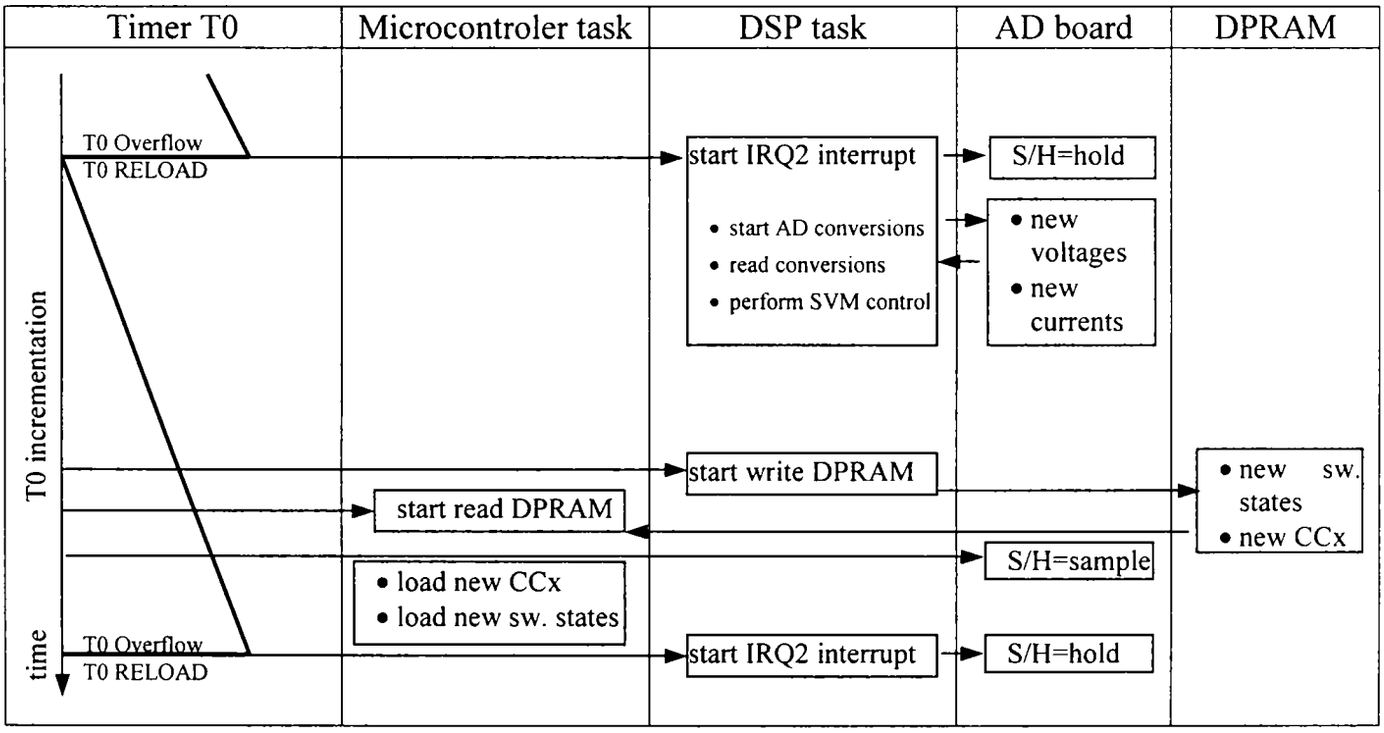

The generation of the switching pattern uses the Capture/Compare Unit and the Peripheral Event Controller provided by the C167 microcontroller. This is presented in Fig. 3.9. When the timer T0 match the content of a CCx channel, an automatic transfer from a defined memory location, which contains the new switching state of the converter, to an output port, which consist of the command terminals for the commutation-control unit, is performed. The PEC transfer is performed in one machine cycle, in this way the action is fast and high priority executed and no software resources as interrupt subroutines are required. This produces a double-sided SVM switching pattern, starting with a zero vector, no provide low noise in the moment of acquisitions for the signals.
The tasks of the DSP interrupt, which performs the matrix converter control on the motor and line side, is shown in Fig. 3.10 and these are:

- starts acquisitions of the three input phase voltages;
- performs the motor side control (output voltage reference vector);
- performs the line side control (input current reference vector);
- calculates the imaginary DC-link voltage;

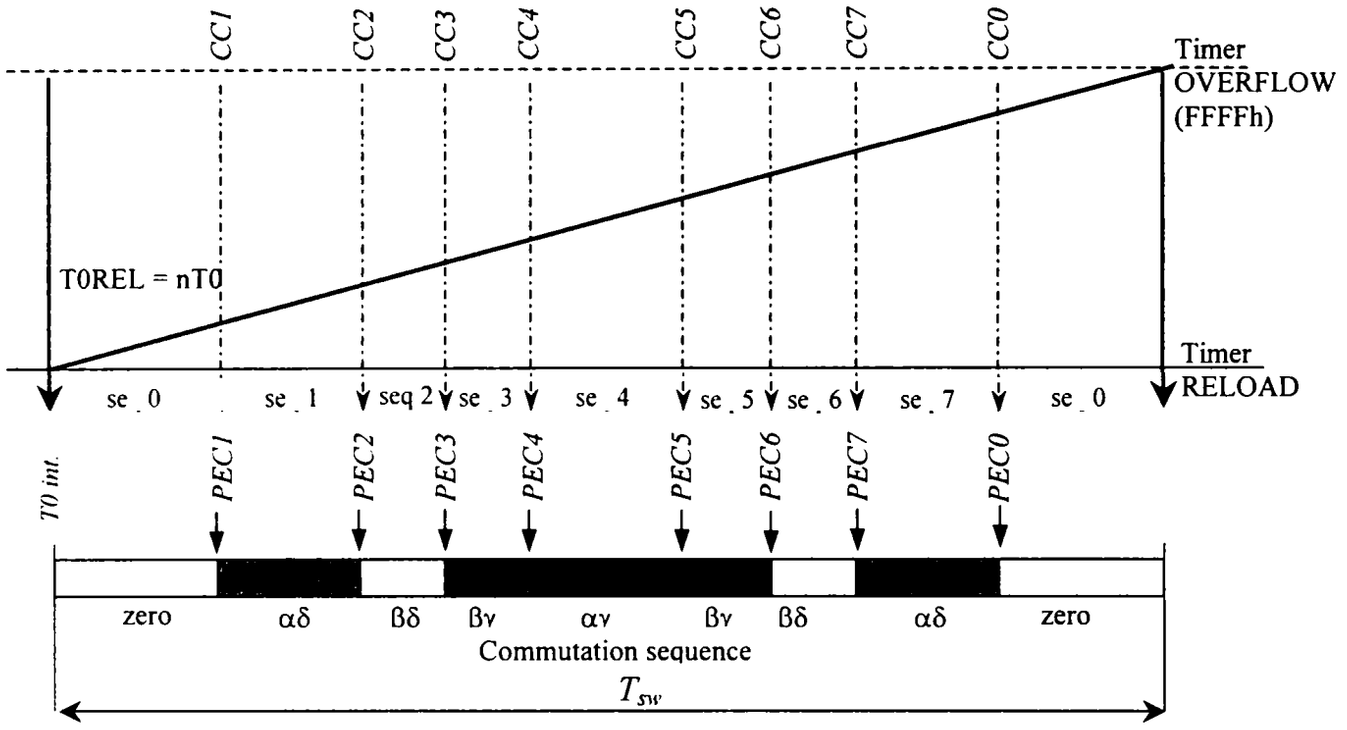

Fig.3.9: Timing diagram for the SVM switching pattern generation

- calculates the modulation index, and forward compensate for input voltage unbalance and distortion;
- calculate the duty-cycles of the double-sided ISVM sequence and the optimised switching pattern;
- send new data to the microcontroller;

In Fig. 3.10 the logic control scheme of the DSP program is shown. The *Ramp Control* block controls the acceleration and deceleration producing the actual frequency f_{out}. This is used to integrate the angle θ_{ref} of the motor reference flux. The amplitude of the motor reference flux Ψ_{ref} is setable, as a fixed value or may be custom variable. By differentiating the reference flux in α-β co-ordinate, the reference output phase voltage vector is found. The amplitude of the output voltage vector U_{out} is used to calculate the modulation index m_U. The angle θ_{out} of the output voltage vector is used to calculate the sector *sec_out* and the angle within the respective sector θ_{out} of the output reference voltage vector, needed to perform the SVM in the invertion stage.

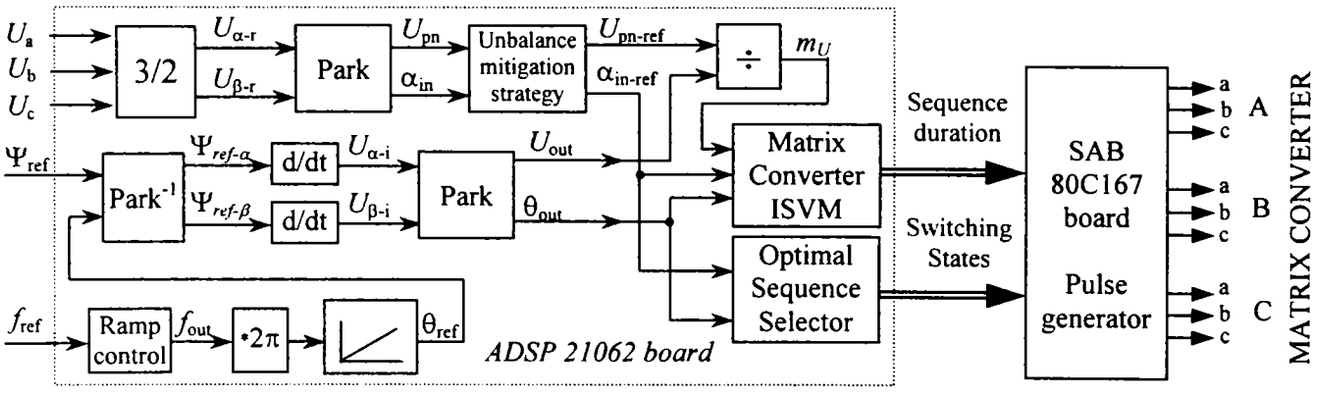

Fig. 3.10: DSP control diagram for the matrix converter prototype

The three input phase voltages U_a, U_b, U_c are used to calculate the angle θ_{in}. This may be subject of unbalance compensation, which produces a new input current reference angle [3.7]-[3.9]. This is used to calculate the sector *sec_in* and the angle within the respective sector θ'_{in} of the input current reference vector, needed to perform the SVM in the rectification stage. Also, this is used to calculate the imaginary DC-link voltage used to calculate the voltage modulation index m_U.
Inside the ISVM Control Block the duty-cycles of the switching sequence are calculated by using the reference vectors: the current vector given by the angle of the input phase voltage vector and the motor reference voltage vector given by angle and magnitude. The computation of the duty-cycles for the indirect SVM technique was presented in details in Chapter 2.
By selecting an optimal switching pattern as was proposed in [3.1], [3.13], which depends on the sector where the two reference vectors are found, the number of switch-commutation is minimised. The microcontroller capture-compare unit performs the pulse timing and produces the matrix converter switching states, as was presented before.

3.5 DESCRIPTION OF THE LABORATORY TEST-BENCH

The matrix converter prototype is fed from a 4 kVA three-phase auto-transformer, which produces a variable input voltage, if needed, or in case variable voltage, frequency and programmable voltage waveform, from a 15 kVA electronic AC Power Source (15003iX from California Instruments). These possibilities can be used when measurements with different line-side conditions are needed as unbalanced and distorted voltage waveforms. The matrix converter is feeding a 4 kW induction motor, which is mechanically coupled with a DC machine. The excitation of the DC machine is connected to an auto-transformer, via a diode rectifier, which provides variable excitation current, when needed. The main circuit of the DC machine consists of a variable resistor, capable to dissipate a high amount of power and an amp-meter. The principle diagram of the test-bench is presented in Fig. 3.11. The parameters of the induction motor and of the DC machine are presented in Appendix 3.3 and 3.4.

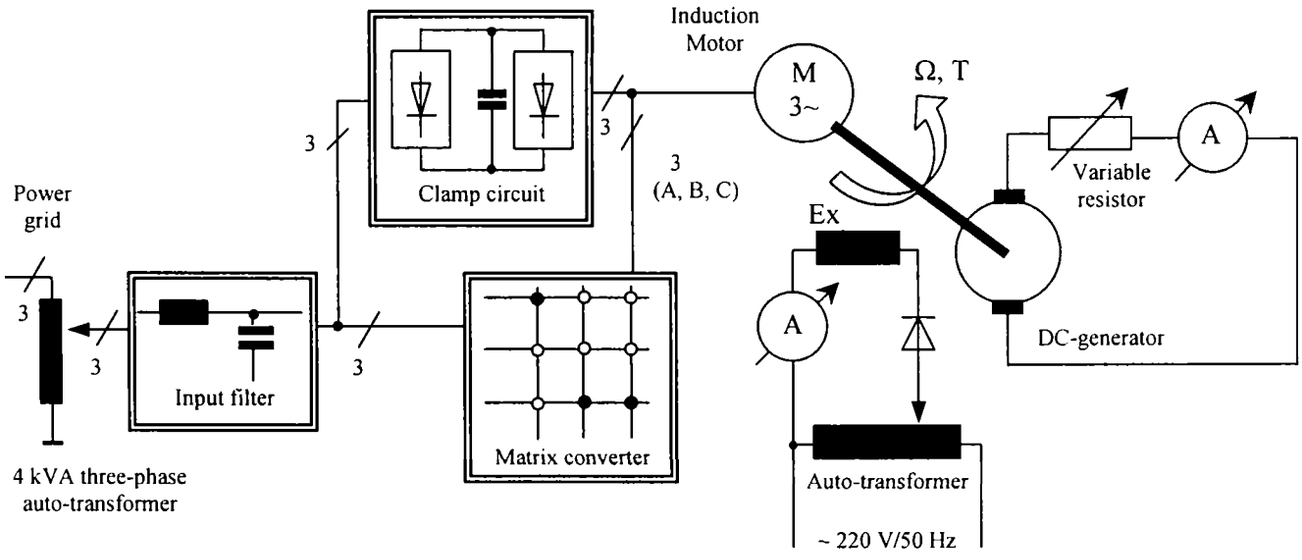

Fig. 3.11: Principle diagram of the laboratory test-bench for prototype evaluation

Taking into account the DC machine parameters, the mechanical torque on the shaft of the induction motor may be determined by multiplying the main DC machine current, which is

measured with an Amp-meter by a coefficient k_{DC}, which gives the torque-current dependence at nominal excitation current of the DC machine.

$$T_{L\text{-}IM} = k_{DC} \cdot I_{DC} \tag{3.17}$$

where $k_{DC} = 2{,}08$ Nm/A.

The most important disadvantage is that the induction motor cannot be loaded at full speed, and therefore full power of the matrix converter prototype cannot be achieved with this set-up.
In Fig. 3.12 an overview of arrangement in the laboratory is shown. Supplementary than was reported before, in this arrangement a three-phase Universal Power Analyser (PM 3000A from Voltech) is used to monitor the electrical parameters on the input side as voltage, current, power (active, reactive), power factor, as well as the harmonic content and the THD of these parameters. A four-channel digital oscilloscope (TDS 420 from Tektronix) is used to monitor the waveforms in the input and output side, collected from the voltage and current transducers available in the system. A vector visualiser is connected on the output side, providing the possibility to visualise the vector locus of the output voltage, current and flux, on a two-channel oscilloscope (HM 305 from Hameg).

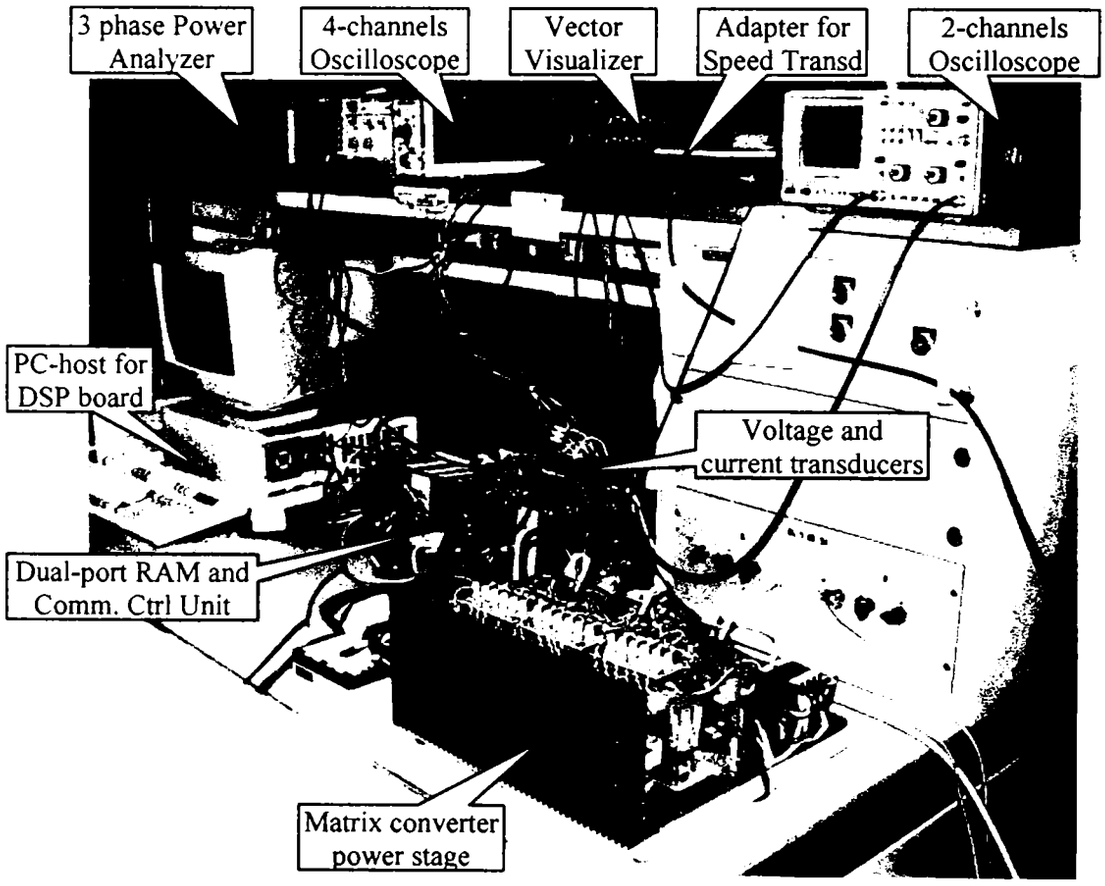

Fig. 3.12: Overview of the setup of matrix converter laboratory prototype

The last aspect presented here was an evaluation of the influence of the minimum sequence duty-cycle due to the commutation. As the four-step commutation and the quantification of the duty-cycle duration use the same clock signal, it was studied how the limit for the minimum sequence duration is influencing the waveform distortion. Three values for minimum conduction duty-cycles have been taken into account: $t_{min} = \{2, 3, 4\} \times t_{clk}$. It was considered possible to use these

values, because by studying the optimal commutation table, successive commutations take place in different output switch groups, which belongs to different output lines. The effect in distorting the output current waveform at low modulation index, due to distorted output voltage waveform, is presented in Fig. 3.13. This is caused because low modulation index cause higher errors when calculating the duty-cycles, which increases more when the reference vectors are near to the sectors boundaries.

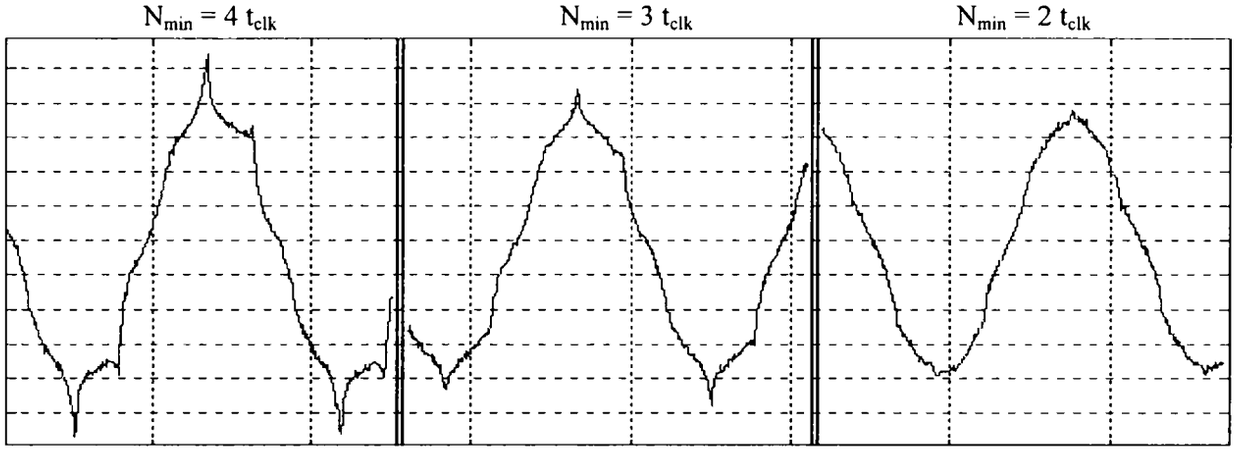

Fig. 3.13: Distortion of the output current waveform caused by synthesis errors of the SVM modulator at lower modulation index due to duty-cycles limitation

Test conditions: U_{in}=3x380 V/50 Hz; m_U=0.06; f_{out}=3 Hz; f_{sw}=4 kHz; Scale: current: 1 A/div; time: 200 ms/div

SUMMARY

Based on a previous work carried out at Institute for Energy Technology, Aalborg University, Denmark, in 1992-1996 during a Ph.D. Program, which develop the first prototype, the research effort was directed to improve the performance in the following directions:

- to increase the computational power of the control system, by employing a powerful dual-processor system, giving the opportunity to implement various time-consuming tasks, as strategies to compensate the effect of unbalanced and distorted input voltage;
- to increase the quantity and the resolution of information available from the drive;
- to reduce the size of the system, by integrating the whole commutation control units in a single control board, due to a high-performance PLD chip;

In parallel, theoretical investigation has been done in order to determine the real requirements for the passive components, in order to achieve high integration, by decreasing the weight and the volume, while the performance was not affected. It has been shown that no special requirement for higher du/dt capacitors in the clamp circuit are needed. Also, arbitrary design rules previously proposed, which provided higher power factor in a wide power range, does not provide a best use of the system weight and volume, as usually chokes have a lower power density than film capacitors.

APPENDIX 3.1

The characteristics of the input filter

L_{in}/*phase*	1.2 mH/10 A_{pk} (0.013 p.u.), type: B82505-W-A4 (S+M). weight: 0.6 kg, size: 43x24x111 mm
C_{in}/*phase*	6x 1 µF/250 V (X2 class), type: PHE 830MF7100M (EvoxRifa). weight: 15.5 g, size: 14.5x24.5x31.5 mm (for one piece)
f_0	1876 Hz
$\cos \varphi_{min}$	0.877_{CAP}@P_{out} = 10% P_n (273.7 VAr@500 W)
$\Delta U_{Lin}/U_n$	0.0083 % @ 7.5A_{rms}, 50 Hz

APPENDIX 3.2

The characteristics of the clamp circuit

Diode	BYPT 12PI-1000 V_{RRM} = 1000 V; I_{FSM} = 12 A; I_{FSM} = 75 A; I_{FRM} = 150 A;
C_{clamp}	9.4 µF/1050 V_{DC}, $(dU/dt)_{max}$=1000 V/µs (snubber capacitor type)
$(L_{\delta S}+L_{\delta R})_{IM\text{-}max}$	10.7 mH @ i_{max}=20 A, U_{max}=1000 V
ΔE_{FAULT}	3.2 J @ U_{max}=1000 V, U_n=565 V

APPENDIX 3.3

Data on the induction-motor nameplate:

U_n = 380 V (delta); I_n = 7,9 A; n_n = 2880 rpm; P_n = 4 kW; T_n = 13,3 Nm;

APPENDIX 3.4

Data on the DC machine nameplate:

U_n = 400 V_{DC}, I_n = 9,7 A_{DC}; I_e = 0.7 A_{DC}; P_n = 3,3 kW; n_n = 1560 rpm; T_n = 20,2 Nm;

APPENDIX 3.5

Technical specification for the matrix converter laboratory prototype:

Input terminals:

- Input voltage: 0 - 380 V/±10% and 50Hz;
- Rated input current: 7.5 A;
- cos φ = 1;

Motor terminals:

- Motor control strategy: scalar;
- Switching frequency: 2…6 kHz;
- Overcurrent protection level: 20 A_{peak};
- Output apparent power: 8.5 kVA;

Characteristics of the transducers:

- Input voltage transducer scale: -400 V ... +400 V / - 5V ... + 5 V
- Output current transducers scale: -25 A ... +25 A / - 5V ... + 5 V
- Input current transducer scale: -12.5 A ... + 12.5 A / -5 V ... + 5 V
- Speed transducer scale: 0 .. 4000 rpm / 0 V ... +5 V

REFERENCES

[3.1] P. Nielsen. "*The matrix converter for an induction motor drive*", Industrial Ph.D. project EF493, ISBN 87-89179-14-5, 296 pages, Aalborg University, Denmark, 1996.

[3.2] C. Klumpner, I. Boldea, F. Blaabjerg, "*The matrix converter: Overvoltages caused by the input filter, bidirectional power flow, and control for artificial loading of induction motors*" Electric Machines and Power Systems Journal, vol. 28, no. 2, pp. 129-142, Taylor & Francis Group, 2000.

[3.3] C. Klumpner, I. Boldea, F. Blaabjerg, P. Nielsen, "*A new modulator for matrix converters allowing for the reduction of input current ripple*", Proc. of OPTIM, vol. 2, pp. 487-492, 2000.

[3.4] D. Casadei, M. Matteini, G. Serra, A. Tani, C. Klumpner, "*Input power quality in matrix converters: Minimisation of the RMS value of input current disturbances under unbalanced and nonsinusoidal supply voltages*", Proc. of NORpie, pp. 129-133, 2000.

[3.5] C. Klumpner, I. Boldea, F. Blaabjerg, "*Artificial loading of the induction motors using a matrix converter*" Proc. of IEE/PEVD, pp. 40-45, 2000.

[3.6] C. Klumpner, P. Nielsen, I. Boldea, F. Blaabjerg, "*New steps toward a low-cost power electronic building block for matrix converters*", IEEE/IAS Annual Meeting, vol. 3, pp. 1964-1971, 2000.

[3.7] M. Matteini, D. Casadei, C. Klumpner, F. Blaabjerg, "*Comparison of two current modulation strategies for matrix converters under unbalanced input voltage conditions*", Proc. of ISIE'00, december 2000, in press.

[3.8] C. Klumpner, P. Nielsen, I. Boldea, F. Blaabjerg, "*A new matrix converter-motor (MCM) for industry applications*", Proc. of IEEE/IAS Annual Meeting, vol. 3, pp. 1394-1402, 2000.

[3.9] D. Casadei, G. Serra, A. Tani, P. Nielsen, "*Theoretical and experimental analysis of SVM-controlled matrix converters under unbalanced supply conditions*", Electromotion Journal, vol. 4, no. 1-2, pp 28-37, 1997.

[3.10] C.L. Neft, C.D. Shauder, "*Theory and design of a 30-hp matrix converter*", IEEE Trans. on Industrial Applications, vol. 28, No. 3, pp. 546-551, 1992.

[3.11] P. Nielsen, F. Blaabjerg, J.K. Pedersen, "*Novel solutions for protection of matrix converter to three phase induction machine*", IEEE/IAS Annual Meeting, vol. 2, pp. 1447-1454, 1997.

[3.12] N. Burany, "*Safe control of 4-quadrant switches*", IEEE/IAS Annual Meeting, vol. 1, pp. 1190-1194, 1989.

[3.13] P. Nielsen, F. Blaabjerg, J.K. Pedersen, "*Space vector modulated matrix converter with minimized number of switchings and feedforward compensation of input voltage unbalance*", Proc. of PEDES'96, vol.2, pp. 833-839, 1996.

[3.14] Siemens Matsushita Components, "*Technical Product Information. Passive Components. Databook Library*", Ordering no. B465-P6580-X-X-7400, Germany, 1997.

[3.15] SGS-Thomson Microelectronics, "*BYPT 12PI-1000 Fast recovery rectifier diode*", Datasheet, Italy, 1994.

[3.16] LEM, "*Current transducer LA 25-NP*", 980909/6, LEM Components, 1998.

[3.17] Xilinx, "*AppLINX CD-ROM*", USA, 1999.

[3.18] Analog Devices, "ADSP-2106x Sharc User's Manual", 82-000795-02, USA, 1995.

[3.19] Analog Devices, "*ADSP-21000 Family. C Runtime Library Manual*", 31-000007-03, USA, 1995.

[3.20] Siemens, "*C167 Derivatives - 16 Bit CMOS Single-Chip Microcontrollers - User' Manual 03.93 Version 2.0*", Siemens AG, Munchen, 1996.

[3.21] Toshiba, "*TLP-250 IGBT Gate drive*", Technical data, 1996-4-8.

Chapter 4

Hardware Improvements for Matrix Converters

This chapter reports new hardware improvements of the matrix converter. A structure of a power electronic building block for matrix converters is proposed, to provide the user with a reliable hardware, with built-in protection and bi-directional switch commutation control. Solutions to reduce the costs in the low power range are proposed, consisting in a new silicon power stage structure and of a new input filter topology [4.1].
The influence of the input filter and the clamp circuit are studied, when a voltage step disturbance is applied on the input side, to verify the design of the input filter-clamp circuit assembly to overvoltage restrictions, caused by severe grid disturbances as voltage sags or momentary power interruptions. An additional circuit consisting of damping resistors and a relay is proposed to prevent the overvoltage risk during the matrix converter power-up [4.2].

4.1 POWER ELECTRONIC BUILDING BLOCK FOR MATRIX CONVERTERS

The way of developing the frequency converter technology for industry application has evolved during the last 40 years, driven by the power switches technology and control circuits technology [4.3]. At the beginnings, power stages were built with discrete power devices, because snubber circuits were needed and were easy to repair. The maturation of the power switch technology allowed for integration of power devices in power modules, in order to decrease production costs. Further, power electronic building blocks provide safe and optimal operation of a power stage and control circuits assembly due to an integrated design.

4.1.1 Consideration for integrating the bi-directional switches in a power module

During the last 15 years many matrix converter prototypes have been reported in the literature [4.4]-[4.12]. Almost all those prototypes were build using discrete power devices. The use of a specially designed 3-phase-to-1-phase (3∅/1∅) power module with bi-directional switches has been first reported in 1996 [4.4], and later in 1997 [4.5] and 1999 [4.6].
The purposes of integrating the bi-directional switches into a power module are:

- to reduce the volume occupied by the solid-state devices, as discrete devices takes much space compared to integrated devices in power modules;
- to reduce the count of power module terminals due to internal wiring, with influence in reducing the leakage inductance of the main current path due to shorter connections and in reducing the converter manufacturing costs;
- to allow an optimal integration of the hardware protection and the commutation control logic inside the gate-driver stage, in order to develop an integrated power electronic building block for matrix converters;

The converter power range is an important criterion in choosing the optimal topology of the power module. For example, in the DC-link VSI technology, this aspect has led to the optimal power module topology of today's industrial frequency converters as follow:

- in the low power range, the manufacturers integrate all the silicon devices inside of a single power module: the IGBT's, the fast recovery diodes (FRD), the rectifier diodes, the braking chopper and the temperature sensor;
- in the high power range, the manufacturers integrate into a power module a single inverter leg or a six-pack IGBT module is used as an inverter leg.

The difference of approach is justified by the production specific costs ($/kW), which are high in the low power range, by the cooling problems and also by the complex functions required for the gate-driver. Therefore, in the high power range, where the converter efficiency and reliability are more important than the cost, the IGBT gate-driver has to perform complex functions as overcurrent protection, active turn-on/turn-off switching, which reduces the commutation losses, du/dt and EMI, or in paralleling the IGBT's [4.13], [4.14]. All these features are based on monitoring the collector-emitter voltage of the IGBT's. As a result, the power-module and the gate-driver board should be designed to match each other with minimized size, power loss and number of terminals, allowing the user to build the converter without taking into account the specific problem of operating and protecting the power switches.

The CE and CC anti-paralleled switch topologies, which have been presented in Section 2.2, are analyzed in order to obtain the optimum configuration of a power module with bi-directional switches for matrix converters. The purpose of this analysis is to establish the optimum topology for both types of power modules: 3∅/1∅ and 3∅/3∅. This includes the reduction of the insulated power supplies count, the reduction of the terminals count per power module, the possibility to feed input voltage and output current transducers from the gate-driver supplies. Scheme of 3∅/1∅ power module topologies, with CE or CC connected IGBT's, are shown in Fig. 4.1.

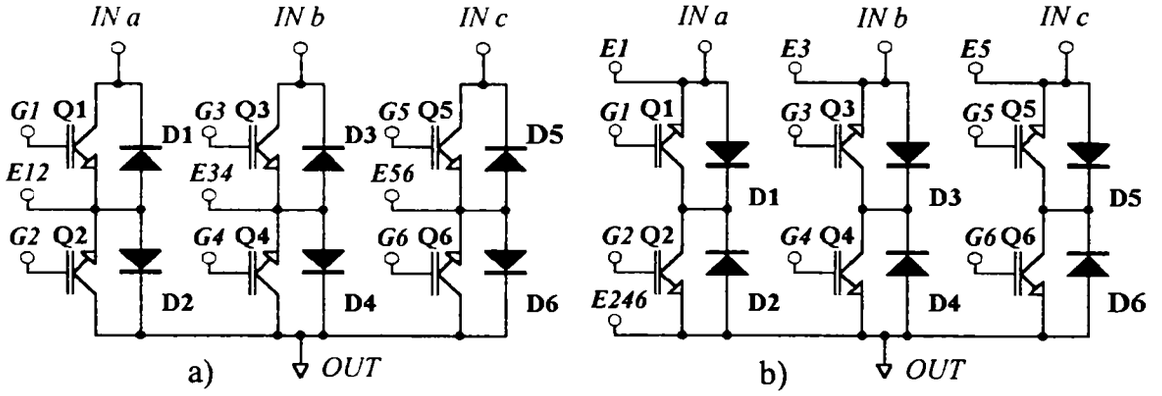

Fig. 4.1: The scheme of a 3∅/1∅ power module using:
a) CE-IGBT's; b) CC-IGBT's

Table 4.1 summarizes the analysis of the two bi-directional switches, concluding that the choice depends on the power range for which the power module is designed. The CE topology is recommended to build a 3∅/1∅ power module for high power range, where the possibility to monitor the collector-emitter voltage (V_{CE}) makes possible to use a smart gate-driver, with short-circuit detection and adaptive switching, which is recommended in the high power range. A reduced count of control terminals per power module (9 pcs.), no connections needed between the different gate-driver boards that belong to different power modules and reduced count of galvanic-insulated signal channels, are other advantages of the CE topology.

The CC topology is recommended to build a 3∅/3∅ power module for low power range due to the reduced count of insulated gate-driver power supplies (6 pcs.) and the small size characteristic of

an one-chip solution. The reduced count of control terminals per power module (24 pcs.) and the possibility to feed the input voltage transducers and the output current transducers from the gate-driver power supplies are other advantages of the CC topology.

Table 4.1
Hardware requirements for a matrix converter depending on the bi-directional switch topology

	COMMON EMITTER (Fig. 4.1a)	COMMON COLLECTOR (Fig. 4.1b)
Insulated gate-driver power supplies:	9 pcs	6 pcs
Galvanic-insulated signal channels:	9 pcs distributed commutation control unit in the gate-driver stage	18 pcs centralised commutation control unit is used
Access to the IGBTs terminals:	YES (suitable for V_{CE} monitoring)	NO
Minimum number of control terminals (single emitter)):	• 9 (3∅/1∅ power module) • 27 (3∅/3∅ power module)	• 10 (3∅/1∅ power module) • 24 (3∅/3∅ power module)
If the bi-directional switches are integrated in a 3∅/1∅ power module:	• no external connection to other modules necessary • gate-driver integration with power module is possible	external connections between module are required for the gate-driver power supplies
Remarks:	Possible to implement overcurrent protection and adaptive switching (using V_{CE})	Possible to feed the voltage and current transducers from the gate-driver power supplies
Recommendation:	Suitable for a 3∅/1∅ power module (high power range)	Suitable for a 3∅/3∅ power module (low power range)

4.1.2 Designing considerations for a Power Electronic Building Block for matrix converters

A new trend to increase reliability and to reduce development time of products in customized applications is to develop fully integrated power electronic systems, which lead to low-cost products with shorter design cycles [4.15]. A stand-alone power electronic building block (PEBB) for matrix converters must include decoupling capacitors near to the power terminals to reduce the commutation overvoltages, the insulated power supplies to feed the gate-drivers, an integrated commutation control logic and overcurrent protection and protection against a faulty command. In order to provide convenient external interface, the PEBB requires a reduced number of supply terminals and reduced number external signals, which has to be TTL compatible.
In the low power range, the power modules are mounted on PCB and a shunt are employed to measure the currents, but the power module must employ CC-connected IGBT's to allow the gate-driver power supplies to feed the electronics as well. In the high power range, the PCB cannot be used for the main current path and it is more convenient to use the V_{CE} for protection and commutation control, but the power module has to employ CE connected IGBT's [4.19].
A block scheme of a matrix converter PEBB proposed in the low-power range is shown in Fig. 4.2. The "*Logic Control*" block monitors the functionality of the matrix converter. The "*Overcurrent*" signal is produced by the "*Overcurrent Protection*" block, caused by an overcurrent

situation. As a result, all the IGBT's are turned off and the "*Fault*" signal is generated. An external controller produces the following control signals: "*Reset*", which clears an overcurrent error memorized by the control board, "*Enable*" and the state of the matrix converter switches (*A0, A1, B0, B1, C0, and C1*), which are 2-bit encoded.

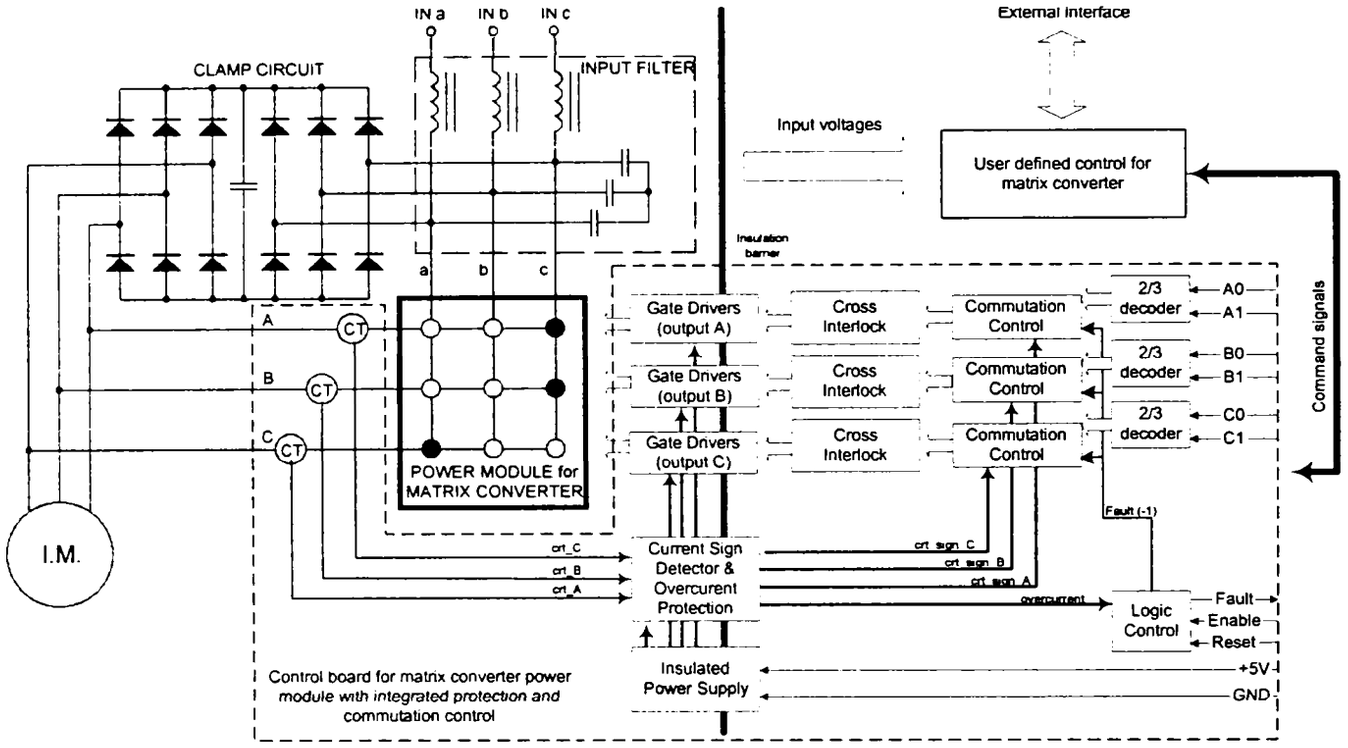

Fig. 4.2: The block scheme of a PEBB for matrix converters

The output current information is processed on the gate-driver stage, thus no analogue signal has to be transferred through the insulation barrier. Four optocouplers are used to transfer the overcurrent and the three output current signs, which are needed to control the bi-directional switch commutation. All the necessary logic to control the matrix converter is implemented on a PLD chip. The proposed control board for the matrix converter uses only 11 external connections to supply the electronic board, to achieve the complete control and to provide safe-operation of the matrix converter.

The practical observations in building a matrix converter as a PEBB in order to optimize the interface with a higher level processor unit reported in this section are used in Chapter 8, where the hardware and software implementation of an integrated motor drive, the matrix converter-motor (MCM) is described.

4.1.3 Faulty command protection

Internal short-circuits caused by faulty command signals are fatal for the matrix converter power stage because:

- usually there is no current sensor on the input phases able to detect short-circuits between the input phases;
- the value of the input filter inductance is small (1-3% p.u.) and in the case of a short-circuit between two input phases, the circulating current will exceed the maximum value very quickly.

A faulty command is defined by closing two bi-directional switches that connect two different input phases to a common output phase. An internal short-circuit could occur in Fig. 4.3 when only two switches Q2 and Q3 are turned on and the potential on phase *a* is higher than the potential on phase *b*: a circulating current from input phase *a* to input phase *b* will flow through D1-Q2-D4-Q3. The internal short-circuit may be avoided if a cross-interlock protection is used. This means to condition the command for an IGBT with the open state of all the other IGBT's, which allow for circulating currents between the input phases.
For example, if a switch connected to one side (an input phase) has to be turned on (e.g. Q3), it should be verified that there is no switch turned on in opposite side, excepting the switch in series on the respective input phase (e.g.: Q2 and Q6). This situation is shown in Fig. 4.3.

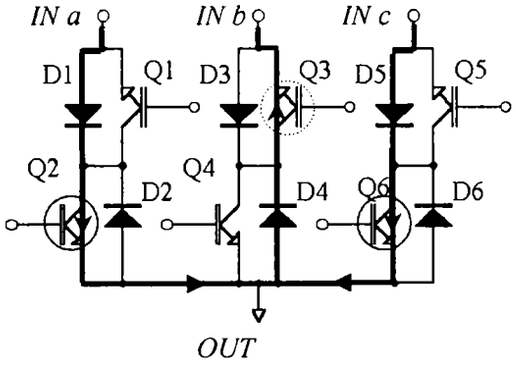

Fig. 4.3: Internal short-circuit path in a 3∅/1∅ power module

This protection is recommended for the gate-driver stage, without the commutation control logic included, where the risk of receiving a faulty command signal induced by noise, exists. The implementation requires only a few logic gates.

4.1.4 Novel matrix converter topology using three insulated supplies for the gate-drivers

The optimum matrix converter topology in order to minimize the number of the necessary insulated power supplies was already investigated [4.4], [4.5] and it was found that using CC bi-directional switches, the number of insulated gate-driver power supplies is minimized (6). This number is higher compared to a standard diode bridge VSI, but it is the same compared to a back-to-back VSI, which is another regenerative converter topology (AC/DC/AC).
In low power applications there is no need to use differential power supplies to feed the gate-drivers, because the IGBT's can be switched off with zero potential on the gates [4.16]. The power modules easily support the extra-losses caused by the increased switching losses due to zero voltage blocking because low power IGBT's are available for high switching frequency providing low switching losses. An economical solution used in DC-link VSI is to generate the supply for the upper IGBT gate-driver using a bootstrap supply, which consist of a capacitor and a diode [4.17]. When the lower IGBT is turned on, the V_{CE} drops to a few volts and the bootstrap capacitor is charged from the lower IGBT gate-driver power supply.
By changing the matrix converter topology, it is possible to implement the bootstrap method to generate several power supplies. The operating principle is presented in Fig. 4.4. If a CE bi-directional switch (Q3-D3-Q4-D4) connects an input line IN to an output line OUT, a single insulated power supply is needed to feed the two IGBT gate-drivers Q3 and Q4, which will be called the master-switches. If two bootstrap diodes D_{IN} and D_{OUT} and two bootstrap capacitors C_{IN} and C_{OUT} are introduced, as is shown in Fig. 4.4, each time when a master-switch Q3

respectively Q4 is turned on, the corresponding bootstrap capacitor (C_{IN} or C_{OUT}) is charged from the DC/DC power supply. In this way, two other power-supplies with reference to the input line IN and to the output line OUT, are produced.

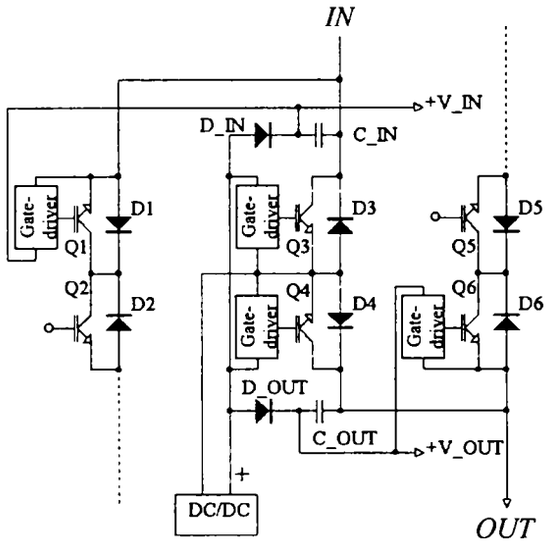

Fig. 4.4: Generation of bootstrap supplies in the new bi-directional switch arrangement

If two other bi-directional switches in the CC topology are connected, one to the input phase IN and the other one is connected to the output phase OUT, it is possible to feed the Q1 and Q6 gate-drivers from the V_{IN} and V_{OUT} power supplies. A similarity to use the bootstrap circuit into a standard VSI to feed the upper IGBT gate-drivers is evident. Q1-Q3 and Q6-Q4 forms virtual VSI legs, with the negative potential of the DC-link considered in the master-switches Q3 and Q4 emitters. If this idea is expanded to a 3Ø-3Ø matrix converter, the power stage topology will employ three CE bi-directional switches and six CC bi-directional switches, allowing the reduction of the count of insulated power supplies to three, as shown in Fig. 4.5.

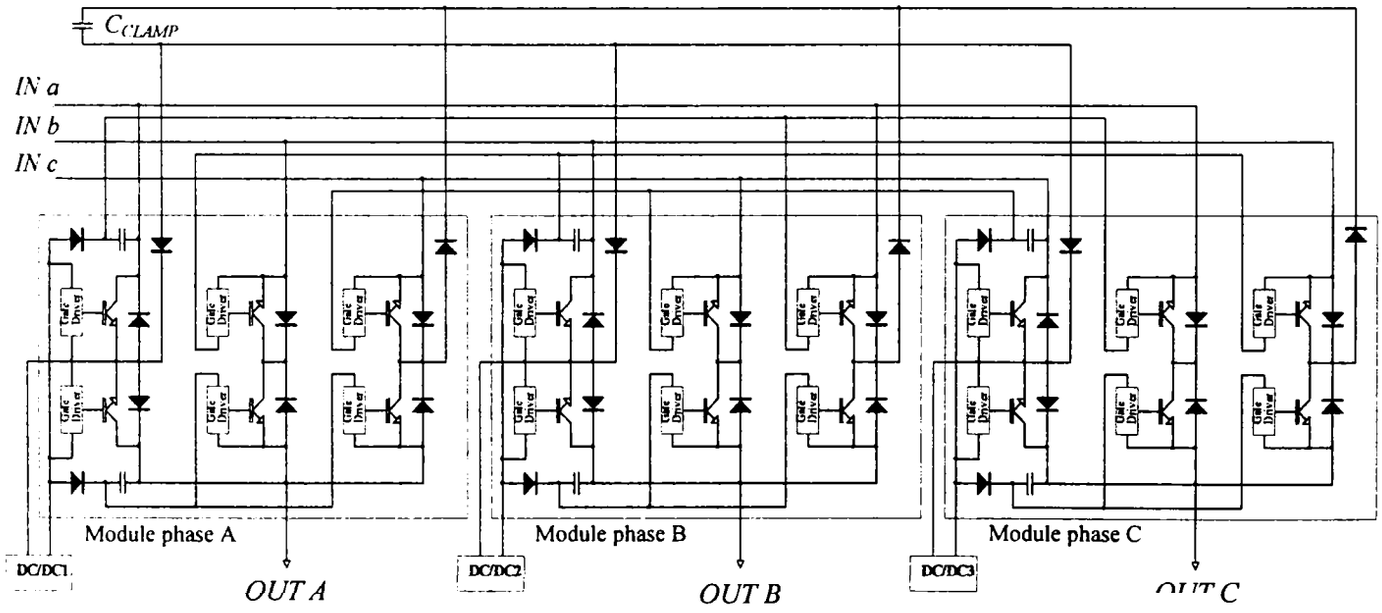

Fig. 4.5: The novel matrix converter topology with reduced count of insulated power supplies (3) and clamp diodes (6)

It has previously been shown that a similar arrangement of bi-directional switches allows for the reduction of the clamp circuit diodes to six [4.4] compared to the standard arrangement presented in Fig. 4.2. Using both ideas, it is possible to develop a new 3∅/3∅ power module with integrated bi-directional switches and clamp diodes with no other external power semiconductor devices needed, requiring only three insulated power supplies to feed all the gate-drivers.
It is necessary to run a specific "warm-up" sequence before the matrix converter is ready to start, in order to charge the bootstrap capacitors by turning on the master-switches, depending on the line-to- line input voltage, in such a way that the bi-directional switch will not conduct. When the input voltage changes polarity, the other master-switch is turned on, providing power supply for all the other IGBT gate-drivers, with no risk of having hazardous potentials on the output. In this way, the start-up sequence is completed in less than a semi-period of the input voltage. The value of the bootstrap capacitors should be chosen in order to keep the required voltage constant during the start-up procedure. Also considering that each master-switch operates at least a sixth part of input voltage period, the value of the bootstrap capacitors should be chosen to store energy to feed three gate-drivers during the period the master-switch does not conduct, which is about 3.3 ms at 50 Hz input frequency.

4.2 SAFE OPERATION ISSUES IN CONJUCTION WITH THE INPUT FILTER

Due to the lack of a DC-link, which provide stability for line disturbances to a VSI, the matrix converter is sensitive to line disturbances, which may affect the semiconductor structure. Therefore, an auxiliary circuit including a clamp capacitor is needed to prevent overvoltage caused by shutting down the matrix converter while the motor is still magnetized and to protect against overvoltage from the input side. The power grid disturbances, in conjunction with the L-C input filter and the clamp circuit, connected as was shown in Fig. 4.2, may produce overvoltages on the matrix converter inputs and overcurrents on the clamp circuit diodes during the capacitor charging. Similar to standard diode-bridge VSI, where due to the large DC-link capacitors, a direct on-line power-up involves large in-rush currents which destroys the diode-rectifier, in matrix converters a safe power-up circuit is also necessary to minimize the overvoltage risk due to the L-C topology of the input filter. When the reactive elements are designed, the analysis should take in account the influence of the power grid and the overall topology of the matrix converter, which affect the transients on the input side.
Caused by the L-C series configuration of the input filter, oscillations appear during input voltage disturbances. A classification of possible disturbances from the mains include:

- power-up of the matrix converter;
- voltage sags or momentary power interruptions;

First type of disturbances may be prevented, involving auxiliary circuits, designed in the worst case condition in the power-up moment. Second type of disturbances could not be prevented, but worst case condition may become input variables for a new design criterion of the input filter and clamp circuit elements.

4.2.1 Transients in RLC series circuits

The response of an R-L-C circuit is analyzed in simple situation, when a DC step voltage U_{step} is applied to this circuit. Depending on the value of the resistance of the circuit compared with the "critical resistance" (4.1) of the circuit, there are two types of responses.

$$R_K = 2\sqrt{\frac{L}{C}} \tag{4.1}$$

- If $R<R_K$, the voltage across the capacitor oscillates and reaches a maximum level of two times the input step voltage, as is shown in Fig.4.6a. The expression of the voltage across the capacitor terminals becomes:

$$u_c = -\frac{U_{step}}{\omega_0} \cdot \exp^{-\delta_0 \cdot t} \cdot [\delta_0 \cdot \sin \omega_0 t + \omega_0 \cdot \cos \omega_0 t] + U_{step} - U_{ini} \tag{4.2}$$

where U_{ini} is the capacitor initial voltage. The pulsation ω_0 and the damping factor δ_0 have the following expressions:

$$\omega_0 = \sqrt{\frac{1}{L \cdot C} - \left(\frac{R}{2 \cdot L}\right)^2} \tag{4.3}$$

$$\delta_0 = \frac{R}{2 \cdot L} \tag{4.4}$$

Voltage overshot, higher that twice the voltage step is possible to appear, when the sign of the residual voltage U_{ini} in the capacitor is different from the sign of the voltage step U_{step}.

- If $R>R_K$ no oscillations occurs and the voltage across the capacitor reach the steady-state level, which is also the applied voltage step U_{step}, as is shown in Fig. 4.6b.

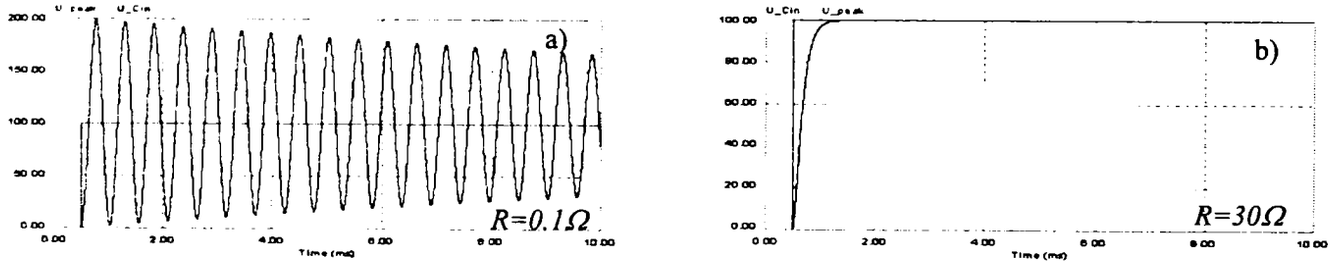

Fig. 4.6: Response of an RLC circuit (L=1.2mH, C=6μF, R_k=28Ω) to a voltage step(100V)

The overvoltage level depends on the relative circuit resistance (R'/R_k). This is shown in Fig. 4.7, where the curve was plotted resolving (4.2) for different values of the circuit resistance, but using the constant values of the reactive elements of the input filter and zero voltage across the capacitor as initial condition. A higher relative resistance of the circuit reduces the overvoltage level.

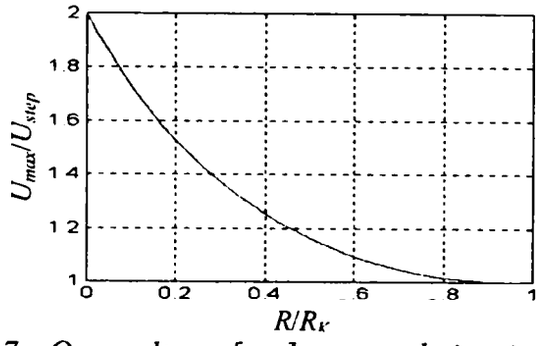

Fig. 4.7: Overvoltage [p.u] vs. rated circuit resistance (zero initial voltage in the capacitor of the filter)

If the total resistance of the circuit R' is known or may be estimated, including the power grid influence, by imposing a restriction for the overvoltage level U_{max}/U_{step}, the critical resistance of the input filter R_K' may be determined in Fig. 4.7. By knowing the total inductance of the input filter L', with the power grid influence included, and the desired cut-off frequency of the input filter, the minimum value of the input filter capacitors, which comply with the maximum overvoltage level is found:

$$C' = \frac{\sqrt{2}}{\omega_0 \cdot R'_K} \tag{4.5}$$

The designer should compare this value with the one determined by other design criteria, more restrictive.

$$C_{in} \geq C' \tag{4.6}$$

In general (4.6) gives a higher value for the input filter capacitor. A numerical example, which is representative for the 8.5 kVA prototype presented in Chapter 3 is given: R'=0.2 Ω, U_{max}/U_{step} = 1.4, L' = 1.4 mH, and f_0 = 1.7 kHz, results C' = 180 μF, while C_{in} = 6 μF (C'/C_{in} = 30 !!).
Considering that electrical loads in a given power range (e.g. 5-50 kVA) benefit of identical power grid conditions, it is concluded that the overvoltage risk is higher for smaller matrix converter units, which use smaller input filter capacitors and give a higher critical resistance.

4.2.2 Influence of adding a clamp circuit to the input filter transients

The clamp circuit is used as a general protection against input voltage disturbances in various electrical circuits and consists of a clamp capacitor and a rectifier (a diode or a bridge), to absorb the incoming energy, while keeping the overvoltage level below dangerous level. In standard VSI, the DC link capacitor and the input bridge provide effective clamping for input voltage disturbances, while the same DC-link capacitor and the freewheeling diodes from the IGBT inverter provide clamping on the motor side. A matrix converter needs the same protections, therefore a clamp circuit is connected through B6 diode rectifiers on the input and output sides, as is shown in Fig. 4.2.
In order to analyze how a clamp circuit works, lets considering a single-phase LC circuit (R=0) and a clamp circuit connected across the capacitor in the input filter, where a sensitive may be connected. The maximum overvoltage level is determined by applying a voltage step U_{step} disturbance to the LC circuit in both situations: with and without the clamp circuit. The initial state of the filter capacitor is discharged (U_{in_ini} = 0), while the initial state of the clamp capacitor is charged with the same step voltage (U_{c_ini} = U_{step}). This hypothesis emulates the situation when total power outage situation occurs, discharging the input filter capacitor, while the clamp capacitor remains charged with the magnitude of the nominal voltage.

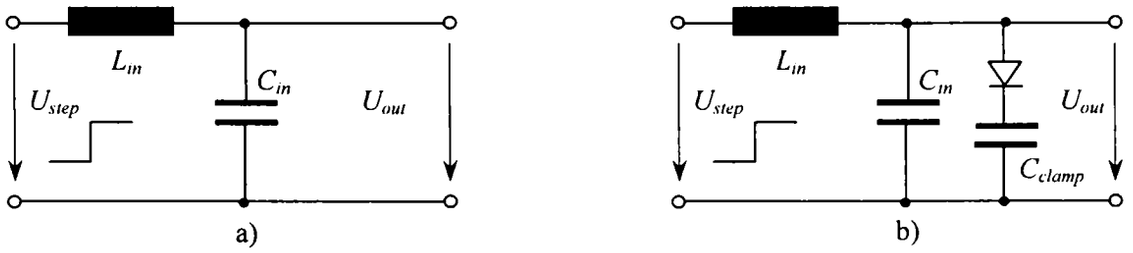

Fig. 4.8: Circuit diagrams of an LC filter to study the transient to a voltage step: a) without a clamp circuit; b) with clamp circuit

The oscillating energy W_{osc} in a simple L-C series circuit without a clamp circuit connected is:

$$W_{osc} = \frac{L_{in} \cdot i^2}{2} + \frac{C_{in} \cdot (u - U_{step})^2}{2} = \frac{C_{in} \cdot U_{step}^{\ 2}}{2}\Big|_{t=0} \tag{4.7}$$

where L_{in}, C_{in} are the inductance and the capacitance of the LC circuit, i is the momentary current trough the inductor, $(u\text{-}U_{step})$ is the momentary transient voltage across the capacitor, and U_{step} is the voltage step applied to the circuit and also the steady-state voltage across the capacitor.

If the clamp circuit is connected across the filter capacitor, the effect is that the equivalent capacitance in the LC circuit is increased while the clamp voltage is below the voltage level across the capacitor of the L-C filter. The voltage overshoot is determined by making the oscillating energy equivalent in both conditions: without and with the clamp circuit connected, in the initial condition presented before.

$$\frac{C_{in} \cdot U_{step}^{\ 2}}{2} = \frac{(C_{in} + C_{clamp}) \cdot (U_{\max} - U_{step})^2}{2} \tag{4.8}$$

$$\frac{C_{clamp}}{C_{in}} = \frac{1}{\left(\frac{U_{\max}}{U_{step}} - 1\right)^2} - 1 \tag{4.9}$$

Imposing a maximum admissible overvoltage level, *e.g.* U_{max}/U_{step} = 1.4, the same as in the previous numerical example, the clamp capacitor value is found: $C_{clamp} > 5.25 C_{in}$. A simple simulation in Simcad® validates (4.9) and clearly shows the clamping effect, depending on the initial voltage of the clamp capacitor. The simulation results are presented in Fig. 4.9.

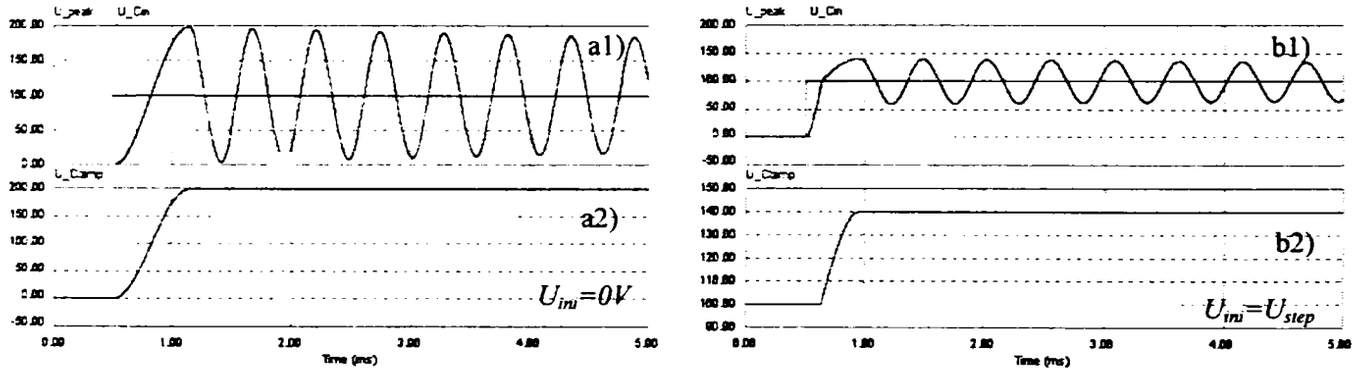

Fig. 4.9: The response of an L-C filter (L_{in}=1.2mH, C_{in}=6μF) with clamp circuit added (C_{clamp}=30μF) to a step voltage (U_{step}=100V), depending on the initial condition (U_{ini})

The clamping is effective when the clamp capacitor is already charged with the peak nominal voltage, as shown in Fig. 4.9b1 and Fig. 4.9b2. In case the clamp capacitor is initially discharged, the oscillating energy will increase, causing higher current peak and no improvement in the transients is obtained, as is presented in Fig. 4.9a1 and Fig. 4.9a2.

This method to reduce the overvoltage level caused by input voltage disturbance (step voltage) give smaller values for the reactive elements than (4.5). Also if the input filter capacitors are minimized, a smaller value for the clamp capacitor is obtained because the overvoltage depends on the C_{clamp}/C_{in} ratio.

4.2.3 Methods to mitigate overvoltages caused by the power grid transients in conjunction with the input filter

As was presented before, there are three ways to reduce the overvoltage level caused by the input filter, all reducing the L-C oscillating energy:

- by increasing the circuit resistance with series damping resistors, higher than the critical resistance (4.1);
- by-passing the input filter inductance during voltage disturbance;
- by using a large clamp capacitor in order to cut-off a higher amount of the oscillating energy, limiting the overvoltage level;

The first method is suitable for the matrix converter power-up situation. This eliminates completely the transient, but after power-up, the damping resistors should be by-passed in order to avoid higher power loss. The principle diagram is presented in Fig. 4.10a. The disadvantage is that the by-pass relay should be able to handle the nominal current of the converter continuously.

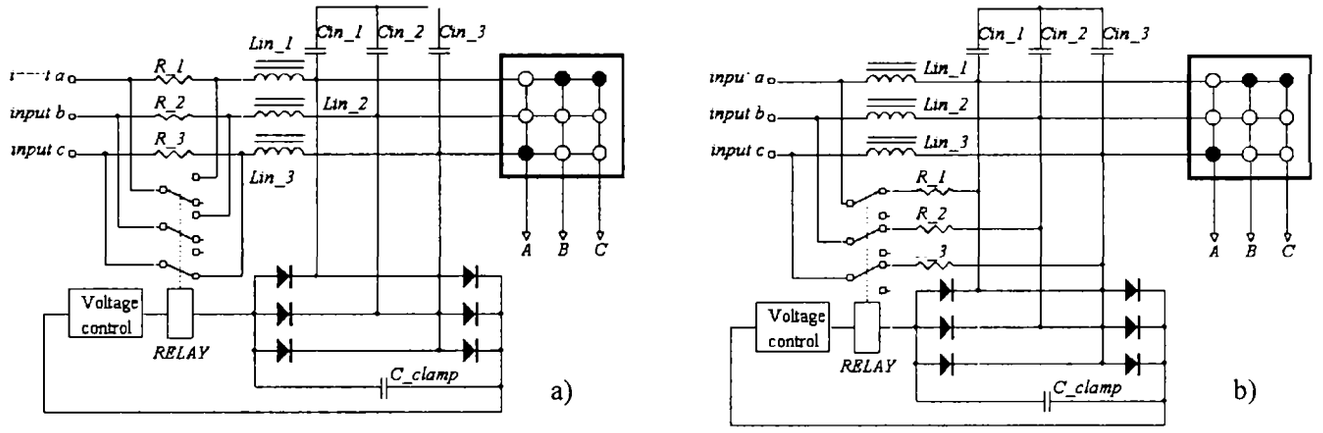

Fig. 4.10: Power-up circuits for matrix converters: a) using series damping resistors; b) using parallel damping resistors

The voltage across the clamp capacitor controls the by-pass relay, which has normal open (NO) armatures: if the voltage is low, the relay is de-energized, therefore the damping resistors are introduced in the main circuit, in series with the filter inductance. The value of the series damping resistors should satisfy (4.1), in order to eliminate the transients.

The second method consists in reducing the level of oscillating energy, which accumulates in the filter inductance during the transients, by-passing the inductors with parallel damping resistors. The principle diagram is presented in Fig. 4.10b. The value of the damping resistors should be smaller than the reactance of the choke, calculated at the cut-off frequency ω_0 of the input filter.

$$R << \omega_0 \cdot L_{in} \tag{4.10}$$

The voltage across the clamp capacitor controls the relay. If the voltage is low, the relay is de-energized and the normal closed (NC) armatures introduce the damping resistors in the circuit, by-passing the input filter inductance. If the voltage increases above a certain level, the relay is energized and the damping resistors are disconnected. The relay contacts are used only during the power-up. The in-rush current into the clamp circuit is higher, but is similar to the situation when no overvoltage reduction scheme is used, as is shown in Fig. 4.12, where all three situations are simulated. In this case, the disadvantage is that the diodes from the clamp circuit should be able to handle large currents during power-up.

If no neutral current flows in the input filter circuit, it is possible to simplify these schemes, by damping the input filter only in two phases, as is shown in Fig. 4.11a for series damping situation and in Fig. 4.11b for a parallel damping situation. The circuit becomes asymmetric, influencing the transient in the third phase by reducing the overvoltage level. Therefore, the value of the damping resistors has to be calculated differently.

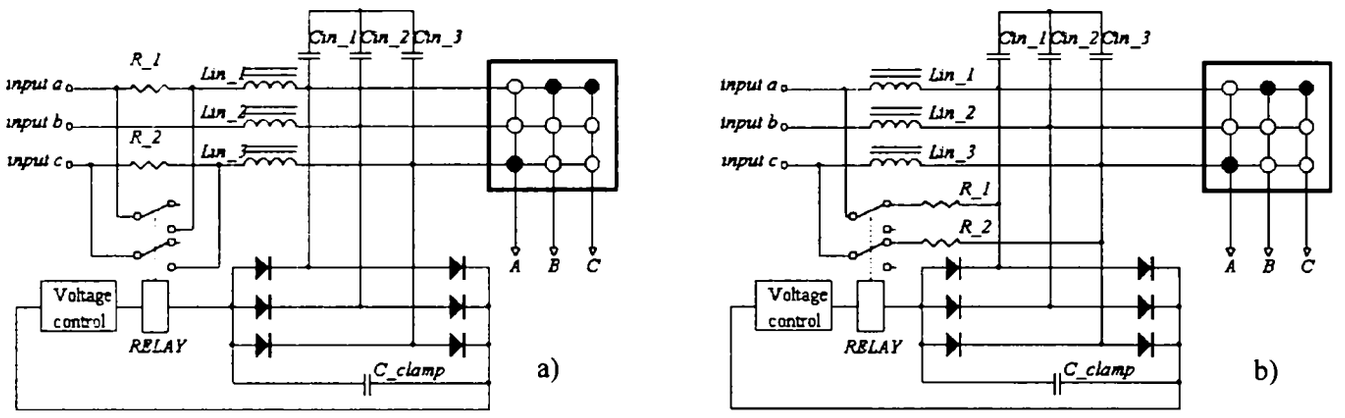

Fig. 4.11: Economical version of the power-up circuits for matrix converters: a) using series damping resistors; b) using parallel damping resistors

In the case of a series damping, the value of the damping resistors should satisfy the following condition, in order to eliminate the overvoltages, considering the higher line-to-line voltage between *input_a* (or *input_c*) and *input_b*, the equivalent inductance ($2L_{in}$) and the equivalent capacitance ($C_{in}/2$):

$$R \geq 4\sqrt{\frac{L_{in}}{C_{in}}} \tag{4.11}$$

Simulations in Simcad® show the matrix converter performing the power-up procedure in the worst connecting conditions, for the asymmetric topologies of the power-up circuit presented in Fig. 4.12. The same configuration of the input filter, as used in the previous simulations, is considered: C_{in} = 6 μF, L_{in} =1.2 mH, C_{clamp} =30 μF. The figures present the input filter capacitor voltages U_{in_1}, U_{in_2}, U_{in_3}, the clamp capacitor voltage U_{clamp} that "memorize" the maximum line-to-line voltage and the clamp capacitor current in the most affected line I_{clamp}, showing the stress of the diodes from the clamp circuit during power-up. The simulation have been made considering the voltages U_{in_1}, U_{in_2}, U_{in_3} with 0°, 120°, 240° initial angles in the power-up moment, applied to *input_a*, *input_b*, *input_c*.
Three situations are considered, as follow:

- no overvoltage reduction scheme employed (Fig 4.12a);
- employing a series damping scheme (Fig. 4.12b), with two resistors ($R_1 = R_2 = 60\ \Omega$);
- employing a parallel damping scheme (Fig. 4.12c), with two resistors ($R_1 = R_2 = 5\ \Omega$).

A solution to reduce the risk of damaging the clamp diodes when the parallel-damping scheme is used, is to oversize the diode on the phase, which is not by-passed. However, saturation of the input filter choke reduces the current peak, as it will be further shown.

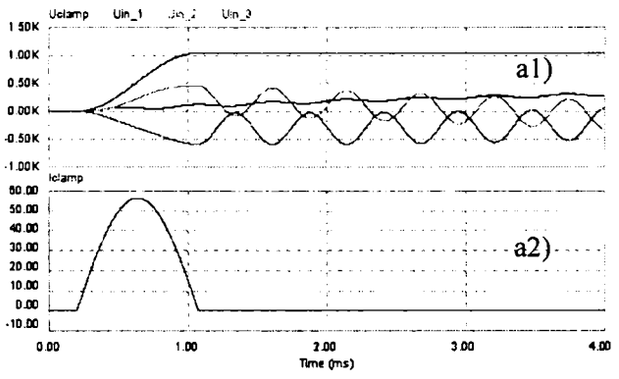

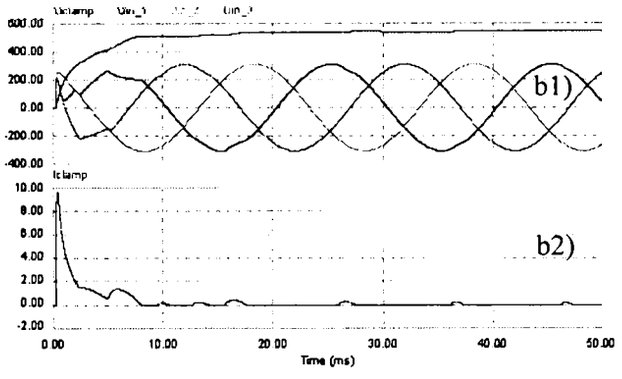

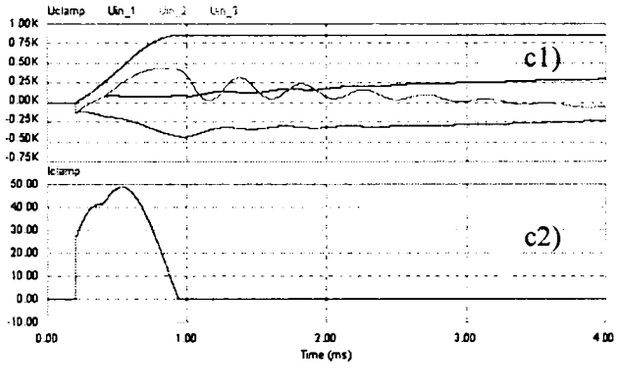

Fig. 4.12: Matrix converter power-up:

a) without overvoltage reduction circuits:
a1) U_{clamp}=1050 V_{max}; a2) I_{clamp}=56 A_{max};

b) using two series resistors (60Ω):
b1) U_{clamp}=548V_{max}; b2) I_{clamp} = 9.5 A_{max};

c) using two by-pass resistors (5Ω):
c1) U_{clamp}=853V_{max}; c2) I_{clamp}=49 A_{max};

4.2.4 Saturation effect of the input filter choke

In order to investigate the influence of the choke saturation in the input filter transient, a simulation in TurboPascal® was developed, due to the fact that simulation programs for electric circuits used in the previous examples, as Simcad®, have no possibility to define a custom characteristic for a saturated inductance. The simulation program resolves the equations of the R-L-C circuit by considering in each sampling moment different values of the inductance. This depends on the current, which flows through the choke, and was previously defined as a table. Simulations are performed considering zero voltage in the filter capacitors and zero current in the choke filter, as initial conditions, while the choke inductance is constant or is affected by saturation. Two situations are taken into account:

- the clamp circuit is not connected in parallel to the filter capacitor;
- a clamp circuit (C_{clamp}=5·C_{in}) is connected in parallel to the filter capacitor and initially charged, to simulate a power interruption disturbance;

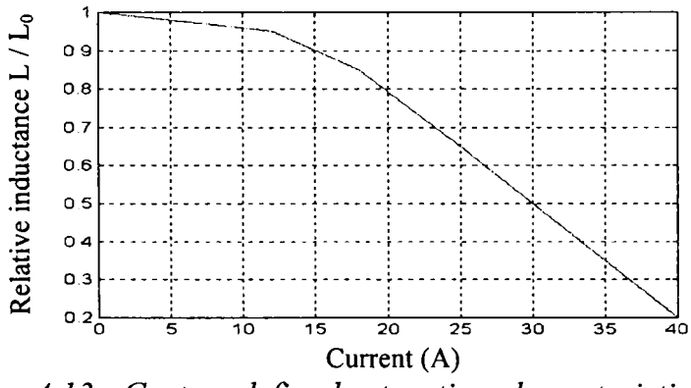

Fig. 4.13: Custom defined saturation characteristic used in the simulation (choke rated current: 8 A_{RMS})

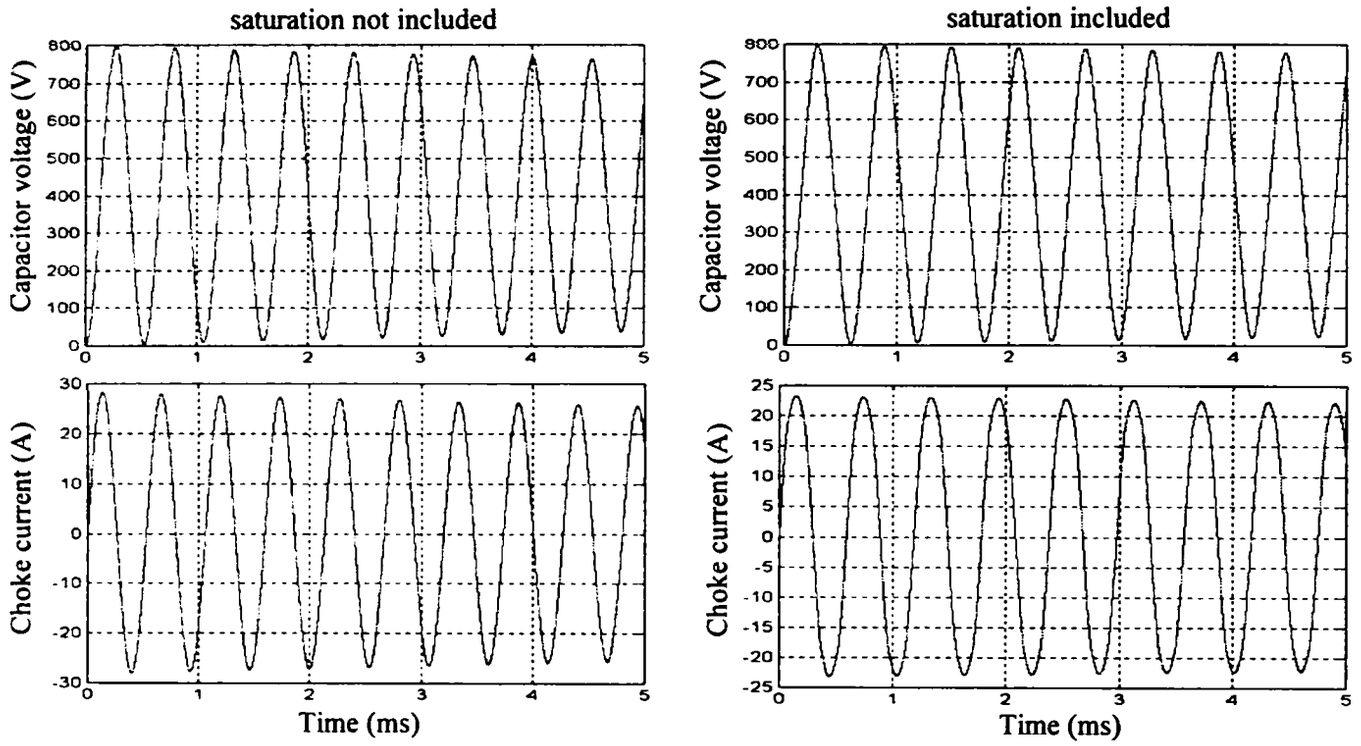

Fig. 4.14: Influence of the choke saturation in the transient response of an R-L-C circuit (0.05 Ω, 1.2 mH, 6 μF) to a voltage step (400 V) without clamping: unsaturated (U_{max} = 797.8 V, I_{max} = 28.2 A) and saturated (U_{max} = 798.1 V, I_{max}=23.3 A)

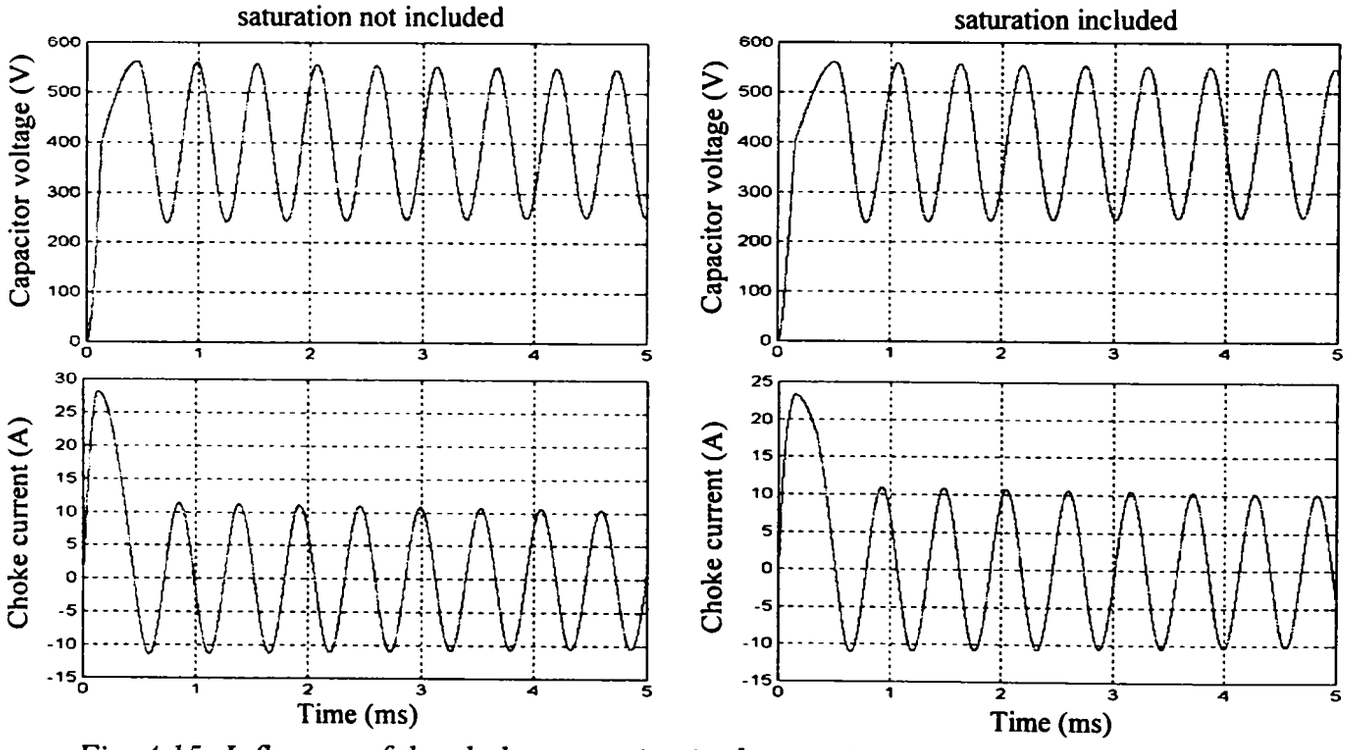

Fig. 4.15: Influence of the choke saturation in the transient response of an R-L-C circuit (0.05 Ω, 1.2 mH, 6 μF) to a voltage step (400 V) with clamping (C_{Clamp} = 5 C_{in}, U_{ini} = U_{step}): unsaturated (U_{max} = 561.7 V, I_{max} = 28.2 A) and saturated (U_{max} = 562.0 V, I_{max}=23.3 A)

The saturation characteristic of the choke has been defined, considering the input filter designed for a 5kW input power, which has a nominal current of 8 A_{RMS}. Both situations show that there is no improvement in reducing the overvoltage level when the choke saturation is taken into account, but the current peak during transient decrease with 14.5%. The reason is that when the choke starts to saturate, energy stored in the magnetic field remains constant. Therefore, is less energy to oscillate in the reactive elements. Small variations in the maximum voltage values are caused by different losses in the choke resistance, caused by different value of the currents.
The reduction in the current peak due to choke saturation may be taken into account when the auxiliary elements, as the diodes in clamp circuit or the relay, are sized.
An another aspect, which may influence transients in the input filter, is the increasing of the choke resistance due to the skin effect, because the transients are characterized by higher frequency, causing an increase of the R'/R_K ratio. Therefore, the overvoltage level decrease, as was shown in the previous section. However, the chokes has to be designed in order to reduce losses caused by the high frequency ripple in the input current, so the increasing of the choke resistance at frequencies (f_0) below the switching frequency should not important.

4.3 SIZE REDUCTION OF THE INPUT FILTER IN LOW POWER MATRIX CONVERTER

According to the previous proposals, the possibility to reduce the size of the input filter is investigated, in order to reduce the price and the volume of the matrix converter.
The input filter is used to improve the input current waveform by reducing the high-harmonics content. It is desired to have sinusoidal and balanced input currents in order to have a friendly interaction with the grid. In this way, the trajectory of the input current vector will become circular. If the input currents are unbalanced, the trajectory becomes elliptic. If high order harmonics are present into the input currents, the trajectory of the input current will show a circular envelope. The envelope thickness depends on the current ripple magnitude. By improving the filtering, the envelope thickness of the input current vector decreases.
The Clarke transformation, from a three-phase system (*a-b-c* coordinates) to a two-phase system (α-β coordinates), is widely used in electrical engineering, with implications in reducing the computation effort. If the input currents are transferred into the α-β coordinates (4.12)-(4.13), only two chokes to filter the two currents i_α and i_β are required in order to reduce the input current vector envelope.

$$i_\alpha = i_a; \tag{4.12}$$

$$i_\beta = \frac{i_b - i_c}{\sqrt{3}}; \tag{4.13}$$

4.3.1 Low-cost input filter implementation

No change is required to filter the α coordinate current, but a special configuration to filter the β coordinate current is required. However, the filter will use only two choke cores. One is a normal choke, but the other one will have two windings, as shown in Fig. 4.16. Because a common core is used for the phase *b* and phase *c* windings, an interaction between the phase currents is expected to appear, with the effect in the leveling the current ripple on phase *b* and phase *c* and a small asymmetry on the phase voltages.

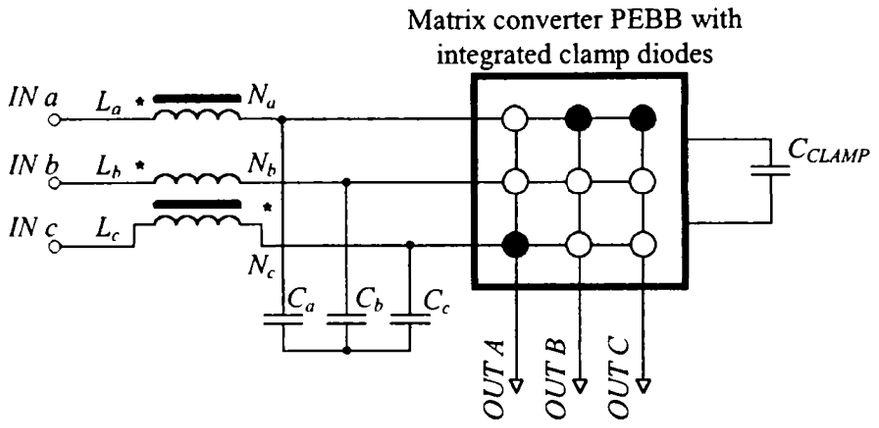

Fig. 4.16: Proposed configuration of a low-cost low volume input filter for matrix converter

If the same core section is chosen for the second choke (β), the number of turns should be decreased (same magnetic energy) to avoid saturation:

$$N_B = N_C = \frac{N_A}{\sqrt[4]{3}} \text{ [turns]} \tag{4.14}$$

If the same phase inductance is chosen, the core section should be increased corresponding to a higher energy stored into the core, but the number of turns decreases:

$$A_{L-\beta} = \sqrt{3} \cdot A_{L-\alpha} . \text{ [nH/turns}^2\text{]} \tag{4.15}$$

However, both situations produce a smaller size of the input filter chokes.

4.3.2 Experimental evaluation of the low-cost input filter

The proposed input filter is tested on a 8.5 kVA matrix converter prototype which uses three specially designed 3∅-1∅ power modules (1200V/25A), already reported in [4.3], [4.4]. The standard version of the input filter uses three star-connected capacitors of 6μF/250Vac and 1.4 mH/10A industry manufactured inductors. The inductance for the α coordinate core that corresponds to phase *a* was one of the inductors used in the test with the standard input filter and the new inductor for the β coordinate was built using an U+I ferrite core of 8.25 cm^2 with 1 mm total airgap. The inductance for the two β coordinate windings was chosen 0.95 mH in order to have the same energy stored into the core (4.14). The frequency characteristics of the inductors are presented in Fig. 4.16. The matrix converter operates with full input voltage and with 4 kHz

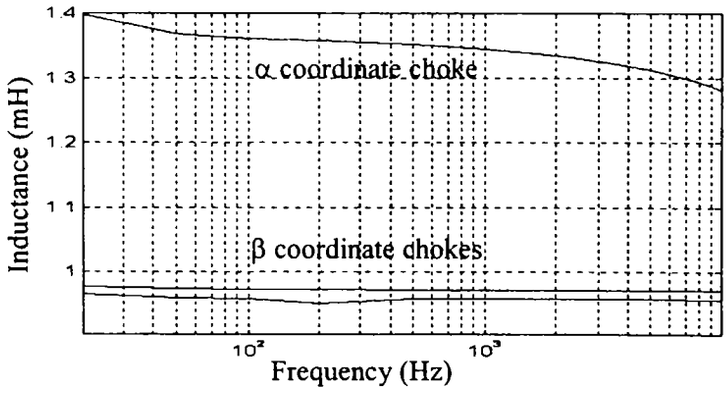

Fig. 4.17: The inductance of the two chokes vs. frequency

switching frequency. The modulation uses a double-sided SVM with minimized number of commutations [4.12] and the commutation of the bi-directional switches inside the 3∅-1∅ power module is performed in 4-steps depending on the output current sign [4.4], [4.5].
The test consists of driving a 4 kW-induction motor (see Appendix 4.1 for the motor parameters) at 30 Hz and 50% load torque by using three inductors in standard input filter configuration or by using the proposed input filter topology, with the same input filter capacitors. The input currents have been acquired by using Hall transducers and a 4-channel TDS3014 (Tektronix) oscilloscope with built-in FFT function and monitored by a three-phase power analyzer PM3000A (Voltech).
Fig. 4.18 shows the output line-to-line voltage at a 30 Hz output frequency and the FFT analysis. High order harmonics are present in the output voltage spectrum with a multiple of the switching frequency (4 kHz). Fig. 4.19 shows the output current and FFT analysis in the same test condition.
Fig. 4.20 and Fig. 4.21 compare the input phase voltage U_a and the three input phase currents I_a, I_b, I_c in two situations: using the standard and the proposed input filter. The current ripple on phase *a* is higher for the proposed input filter topology, caused by the circuit asymmetry and by the mutual coupling between phase *b* and *c*, which cancel the noise in β coordinate, but increase the noise in α coordinate, despite of the higher phase inductance.
Fig. 4.22 and Fig. 4.23 show the locus of the input current vector that corresponds to the currents presented in Fig. 4.20 and Fig. 4.21. In Fig. 4.23 the higher ripple on phase *a* causes an asymmetric envelope of the input current vector on the α-coordinate.

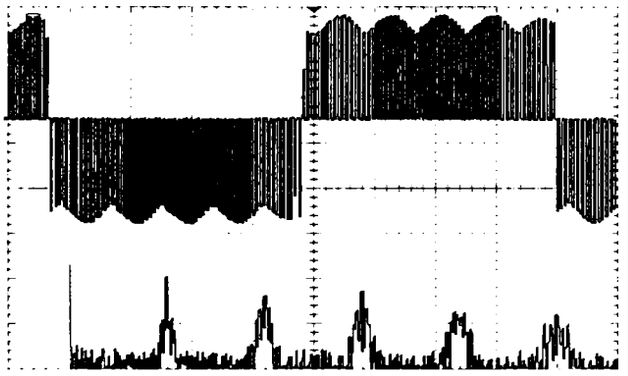

Fig. 4.18: The output line voltage (250 V/div, 4 ms/div), and FFT (20 dB/div, 2.5 kHz/div) at 30 Hz output frequency

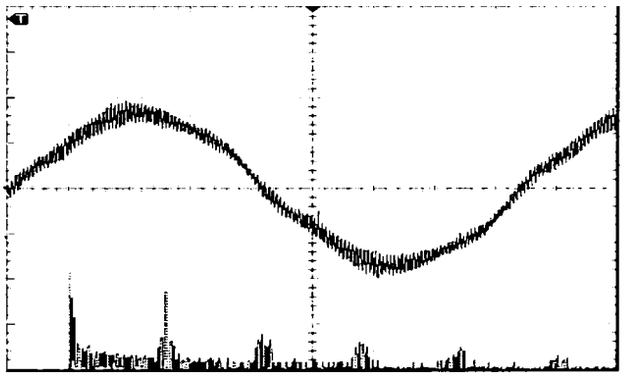

Fig. 4.19: The output current (5 A/div, 4 ms/div), and FFT (20 dB/div, 2.5 kHz/div) at 30 Hz output frequency

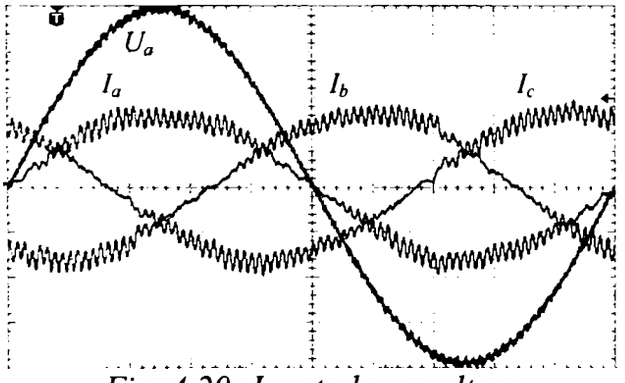

Fig. 4.20: Input phase voltage U_a (80 V/div) and the three input currents I_a, I_b, I_c (2.5 A/div) vs. time (4 ms/div) (standard input filter topology)

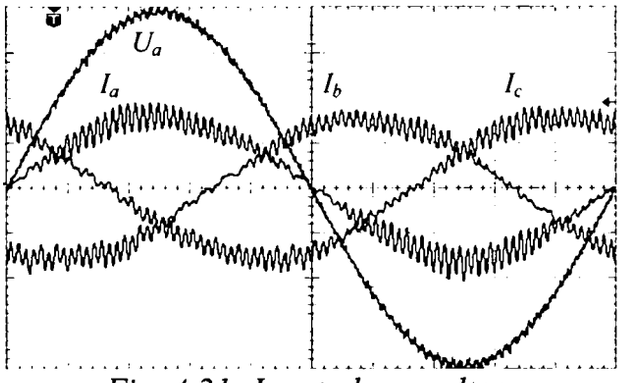

Fig. 4.21: Input phase voltage U_a (80 V/div) and the three input currents I_a, I_b, I_c (2.5 A/div) vs. time (4 ms/div) (proposed input filter topology)

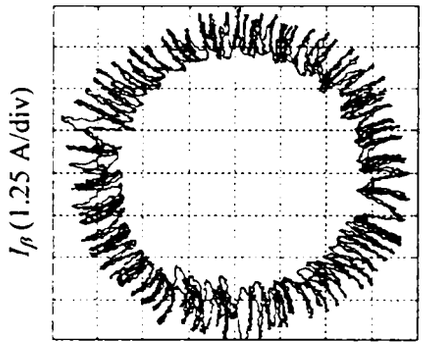

Fig. 4.22: Input phase current locus (standard input filter topology)

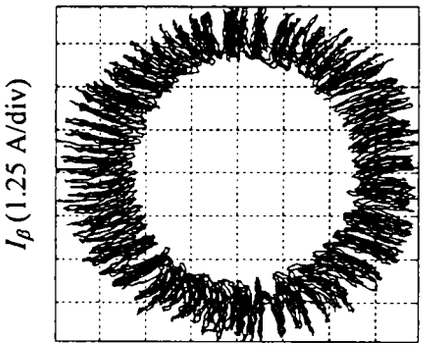

Fig. 4.23: Input phase current locus (proposed input filter topology)

The input phase currents and the corresponding FFT analysis are presented in Fig. 4.24 and Fig. 4.25. Excepting phase *a* where the harmonic content is slightly higher, the harmonic spectrum on phase *b* and phase *c* are similar.

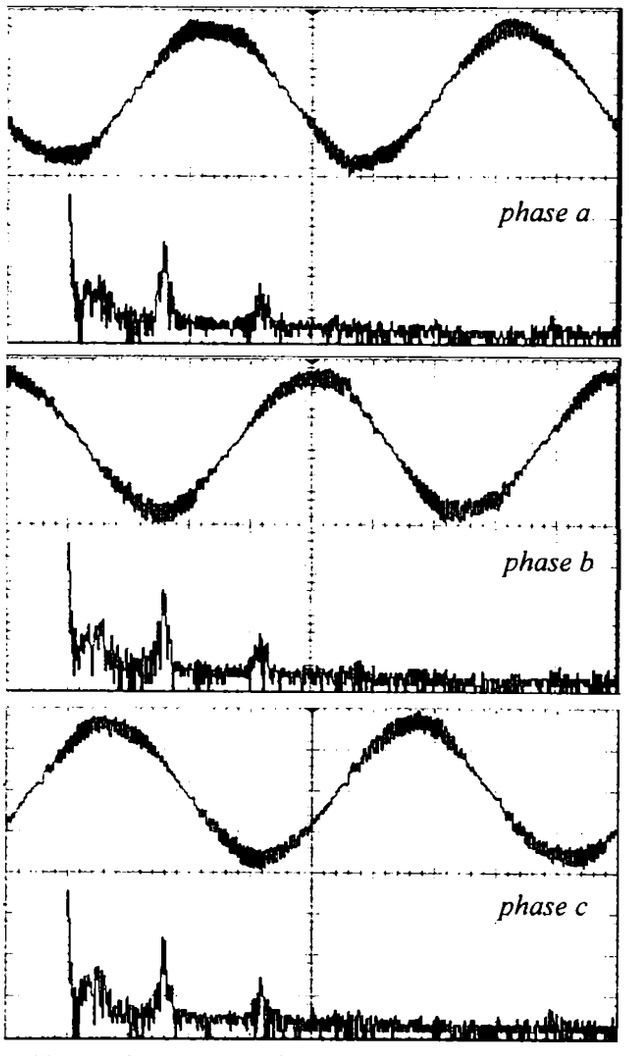

Fig. 4.24: Input phase currents (2.5 A/div, 4 ms/div) and FFT (20dB/div, 2.5 kHz/div) (standard input filter topology)

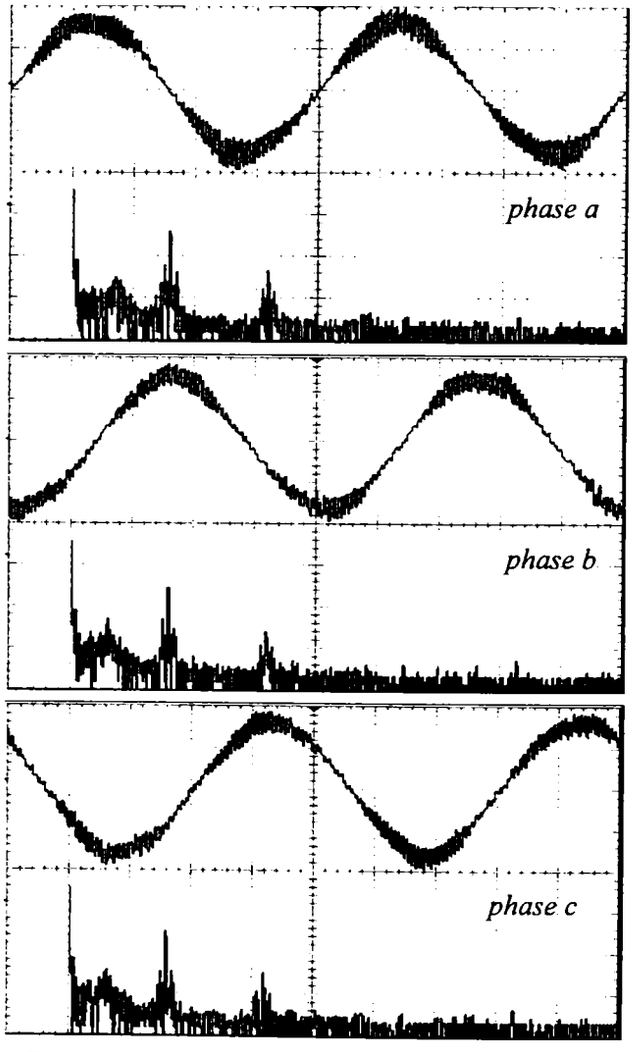

Fig. 4.25: Input phase currents (2.5 A/div, 4 ms/div) and FFT (20dB/div, 2.5 kHz/div) (proposed input filter topology)

Measurements on the input side are presented in Table 4.2, which compare the performance of the two input filter topologies. For the THD calculation, the power analyzer uses 99th harmonics. This means that the current harmonics, which correspond to the switching frequency, are included in the THD calculation. It is shown that a higher current THD on phase *a* appears when the proposed input filter topology is used.

Table 4.2
Comparative measurements on the input side of the matrix converter

	Standard input filter configuration			*Proposed input filter configuration*		
	phase *a*	phase *b*	phase *c*	phase *a*	phase *b*	phase *c*
U [V_{rms}]	219	219	219.1	219	219	219.2
I [A_{rms}]	3.19	3.15	3.14	3.16	3.11	3.12
P [W]	694	682.2	681.3	679	673.3	677
Q [Var]	92	90	91.3	128.8	104	102.8
U_{THD} [%]	1.5	1.2	1.2	1.6	1.35	2
I_{THD} [%]	13	12.8	12.8	18.1	14.8	14.8
Power Factor	0.991	0.991	0.991	0.982	0.988	0.988

SUMMARY

In this chapter a topology of a PEBB for matrix converters is proposed, as a first step to increase the reliability, by integrating the protections and the bi-directional switch commutation. Therefore, protection issues in a matrix converter are discussed, showing that the integration should take into account the design of the gate-driver board.
A new low-cost topology to dispose the matrix converter IGBT's, suitable for the low power range, is proposed. This is based on a new configuration of the bi-directional switches, suitable for integration in a three-phase to one-phase power module. In this way reduction of the insulated power supplies to a count of three and reduction of the clamp diodes to a count of six is achieved.
Solutions to mitigate overvoltages induced by the presence of an L-C topology on the input side, as well as the necessity of clamping in the input side, are discussed. It is shown that a power-up circuit is necessary to eliminate the overvoltage risk. Auxiliary effects, as saturation of the input filter choke and interaction input filter – clamp circuit, are presented.
A solution to reduce the size of the input filter chokes is proposed, based on the observation that in α-β coordinates only two currents should be filtered. This solution allows for the reduction of the input filter size. Experimental results show that by using only two cores, the input current waveforms and THD are similar, compared to the standard topology. The two proposed solutions constitute steps towards implementation the matrix converters in the low-power range for industry applications.

APPENDIX 4.1:

Type: MBT 112M (ABB), P_n = 4 kW; U_n= 380 V(Δ); I_n = 7.9 A; cos φ_n = 0.9; n_n = 2880 rpm;

REFERENCES:

[4.1] C. Klumpner, P. Nielsen, I. Boldea, F. Blaabjerg, "*New steps toward a low-cost power electronic building block for matrix converters*", Proc. of IAS Annual Meeting, vol. 3, pp. 1964-1971, 2000.

[4.2] C. Klumpner, I. Boldea, F. Blaabjerg, "*The matrix converter: Overvoltages caused by the input filter, bidirectional power flow, and control for artificial loading of induction motors*", Electric Machines and Power Systems Journal, vol. 28, no. 2, pp. 129-142, Taylor & Francis Group, 2000.

[4.3] J.D. Van Wyk, F.C. Lee, "Power electronics technology at the dawn of the millennium – status and future", Proc. of PESC'99, paper 1.1 (plenary), CD-ROM version, 1999.

[4.4] P. Nielsen, "*The matrix converter for an induction motor drive*", Industrial Ph.D. Fellowship EF 493, ISBN 87-89179-14-5, Aalborg University, Denmark, August 1996.

[4.5] P. Nielsen, F. Blaabjerg, J.K. Pedersen, "*Novel solutions for protection of matrix converter to three phase induction machine*", IEEE/IAS Annual Meeting Conference Record'97, vol. 2, pp. 1447-1454, 1997.

[4.6] J. Chang, D. Braun, "*High-frequency AC-AC converters using 3-in 1 IBPMs and adaptive commutation*", Proc. of PESC'99, pp. 351-357, 1999.

[4.7] C.L. Neft, C.D. Shauder, "*Theory and design of a 30-hp matrix converter*", IEEE Trans. on Industrial Applications, vol. 28, No. 3, pp. 546-551, 1992.

[4.8] R. R. Beasant, W.C. Beattie, A. Refsum, "*An approach to realization of a high-power Venturini converter*", Proc. of PESC'90, pp. 291-297, 1990.

[4.9] L. Empringham, P.W. Wheeler, J.C. Clare, "*Intelligent commutation of matrix converter bi-directional switch cells using novel gate drive techniques*", Proc. of PESC'98, pp. 707-713, 1998.

[4.10] N. Burany, "*Safe control of 4-quadrant switches*", Proc. of IAS Annual Meeting, pp. 1190-1194, 1989.

[4.11] A. Shuster, "*A matrix converter without reactive clamp elements for an induction motor drive system*", Proc. of PESC'98, pp. 714-720, 1998.

[4.12] P. Nielsen, F. Blaabjerg, J.K. Pedersen, "*Space vector modulated matrix converter with minimized number of switchings and feedforward compensation of input voltage unbalance*", Proc. of PEDES'96, vol.2, pp. 833-839, 1996.

[4.13] R. Chokhawala, J. Catt, B. Pelly, "*Gate drive considerations for IGBT module*", Proc of IAS Annual Meeting, pp. 1186-1195, 1992.

[4.14] V. John, B.S. Suh, T.A. Lipo, "*High-performance active gate drive for high-power IGBT's*", IEEE/IAS Annual Meeting Conference Record'98, vol. 2, pp. 1519-1529, 1998.

[4.15] L. Aftandilian, V. Mangtani, A. Dubhashi, "*Advances in power semiconductors and packaging lead to a compact integrated power stage for AC drives*", Proc. of Wescon'97, pp. 334-339, 1997.

[4.16] G. Mackert, E. Schimanek, "*Comparison of switching off an IGBT with 0V and -8V*", Proc. of PCIM'97, Power Conversion, pp. 383-384, 1997.

[4.17] J. Adams, "*Boostrap component selection for control IC's*", Design Tip DT 98-2, International Rectifier, http://www.irf.com/technical-info/designtp/dt98-2.pdf, 1998.

Chapter 5

Investigations to reduce the Input Current Ripple of a Matrix Converter Drive

This chapter deals with quality aspects involved by using different switching patterns based on Indirect Space Vector Modulation (ISVM) for matrix converters. It is known that electrical equipments connected to the power grid must comply with the EMC emission requirements in the low frequency and high frequency range. This is much critical for an electrical equipment, which uses power electronics and therefore, produces current ripple of higher magnitude in a wide frequency range. High order harmonics above 1 kHz in the filtered input current caused by the PWM switching is called current ripple and increases the THD, even though the low order harmonics (5-th to 13-th order) content is low. This ripple is caused by the specific PWM switching in the input side of the matrix converter, because this acts as a Current Source Inverter (CSI) or by resonance, caused by the second order characteristic of the L-C input filter.
In order to reduce the ripple, the influence of different factors on the ripple magnitude is simulated. The influence of the load displacement factor and the density of zero-vectors in the input current are discussed. It is proven that by increasing the number of zero-vectors in the switching period, the input current ripple at lower modulation index is notably reduced at the same number of the switch commutation per second, which means lower switching frequency. The implementation of a modulator for a matrix converter is also proposed, which is based on a microcontroller and an EPROM table. A high pulse-width resolution is achieved by using four dedicated PWM channels. The system is able to change the SVM pattern (single or two zeros per switching period) depending on the modulation index, providing a low input current ripple in the whole modulation index range.

5.1 INTRODUCTION

Since the Venturini modulation technique for matrix converter was proposed [5.1] providing sine wave in - sine wave out operation, but using a complicated mathematical model and having serious limitations in the voltage transfer ratio (0.5), improvements have been reported on the following research directions:

- to increase the voltage transfer ratio of the Venturini modulator [5.2], [5.3], [5.8];
- to propose new modulators with a simpler mathematical models [5.4] - [5.7];
- to decrease the number of sequences inside the switching period, in order to decrease the number of switch commutations per second [5.6];
- to compare different modulation strategies [5.8];
- to propose methods that improve the matrix converter sensitivity to input voltage disturbances [5.7], [5.9];

Characteristic for the research work in this area is that the effect of decreasing the number of sequences inside the switching period on the quality of the input current has not been analyzed. Also evaluation of different modulation strategies was made at the same switching frequency, without taking into account that the number of switch commutation per second was different.
The upper limit of the switching frequency for a frequency converter is given by the maximum switching losses in the semiconductor devices, as the conduction losses may be considered constant for certain load conditions. This means that it is recommended to evaluate different modulation strategies at the same number of switch commutations per second (same switch stress), although the performance in both sides, the grid and the motor, increases by increasing the switching frequency.
The matrix converter instantaneously transfers energy from one side to the other side though the matrix switches, which galvanic connect the input phases to the output phases. If the modulation strategy does not use rotating vectors, excepting the moments when a zero-vector is produced, one of the output currents given by the matrix switch state appears in two of the input phases which forms the virtual DC-link, while the other input phase remains disconnected. This situation is shown in Fig. 5.1, where an active vector (*cca*) causes a pause in the current of the input phase *b* (left side), while a zero-vector (*ccc*) causes a pause in all the input phase currents (right side).

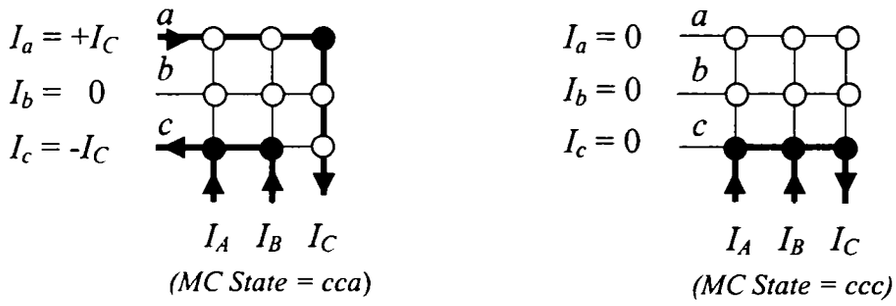

Fig. 5.1: Situations with zero currents in the input phases caused: by an active vector (left side)or by a zero-vector (right side)

Because the switching state of the converter changes many times during the switching period, the current waveform in the input phases will look as a succession of pulses. These are slides from the output currents, with pauses caused by zero vectors in all input phases or by an active vector only in the unused input phase. This is shown in Fig. 5.2 where the input currents are reconstructed from a hypothetical-switching pattern, presented in Table 5.1. The variation in magnitude of the current slides depends on the load displacement factor, while the duration of the zero vectors depend only on the modulation index.
The influence of the load displacement factor on the input current vector can be studied for two situations: ideal resistive load and ideal inductive load. Having the results, by applying the superposition principle, any particular situation can be predicted with a good accuracy.
The modulation index is fixed, imposed by the control and usually depends on the output frequency. For a given input filter and zero-vector duration the ripple may be modified only by dividing the duration of the zero-vector in few fragments and by inserting them in the switching pattern. This method is effective in the lower modulation index range where the duration of the zero-vector fragment is comparable to the fragments of output currents. In the higher range, where the duration of the zero vector decreases and becomes comparative to the clock resolution used to

quantify the pulse width of the sequences inside the switching period, errors appears and filtering becomes less effective.

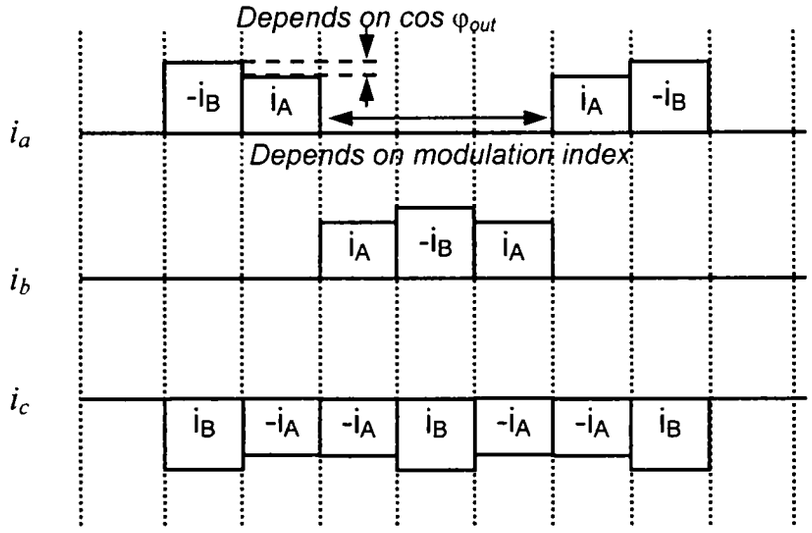

Fig. 5.2: Formation of the input current from output current slides corresponding to the switching pattern presented in Table 5.1

Table 5.1
Switching pattern and reconstructed input currents from output currents

Switching pattern	Switching state	Correspondence in input phase: a	b	c
	aaa	0	0	0
	aca	$-i_B$	0	i_B
	acc	i_A	0	$-i_A$
	bcc	0	i_A	$-i_A$
	bcb	0	$-i_B$	i_B
	bcc	0	i_A	$-i_A$
	acc	i_A	0	$-i_A$
	aca	$-i_B$	0	i_B
	aaa	0	0	0

5.2 THE INFLUENCE OF ACTIVE AND REACTIVE COMPONENTS OF THE OUTPUT CURRENT ON THE INPUT CURRENT RIPPLE

To investigate the influence of the input current ripple and the factors that determine the magnitude of the ripple, it is necessary to compare how the reactive power flows through a standard DC-link VSI and through a matrix converter.
Into a DC-link VSI the reactive power is exchanged with the DC capacitor during the freewheeling diodes conduction and no reactive exchange with the grid occurs because the input diode-bridge acts as a barrier. Into a matrix converter there is no intermediary reactive elements and the reactive energy is taken from the input filter capacitors and from the power grid. If the

matrix converter operates at cos φ_{in}=1 condition and the modulation strategy provides sinusoidal input current, all the necessary reactive power for the load is converted into high frequency input current ripple. This means a correlation between the reactive output power and the input current ripple may exist and this is further investigated.
Therefore, if an induction motor runs at no load, the output current consists of the motor magnetizing current, which is 40-60% of the rated current with 90° lagging the output phase voltage. The fundamental of the input current drawn form the grid by the matrix converter is given by the active power taken by the load, for instantaneous unitary displacement power factor, which is close to zero. The ripple in the unfiltered input current reaches the maximum level, when the power factor of the motor is low and the two slides of the output current have opposite signs, and this has to be filtered effective.
The influence of the output current displacement factor on the input current ripple is simulated using simplified conditions:

- the output currents are imposed sinusoidal and balanced without taking into account the direct transformation of the input voltages into output voltages;
- the influence of the voltage drop across the input filter chokes are neglected, therefore the input reference angle of the input current vector and the duty-cycles corresponding to the sequence pulses width are calculated using ideal supply conditions;

In this simulations the output current was imposed because:

- the purpose of this simulation is to find the correlation between the displacement angle of the output current and the ripple in the input currents, and is desired to eliminate parasitic influence as load oscillations, ripple in the output current produced by the switching frequency of the converter, unbalance or by load model errors;
- it is easy to impose custom defined conditions on the output side as: constant magnitude and variable displacement angle or constant amplitude of the reactive current component and variable displacement angle, similar to the induction motor case;

Also, the influence of the input voltage ripple when performing the direct transformation matrix to calculate the output voltages has been neglected because:

- the output currents are imposed as sinusoidal and balanced with given magnitude, and variation of input voltage does not produce any changes in the output currents;
- the only influence may be in the rectification stage of the indirect modulation model, by introducing noises in the input current angle and on the modulation index;

In both situations, the matrix converter is using the same switching pattern and modulation technique (double sided ISVM) and produces a pure three-phase sinusoidal output current of constant amplitude but variable displacement factor. The tests consists of two limit conditions: resistive output current (cos φ_{out}=1) and inductive output current (cos φ_{out}=0) and voltage and current waveforms are represented. The output phase voltage and the imposed current are shown in Fig. 5.3a (cos φ_{out}=0) and Fig. 5.3b (cos φ_{out}=1). The input phase voltage and the unfiltered current are presented in Fig. 5.3c (cos φ_{out}=0) and Fig. 5.3d (cos φ_{out}=1), which shows that the magnitude of the current ripple reaches, in both situations, the level of the output current envelope. In Fig. 5.3e (cos φ_{out}=0) and Fig. 5.3f (cos φ_{out}=1) the input phase voltage and the filtered current are presented. As expected, the fundamental component of the filtered current in the inductive load case is zero and the ripple magnitude has a lower value.

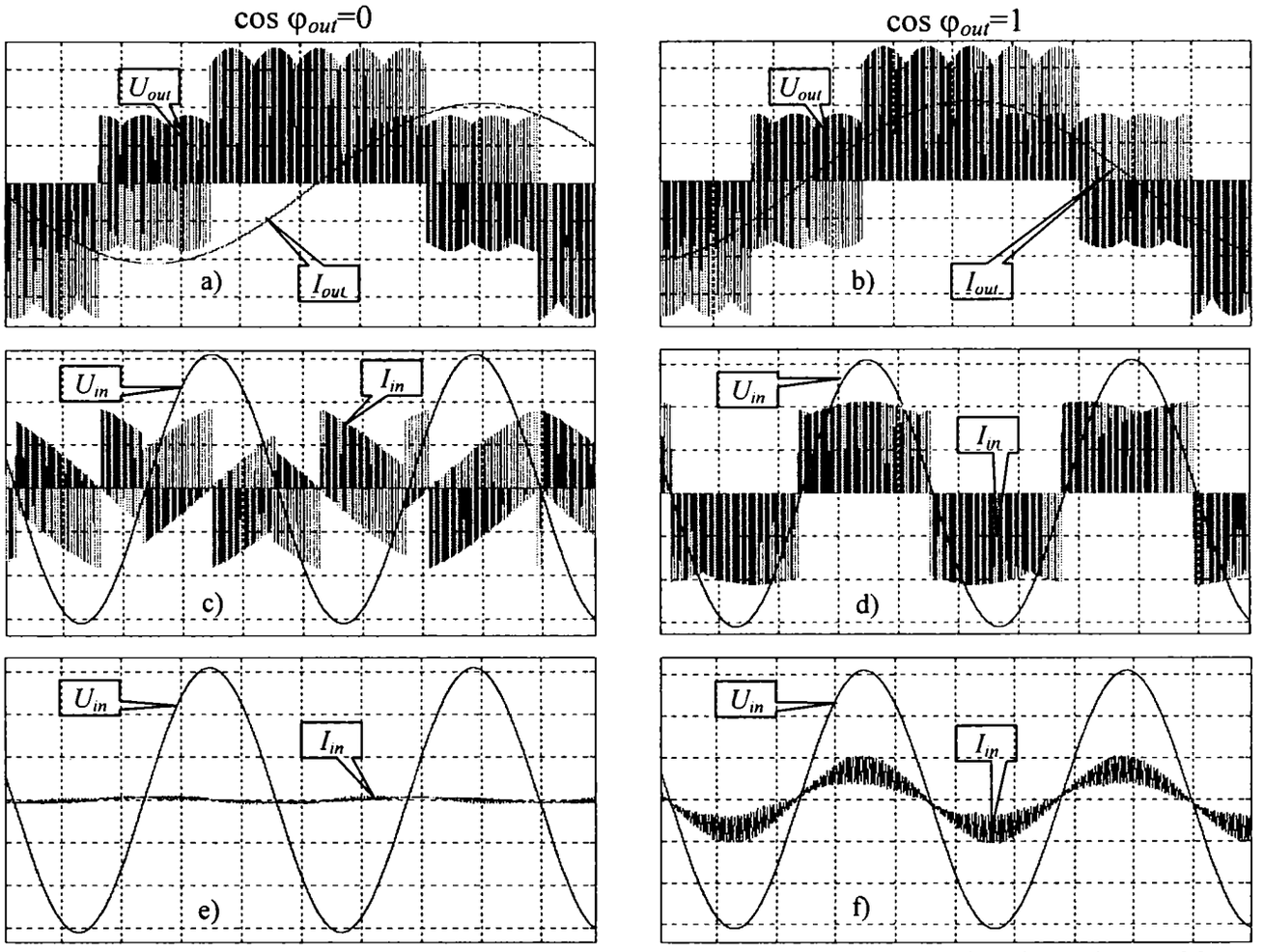

Fig. 5.3: Matrix converter operation at constant output current amplitude and variable displacement factor: a), b) Output phase voltage and current; c), d) Input phase voltage and unfiltered current; e), f) Input phase voltage and filtered current;
Simulation conditions: U_{in_f}=310 V; f_{in}=50 Hz; I_{out}=15 A; f_{out}=20 Hz; m_U=0.4;
Voltage scale 100 V/ div, current scale 10 A/ div, time scale 5 ms/div;

5.3 THE INFLUENCE OF ZERO-VECTORS ON THE INPUT CURRENT RIPPLE

A zero-vector is produced when the matrix switches are configured in a way that all the output phases are connected to a single input phase *a*, *b* or *c* as shown in Fig. 5.4. Therefore the matrix converter drew no current from the input side.

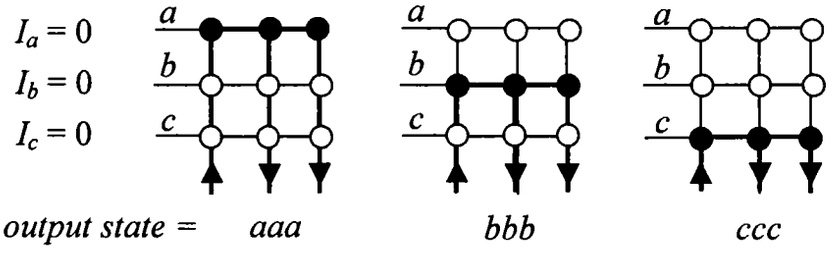

Fig. 5.4: Zero vectors switch states in a matrix converter

The effect of a zero-vector is well known. On the output stage the zero-vector duty-cycle modifies the magnitude of the output voltage vector which gives the motor flux magnitude. On the input stage the zero-vector duty-cycle modifies the magnitude of the input current vector, which gives the active power level for a constant displacement angle of the reference input current vector.
The input current ripple depends on the switching frequency seen from the input side and on the characteristics of the L-C input filter, given by the value of the capacitors and chokes. In order to reduce the size of the input filter, smaller values of the components are desired, which gives a higher cut-off frequency of the input filter. For a given input filter, resulted from prior design restrictions, the only way to decrease the input current ripple is to increase the switching frequency seen from the input side. If the input current taken by the matrix converter is considered as a succession of short current pulses, as it was presented in the previous section, the switching frequency seen from the input side is determined by the number of breaks in the unfiltered current drawn from the input filter. The most convenient situation occurs during a zero-vector when all three input currents are zero and this possibility is further investigated.
For a given modulation strategy, the number of zero-vectors n_{zero} into the switching pattern is constant. However, effort was made to reduce the number of zero-vectors, which naturally result from combining the rectification stage sequences (0-γ-δ) with the inversion stage sequences (0-α-β), in order to reduce the number of commutations inside the switching pattern, the hardware requirements for the modulator and to increase the switching frequency. In order to reduce the ripple in the input current by increasing the switching frequency seen from the input side, at constant or higher switching period to produce equal number of switch commutation per second, it is necessary to change the switching pattern by inserting zero-vectors in a convenient way. To prove the validity of this solution, two double-sided ISVM switching patterns are considered by using a combination of switching states to provide a single bi-directional switch commutation of the converter when the sequence is changed. In [5.7] it was shown this may be achieved by arranging the sequences inside the pattern in a certain way.
If the switching frequency ratio of the two patterns f_{sw_2} / f_{sw_1} is chosen to provide the same number of switch commutations per second condition (5.3), the ratio between the switching frequency seen from the input side $f_{sw\_in\_2} / f_{sw\_in\_1}$ is given by (5.4).

Pattern 1: 8 commutations/single zero-vector (0-αγ-αδ-βδ-βγ-βδ-αδ-αγ-0) (5.1)
Pattern 2: 10 commutations/two zero-vectors (0-αγ-αδ-βδ-βγ-0-βγ-βδ-αδ-αγ-0) (5.2)
$f_{sw\_2} / f_{sw\_1} = n_{comm\_1} / n_{comm\_2} = 8/10 = 0.8$ (5.3)
$f_{sw\_in\_2} / f_{sw\_in\_1} = f_{sw\_2} / f_{sw\_1} \times n_{zero\_2} / n_{zero\_1} = 1.6$ (5.4)

This means that a double sided SVM pattern with two zero-vectors per switching period should provide a higher switching frequency (+60%) on the input side compared to a single zero-vector switching pattern, even though the switching frequency of the matrix converter is lower. Other switching patterns with 3-6 zeros per switching period are investigated and the conclusions are summarized in Table 5.2. The proposed switching patterns result by fragmenting certain active vectors and by inserting a zero-vector, which provide single switch commutation. A zero vector may be inserted between two different active vectors, in this way no fragmentation is required, but one switching requires multiple switch commutations and the result regarding the number of switch commutations per second is identical with the fragmentation method, but hardware implementation requires less counter units.

Table 5.2
Possible multi-zero switching patterns in a matrix converter using ISVM

No. zeros	Possible switching patterns and timings	No. sw. commut.	f_{sw_in} (gain)
1	0-αγ-αδ-βδ-βγ-βδ-αδ-αγ t_0-t_1/2-t_2/2-t_3/2-t_4-t_3/2-t_2/2-t_1/2	8	1× (refer.)
2	0-αγ-αδ-βδ-βγ-0-βγ-βδ-αδ-αγ t_0/2-t_1/2-t_2/2-t_3/2-t_4/2-t_0/2-t_4/2-t_3/2-t_2/2-t_1/2	10	1.6× (+60%)
3	0-αγ-αδ-βδ-0-βδ-βγ-βδ-0-βδ-αδ-αγ t_0/3-t_1/2-t_2/2-t_3/4-t_0/3-t_3/4-t_4-t_3/4-t_0/3-t_3/4-t_2/2-t_1/2	12	2× (+25%)
4	0-αγ-αδ-0-αδ-βδ-βγ-0-βγ-βδ-0-βδ-αδ-αγ t_0/4-t_1/2-t_2/3-t_0/4-t_2/3-t_3/3-t_4/2-t_3/3-t_0/4-t_3/3-t_2/3-t_1/2	14	2.3× (+15%)
5	0-αγ-αδ-βδ-0-βδ-βγ-0-βγ-βδ-0-βδ-αδ-0-αδ-αγ t_0/5-t_1/2-t_2/3-t_3/4-t_0/5-t_3/4-t_4/2-t_0/5-t_4/2-t_3/4-t_0/5-t_3/4-t_2/3-t_0/5-t_2/3-t_1/2	16	2.5× (+9%)
6	0-αγ-αδ-0-αδ-βδ-0-βδ-βγ-0-βγ-βδ-0-βδ-αδ-0-αδ-αγ t_0/6-t_1/2-t_2/4-t_0/6-t_2/4-t_3/4-t_0/6-t_3/4-t_4/2-t_0/6-t_4/2-t_3/4-t_0/6-t_3/4-t_2/4-t_0/6-t_2/4-t_1/2	18	2.7× (+7%)

It is possible to increase the number of zeros per switching period and to increase the switching frequency seen from the input side even if the switching period is reduced in order to maintain the same number of switchings per second. The most significant increase in the switching frequency seen from the input side is obtained when the pattern is changed from a single zero-vector to two zero-vectors (+60%), while at more than five zero-vectors per switching period, the gain compared to the previous pattern is ineffective (+7%).
Another aspect is that for a higher number of steps it is necessary to divide each active sequence in too many fragments. As the clock resolution is not indefinitely small, this causes a decrease of the pulse width resolution and the increase of the harmonics content due to a low switching frequency. It is possible to correct the conduction duration during the switching period and actualize the sequences duration values in respect to the new measured and reference values. However, this will imply a more complicated hardware for the modulator that is not justified by the increase in performance.
Therefore, the reduction of the input current ripple with single and two zeros switching pattern is further analyzed in order to determine how the current flows through each input phase of the matrix converter (Table 5.2 and 5.3).

Table 5.3
Example of a single zero-vector switching pattern

In conduction:	aaa	aca	acc	bcc	bcb	bcc	acc	aca	aaa	Zeros
phase a*		■	■				■	■		2
phase b				■	■	■				1
phase c		■	■	■	■	■	■	■		1

Table 5.4
Example of a two zero-vectors switching pattern

In conduction:	aaa	aca	acc	bcc	bcb	bbb	bcb	bcc	acc	aca	aaa	Zeros
phase a		■	■						■	■		2
phase b				■	■		■	■				2
phase c		■	■	■	■		■	■	■	■		2

For the single zero-vector switching pattern presented in Table 5.2 there are two zeros in one of the input phases but that will change when the sectors of the reference vectors change. It is expected to have portions in the input current with smaller ripple even when a single zero-vector switching pattern is used and uniform current ripple waveform when the two-zero vectors switching pattern is used.
Below a voltage transfer ratio of 0.5, it is expected a more effective filtering of the input current, when the duration of the zero-vectors exceed the duration of active vectors.

5.4 SIMULATION STUDY THE INPUT CURRENT RIPPLE REDUCTION

In order to compare the influence on the input current ripple of two switching patterns, a simplified model of a matrix converter was simulated in a program written in TurboPascal™. The following assumptions have been taken in order to exclude non-relevant parasitic effects:

- the duty-cycles of each switching sequence are calculated using the input phase voltages, which are sinusoidal and balanced, sampled at the beginning of the switching period, without taking into account the voltage ripple across the input filter chokes;
- the output currents are forced sinusoidal and balanced (similar to a current source), with given amplitude and constant displacement to the reference output phase voltage, to eliminate any disturbance caused by an electromechanical load and to reduce the computational effort;
- the reconstruction of the input currents is made by applying in each sample period the inverse transformation to the output currents and calculating the input filter model;

In Table 5.5 the simulation conditions and setup parameters are presented. Simulations have been carried out for a fiction current source inductive load of constant current and displacement factor. The modulation index is proportional with the output frequency with the following values: 15 Hz, 20 Hz, 25 Hz, 30 Hz, 35 Hz. Waveforms including the input phase voltage, the filtered input current and the FFT of the filtered and unfiltered input current are presented only for three situations: 15 Hz (in Fig. 5.5), 25 Hz (in Fig. 5.6) and 35 Hz (in Fig. 5.7).

Table 5.5
Conditions for the matrix converter simulation with constant output displacement current angle

Electrical parameters				Input filter			Simulation parameters		
U_1	f_1	I_2	$\cos\varphi_2$	L_{in}	C_{in}	R_{in}	f_{sw} (ref)	t_{sim}	t_h
220 V_{rms}	50 Hz	8.3 A_{rms}	0.8	1.2 mH	6 µF	0.1 Ω	4 kHz	100 ms	400 ns

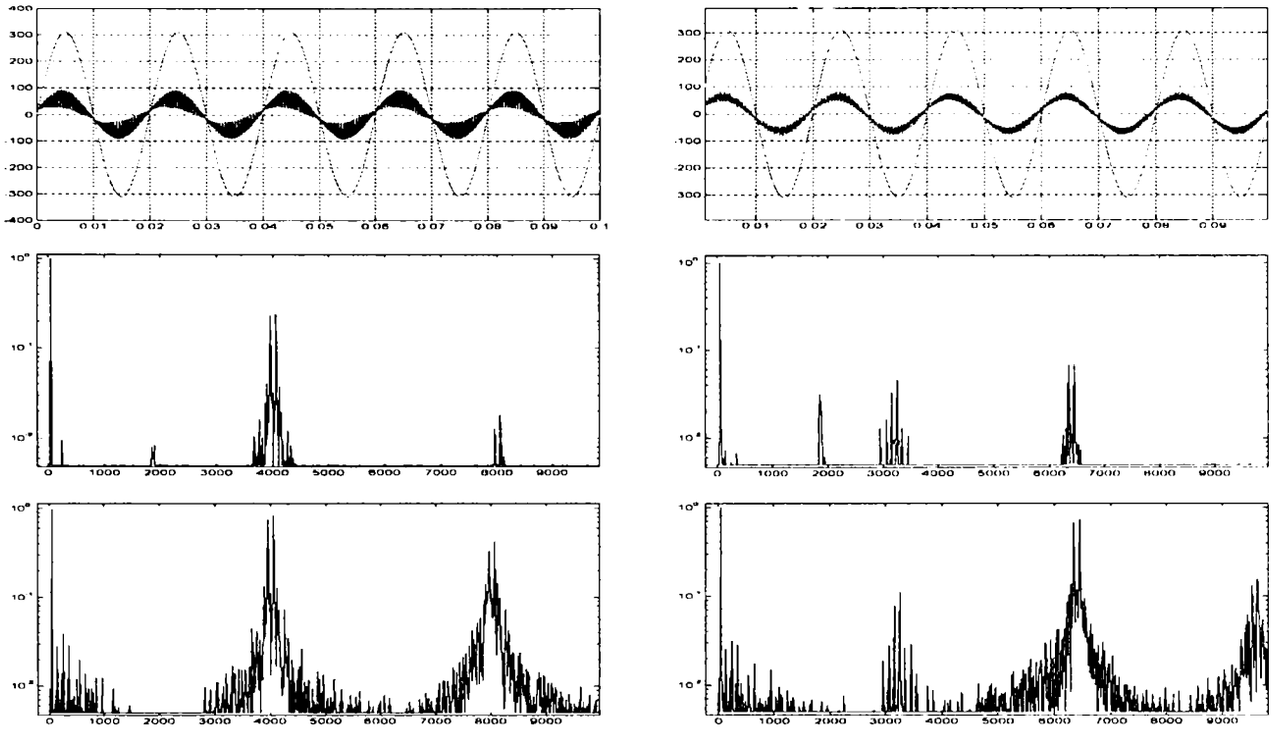

Fig. 5.5: Single-zero (left side) versus two-zeros (right side) switching pattern: a), b) Input phase voltage (V) and filtered current (0.01A) vs time (s); c), d) FFT of the filtered input current; e), f) FFT of the unfiltered input current vs. frequency (Hz)
Simulation conditions: f_{out}=15 Hz, f_{sw}=4kHz (left side) / 3.2 kHz (right side)

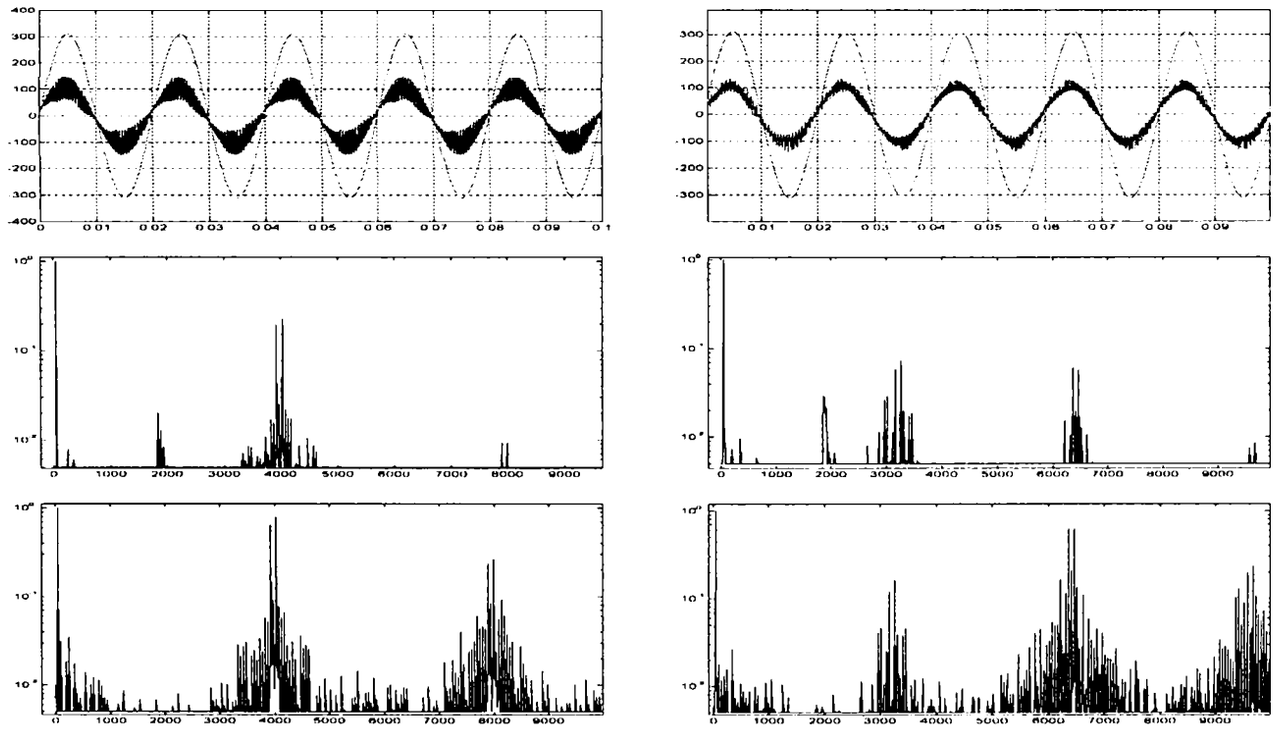

Fig. 5.5: Single-zero (left side) versus two-zeros (right side) switching pattern: a), b) Input phase voltage (V) and filtered current (0.01A) vs time (s); c), d) FFT of the filtered input current; e), f) FFT of the unfiltered input current vs. frequency (Hz)
Simulation conditions: f_{out}=25 Hz, f_{sw}=4kHz (left side) / 3.2 kHz (right side)

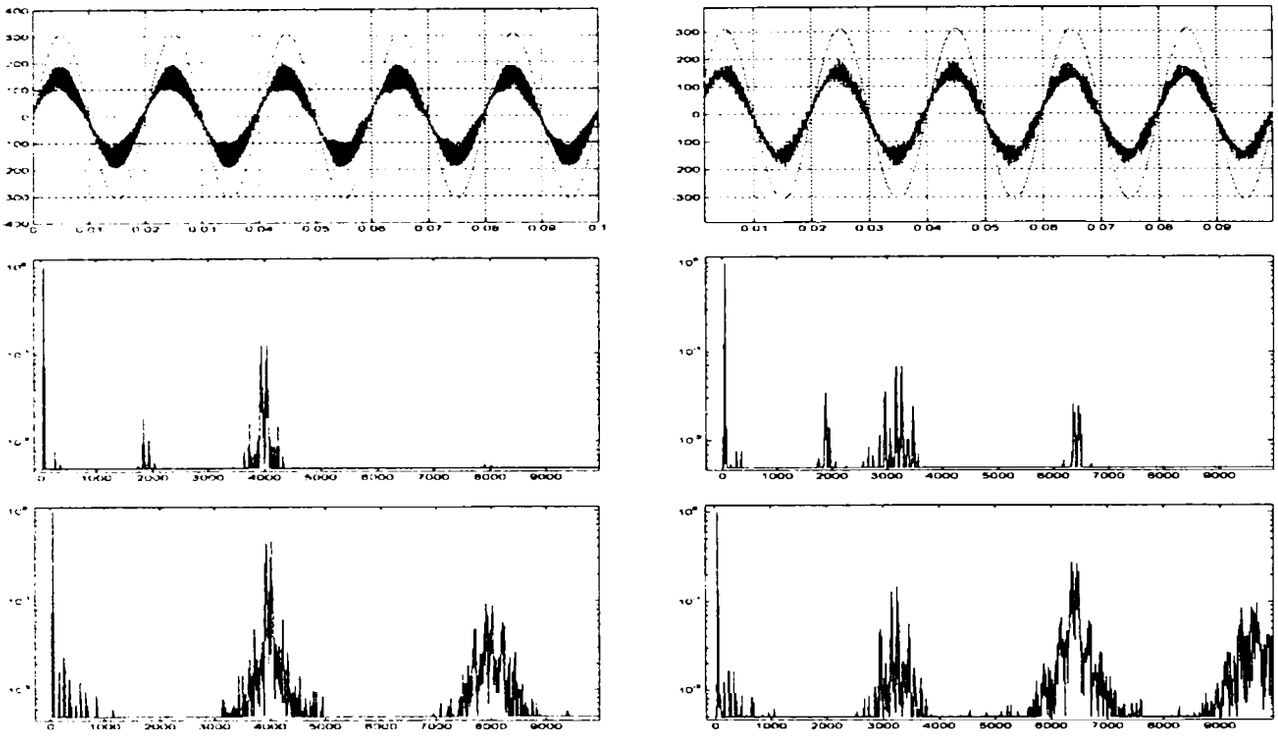

Fig. 5.5: Single-zero (left side) versus two-zeros (right side) switching pattern: a), b) Input phase voltage (V) and filtered current (0.01A) vs time (s); c), d) FFT of the filtered input current; e), f) FFT of the unfiltered input current vs. frequency (Hz)
Simulation conditions: f_{out}=35 Hz, f_{sw}=4kHz (left side) / 3.2 kHz (right side)

After filtering, in the spectrum of the filtered current appears harmonics around the input filter cut-off frequency. As the cut-off frequency is smaller than the switching frequency, the effect in the input current THD is notable, despite of the lower magnitude. The magnitude of the harmonics around the input filter cut-off frequency increases if the switching frequency decreases (similar load condition). This is summarized in Table 5.6. If the switching frequency is closer to the cut-off frequency, resonance increases and filtering becomes ineffective.

Table 5.6
Highest harmonic magnitude of the filtered current around the filter cut-off frequency

Harmonic order \ Output frequency		15 Hz	25 Hz	35 Hz
Input filter cut-off frequency (1.8 kHz)	8 pulses	0.9 %	2 %	1.8 %
	10 pulses	3.2%	3 %	3.5 %
Switching frequency	8 pulses (4 kHz)	25 %	~23 %	~13 %
	10 pulses (3.2 kHz)	~4.8 % 3.2 kHz 7 % 6.4 kHz	~8.5 %	7 %

In Fig. 5.8a and Fig. 5.8b it is shown by comparison the calculated THD for the first 40 harmonics of the filtered and unfiltered input current for the two switching patterns. The frequency range ($f <$ 2 kHz) includes the cut-off frequency of the input filter but does not include the switching frequency. In both situations the THD of the unfiltered input current decreases slowly, while the THD of the filtered current is increasing slowly.
In Fig. 5.8c and 5.8d it is shown by comparison the calculated PWHD for the 14-th to 40-th harmonics of the filtered and unfiltered input current for the two switching patterns. As the switching frequency is not included in this frequency range (700 Hz $< f <$ 2 kHz), it is clearly shown that the input filter increases the harmonic content, producing current harmonics around the L-C filter cut-off frequency.

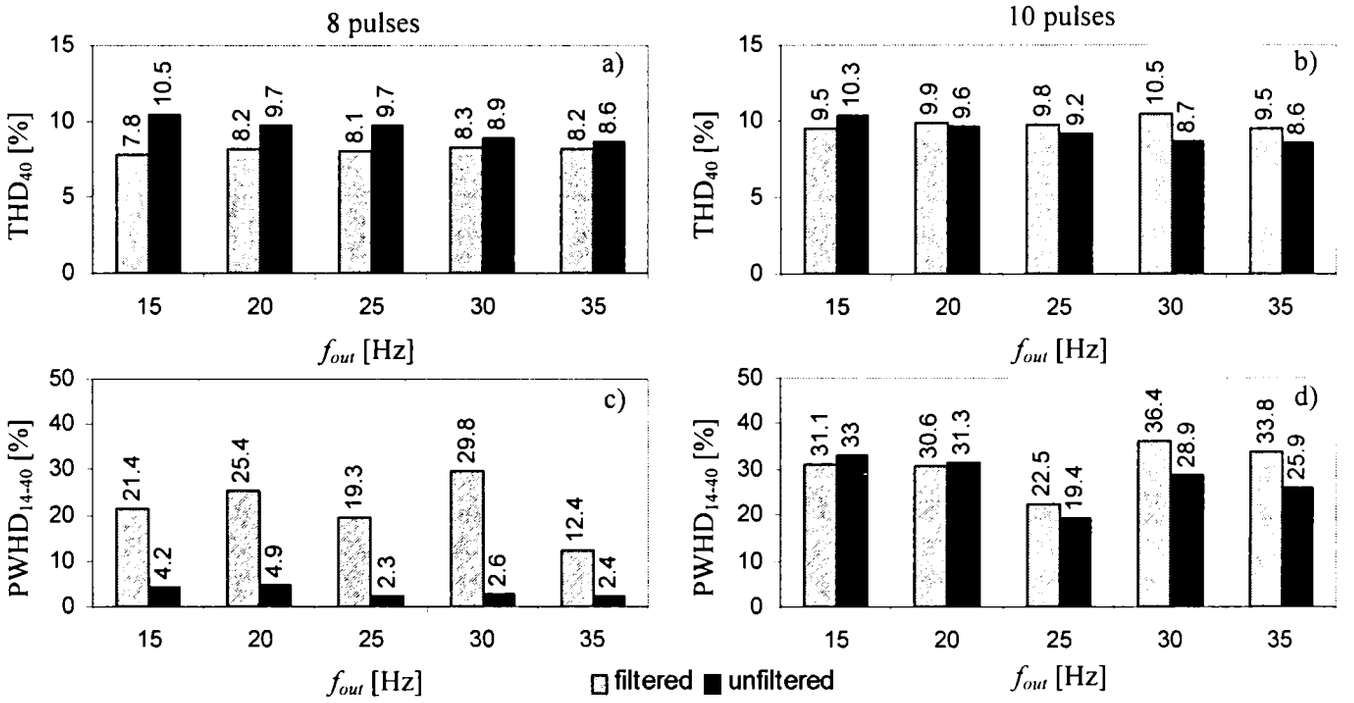

Fig. 5.8: Calculated THD and PWHD of the filtered and unfiltered input current for the single zero-vector (left side) and the two zero-vectors (right side) switching patterns

In Fig. 5.9a and Fig 5.9b shows a direct comparison of the calculated THD considering the first 40 harmonics (left side) and considering the first 100 harmonics (right side) of the filtered input current, for the two switching patterns. In the first case, the frequency range ($f <$ 2 kHz) does not include the switching frequency, but includes the cut-off frequency of the input filter (f_0 = 1.8 kHz). The THD is higher for the 10-step switching frequency because a lower switching frequency is used, causing a lower PWM synthesis resolution and a stronger interaction with the input filter. In the second case, the frequency range ($f <$ 5 kHz) cumulates the effect of the switching frequency and the cut-off frequency of the input filter. The THD is much lower for the 10-step switching pattern compared to the 8-step switching pattern and the difference decreases as the output frequency increases. This is due the fact that the THD has a decreasing variation for the 8-step switching pattern while the 10-step switching pattern causes an increasing of the THD with the output frequency.

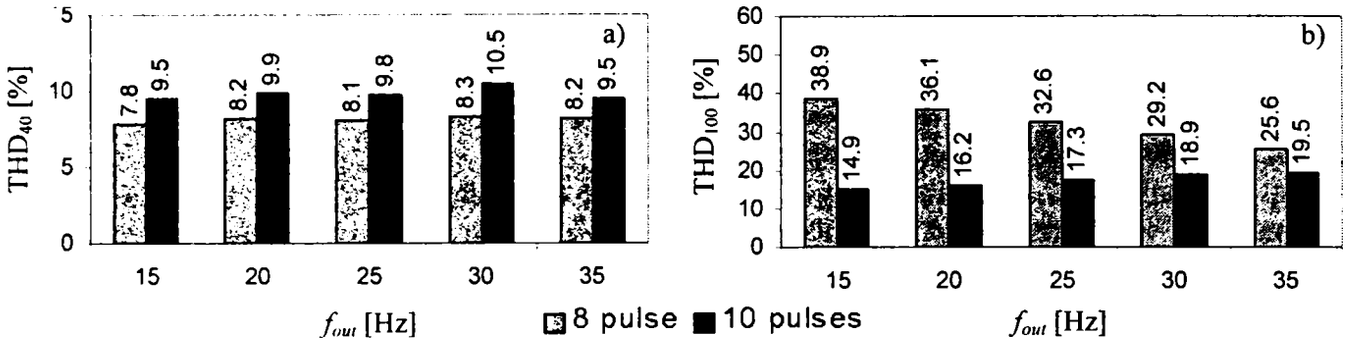

Fig. 5.9: Calculated THD for a single-zero vector and two-zero vector switching patterns: a) THD until 40-th order (left side); b) THD until 100-th order (right side);

5.5 PROPOSAL FOR A MATRIX CONVERTER SVM MODULATOR WITH INPUT CURRENT RIPPLE REDUCTION

The details about the optimal commutation pattern have been presented in [5.7] and this provides a minimum number of commutations in the matrix converter, by eliminating the double commutations. The method is implemented as a look-up table and addressed by knowing the sectors where the reference vectors (the input current and the output voltage) are placed. The optimal switching pattern has been extended to two zeros per switching period by inserting a zero-vector state following the criteria where the number of "Branch Switch Over" is minimized.
The modulator consists of an 80C167-microcontroller board and a 2 kB EPROM where the two optimal switching pattern are stored. The principle scheme is shown in Fig. 5.10.

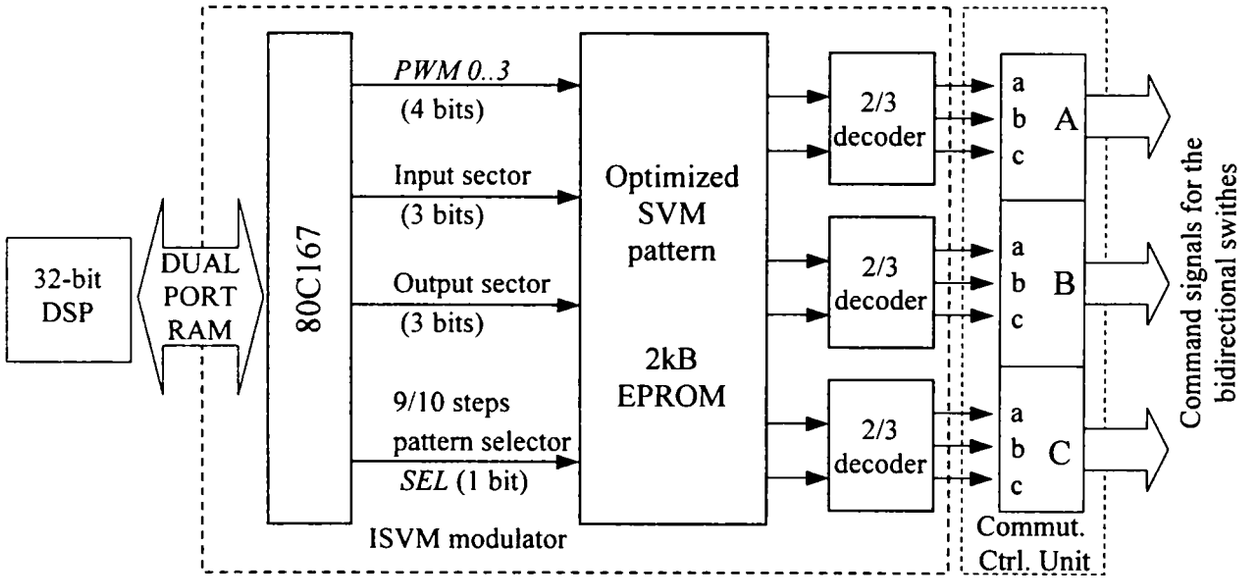

Fig. 5.10: The proposed matrix converter modulator

To provide a good resolution of the sequence pulse width into the switching period, four 16-bit PWM channels *PWM 0...3* working with 50 ns clock resolution are used. In order to obtain 9 command signals for the bi-directional switches, a 2-bit to 4-state decoder is used. In this way the

conduction of two switches that belongs to an output phase and may produce short-circuit on the input is not allowed and the implementation can use 8-bit logic IC's.
The optimal switching pattern table is stored into an EPROM and it is addressed as follows:

- 3 bits select the rectification stage sector (value from 0 to 5);
- 3 bits select the inversion stage sector (value from 0 to 5);
- 1 bit to select the appropriate switching pattern;
- 4 bits to select the current sequence inside the switching pattern;

Fig. 5.11 shows the generation of the single zero-vector and the two zero-vectors, by using the four PWM channels and the *SEL* bit. To generate a single-zero vector switching pattern, the four PWM channels must work in the symmetrical PWM generation mode (*SEL*=0) [5.13]. To generate a two zero-vectors switching pattern, the four PWM channels are configured in the standard PWM generation mode and the *SEL* bit is toggled in the middle of the switching period by the microcontroller logic. Also the content of the PWM counters is changed to assure the symmetry of the double-sided SVM pattern.

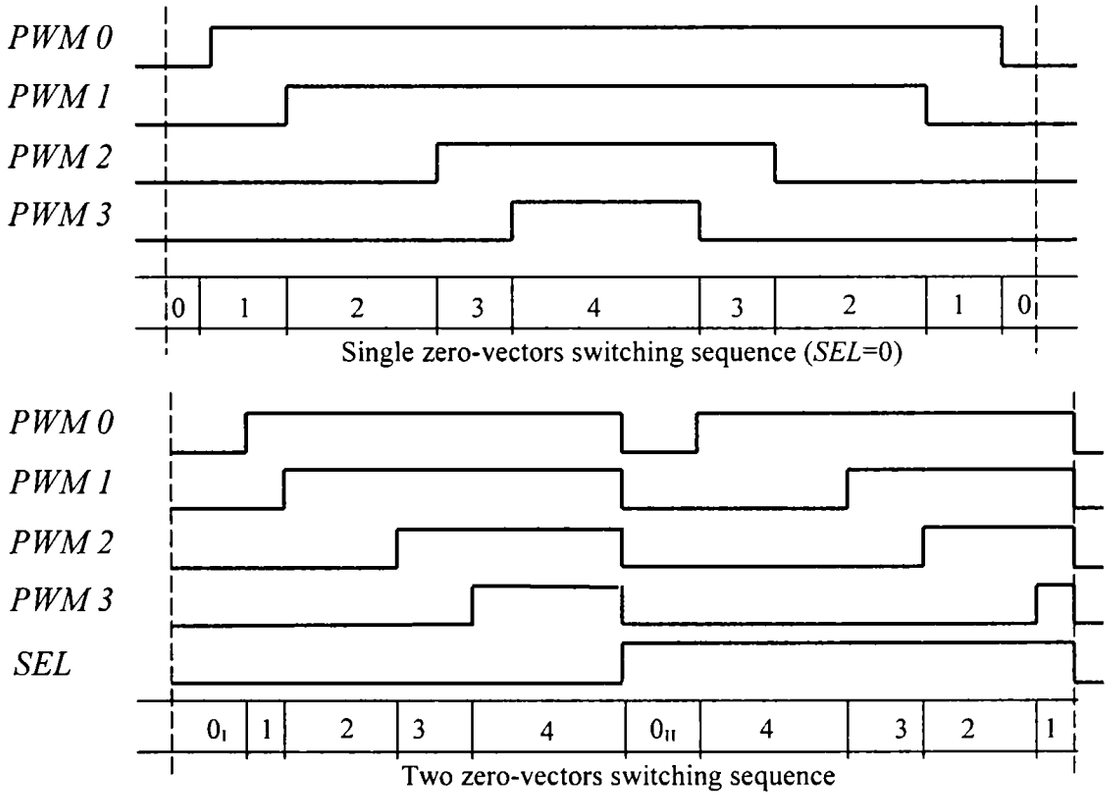

Fig. 5.11: Generation of the switching sequences by using four PWM channels

The control diagram of the matrix converter using the proposed SVM modulator is presented in Fig. 5.12. The control is implemented into a DSP (ADSP-21062 board) and uses the three input phase voltages U_a, U_b, U_c and the reference frequency f_{ref} as inputs.
In order to obtain $cos\ \varphi_{in}=1$ operation the position of input current reference vector θ_{in} is synchronized to the input voltage vector. Depending on the output frequency f_{out}, the *MODE* flag is set, which selects the switching pattern into the SVM modulator *SEL bit* in order to provide minimum input current ripple. The estimated imaginary DC-link voltage U_{pn} is used to determine the modulation index and using the ISVM equations (Chapter 2) the PWM registers content *PW0...3* is calculated. Necessary data are sent to the microcontroller through a dual-port RAM.

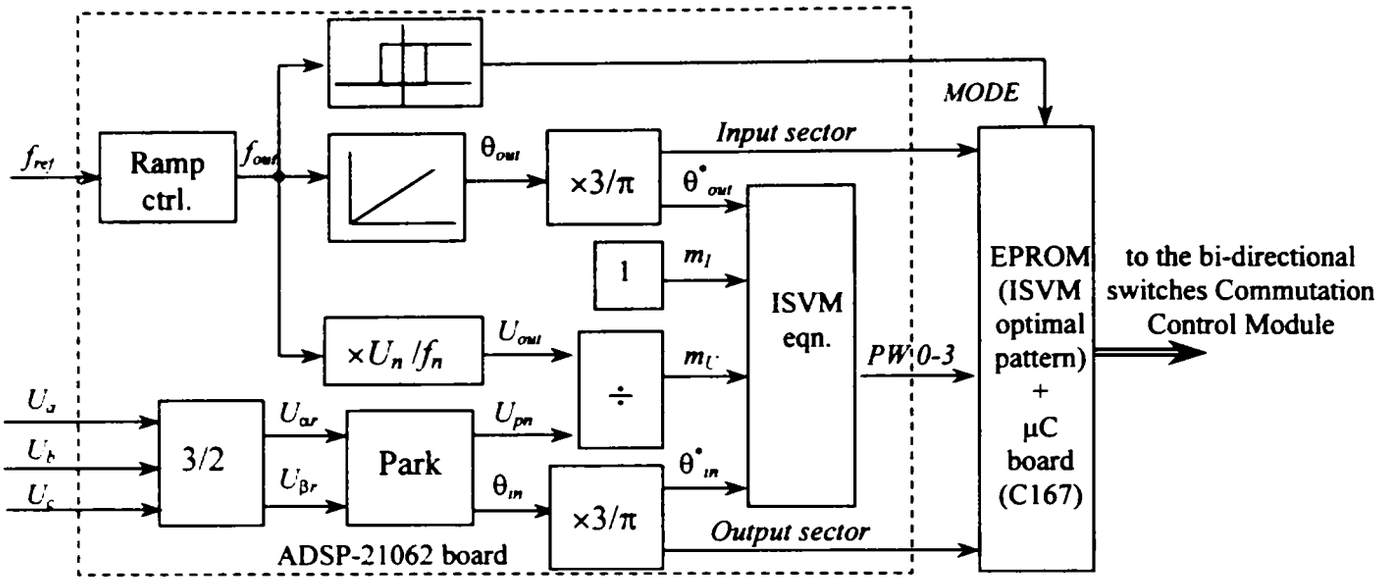

Fig. 5.12: The control diagram of the matrix converter

5.6 EXPERIMENTAL EVALUATION

The tests were performed on the 8.5 kVA matrix converter prototype described in Chapter 3. The input filter uses 1.2 mH/ 16 A_{rms} line chokes and 6 µF/ 250 V_{ac} capacitors star connected, giving a calculated input filter cut-off frequency of 1.8 kHz. The induction motor nameplate data are presented in Appendix 5.1. Two switching patterns have been tested:

- a single zero-vector switching pattern (8 commutations per switching period) with 4 kHz switching frequency;
- a two zero-vectors switching pattern (10 commutations per switching period) with 3.2 kHz switching frequency;

During the tests, the input current THD was monitored using a PM100 single-phase power analyzer (Voltech), which take into account 50th harmonics (f < 2.5 kHz) to calculate the THD. Voltage and current waveforms have been acquired using a TDS3014 oscilloscope and an AM503 current probe with amplifier (Tektronix). The oscilloscope sampling method was set to *"Peak detect"* to show precisely the amplitude of the input current ripple. The built-in Fast Fourier Transform (FFT) function was used to represent the spectrum.

Fig. 5.13 shows commutation details in the filtered input current for the single zero-vector switching pattern (a) and the two zero-vectors switching pattern (b). Oscillations start and are rapidly damped in the moment the rectification vector is changed. The commutations of the active vectors of the rectification stage are marked in the figure, using specific symbols.

The zero-vectors can be distinguished by the lack of the high frequency noises, which are characteristic only to active vectors. Therefore, during a zero vector, only the input filter is connected on the mains and oscillations take place, having initial conditions determined by the last moment when the previous active vector was applied. This explains the presence of current harmonics around the cut-off frequency. Despite of a lower switching frequency, the two zero-vectors switching pattern provides a higher switching frequency seen from the input side. Test conditions were: f_{out} = 15 Hz, m_U = 0.3 and no load.

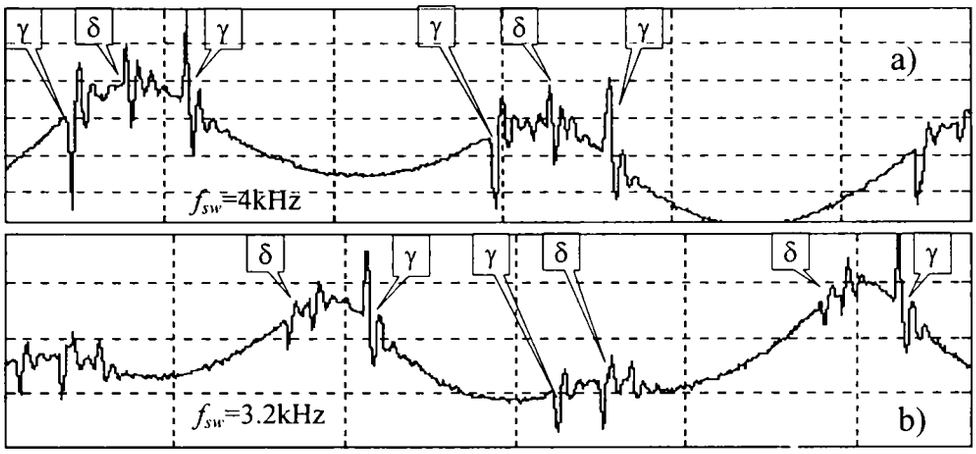

Fig. 5.13: The input current shape during commutation for a single-zero (a) or two-zeros (b) switching patterns (100 µs/div)

Fig. 5.14 and Fig. 5.15 shows the filtered input current and spectrum when the matrix converter operates in the lower modulation index range: m_U=0.3, f_{out}=15 Hz, and 50 % load torque. The current ripple is notably reduced when the matrix converter uses two zero-vectors in the switching pattern. By analyzing the input current spectrum, it is noticed that in the case of two zero-vectors in the switching pattern, the highest harmonic magnitude corresponds to 6.4kHz, which means the matrix converter acts on the input side with a doubled switching frequency. However, the 3.2 kHz harmonic is present in the spectrum and the peaks are multiple of 3.2 kHz. The inductive influence of the power grid decreases the input filter cut-off frequency from 1.8 kHz (calculated) to about 1.6 kHz, which is shown in the filtered input current spectrum.

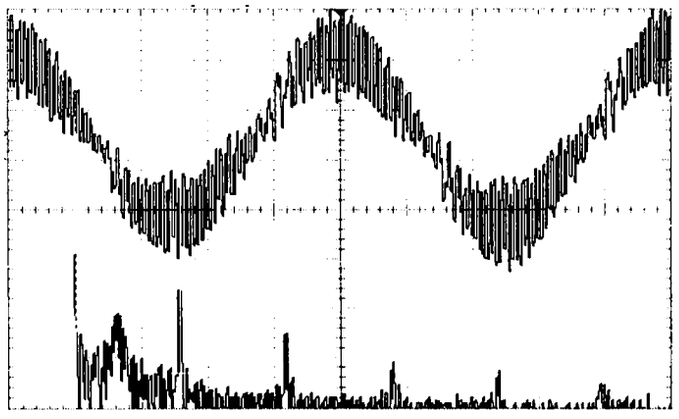

Fig. 5.14: The input current (1 A/div, 4 ms/div) and the FFT (20 dB/div, 2.5 kHz/div) for a single-zero switching pattern (peak detect).
f_{out}=15 Hz; f_{sw}=4 kHz; T=50 % T_N; THD_{50}=21 %;

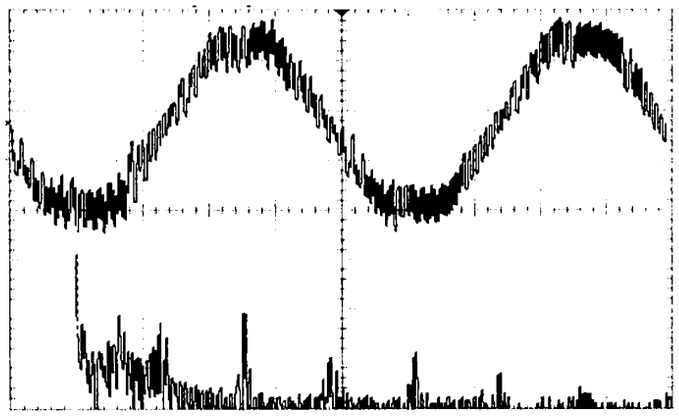

Fig. 5.15: The input current (1 A/div, 4 ms/div) and the FFT (20 dB/div, 2.5 kHz/div) for a two-zeros switching pattern (peak detect).
f_{out}=15 Hz; f_{sw}=3.2 kHz; T=50 % T_N; THD_{50}=15 %;

At higher modulation index, the current spectrum around the switching frequency will enlarge and the interaction with the input filter becomes stronger. Also a higher current is expected to flow through the input filter inductance and oscillations in the input filter caused by the current spikes may easily amplify due to input filter resonance. In the high modulation index range a single zero-vector in the switching pattern allows a higher switching frequency and the interaction with the input filter will be reduced. Fig. 5.16 and Fig. 5.17 shows the output line voltage and voltage spectrum for single zero-vector and two zero-vectors in the switching pattern.

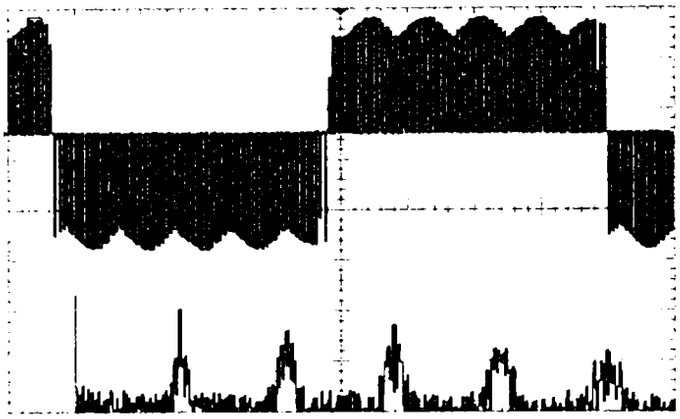

Fig. 5.16: The output line voltage (250 V/div, 4 ms/div), and FFT (20 dB/div, 2.5 kHz/div) for a single-zero switching pattern (peak detect).
f_{out}=30 Hz; f_{sw}=4 kHz;

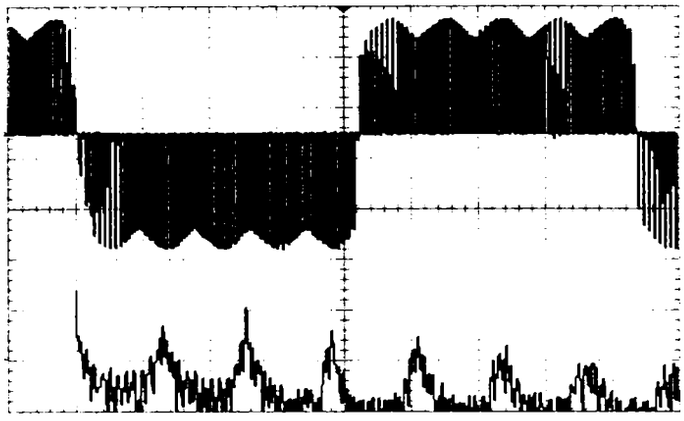

Fig. 5.17: The output line voltage (250 V/div, 4 ms/div), and FFT (20 dB/div, 2.5 kHz/div) for a two-zeros switching pattern (peak detect).
f_{out}=30 Hz; f_{sw}=3.2 kHz;

Fig. 5.18 shows the input voltage and input current when the matrix converter operates in the higher modulation index range: m_U=0.6, f_{out}=30 Hz and 50% load torque. Fig. 5.19 shows the output current and the spectrum for 30 Hz output frequency and 50% load torque.

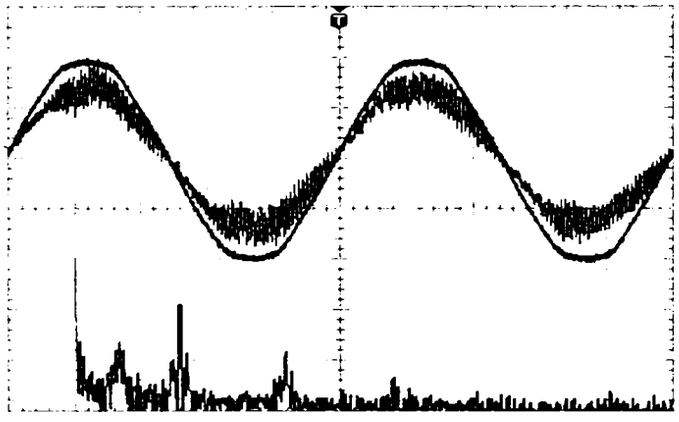

Fig. 5.18: The input phase voltage (160V/div, 4ms/div), current (2 A/div, 4 ms/div) and the input current FFT (20 dB/div, 2.5 kHz/div) for a single-zero switching pattern (peak detect).
f_{out}=30 Hz; f_{sw}=4 kHz; T=50 % T_N ; THD_{50}=12%;

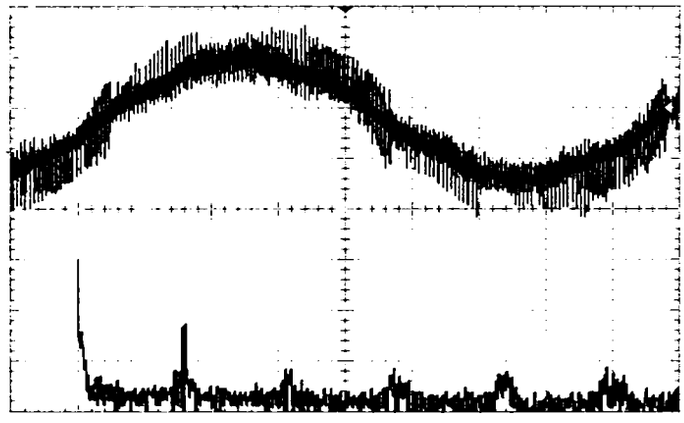

Fig. 5.19 The output current (5 A/div, 4 ms/div), and FFT (20 dB/div, 2.5 kHz/div) for a single-zero switching pattern (peak detect).
f_{out}=30 Hz; f_{sw}=4 kHz; T=50 % T_N;

SUMMARY

In this chapter the factors with influence on the input current ripple are analyzed. A method to reduce the input current ripple is proposed, based on the observation that the number of zero-vectors in the switching pattern influences the switching frequency seen from the input side and this may be easily changed. It is shown that by using a multi-zeros switching pattern it is possible to reduce notably the input current ripple in the low modulation index range despite of a lower switching frequency, to accomplish the same number of switch commutation per second.
A new SVM modulator for matrix converters, which is able to generate two switching patterns, is proposed. In this way the control changes the switching pattern depending on the modulation index, in order to minimize the input current ripple in the whole range of the modulation index.

APPENDIX 5.1:

Type: MBT 112M (ABB), P_n = 4 kW; U_n= 380 V(Δ); I_n = 7.9 A; cos φ_n = 0.9; n_n = 2880 rpm;

REFERENCES

[5.1] M. Venturini, "*A new sine wave in sine wave out, conversion technique eliminates reactive elements*", Proc. of Powercon 7, E3_1-E3_15, 1980.

[5.2] M. Venturini, A. Alesina, "*The generalised transformer: a new bidirectional sinusoidal waveform frequency converter with continuously adjustable input power factor*", Proc. of PESC'80, pp. 237-247, 1980.

[5.3] A. Alesina, M. Venturini, "*Analysis and design of optimum-amplitude nine-switch direct AC-AC converters*", IEEE Trans. on Power Electronics, vol. 4, no. 1, 1989.

[5.4] C.L. Neft, C.D. Shauder, "*Theory and design of a 30-hp matrix converter*", IEEE Trans. on Industry Applications, vol. 28, no. 3, pp. 546-551, 1992.

[5.5] L. Huber, D. Borojevic, "*Space vector modulator forced commutated cyclo-converters*", Proc. of PESC'89, pp. 871-8761, 1989.

[5.6] E.P. Wiechmann, J.R. Espinoza, L.D. Salazar, J.R. Rodriguez, "*A direct frequency converter controlled by space vectors*", Proc. of PESC'93, pp. 314-317, 1993

[5.7] P. Nielsen, F. Blaabjerg, J.K. Pedersen, "*Space vector modulated matrix converter with minimized number of switchings and feedforward compensation of input voltage unbalance*", Proc. of PEDES'96, vol.2, pp. 833-839, 1996.

[5.8] L. Zhang, C. Watthanasarn, W. Shepherd, "*Analysis and comparison of control techniques for AC-AC matrix converters*", IEE Proc.-Electr. Power Appl., pp. 284-294, vol. 145, no. 4, 1988.

[5.9] D. Casadei, G. Serra, A. Tani, P. Nielsen "*Theoretical and experimental analysis of SVM-controlled matrix converters under unbalanced supply conditions*", Electromotion Journal, no. 4, pp.28-37, 1997.

[5.10] J. Oyama, X. Xia, T. Higuchi, E. Yamada, T. Koga, "*Effects of the filter on matrix converter characteristics under a new control method*", Proc. of SPEEDAM Symposium, section A5 pp. 7 –14, 1996.

[5.11] P. Wheeler, D. Grant, "*Optimized input filter design and low-loss switching techniques for a practical matrix converter*", IEE Proc.-Electr. Power Appl., vol. 144, no. 1, pp. 53-60, 1997.

[5.12] C. Klumpner, I. Boldea, F. Blaabjerg, "*A new modulator for matrix converters allowing for the reduction of input current ripple*", Proc. of OPTIM'00, vol. 2, pp. 487-492, 2000.

[5.13] Siemens, "*C167 Derivatives - 16 Bit CMOS Single-chip microcontrollers - User's manual 03.93 Version 2.0*", Siemens AG, Munchen, 1996.

Chapter 6

Matrix Converter used in Artificial Loading of Induction Motors

This chapter discuses implementation aspects of using a frequency converter in artificial loading of induction motors. The characteristic of the artificial loading process requires a cyclic circulation of energy between the converter and the motor, in order to increase the motor current and electromagnetic torque to the rated values, without any load connected to the motor shaft. It is known that standard converters have serious limitations regarding the maximum level of the circulating energy, and if the incoming energy exceeds the storage capacity of the DC-link capacitors, an overvoltage fault may occur in the converter. This limitation can be overridden by using unidirectional power flow converters with high energy-storage capability in the DC-link or by using a bi-directional power flow converter with minimal energy storage capability.
Two possible bi-directional power flow converter topologies are investigated: the back-to-back voltage source inverter (VSI) and the matrix converter. A comparative analysis of the two bi-directional power flow converters shows that the energy stored in the passive components of a matrix converter is minimised. Due to the instantaneous transfer of the electrical power in both directions, the matrix converter topology constitutes an attractive alternative to other solutions, which store the circulating energy during the artificial loading process. Tests on an induction motor validate the use of the matrix converter in artificial loading of the induction motors.

6.1 INTRODUCTION

The principle of artificial loading of the induction motors, known as "*the dual-frequency method*" was first proposed by Yetterberg [6.1] in 1921. The original idea uses two series connected synchronous generators SG_1 and SG_2 to produce a dual frequency voltage system to feed the induction motor *IM*, as shown in Fig. 6.1a.

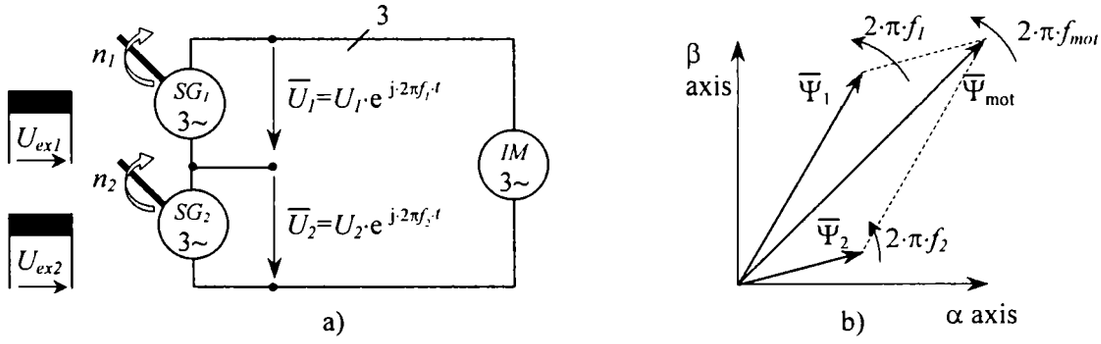

Fig. 6.1: Artificial loading of an induction motor (IM) through the dual frequency method: a) principle scheme using two synchronous generators (SG_1, SG_2); b) the resultant flux vector Ψ_{mot} generation from the flux components Ψ_1 and Ψ_2;

By considering the superposition principle, each voltage system produces in the induction motor a circular magnetic flux of different magnitudes (Ψ_1 and Ψ_2) and different pulsation ($2\pi \cdot f_1$ and $2\pi \cdot f_2$), which determines a resultant magnetic flux of variable magnitude (Ψ_{mot}) and pulsation ($2\pi \cdot f_{mot}$), as shown in Fig. 6.1b. In Fig. 6.2, the magnitude and the instantaneous frequency of the resultant flux are shown in a particular situation. It is seen that the instantaneous frequency of the resultant flux is varying around the frequency of the highest flux magnitude, for this reason called the dominant flux.

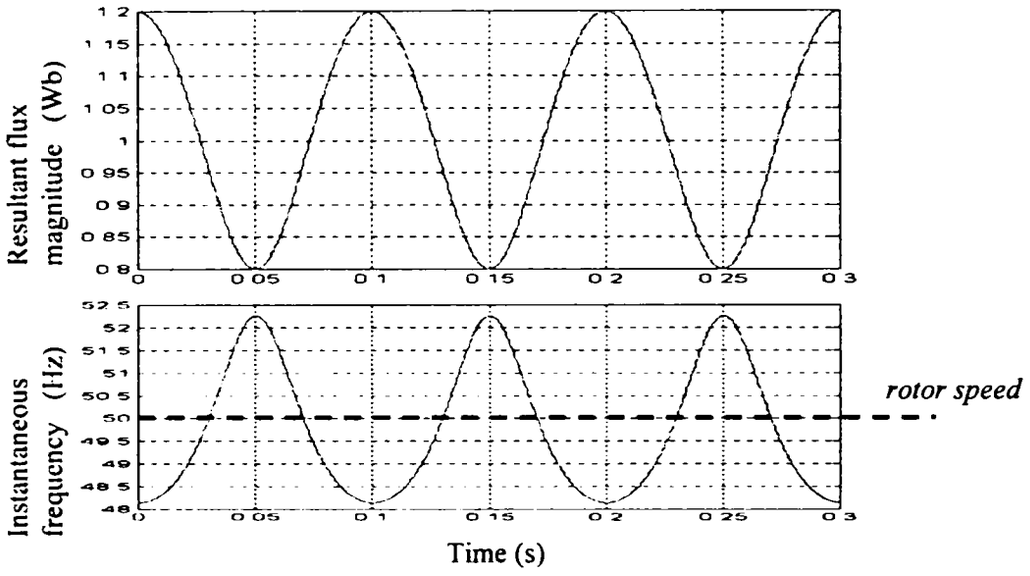

Fig. 6.2: The magnitude and the instantaneous frequency of the flux vector during the artificial loading test of an induction motor using the dual frequency method
(Ψ_1=1 Wb, Ψ_2=0.2 Wb, f_1=50 Hz, f_2 = 40 Hz)

If the mechanical inertia of the motor is high enough, the rotor speed may be considered constant. If the frequency of the dominant flux is the nominal frequency of the motor, then the instantaneous frequency of the resultant flux is varying around the synchronous frequency and makes the induction motor to oscillate between motor and generator regime, using the mechanical inertia as a load. The energy preservation principle, considered for a cycle of motoring-generating, may be written as:

$$W_{mot} = W_{gen} + W_{motor\ losses} \tag{6.1}$$

The purpose of this test is to produce rated losses in the induction motor, similar to a conventional loading test, in order to test the thermal regime of the motor. The motor losses includes mechanical losses which depends on the shaft speed, copper losses which depends on the RMS motor current and iron losses which depends on the flux level. This means that the motor should run at nominal shaft speed, with nominal RMS motor current and with a magnetic flux around the rated level. This concludes that the main requirement for an equipment designed to be used in artificial loading tests for induction motor is to provide cyclic bi-directional circulation of the energy with the motor, even though this equipment may take from the power grid only the motor losses.

Although the first implementations have used synchronous generators driven by variable speed DC motors to produce the variable frequency and variable voltage sources, this takes a lot of space, implies many circuits to control the excitation of DC motors and AC generators and requires a higher installed power. Multiplied by the overall efficiency of the electromechanical system, this provides low efficiency and low flexibility.

6.2 MICROPROCESSOR CONTROLLED POWER ELECTONICS EQUIPMENTS USED IN ARTIFICIAL LOADING

Some authors [6.2] - [6.5] have showed interest in the artificial loading method by using equipments with microprocessors controlled power electronics to produce a supply voltage in order to test the induction motors, due to a higher flexibility, a higher efficiency and a lower volume. Also it has been proven that there is not a major difference in the thermal regime of a motor fed from such a voltage source generated by power electronics equipment compared to the conventional loading test.
However, no investigation for the requirements of equipments designed to be used in artificial loading applications has been carried out, as authors have used in their experiments the hardware of a standard frequency converter oversized compared to the motor current and controlled by an external microcontroller or DSP system. A few disadvantages of the dual frequency method implemented by using a standard frequency converter have been observed as:

- the necessity to oversize the converter, which has to produce the peak motor current compared to the motor nominal current by a factor of 2.5 [6.4];
- the impossibility of producing the peak value of the resultant flux due to a limited DC-link voltage;
- the risk of producing an overvoltage fault in the converter during the regenerative operation of the motor;
- the risk of producing other faults (e.g. input phase loss) in the converter due to the built-in protections, caused by a higher ripple of the DC-link voltage;

In order to override these inconveniences, the authors have proposed solutions to change the classic dual frequency method to allow a better usage of the frequency converter (higher ratio between the RMS motor current and the inverter rated current) and to reduce the incoming energy in the DC-link during regeneration. As a result, other methods have been developed: the sweep frequency method, the constant speed of rotating magnetic field varying amplitude method [6.3] and the square-wave electromagnetic torque reference method [6.4].
One possibility is to use a standard frequency converter but the main limitation to circulate a higher amount of energy between the motor and DC-link capacitors during the artificial loading process is caused by an unacceptable increase of the DC-link voltage during regenerative operation. Possible solutions to avoid this problem are:

1. to use increased flux braking [6.2] which consists of increasing the stator flux reference during regenerative operation, and thereby increasing the losses in the motor;

2. to use a braking chopper in the DC-link to dissipate the incoming energy which exceeds the DC-link storage capacity during regenerative operation;
3. to increase the value of the DC-link capacitors to store the maximum level of the incoming energy during tests;
4. to use a bi-directional power flow converter [6.10], [6.11];

The first solution uses only a standard frequency converter, but is not possible to make the losses equivalent to the conventional test condition, because the purpose of the method is to increase the flux during braking and therefore the motor losses above the rated level to avoid overvoltages in DC-link. The energy flow diagram in this situation is shown in Fig. 6.3.

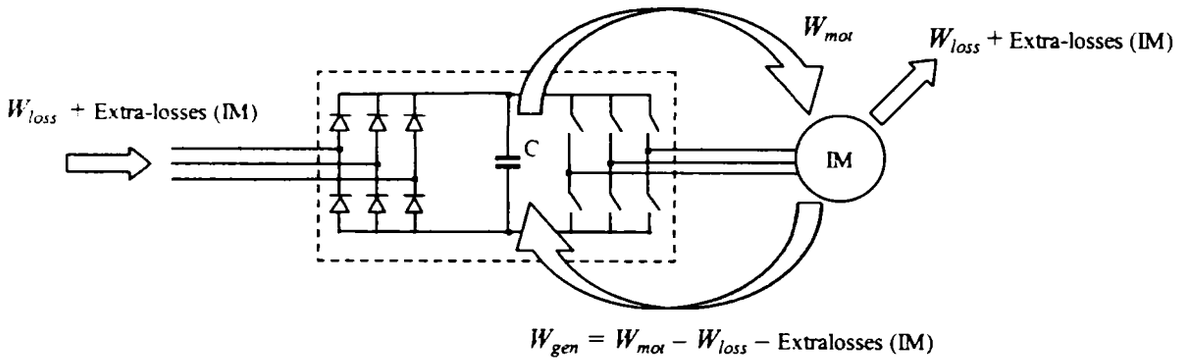

Fig. 6.3: The energy flow diagram when a standard frequency converter is used in artificial loading of induction motors by increasing the flux during deceleration

The second solution requires the use of auxiliary power devices. Some power modules used to build standard frequency converters integrate the chopper (IGBT + freewheeling diode), which makes easier for some manufacturers to provide the frequency converter with an integrated chopper, controlled by the DC-link voltage error. However, an external mounted braking resistor (BR) is always required. The energy flow diagram in this situation is shown in Fig. 6.4.

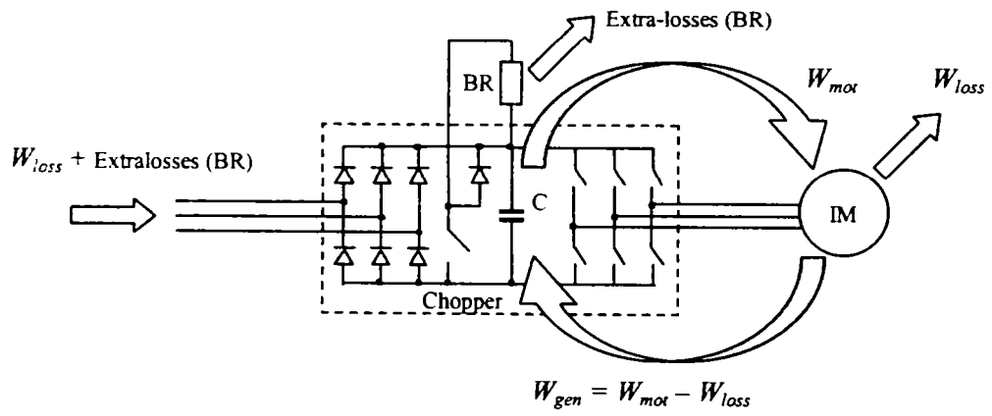

Fig. 6.4: The energy flow diagram when a standard frequency converter with chopper and an external mounted braking resistor (BR) are used in artificial loading of induction motors

The first two solutions dissipate an important part of the incoming energy during regenerative operation, which causes a significantly decreases in the overall efficiency of the testing equipment. The third solution consists of adding extra capacitors in the DC-link. The DC-link capacitor bank should be able to store the incoming energy without exceeding the maximum operating DC-link voltage. The energy flow diagram in this situation is shown in Fig. 6.5.

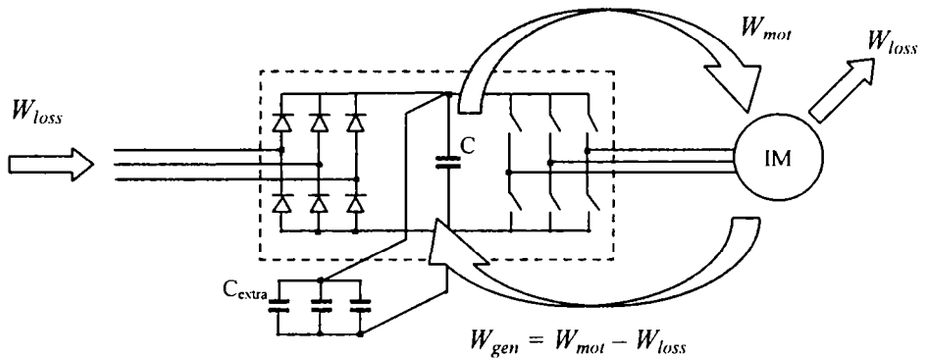

Fig. 6.5: The energy flow diagram when a standard frequency converter with extra-capacitors added in the DC-link are used in artificial loading of induction motors

Because of these problems, it may be concluded that it is very difficult to use a standard frequency converter in artificial loading of induction motors.
The fourth solution requires a more expensive frequency converter but the capacity to load the induction motor is limited only by the overcurrent protection level. The energy flow diagram in this situation is shown in Fig. 6.6.

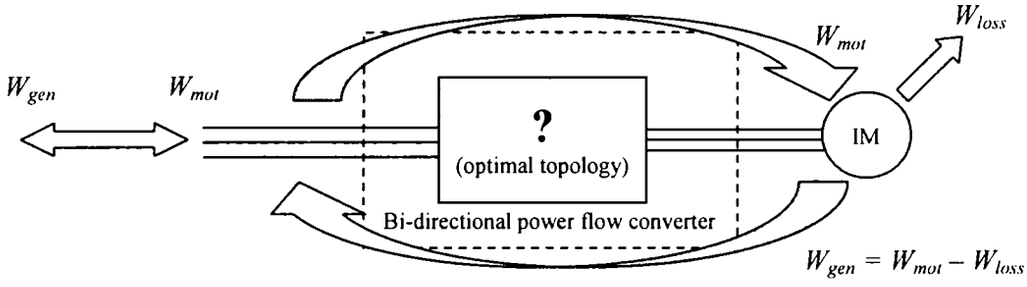

Fig. 6.6: The energy flow diagram when a bi-directional power flow frequency converter is used in artificial loading of induction motors

Discussions about the optimal topology of the bi-directional power flow converter will be presented in the next section. The bi-directional converter built with a thyristor rectifier bridge do not provide high dynamics for frequent motoring-regenerating transitions and may easily stop due to a DC-link overvoltage fault. This is the reason why the two valid topologies, which will be discussed, are the back-to-back voltage source inverter and the matrix converter.

6.3 THE MATRIX CONVERTER AND THE BACK-TO-BACK VOLTAGE SOURCE INVERTER: COMPARISON OF TOPOLOGIES FOR ARTIFICIAL LOADING

If circulating the energy with the power grid is the method chosen in the artificially loading process of the induction motor, the two converter topologies able to provide bi-directional power flow are analysed in order to determine the optimal solution. The comparison criteria in choosing the converter topology are the hardware requirements in building the converter and in controlling the process as: the number of the active switches, insulated gate-driver power supplies, current and voltage transducers and the amount of energy stored into the passive components.
In Fig. 6.7 is shown the topology of a back-to-back VSI. This configuration requires on the power stage 12 IGBT's and 12 Fast Recovery Diodes (FRD's), one large DC-link capacitor and three large AC chokes connected on the input side. Six insulated power supplies are needed to feed the upper IGBT's gate-drivers. In order to control this topology, three (two) output current transducers, a DC-link voltage transducer and three (two) input current transducers are basically needed. Some authors have been reported the use of three (two) supplementary input phase voltage transducers in order to perform the control of the regenerative rectifier [6.13].

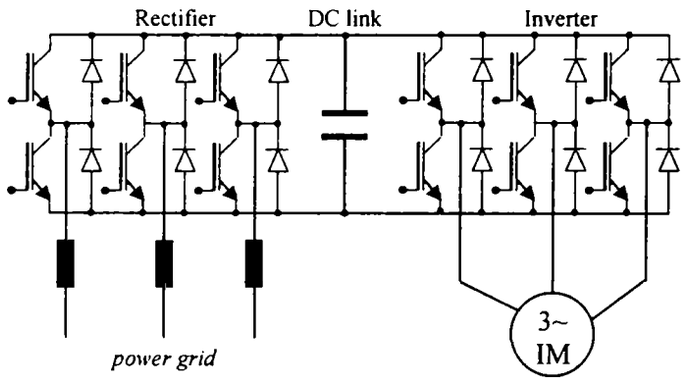

Fig. 6.7: The topology of the back to back VSI

The main advantage of this topology is that this configuration can be assembled from two standard DC-link VSI connected through the DC-link and three line inductors, which reduces the developing and the production costs necessary for a new converter topology. The only change required is to develop new software for the rectifier unit. Drawbacks: even though this is a bi-directional power flow converter, the energy stored in passive components is higher and includes limited lifetime components as electrolytic capacitors.
In Fig. 6.8 the topology of a matrix converter is shown. This configuration requires on the power stage 18 IGBT's and 18 FRD's, three AC chokes (smaller than the previous topology), three film capacitors connected on the input side in a low pass filter configuration, 12 FRD's and one capacitor, smaller than the DC-link capacitor in a clamp circuit configuration. Six insulated power supplies are needed to feed the IGBT's gate-drivers if the bi-directional switch uses a common collector (CC) configuration. In order to control this topology, three (two) output current transducers and three (two) input phase voltage transducers are needed.
The matrix converter has commanded attention due to the following advantages: the lack of the bulky DC-link capacitors with limited lifetime and the instantaneous bi-directional power flow transfer which provides smaller energy stored in passive elements compared to the other topology.

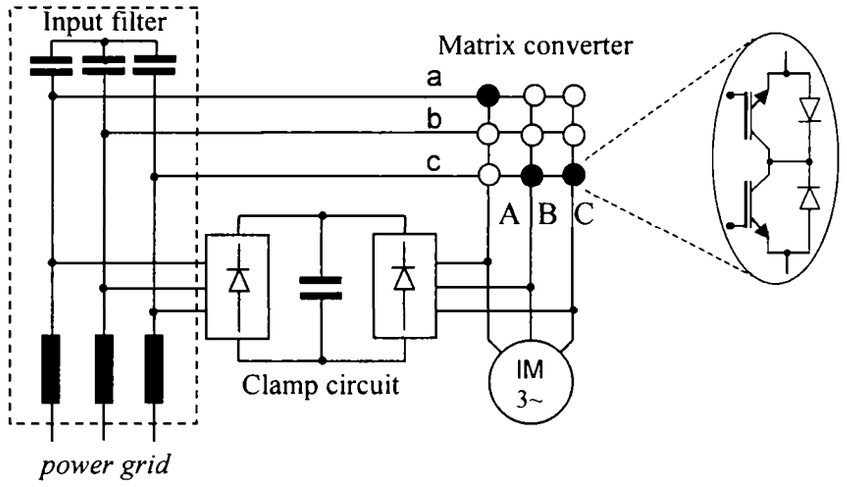

Fig. 6.8: The topology of a matrix converter

Drawbacks: the voltage transfer ratio is theoretically limited at 0.86, the absence of bi-directional switches from the semiconductor market, a higher number of power semiconductor devices needed to build the converter and a low immunity to power grid disturbances.
In Table 6.1 a few hardware requirements for the two bi-directional power-flow topologies are summarised. Despite the high number of power semiconductor devices (3:2 ratio) the matrix converter requires less transducers and bulky passive components than the back-to-back VSI.

Table 6.1
Comparative aspects for hardware requirements of two bi-directional power flow converters

Topology Criteria	BACK-TO-BACK VSI	MATRIX CONVERTER
Unidirectional switches (IGBT + DIODES)	12+12	18+18
Insulated gate-driver power supplies	6+(1)	6
Output current transducers (and A/D channels)	2 (or 3)	2 (or 3)
Input voltage transducers (and A/D channels)	2 (or 3)	2 (or 3)
DC-link voltage transducer (and A/D channel)	1	-
Input current transducers (and A/D channels)	2 (or 3)	-
Input filter topology and Installed kVAr (in p.u.)	L 10-20 p.u.	L-C 1-3 p.u.
Other components	DC-link capacitors	Clamp circuit

The limitation in the voltage transfer ratio, means that it is not possible to reach the nominal induction motor flux at nominal frequency. Practical solutions to eliminate this disadvantage are to change, if possible, the connection of the stator windings to delta (220 V) during tests or to use an auto-transformer on the input side to compensate the voltage transfer ratio. The required kVA for the auto-transformer is around 15% of the installed power and may replace the inductors from the input filter. As the typical line inductance for a back to back topology is 10-20 p.u. [6.12], it is expected that the size of the line inductors to be the same as the size of an auto-transformer used to compensate the matrix converter voltage transfer ratio.

6.5 ARTIFICIAL LOADING OF INDUCTION MOTORS USING A MATRIX CONVERTER

A new method for artificial loading induction motors, by using a matrix converter with space vectors, is developed. This uses a flux reference Ψ_{ref} of constant magnitude but variable frequency f_{out}, with no feedback (currents to correct the flux) from the tested motor, as it is shown in Fig. 6.9. In this way, it may be considered that conditions of making the stator iron losses equivalent to the conventional loading test, are accomplished, while the rotor iron losses are below the rated level.

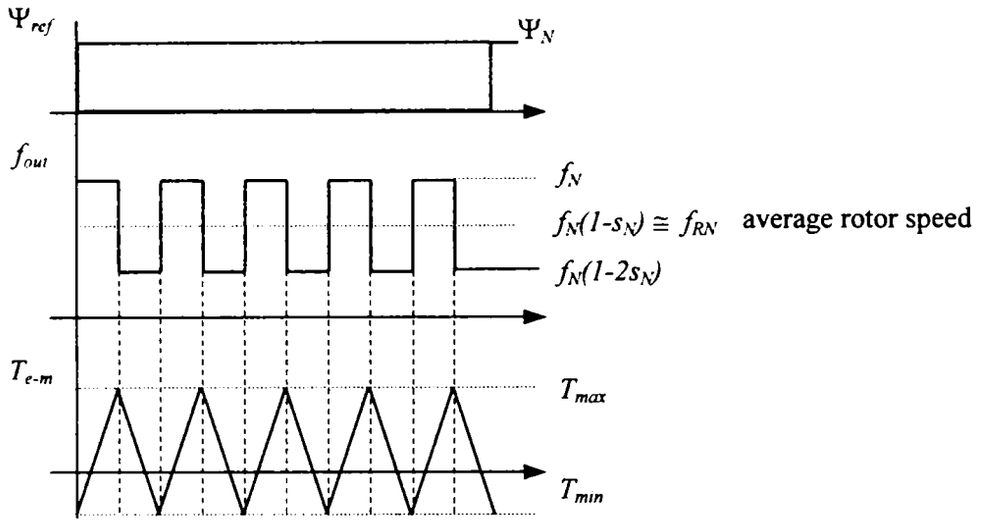

Fig. 6.9: The variation of the reference flux and pulsation for artificial loading and the expected shape of the electromagnetic torque in the induction motor

$$f_{out} = \begin{cases} f_N \\ (1-2\cdot s_N)\cdot f_N \end{cases} \tag{6.2}$$

$$\theta_1(N) = \theta_1(N-1) + 2\cdot\pi\cdot f_{out}\cdot T_{sw} \tag{6.3}$$

$$\overline{\Psi}_{ref} = \Psi_N \cdot e^{j\theta_1} \tag{6.4}$$

where θ_1 is the angle of the stator flux reference vector, which is incremented each switching period T_{sw}, and $\overline{\Psi}_{ref}$ is the reference flux vector of constant magnitude Ψ_N.

By using this method, the rotor slip is limited to the nominal slip $\pm s_N$ (6.2) and if the frequency of changing the instantaneous frequency is high enough, the rotor speed may be considered constant and close to the nominal speed during the artificial loading process. The rotor speed varies around the nominal rotor speed $f_N(1-s_N)$ and gives a similar regime as the conventional loading test for the mechanical losses of the motor. As the instantaneous frequency of the motor reference flux is switched between two constant values and the rotor speed variations are small, it may be considered that the shape of the electromagnetic torque will be triangular during the proposed artificial loading method, as is shown in Fig. 6.9. The reason is that when the instantaneous frequency of the stator flux is changed, the induction motor will continue to run in the same regime (motor or generator) because the relative position between the stator flux vector and the

motor current vector is the same (leading or lagging). In that moment, only the derivative of the electromagnetic torque changes sign. The electromagnetic torque will change sign and the induction motor will change regime (generator or motor) only when the relative position between the stator flux vector and the stator current vector will change (lagging or leading).
The control diagram used to test induction motors with the artificial loading method described before is shown in Fig. 6.10. The matrix converter uses an indirect SVM and an optimal switching pattern, which has been generally presented in Chapter 2. The output phase voltage vector U_{out} which corresponds to the inversion stage and the angle of input voltage vector α_{in} , which replace the input current vector for the rectification stage in order to provide instantaneous unitary displacement factor, are reference parameters. The modulation index is permanently corrected using the momentary DC-link voltage U_{pn} in order to provide sinusoidal and balanced output voltages even in the situation of unbalanced and distorted input phase voltages.

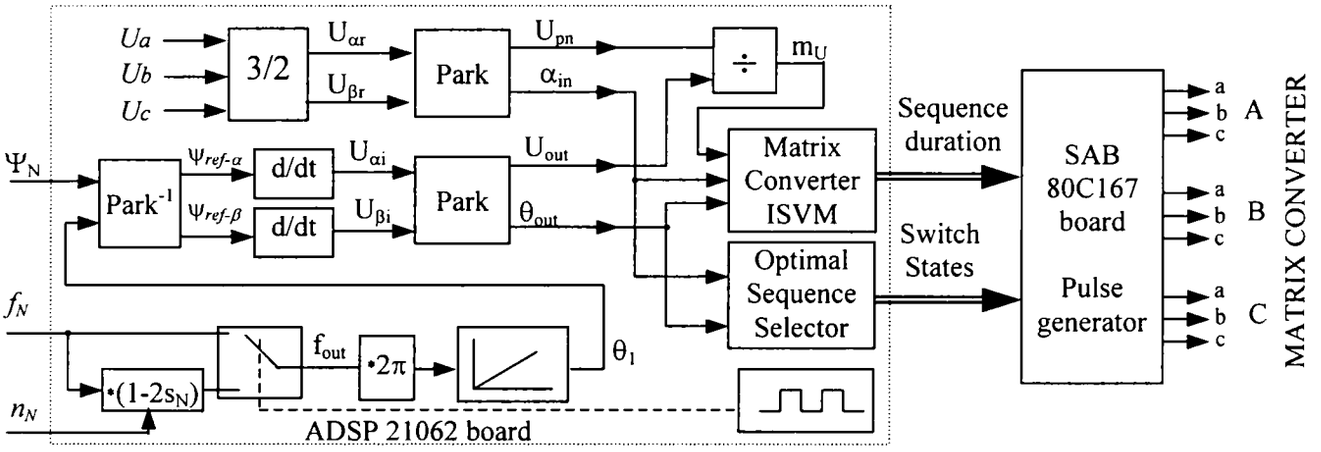

Fig. 6.10 The matrix converter control diagram for artificial loading implemented in the DSP

A correlation between the parameters of the control diagram presented in Fig. 6.10 and the parameters specific for the indirect SVM, presented in Chapter 2, is established:

$$m_I = 1 \tag{6.6}$$

$$\theta_{in} = \alpha_{in} \tag{6.7}$$

$$m_U = \frac{\sqrt{3} \cdot U_{out}}{U_{pn}} \tag{6.8}$$

where α_{in} represents the angle of the input phase voltage vector;
U_{out}, θ_{out} are the magnitude and angle of the reference output voltage vector;
U_{pn} is the instantaneous "DC-link voltage" provided by the rectification stage.

The input variables are the motor rated flux Ψ_N, the motor nominal frequency f_N and the motor rated shaft speed n_N, which gives the two frequency between the output frequency is periodically switched. The toggle period of the output frequencies is decreased until the RMS value of the motor current reaches the nominal value.

The reference flux vector (6.4), is used to calculate the output voltage reference by using

$$\overline{U}_{out} = \frac{\overline{\Psi}_{ref}(N) - \overline{\Psi}_{ref}(N-1)}{T_{sw}} \tag{6.5}$$

6.6 THE LABORATORY SETUP AND EXPERIMENTAL RESULTS

The control system is using a DSP board with ADSP 21062 to perform the digital control, a microcontroller board (SAB 80C167) to generate the double-sided ISVM pattern and an 8 channel /12 bit A/D board. Three input voltages, three output currents and one input current, which is not used in control, are acquired in order to get the necessary information about the process.
The duty-cycles and the switch states are transferred from DSP to the microcontroller through a dual port RAM memory. A four-step commutation strategy for the bi-directional switches is implemented by using programmable logic devices.
The switching frequency of the matrix converter can be varied between 2.5 to 5 kHz. A 7 kVA matrix converter prototype and an 1.1 kW induction motor have been used during tests. The current limit of the hardware protection of the matrix converter is set to 20 A. The input filter uses three 1.2 mH inductance and three star-connected 8.2 μF capacitors.
During the tests, the matrix converter runs with 4 kHz switching frequency and full input voltage (380 V). The induction motor stator windings are delta connected (220 V), which gives a flux reference of 0.5 Wb. The motor data are shown in Appendix 6.1.
Three tests are performed: a no-load test, an artificial loading test using the proposed method and an artificial loading test using the dual frequency method, for comparison purpose only. In Fig. 6.11 comparison between the no-load test and the artificial loading test using the proposed method is showed. The value of the electromagnetic torque seen on the matrix converter output phases T_{e-c} is estimated from the reference stator flux Ψ_{ref} and the measured output currents and this includes the motor losses:

$$T_{e-c} = p \cdot [\Psi_{ref-\alpha} \cdot I_{\beta} - \Psi_{ref-\alpha} \cdot I_{\alpha}] \tag{6.9}$$

The electromagnetic power P_{out} delivered on the output phase of the matrix converter is calculated using the electromagnetic torque and the instantaneous frequency f_{out} of the reference stator flux:

$$P_{out} = \frac{T_{e-c} \cdot 2 \cdot \pi \cdot f_{out}}{p} \tag{6.10}$$

During the no-load test the modulation index varies around 0.58 as is shown in Fig. 6.11a, which corresponds to a line-to-line voltage of 220 V. The ripple in the modulation index is caused by the non-sinusoidal input voltage, which requires compensation on the output stage. Fig. 6.11c shows a 3.1 A amplitude of the output current and the calculated RMS current is 2.4 A. The estimated electromagnetic torque (6.16) shows a very small value around 0.5 Nm, as it is shown in Fig. 6.11e, but includes full iron and mechanical losses and a part of the rated copper losses.
The artificial loading test based on the proposed method uses the 43.5 Hz/50 Hz to toggle the output frequency, in order to reach the nominal RMS motor current. This gives an average of the reference flux speed of 1402 rpm, which is close to the nominal motor speed (1410 rpm).

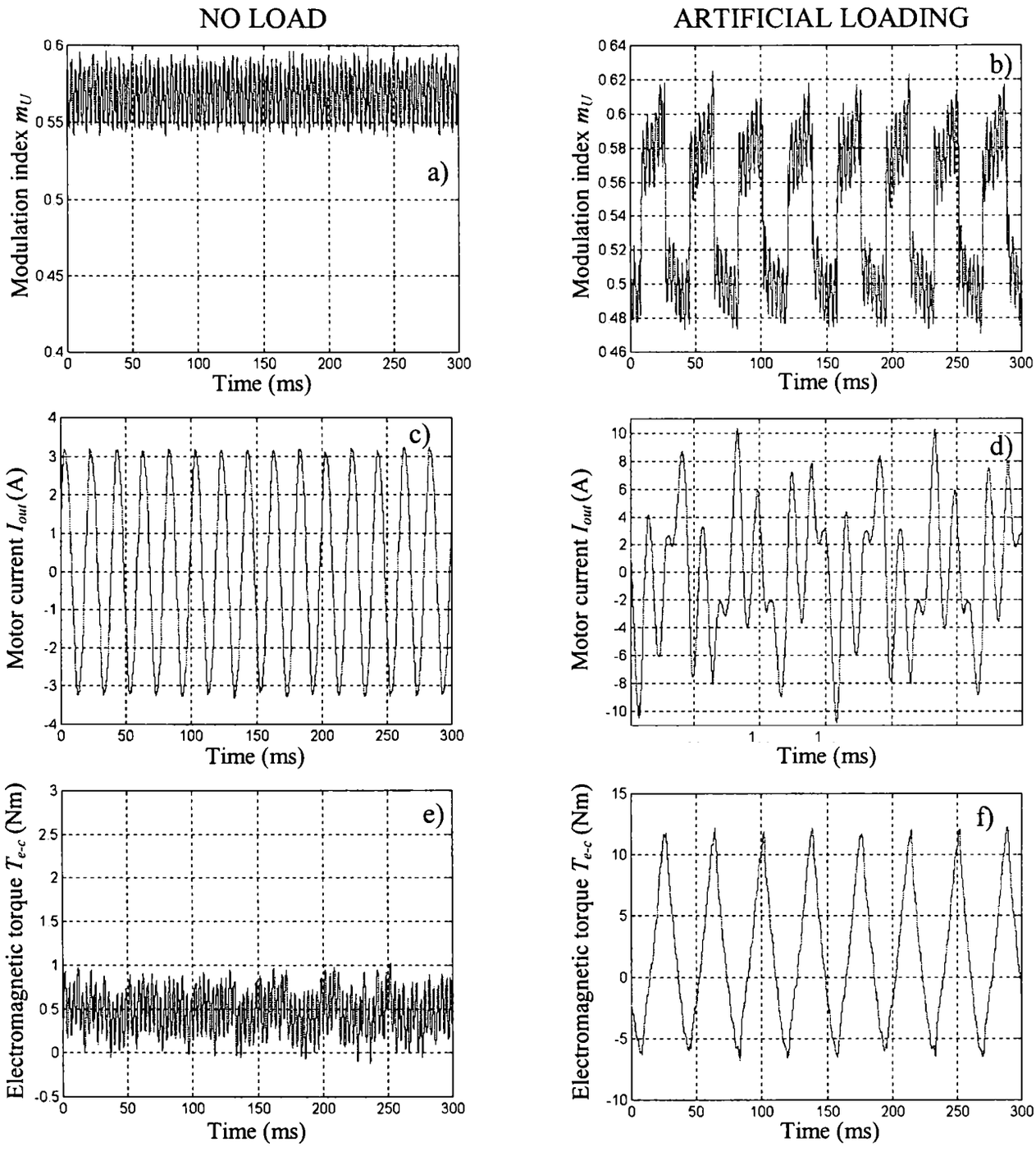

Fig. 6.11: 1.1 kW induction motor fed from a matrix converter: no-load (left side) and artificial loading (right side)

Fig. 6.11b shows the modulation index m_U changing between 0.58 and 0.5. The motor current reaches a maximum peak of 10.5 A as it is shown in Fig. 6.11d, the calculated RMS current is 4.74 A, which gives 100% loading in current. The ratio between the motor peak current and the RMS motor current was 2.2.

The estimated electromagnetic torque presented in Fig. 6.11f shows a triangular variation between –6 Nm and +12 Nm, due to a low inertia of the rotor. The calculated RMS value of the estimated torque seen from the converter is 5.9 Nm.

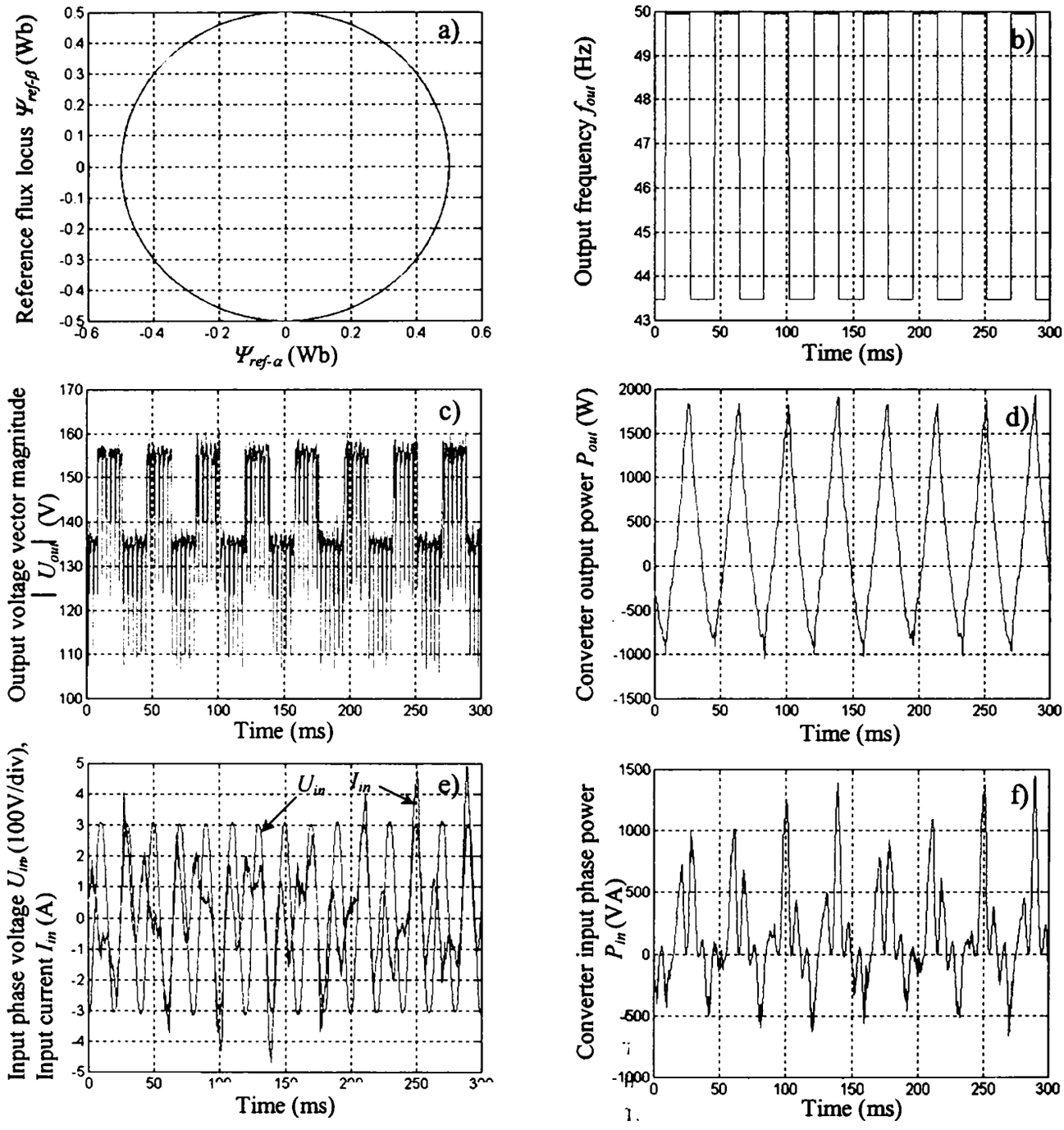

Fig. 6.12: Artificial loading of the 1.1 kW induction motor with a matrix converter using the proposed method

Considering the nominal value of the electromagnetic torque seen from the converter given by (6.11), which for the tested motor is 9.2 Nm. This means that during the artificial loading test the motor was loaded at 64 % rated torque.

$$T_{e-cN} = \frac{P_N}{\eta_N} \cdot \frac{p}{2 \cdot \pi \cdot f_N} \tag{6.11}$$

Fig. 6.12 shows other details of the artificial loading process using the proposed method. Fig. 6.12a and Fig. 6.12b show the reference flux vector locus and the instantaneous output frequency. The magnitude of the reference flux is constant during the artificial loading process, but the instantaneous output frequency has a rectangular variation between 43.5 Hz and 50 Hz. Fig. 6.12c shows the magnitude of the output phase vector, which depends on the instantaneous frequency in order to keep constant the reference flux magnitude. The electromagnetic output power is presented in Fig. 6.12d and shows a variation between –500 W and +1400 W.
The performances on the input side include the input phase voltage and current presented in Fig. 6.12e and the instantaneous input phase power presented in Fig. 6.12f. The displacement between the voltage and the current shows the motoring – regenerating transition regime.
Tests on the same motor have been carried out using the dual frequency method for comparison purpose only and are presented in Fig. 6.13. The two reference magnetic fluxes are: $\Psi_1 = 0.5$ Wb; $f_1 = 50$ Hz; $\Psi_2 = 0.1$ Wb; $f_2 = 40$ Hz. The variation of the reference flux magnitude is presented in Fig. 6.13a and shows that this method requires a higher capability of the equipment to produce flux in the motor. The instantaneous frequency of the reference flux vector is presented in Fig. 6.13b and the noise is produced by the derivative operation during the offline estimation. Variation of the modulation index is presented in Fig. 6.13c and it follows the variation of the flux magnitude. The maximum modulation index has reached 0.75, which is higher than for the proposed method (0.62). The motor current is presented in Fig. 6.13d, showing a peak value of 8 Amps, and a RMS value of 3.42 Amps, which is below the nominal value (73%). In this way, the ratio between the peak motor current and the RMS motor current was 2.34, higher than for the proposed method. The estimated electromagnetic torque (6.9) is presented in Fig. 6.13e, showing variation between –1.5 Nm and 3 Nm, which concludes that the motor is less loaded in torque, with a RMS value of 0.58 Nm (6.3%). The electromagnetic output power delivered to the motor (6.10) is presented in Fig. 6.13f and shows a variation between –250 W to +500 W. The performance on the input side show the input phase voltage and current in Fig. 6.13g and the phase instantaneous power in Fig. 6.13h.

SUMMARY

In this chapter the possibility of using the matrix converter in artificial loading of the induction motors has been investigated. Due to the bi-directional power flow capability, the only limitation in artificial loading is the overcurrent protection level. No restrictions exist regarding the maximum incoming energy due to instantaneous power transfer in the matrix converter.
A method to control a matrix converter for artificial loading applications, using space vectors, is presented. The reference parameters for the control diagram consist of a stator flux vector, of constant magnitude and variable frequency, which provides conditions for equivalent iron losses to a conventional loading test. However, equivalent stator copper losses to conventional loading test are achieved by controlling the RMS value of the stator current. The mechanical losses are close to the nominal value, because the slip frequency is controlled to change sign, around the nominal shaft speed. In this way it is concluded that the proposed method provides test conditions close to the conventional loading test, while the motor under tests develops a significant RMS level of electromagnetic torque. The lower voltage transfer ratio, which is a main drawback of the matrix converter topology, has been override in this application by using a step-up auto-transformer of 15% the matrix converter installed kW or, if possible, connecting the test motor in delta connection (220V).

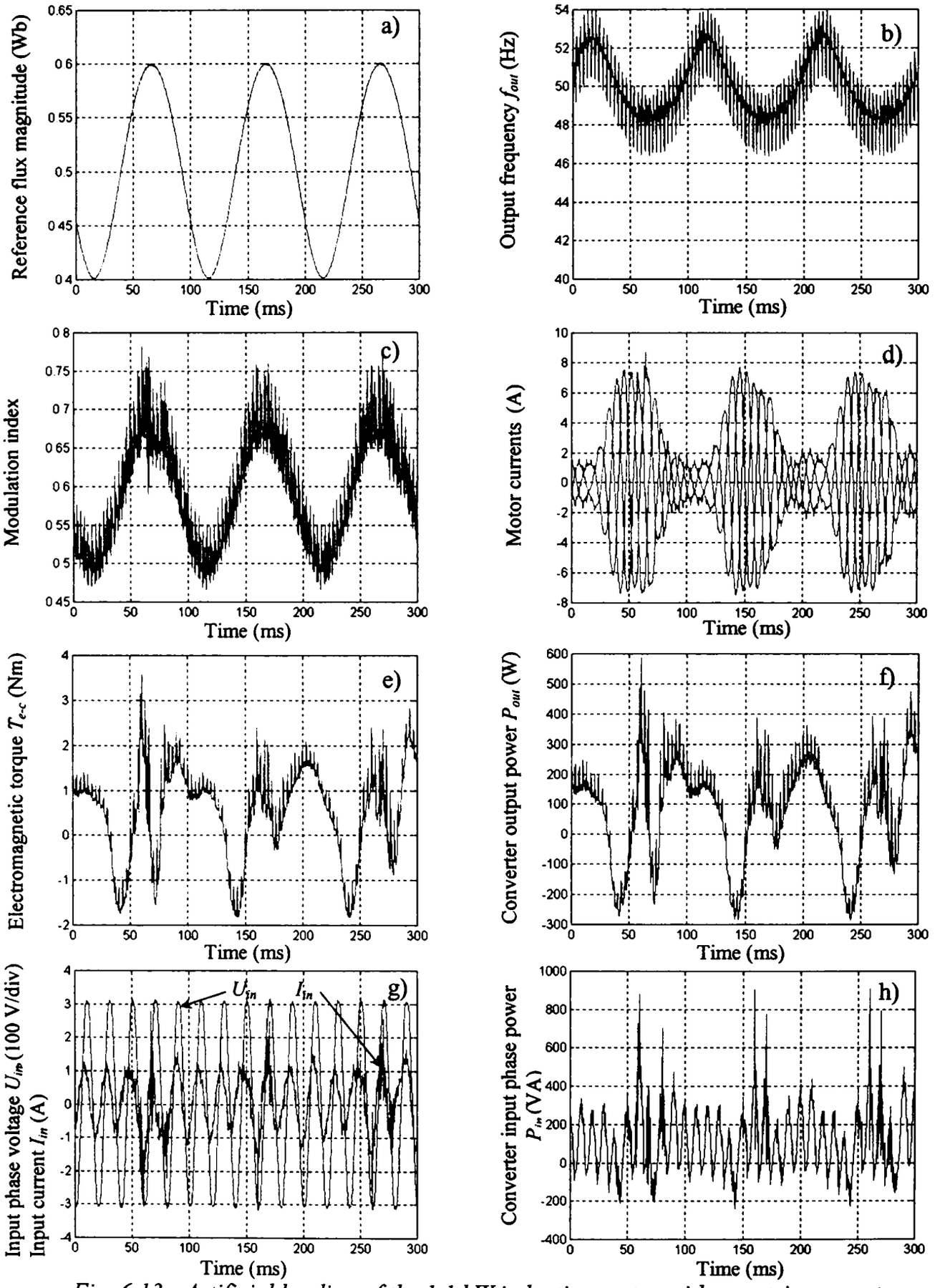

Fig. 6.13: Artificial loading of the 1.1 kW induction motor with a matrix converter using the two frequency method

APPENDIX 6.1

The parameters of the induction motor used for tests:

Motor type: M2AA 090S (ABB); P_N=1.1 kW; n_N=1410 rpm; p=2; η_N=76.3%; $\cos(\varphi)_N$=0.83; U_N=220/380 V; I_N=4.7/2.7 A; f_N=50 Hz; T_N=7.5 Nm; J=0.0032 kg·m^2.

REFERENCES

[6.1] A. Ytteberg, "*Ny method for fullbelassting av electrisca maschiner utan drivmotor eler avlastningsmaskin*", Tekmisktidskrift, pp. S42-44, 1921.

[6.2] P. Lesage, M. Alaküla, L. Gertmar, "*The dynamic thermal loading of an induction machine*", Proc. of EPE'97, vol. 2, pp. 2.520-2.525, 1997.

[6.3] C. Gratham, M. Sheng, "*The synthetic loading of three-phase induction motors using microprocessor controlled power electronics*", Proc. of PEDS'95, vol. 1, pp. 471-476, 1995.

[6.4] P. Templin, M. Alaküla, L. Gertmar, "*Dynamic thermal loading of inverter fed induction machine*", Stockholm Power Tech, pp. 241-244, 1995.

[6.5] L. Tutelea, I. Boldea, E. Ritchie, P. Sandholdt, F. Blaabjerg, "*Thermal testing for inverter-fed induction machines using mixed frequency method*", Proc. of ICEM'98, vol. 1, pp. 248-253, 1998.

[6.6] C. Grantham, "*Full load testing of three phase induction motors without the use of a dynamometer*", Proc. of ICEMA, pp. 147-152, 1993.

[6.7] C. Grantham, H. Tabatabaei-Yazdi, "*A novel machineless dynamometer for load testing three-phase induction motors*", Proc. of PEDS'99, pp. 579-584, 1999.

[6.8] M. Sheng, C. Grantham, "*Synthetic loading of three-phase induction motors by magnetic field magnitude modulation*", IEE Proc. – Electr. Power Appl., vol. 141, no. 2, pp. 95-100, 1994.

[6.9] C. Grantham, M. Sheng, E.D. Spooner, "*Synthetic loading of three-phase induction motors using microprocessor controlled power electronics*", IEE Proc. – Electr. Power Appl., vol. 141, no. 2, pp. 101-108, 1994.

[6.10] C. Klumpner, I. Boldea, F. Blaabjerg, "*The matrix converter: overvoltages caused by the input filter, bi-directional power flow, and control for artificial loading of induction motors*", Electric Machines and Power Systems Journal, vol. 28, no. 2, pp. 129-142, Taylor & Francis Group, February 2000.

[6.11] C. Klumpner, I. Boldea, F. Blaabjerg, "*Artificial loading of the induction motors using a matrix converter*", Proc. of IEE/PEVD'00, pp. 40-45, 2000.

[6.12] V. Manninen, "*Application of direct torque control modulation technology to a line converter*", Proc. of EPE'95, vol. 1, pp. 292-296, 1995.

[6.13] F. Blaabjerg, J.K. Pedersen, "*An integrated high power factor three-phase AC-DC-AC converter for AC-machines implemented in one microcontroller*", Proc. of PESC'93,vol. 1, pp. 285–292, 1993.

Chapter 7

Ride-through Capabilities for Matrix Converters

In the last years many solutions to provide continuous operation of Adjustable Speed Drives (ASD's) during power grid disturbances are proposed, but they are all applied to DC-link ASD's. A classical Direct Frequency Converter (DFC) topology, the cycloconverter, has limitations regarding the output frequency, but a new topology, the matrix converter, which is based on IGBT switches mounted in a bi-directional configuration, allows the implementation of a high performance ASD [7.1].
In this chapter a new solution to provide limited ride-through operation for a scalar controlled matrix converter (MC), for a duration of hundreds milliseconds without any hardware modification, is proposed [7.2]. During the ride-through operation, the drive is not capable to develop torque or to control the motor flux. By recovering the necessary power to feed the control hardware, the MC is able to keep the ASD operating. When normal grid conditions are re-established the MC is also able to accelerate the motor from nonzero speed and flux by initializing the modulator with the correct frequency and angle of the reference voltage vector, which are estimated. The duration of the ride-through operation depends on the initial motor flux, speed level, rotor time constant, load torque and inertia. The main tasks of the proposed control strategy are to provide the power to feed the control hardware and to estimate the initial condition in order to restart the drive immediately, from nonzero speed and flux condition, in order to reach the reference frequency in the shortest time.
The mechanism to provide energy to feed the control hardware in the case of power grid failure and the features provided by this control strategy are discussed. Tests to prove the capability of recovering enough energy from the motor are presented. Based exclusively on the current waveforms during the ride-through operation regime, a frequency observer and an angle observer necessary for the modulator to perform a successfully restart are developed. Tests including ride-through operation and restart from nonzero shaft speed and rotor flux show the validity of the proposed solution.

7.1 INTRODUCTION

During power interruptions or deep voltage sags, an ASD without ride-through capability runs at the reference frequency until an undervoltage fault occurs. Because the energy stored in the DC-link capacitors of a Voltage Source Inverter (VSI) is small, when a power interruption occurs, the ASD trips in a few tens of milliseconds, depending on the energy stored in the DC-link capacitors and the power delivered to the motor. If the ASD has no ride-through capabilities, this should be restarted from zero speed, when normal grid conditions are re-established. Sometimes a reset procedure is necessary before start-up and/or an aligning procedure has to be performed for industrial installations, which require a co-ordination between different movement axis. In this way, important delays are introduced and in the case of a critical process, important damage is caused.

Reasons to cause faults in an ASD without ride through capabilities:

- the Switch-mode Power Supply (SMPS) that feeds the control boards is not able to deliver the necessary voltage, forcing a shutdown of the control system. This causes the control to loose all information regarding the motor state, and after a power-up sequence, which may take seconds, should be initialised with the default (zero) values.
- due to a severe decrease of the DC-link voltage, a fault may be triggered in the ASD power stage, because the converter is not able to deliver the required output voltage level, which may produce overcurrents in the motor.
- there are other auxiliary devices as the inrush circuit (a charging resistor and a by-pass relays or a thyristor-diode rectifier bridge), which has to be turned off immediately, in case the DC-link voltage decreases below a minimum level. Otherwise, if the input voltage is re-established, an overcurrent situation occurs and serious damage in the ASD input stage may be produced.

The research work in this area has focussed:

- on studying the frequency and the effects of voltage sags and power interruptions on the ASD's, from the user's perspective [7.3] – [7.7], in order to classify the power grid disturbances on the damage caused and to estimate specific costs for different type of power grid disturbance;
- on proposing new ride-through solutions applied to an existing frequency converter hardware [7.7] – [7.12];
- on modifying the frequency converter hardware in order to improve the ride-through operation of the ASD's [7.7], [7.13] – [7.21];
- on building a test bench to evaluate the response of different ASD's to the same type of input disturbance [7.22].

Depending on the requirements for the ASD ride-through operation, a few solutions have been proposed in the literature [7.7]-[7.21] and may be classified as:

1. ASDs without output power capability during power grid disturbances: The basic requirements for the converter are to feed the control circuits and to magnetise the motor in order to reach the reference frequency in a short time, when normal grid conditions are re-established. The ride-through strategy uses regenerative operation of the drive in order to keep the DC-link voltage constant and requires a large inertial load, to provide a small decrease of the motor speed. This way the motor is under control all the time. These solutions do not imply any hardware modifications and are a common feature of today's industrial frequency converters. In Fig. 7.1 the operation principle of such a converter (ACS600 from ABB) during a short power interruption is shown [7.23].

The control during the ride-through operation depends on the type of the motor control during normal operation. If a scalar type control is used, which requires less computational resources, it is complicated to completely control the motor (maintain a constant flux level) during ride-through operations, because of missing information (speed). Therefore, proposed ride-through strategies for scalar controlled ASD's require a transition from normal operations to ride-through operation in order to achieve control of the motor [7.10]. Other solutions require supplementary sensors mounted on the output side [7.12] in order to provide the speed, position and magnitude of the residual flux in the motor, information necessary for the restart procedure.

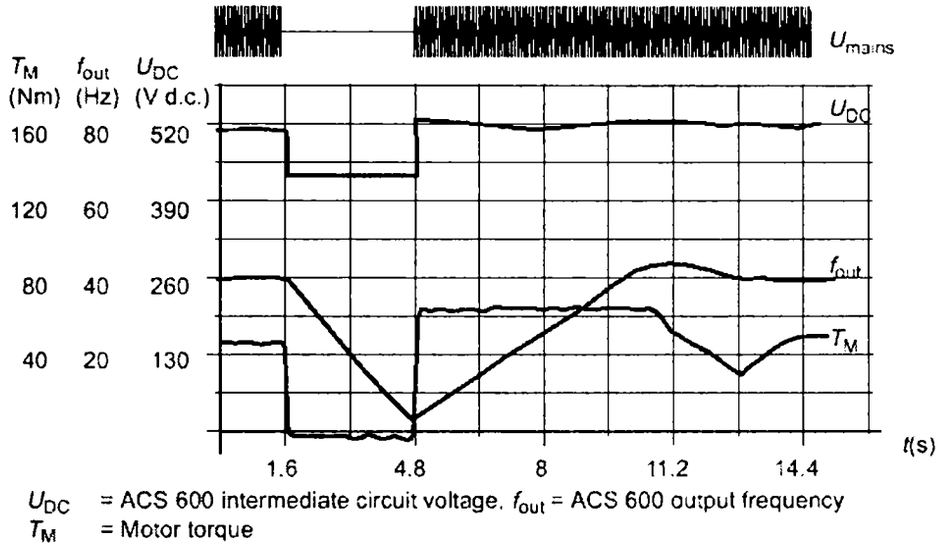

Fig. 7.1: Ride-through operation principle presented in the technical manual of an industrial frequency converter (reprinted from [7.23], Fig. 6-1, pp. 6-2)

If a vector type control is used, which requires more computational resources, it is very easy to control the motor (flux, torque and speed is estimated) during ride-through operation, and to perform a faster restart when normal grid conditions are re-established. Changing the operation from one situation to the other situation does not require any transients in the motor operation, while the motor is accurate controlled during the ride-through operation.
However, if the ASD control is unable to keep the motor "alive" during a power interruption, and the input voltage is restored, the ASD control should be able to perform a restart, while the residual magnetised motor is still spinning. This feature called flying start is used independent of the ride-through operation and is implemented in a wide range of industrial frequency converters.

2. ASDs with partial or full output power capability during power grid disturbances: The energy to feed the control circuits and to drive the load according to the reference speed/frequency or to fulfil a customised grid-fault scenario, is taken from an energy storage unit or from a backup source. These solutions imply normally hardware modifications as elements of energy storage and equipment to convert the stored energy in electrical energy of a certain voltage level or to employ a new ASD topology, as the active rectifier.
Solutions to store or to produce energy are to add extra DC-link capacitors, or to use other solutions as batteries, flywheels, ultra-capacitors, superconductive coils, fuel cells, which have been investigated already [7.7], [7.15] - [7.21]. Each solution has different application [7.7], depending on the following:

- overall efficiency;
- how fast full power should be available;
- typical duration of power interruptions;
- recharging rate, cycle life and cost of auxiliary equipment for recharging;
- specific costs of storing the energy ($/kWh);
- specific losses in stand-by operation (J/hour in standby);

- auxiliary equipment needed to convert and adapt the stored energy to the required voltage level.

Also, if it is desired ride-through capability for partial and/or single phase voltage sags, the active rectifier technology is a convenient alternative by boosting up the voltage to a higher level, but then higher current rating for the active devices is needed [7.7], [7.13] - [7.14], [7.19] - [7.21]. Economical solutions to boost up the voltage have been investigated, using a standard configuration of the DC-link VSI with input diode rectifier and a braking chopper (an IGBT and a freewheeling diode), which is integrated inside the same power module.

7.2 RIDE-THROUGH OPERATION STRATEGY FOR MATRIX CONVERTERS

All the solutions presented in the literature to provide ride-through capabilities are based on the DC-link existence and they are applied exclusively to the DC-link ASDs. This is the reasons that the matrix converter (MC) topology is considered so vulnerable to power grid disturbances and the MC ride-through capability was not investigated. However, this capability is very important in respect to the possibility to an extended use of MC in industrial applications.
The control strategy is developed considering the existence of a clamp circuit to protect the MC against overvoltages from the output side. This appears when the converter is turned off while the motor current has reached the overcurrent limit. The magnetic energy from the leakage motor inductances has to be discharged, and if no current path is provided for the motor currents, a dangerous overvoltage occurs. The clamp circuit consists of a clamp capacitor and a B6 diode bridge connected at the output side of the MC [7.24], [7.25]. Also, it is considered that the MC control hardware is fed from the clamp capacitor using a switch-mode power supply (SMPS) as it is shown in Fig. 7.2. In a DC-link ASD, a decrease of the input voltages during voltage sags will block the input diode-bridge. The ASD is disconnected from the power grid and the energy recovered from the motor feeds only the converter hardware.

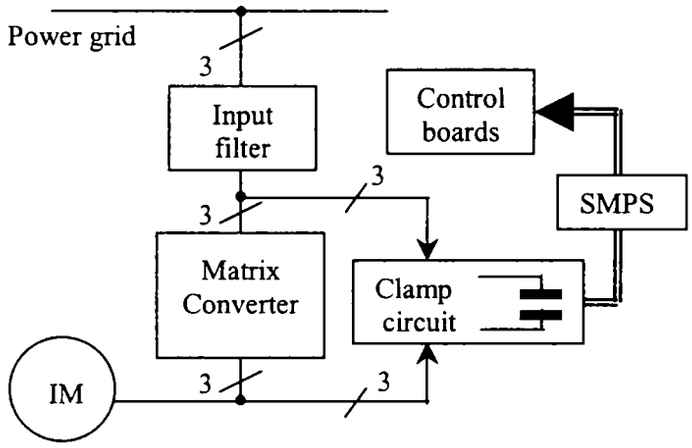

Fig. 7.2: Typical configuration of an ASD with a matrix converter

Because the MC is based on galvanic connections between inputs and outputs, the ride-through control strategy has to provide separation of the motor circuit from the power grid.
Disconnecting all the MC switches, but providing continuity for the motor currents due to the clamp circuit or connecting all the output phases to a single input phase (zero-vector) does the required separation. This is shown in Fig. 7.3, where for a certain direction of the motor currents,

the separation from the grid is obtained by disconnecting all the converter switches (Fig. 7.3a) or by applying a zero-vector (e.g. *bbb* in Fig. 7.3b).

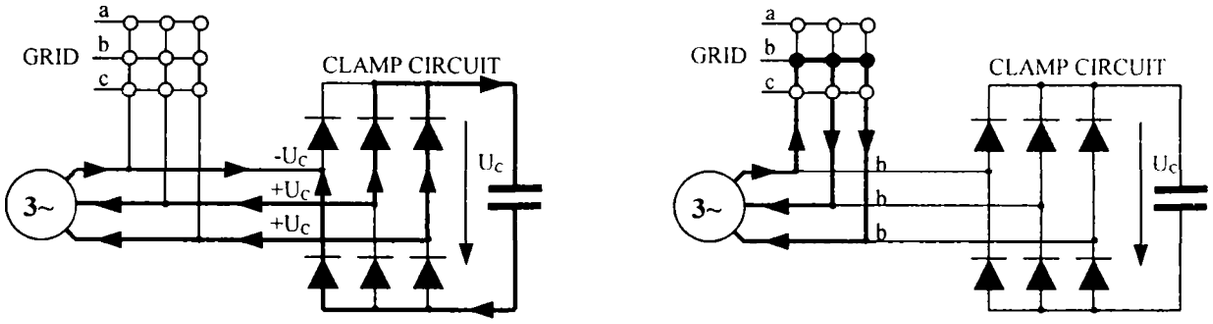

Fig. 7.3: Example of separation of the motor circuit from the grid: a) when all the switches are disconnected; b) when a zero-vector is produced;

By applying a zero-vector, the induction motor current increases and the value of the energy stored in the leakage inductance increases. The stator flux stops moving, but the rotor flux is still moving due to rotor movement. If the rotor flux is leading, the electromagnetic torque changes sign and the increase of energy in the leakage inductance is based on the stored energy in the mechanical system. Disconnecting all the active switches of the MC cause the conduction of the clamp circuit diodes. The stator current decreases and the energy stored in the leakage inductance goes to the clamp capacitor.
By alternating the two-permitted MC states during ride-through operation, it is possible to control the motor currents and to transfer energy from the rotor inertia to the clamp capacitor.
The equivalent scheme of the ASD during the proposed ride-through strategy is presented in Fig. 7.4. The induction motor acts as an AC generator with the EMF produced by the decaying rotor flux. The induction motor leakage inductance $L_{\delta\text{-}r}+L_{\delta\text{-}s}$, the MC and the clamp circuit form a boost converter, which works in AC and uses bi-directional switches.

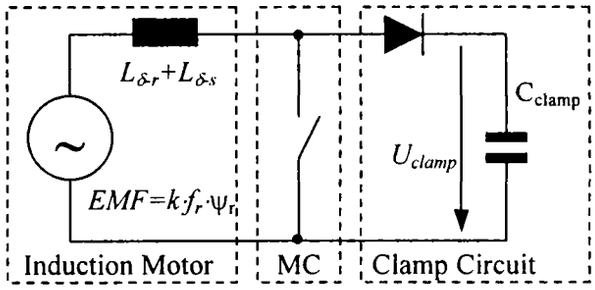

Fig. 7.4: The equivalent scheme of the ASD during ride-through operation

It is not possible to control the magnitude of the rotor flux ψ_r during the ride-through operation, because it is not possible to apply any active voltage vector to the motor, which could increase the flux. The ride-through capabilities depend on the motor parameters (leakage inductances), on the initial conditions of the motor (flux and speed level) and on load characteristic. Each time when the switches are disconnected, another quantity of energy stored in the leakage inductance will be transferred to the clamp circuit. The energy transfer is performed in two steps, as shown in Fig. 7.5.

I During a zero vector, the mechanical energy stored in the rotor inertia is converted into magnetic energy stored in the motor leakage inductance by using the rotor flux.
II Disconnecting the MC switches force the transfer of the energy from the leakage inductance into the clamping circuit.

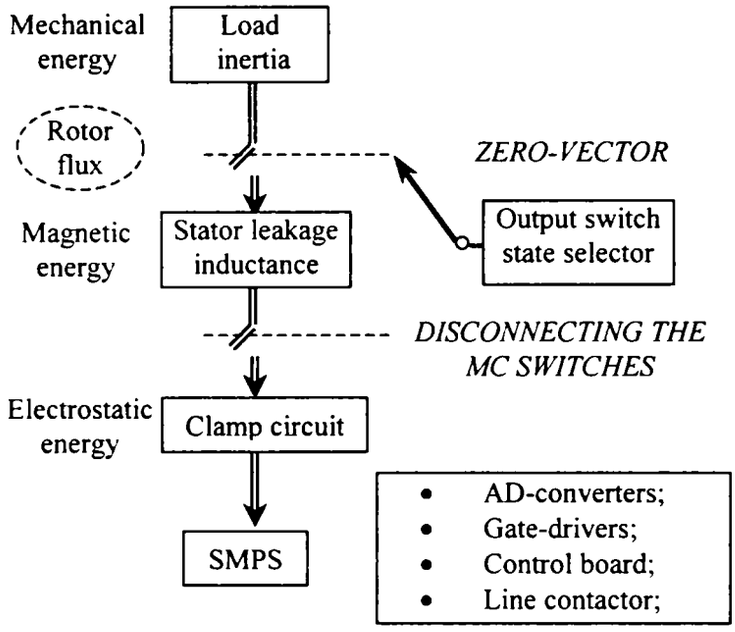

Fig. 7.5: The diagram of the ride-through energy transfer

The proposed operation method for the ride-through strategy is tested on an induction motor feed from a standard DC-link converter, able to emulate the MC functions, during the proposed ride-through strategy. The laboratory set-up is described in Section 7.5. The DC-link capacitor, which is designed to smooth the DC-link voltage, is much higher than the MC clamp capacitor, which is designed only to protect against overvoltages from the motor side in the case of a MC shutdown [7.21], [7.22]. In this way the overvoltage risk due to a higher incoming energy is decreased and the tests are performed safely due to the converter built-in overvoltage and overcurrent protections.
The motor current vector magnitude $|I_s|$ is controlled by changing the MC state according to the following rule:

$$\begin{aligned} &\textit{if} \quad |I_s| > I_{lim} \quad \textit{then} \qquad MC\_STATE = disconnected; \\ &\textit{else} \qquad\qquad\qquad\quad MC\_STATE = zero\_vector; \end{aligned} \tag{7.1}$$

The condition (7.1) was tested and the set-up conditions are mentioned in Table 7.1. This test consists of changing the motor operation from normal operation (constant V/Hz) and steady-state to the proposed ride-through operation and operates in this way as long as possible. The induction motor decelerates until it stops, transferring energy to the DC-link capacitor. The test purpose is to acquire the motor currents, the DC-link voltage and the shaft speed in order to determine the recovered energy and power. The data are acquired and available for other parameter estimation, as is shown in Section 7.3. Sinusoidal and balance of the fundamental motor currents are obtained, as shown in Fig. 7.6, and this gives some advantages, as it will be shown in section 7.3. Also the

quantity of energy transferred each time into the clamp capacitor can be estimated precisely and overvoltages can be avoided without the need of a voltage sensor in the clamp circuit.

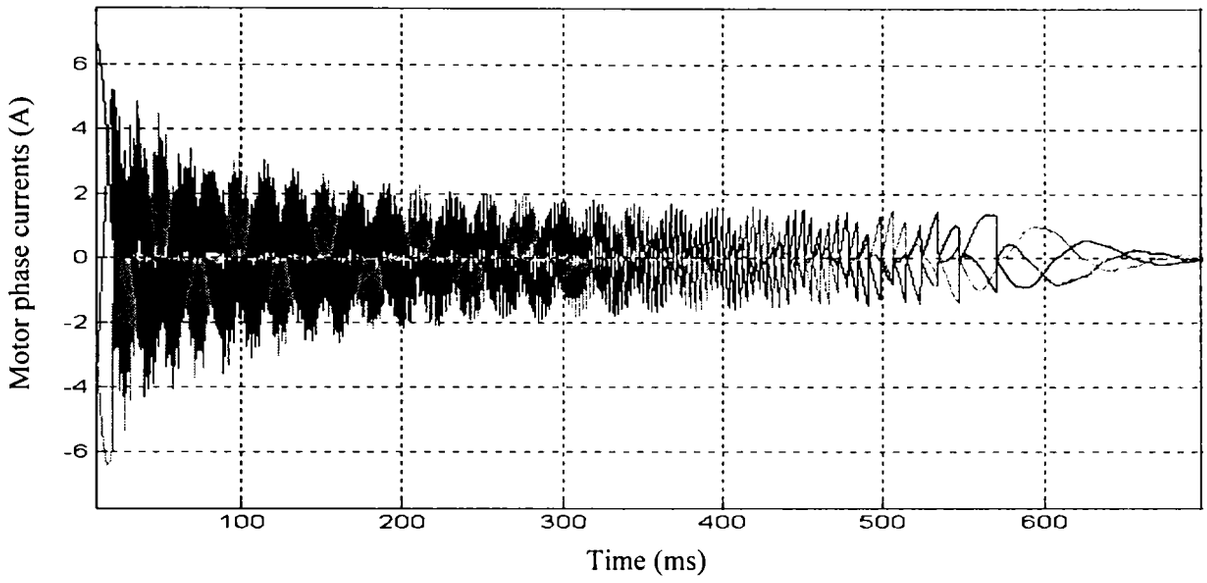

Fig. 7.6: Measured motor phase currents during transition from normal operation to ride-through operation (t_{on}=20 ms)

However, when this strategy is implemented in a matrix converter, it is recommendable to have a "low"/"high" feedback signal from the clamp circuit voltage to enable the ride-through operation, in order to ensure a safer operation of the matrix converter.

Table 7.1
Parameters for the experiment presented in Fig. 7.6 – 7.9

Initial frequency (f_{ini})	25 Hz
Transition moment (t_{on})	20 ms
Switching frequency (f_{sw})	5 kHz
Limit of the current vector magnitude (I_{lim})	1.4 A

The transition from normal operation to the proposed ride-through operation is presented in Fig. 7.7, where both the phase voltage and current are measured during the test described before, using a higher sampling rate (oscilloscope). The operation of the drive is characterised by sinusoidal and balance currents and no reactive power exchange between the motor and the converter, due to a 180° displacement angle between the phase voltage and current fundamental waveforms. A quick change in the current displacement angle is seen in the transition moment. Considering the motor operating at no load, when the current is lagging the voltage by 90°, during transition the displacement angle jumps to 180°. If the motor operates at full load, the jump in the current displacement angle may be higher than 150° in the case of a 0.86 power factor. This is taken into account in Section 7.3, to reduce the errors of estimating the frequency by differentiating the angle of the motor current vector.

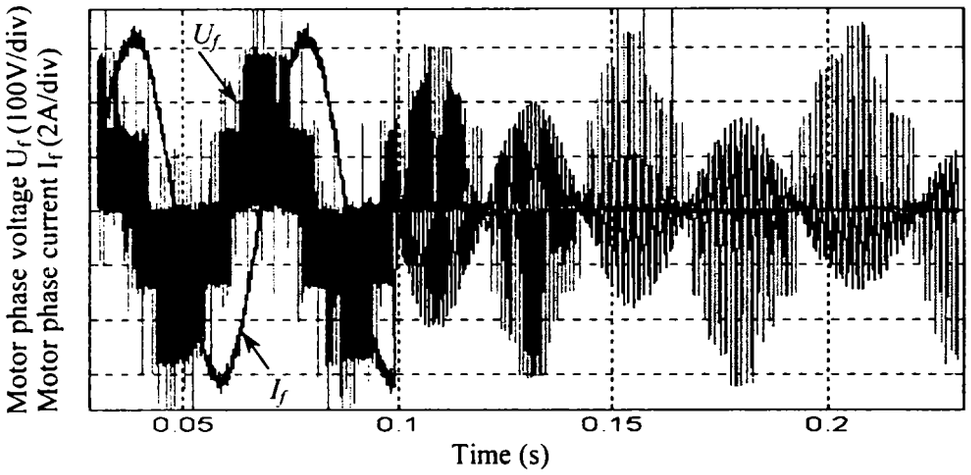

Fig. 7.7: Measured motor phase voltage U_f and current I_f during transition from normal operation to the proposed ride-through strategy

The data acquired in the previous tests are used to estimate offline if the proposed strategy is capable to recover energy from the spinning motor during the proposed ride-through operation. By comparing the motor current vector magnitude to the chosen limit I_{lim} in (7.1), it is possible to reconstruct the phase voltage offline, as shown in Fig. 7.8a. During a zero vector ($|I_s| < I_{lim}$), the phase voltage is considered zero. When the current magnitude has exceeded the limit, the converter is turned off and in order to ensure the continuity for the motor currents, the converter freewheeling diodes will conduct. The sign of the motor currents indicate which freewheeling diode is conducting, and from there the potential on the motor phases and the phase voltages may be determined.
By knowing the values of the DC-link voltage U_{DC} (Fig. 7.8b) and the capacitor value, and using (7.2) it is possible to estimate the recovered energy W_{DC}, as is shown in Fig. 7.8c. A low pass filter with a 10 ms time constant reduces the high ripple in the instantaneous power (7.3) as shown in Fig. 7.8d. Also to determine the peak value of the recovered power, which is highest when the ride-through operation starts, the recovered power is averaged (P_{avrg}) during the ride-through operation using (7.4) and is presented in Fig. 7.8e. During this test, the auxiliary energy taken by the frequency converter is neglected. The filtered recovered power presented in Fig. 7.8d shows a 250 W peak, while the average recovered power presented in Fig. 7.8e shows an 1.5 kW peak. This concludes that it is possible to recover enough energy from the motor to feed the control boards.

$$W_{DC}[k] = C_{DC} \cdot (U_{DC}^{\,2}[k] - U_{DC}^{\,2}[0]) / 2 \tag{7.2}$$

$$P[k] = W_{DC}[k] \cdot f_{sw} \tag{7.3}$$

$$P_{avrg}[k] = W_{DC}[k] / (t[k] - t[0]) \tag{7.4}$$

where: $W_{DC}[k]$ is the recovered energy at the current sample $t[k]$;
$t[0] = t_{on}$, the moment when the ride-through operation starts.

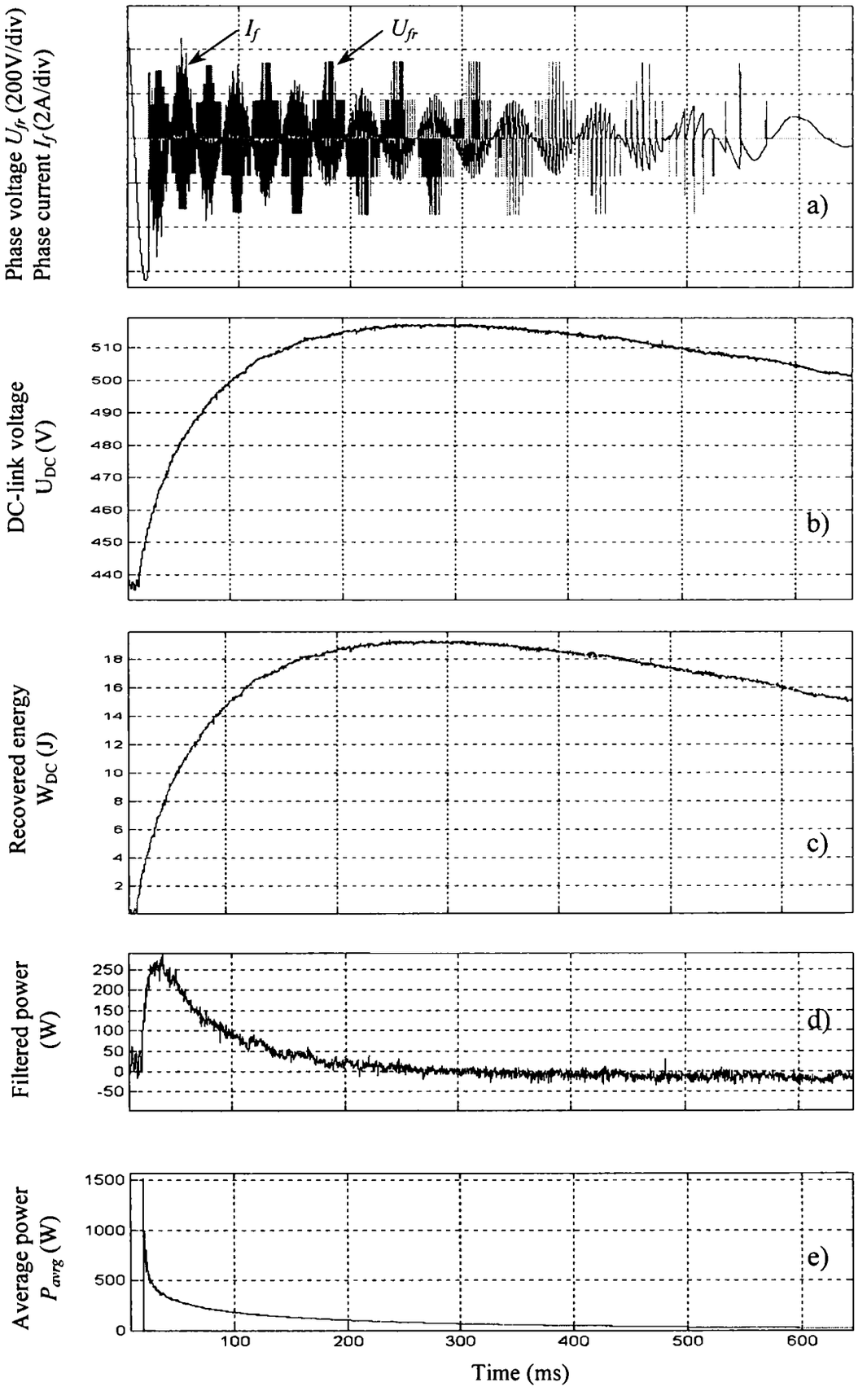

Fig. 7.8: Ride-through operation test:
a) reconstructed phase voltage U_{fr} and measured current I_f; b)DC-link voltage U_{DC};
c) recovered energy W_{DC}; d) filtered recovered power; e) averaged recovered power P_{avrg};

When the strategy is implemented into the MC control software, the designer should pay attention to the lower limit of the switching frequency and to the limit of the current vector magnitude which should not be too close to the overcurrent protection limit. If condition (7.1) is verified once per switching period, but the switching period is too long, or the phase currents rise too fast due to a high motor EMF or a low leakage inductance, the current may reach the overcurrent protection level and cause a fault during the zero-vector. This problem appears especially during the first commutations, due to the higher values of the rotor flux and speed, when the EMF may reach the nominal voltage. For example in Fig. 7.8a, the phase current during ride-through operation reaches 5 Amps, but the current limit I_{lim} is set to 1.4 Amps.

7.3 OBSERVERS FOR VOLTAGE SPACE VECTOR SPEED AND ANGLE

When normal grid conditions are re-established, the control logic should restart the drive as fast as possible. To do this fast, a few parameters for the modulator must be known all the time during the ride-through operation: the actual frequency, the angle of the reference voltage vector and the initial value of the modulation index, which depends on the residual rotor flux level. In the ride-through regime, the induction motor acts as a synchronous motor where the decreasing rotor flux provides the electromechanical conversion of the energy. The load of the "synchronous generator" is the clamp circuit. Because the displacement angle between the phase voltage and current fundamentals is 180°, it acts as a resistive load without any inductive current component and the rotor flux influence is not decreased. This means that it might be easy to estimate the restart conditions from the stator currents, as only the current measurements are usually available on the output side.

To estimate the shaft speed during ride-through operation, two models may be considered. One is based on the flux, which has to be estimated, but the voltage model, which uses integration, accumulates errors. Also the voltage across the clamp capacitor has to be measured, and errors to reconstruct the phase voltage and to estimate the stator flux may appear due to an interrupt current mode, which is characteristic for the proposed ride-through operation strategy.

The second model is based on the stator currents, which are measured. Because the motor acts as a synchronous generator, if the high frequency ripple is neglected, the currents may be considered sinusoidal and balanced (see Fig. 7.6). This means that the shaft speed may be estimated from the instantaneous frequency of the motor current vector, which is true for a synchronous generator with balanced load, when the current vector is moving with constant speed on a circular trajectory, of frequency equal to the shaft speed. Also the initial value of the modulator angle at the restarting moment may be determined too, because the current vector and the voltage vector have opposite direction. The stator current model is based on instantaneous values and therefore not so susceptible to integration errors. Also, if there is no need of energy into the clamp circuit and the ride-through logic disables the commutation, it is possible to actualize the necessary information even if the ride-through logic operates in an intermittent regime, commanded by the clamp voltage error. An important disadvantage of the current model is that the displacement angle jumps in the transition moment and causes a momentary high peak of the estimated speed, which is reduced by limiting the instantaneous value of the estimated frequency. The noise produced by derivative operation is reduced with a low-pass filter.

The results of using the current model in estimating the current vector angle and frequency are presented in Fig. 7.9. The estimation is performed offline on the data sample acquired in the test presented in the previous section. Low pass filters for the current angle and frequency observers

are used to reduce the noise caused by the motor current. The time constants of the low pass filter are implemented as relative value to the switching frequency, to give flexibility of the program to changes, and are show in Table 7.2. In Fig. 7.9a the unfiltered angle of the current vector is shown. Off-line software filtering was used to tune the low-pass filters. No important delay in the filtered angle is introduced, as is shown in Fig. 7.9b. Also the error of the estimated shaft speed is smaller than 1.5 Hz in the time range of 150-500 ms, as shown in Fig. 7.9c.

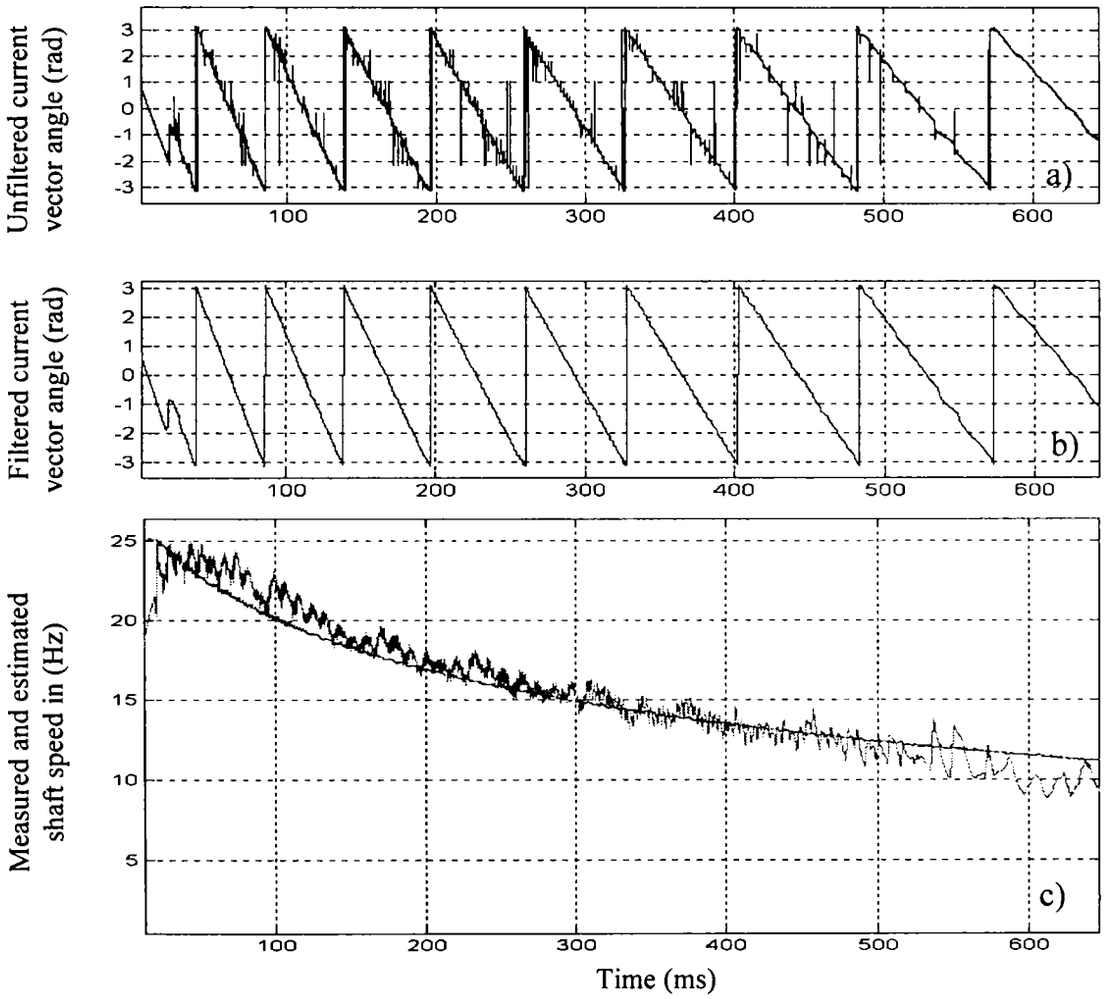

Fig. 7.9: Tuning the filters for the angle and frequency estimators: a) unfiltered angle of the current vector; b) filtered angle of the current vector; c) measured and estimated motor speed;

Table 7.2
Time constants for the filters applied on the current vector angle and frequency

Time constant for the angle filter	0.3 ms ($1.5 \cdot T_{sw}$)
Time constant for the frequency filter	5.6 ms ($28 \cdot T_{sw}$)

7.4 RESTARTING OF THE DRIVE

In order to restart an ASD which uses vector control, the actual shaft speed, the magnitude and the angle of the flux vector has to be known. In the case the ASD uses scalar control, the necessary parameters to initialise the modulator are the initial frequency $\omega_{restart}$ which gives the modulation index m_U according to a constant V/Hz dependency, and the modulator initial angle $\varphi_{restart}$. If the modulation index according to the actual shaft speed frequency is applied in the restarting moment, an overcurrent fault occurs due to the reduced flux level in the motor. This may be avoided if the initial modulation index m_{U0}, which depends on the residual rotor flux, is known. If an exponential variation of rotor flux during ride-through operation is considered, the modulation index in the restarting moment may be estimated using (7.5). In Fig. 7.10 the dependence of the relative value of the modulation index corresponding to the motor used in tests (T_R=117 ms) is shown.

$$m_{U0} \cong f_{restart} / f_N \cdot \exp(-t_{pw\_loss} / T_R) \tag{7.5}$$

where $f_{restart}$ = the motor speed (Hz) in the restarting moment;
f_N = nominal motor frequency (Hz);
t_{pw_loss} = the duration of ride-through operation (s).
T_R = rotor time constant (s);

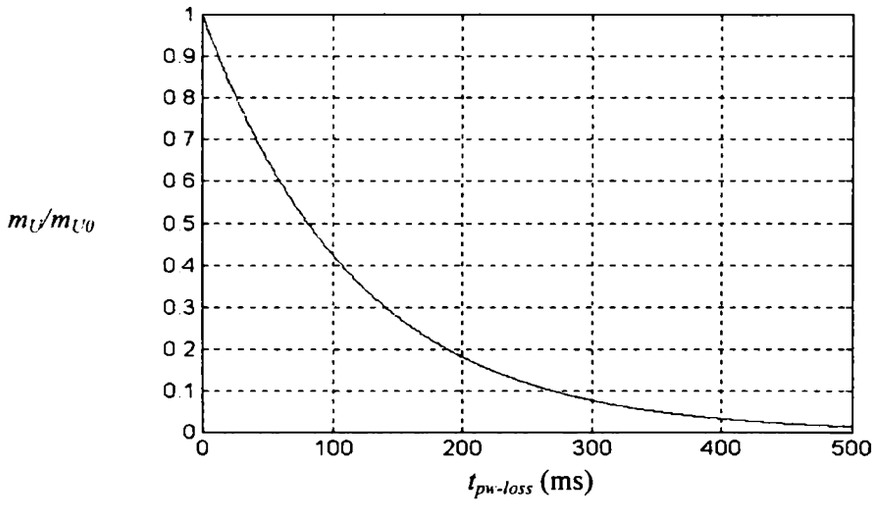

Fig. 7.10: The relative modulation index vs. the duration of the ride-through operation (ms)

A simplification may be done to reduce the computational requirements when implementing (7.5). Considering that the duration of the ride-through operation could not exceed four times the rotor time constant, which corresponds to a residual rotor flux smaller than 2% of the nominal value, the time domain may be divided in a few parts, where the exponential functions may be considered linear. An increase in the modulation index to the actual frequency must be performed in the same way in order to avoid overcurrents. It is not recommended to increase too much the restarting time, because if the drive decelerate under the pull out slip, it won't be able to restart and an overcurrent fault occurs.

In Fig. 7.11 the transition form ride-through operation to normal operation is shown. The test was started with the induction motor running in steady state, with 35 Hz reference frequency. By forcing the software to operate in the ride-through operation mode, a 300 ms power interruption has been simulated (t_{on}=50 ms). After that, the motor is switched to normal operation, by initialising the SVM modulator with the estimated speed (in Hz) and position of the motor current vector. In the restarting moment, only 25 % of the voltage, which corresponds to the actual speed, is applied to the motor in order to reduce the overcurrents but aperiodic transients appears anyway.

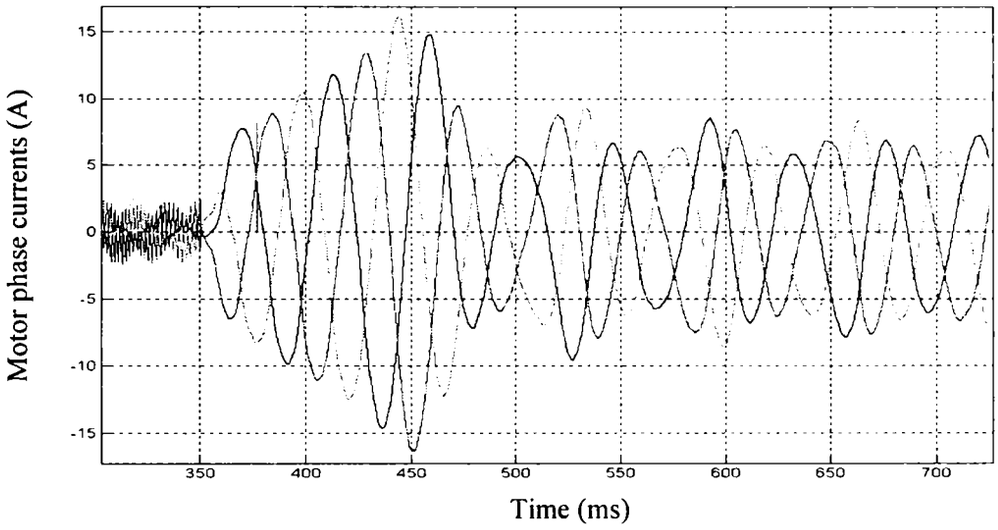

Fig. 7.11: The measured motor currents during the restarting procedure which follows a 300 ms ride-through operation (Test conditions: 8 kHz switching frequency, 35 Hz reference frequency, 25 % initial voltage boost in the restarting moment.)

7.5 LABORATORY SETUP AND EXPERIMENTAL EVALUATION

Tests of the proposed strategy are performed on a 4kW/1435 rpm induction motor (see full parameter list in Appendix 7.1) connected to an 8 kVA industrial frequency converter (Danfoss VLT 3008) with 500μF DC-link capacitors and 20 W losses in the auxiliary circuits. The DC-link capacitors and the freewheeling diodes of the VSI provides a convenient solution to emulate the clamp circuit when the MC is disconnected, while the IGBT's and the freewheeling diodes emulate the MC when a zero-vector is produced. In this way, it is easy to perform the transition from normal operation, when the induction motor is using scalar control (constant V/Hz), to the ride-through operation. The laboratory set-up is shown in Fig. 7.12.

The converter is controlled by a multiprocessor system, which consists of an ADSP-21062 32-bit floating point DSP board to perform the motor control and a SAB80C167 16-bit microcontroller board to perform the pulse generation, connected through a dual port RAM.

Four signals give complete control of the frequency converter: three command signals for the IGBT's (PWM0, PWM1, PWM2) to produce the desired output state of the inverter and a signal (*enable_VSI*) to enable/disable the IGBT's command. The duty-cycle of the three PWM signals is controlled from the DSP program. In normal operation the converter uses a double-sided Space Vector Modulation (SVM) for the pulse generation. During the ride-through operation, the three command signals are forced to produce continuos zero-vector for the whole duration of the ride-through operation. By using the *enable_VSI* signal, the converter may be turned on/off according

to condition (7.1) each sampling period, which is equal to the switching period from the normal operation.

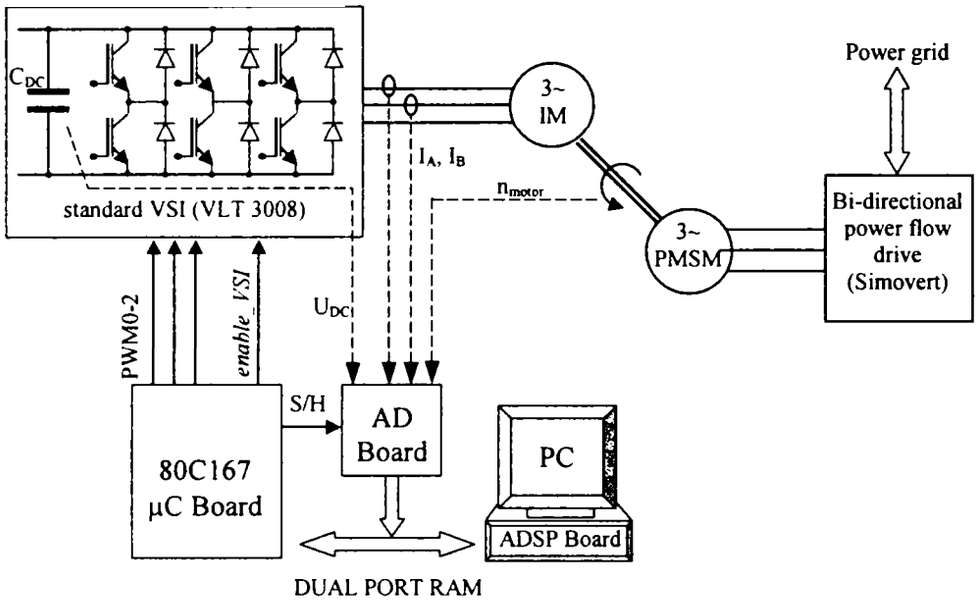

Fig. 7.12: The laboratory set-up used to test the ride-through strategy

All the tests are performed using a reduced value of the DC-link voltage (440...500 V) in order to avoid overvoltage faults during the period when the induction motor acts as a generator. Tests with 40 Hz initial frequency of the motor are presented in order to provide nominal flux of the motor, in the case of reduced DC-link voltage. The control diagram of the system is shown in Fig. 7.13.

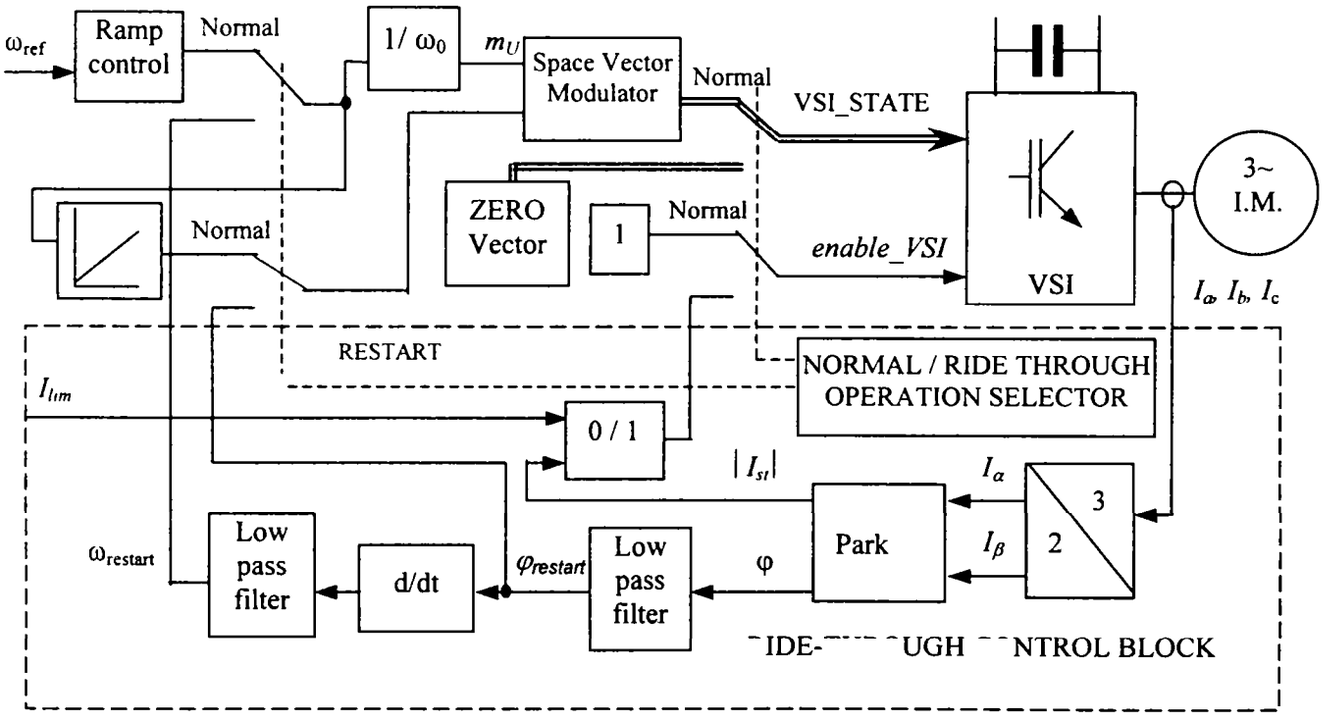

Fig.7.13: The control diagram to test the ride-through strategy

The interface of the DSP program allows the user to modify the switching frequency, the output reference frequency which corresponds to normal operation, the limit of the current vector magnitude which corresponds to the ride-through operation, the duration of the simulated "power grid disturbance" and the acceleration ramp for the restarting sequence. In order to have access to a record for a longer duration, data are stored and saved on three columns: two measured motor currents and alternating, due to a lower dynamics, the measured motor speed and the measured DC-link voltage. The third motor current is reconstituted considering that the sum is zero. The measured speed and the measured DC-link voltage are not used in the control. In this way, a data record of 5500 samples gives the opportunity to analyse the performance of the proposed strategy for a duration of 1100 ms (5 kHz sampling frequency) to 1815 ms (3 kHz sampling frequency).
Fig. 7.14, Fig. 7.16 and Fig. 7.17 show the drive performing a complete ride-through operation cycle in three situations:

- 40 Hz initial frequency and no load torque (Fig. 7.14);
- 40 Hz initial frequency and 10% load torque (Fig. 7.16);
- 50 Hz initial frequency at no load, where due to the reduced DC-link voltage, the motor operates with reduced flux (Fig. 7.17).

The test conditions are presented in Table 7.3.

Table 7.3
Setup parameters for the experiments presented in Fig. 7.14 –7.17

Transition moment (t_{on})	135 ms
Ride-through duration ($t_{pw\text{-}loss}$)	200 ms
Switching frequency (f_{sw})	3 kHz
Limit of the current vector (I_{lim})	2 A
Acceleration ramp after restart	30 Hz/s

It should be noted that supplementary load torque is applied on the shaft during ride-through operation as an effect of the regenerative regime. Fig. 7.15 shows the estimated electromagnetic torque T_{em} during ride-through operation, caused by the energy recovering process. There, a 3 Nm maximum value of the estimated electromagnetic torque during the ride-through operation is shown, which represents 11.5% of the motor nominal torque. This corresponds to the no-load test presented in Fig. 7.14 and it was estimated using the filtered recovered power $P_{filtered}$, which is calculated from the DC-link voltage (similar to Fig. 7.8d), and the measured rotor speed f_R.

$$T_{em} = P_{filtered}/(2 \cdot \pi \cdot f_R \cdot p) \tag{7.6}$$

where p represents the motor pole pairs.

The effect of a load torque on the motor shaft, applied during tests may be seen in the speed drop: from 26 Hz in the no-load situation (Fig. 7.14b) to 18 Hz at 10% load torque situation (Fig. 7.16b). This conclude that in order to ensure operation during power interruption, the ASD inertia should be high enough to provide energy for the mechanical load and also for the ride-through mechanism.

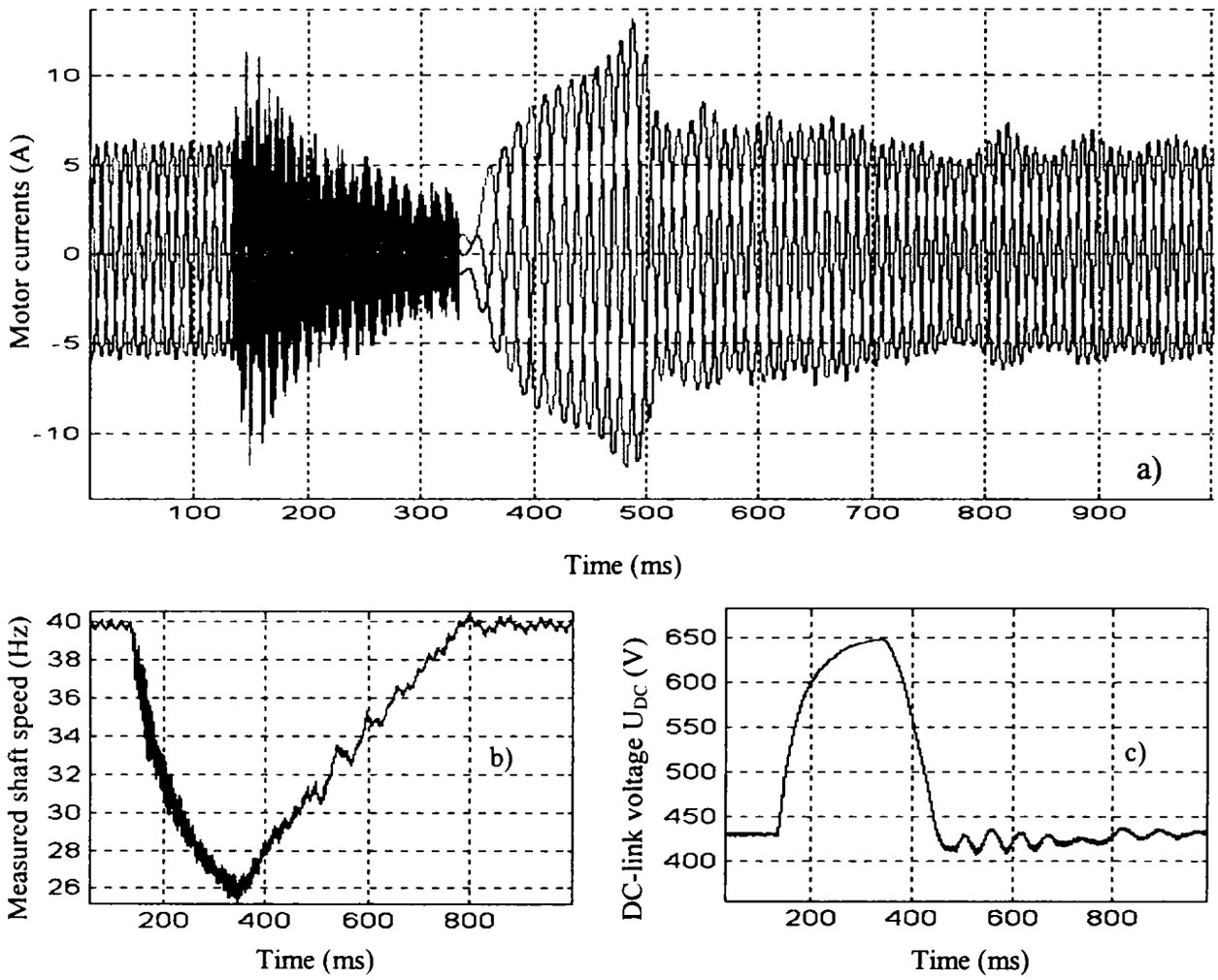

Fig. 7.14: Experimental results of 200 ms ride-through operation
a) Measured motor currents; b) Measured motor speed; c) Measured DC-link voltage.
(Test conditions: 40 Hz reference frequency, 3 kHz switching frequency and no load.)

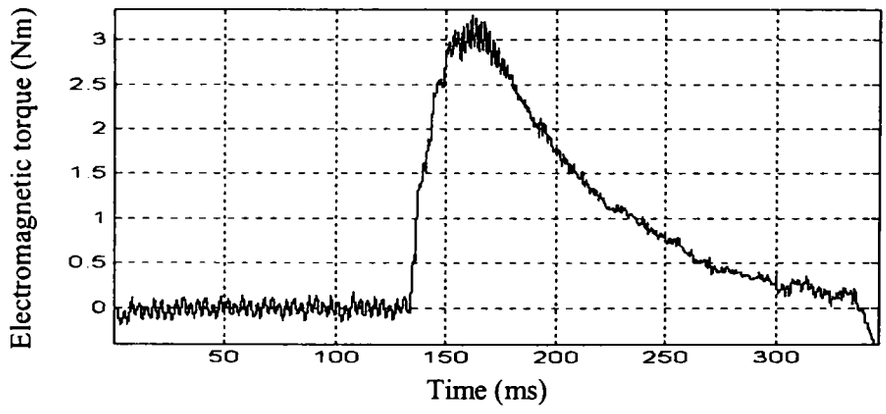

Fig. 7.15: The estimated electromagnetic braking torque vs. time during the ride-through operation in Fig. 7.12 (t_{on}=135ms, t_{off}=335ms)

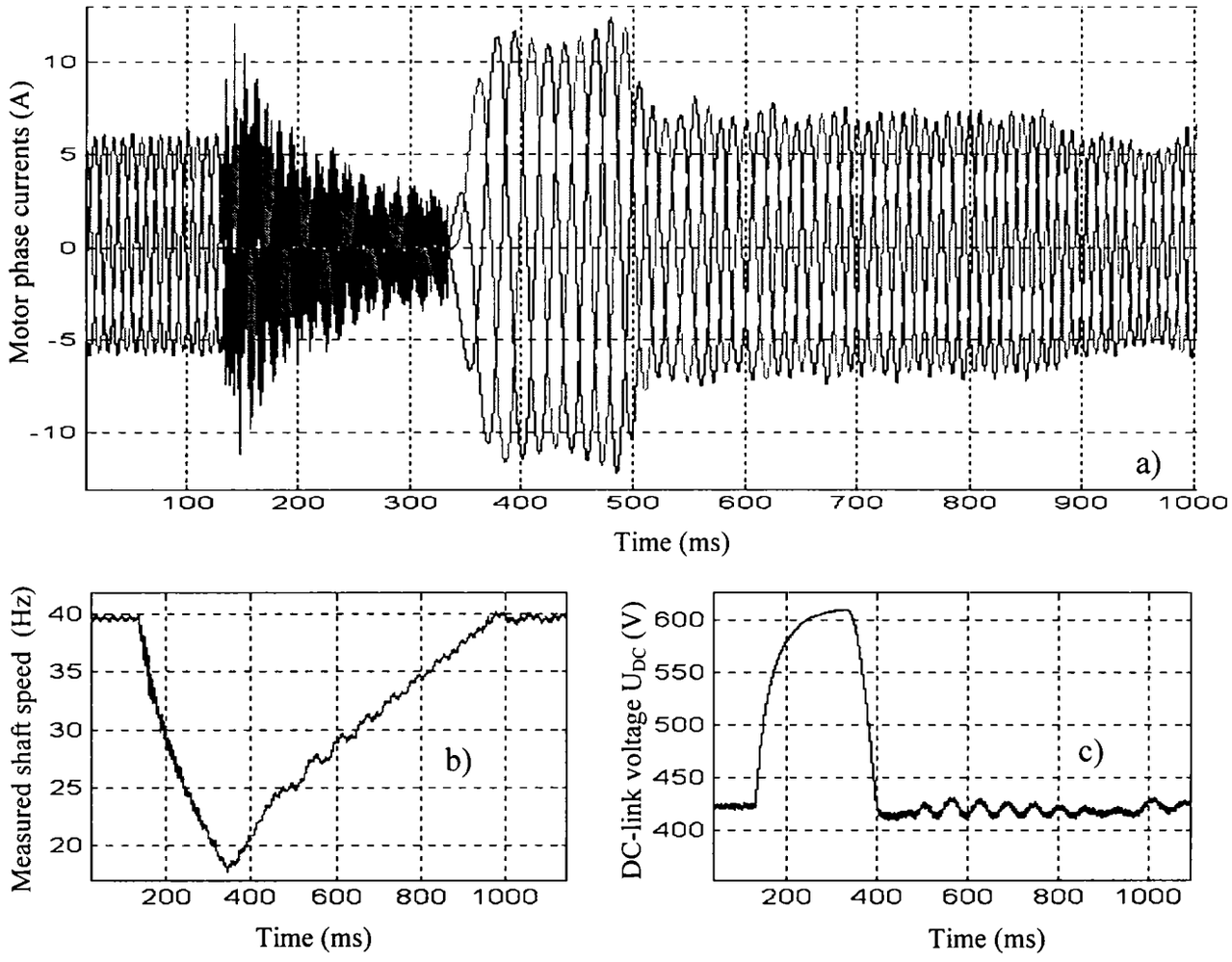

Fig. 7.16: Experimental results of 200 ms ride-through operation
a) Measured motor currents; b) Measured motor speed; c) Measured DC-link voltage.
(Test conditions: 40 Hz reference frequency, 3 kHz switching frequency and 10% load.)

In Fig. 7.17 a ride-through strategy test with 50 Hz reference frequency and no-load condition is shown. This corresponds to a lower level of the motor flux, which may be seen in the motor currents, lower than in the previous no-load test (Fig. 7.14a).
In all the tests, 20 % of the corresponding modulation index is applied in the restart moment, to avoid overcurrents caused by the reduced flux level. The modulation index reaches the full corresponding value within 200 ms. The motor accelerates toward the reference frequency immediately after restart, with an acceleration ramp of 30 Hz/s in both cases. This means that an extra 2 Nm dynamic torque loads the motor during acceleration, due to 0.0215 kgm^2 total rotor inertia (see Appendix 7.1). The flux starts to increase to the nominal value. This takes about 170 ms and results in higher currents, which decrease as the flux increases, as shown in Fig.7.14a, Fig. 7.16a and Fig.17a. During the ride-though operation and the restart the motor current reaches a maximum of 14 Amps, which is slightly higher than the nominal motor current amplitude. In the case the load torque is applied to the motor shaft, the restart is performed from a lower shaft speed and it takes longer. A few phase current peaks appear during the ride-through operation, because the commutation conditions are verified only once per sampling period, which is low (0.33 ms).

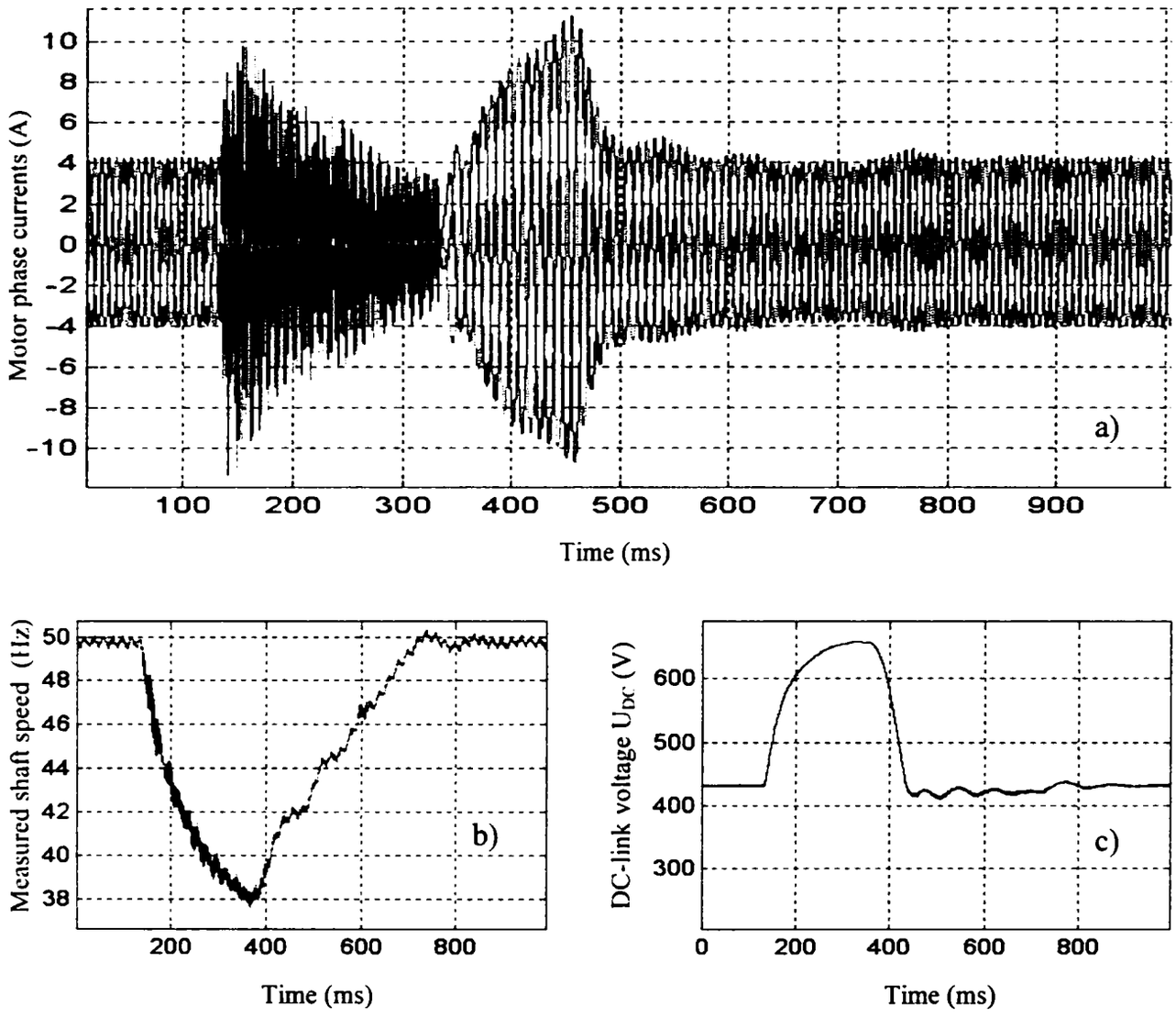

Fig. 7.17: Experimental results of 200 ms ride-through operation
a) Measured motor currents; b) Measured motor speed; c) Measured DC-link voltage.
Test conditions: 50 Hz reference frequency, 3 kHz switching frequency and no load.

7.6 SUMMARY

In this chapter, a new ride-through strategy applied to direct frequency converters has been presented. The maximum duration of the ride-through operation depends on the induction motor parameters and on the initial parameters of the ASD. The main conclusions are:

- it is possible to implement a simple ride-through operation strategy for a scalar controlled MC induction motor drive without any hardware modification;
- the proposed MC ride-through strategy provides not magnetic flux control. The single feature is to provide a mechanism to transfer energy from the motor to the DC-link (clamp capacitor) to feed the hardware;
- the proposed shaft speed and angle observer is based on the instantaneous values of the motor currents and it is not susceptible to cumulate errors;
- no important overcurrents occur during the restart procedure, though the drive is scalar controlled and the switching frequency is low (3 kHz);

- the proposed ride-through strategy is recommended for high-inertia loads where the decrease of the speed during restarting procedure did not exceed the pull out slip frequency. However, the speed drop during the restarting procedure, until the motor flux level is re-established may be estimated, based on the speed variation during ride-through operation;

APPENDIX 7.1

The parameters of the induction motor used for tests in Chapter 7:

P_N = 4 kW, U_N = 400 V, f_N = 50 Hz, I_N=8 A, cos φ = 0.84, n_N = 1435 rpm, η = 85.5%,
T_N = 26.6 Nm, J = 0.014 kgm^2+0.0075 kgm^2 aux. inertia,
R_S = 1.64 Ω, R_R = 1.45 Ω, L_S = L_R = 170 mH, L_m = 164 mH, T_R = 117 ms.

REFERENCES

[7.1] C. Klumpner, P. Nielsen, I. Boldea, F. Blaabjerg, "*A new matrix converter-motor (MCM) for industry applications*", Proc. of IAS Annual Meeting, vol. 3, pp. 1964-1971, 2000.

[7.2] C. Klumpner, I. Boldea, F. Blaabjerg, "*Short term ride through capabilities for direct frequency converters*", Proc. of PESC'00, vol. 1, pp. 235-241, 2000.

[7.3] S. Chattopadhyay, T.S. Key, "*Predicting behaviour of induction motors during electrical service faults and momentary voltage interruptions*", Proc. of Industrial and Commercial Power Systems Technical Conference, pp. 78-84, 1993.

[7.4] A. David, E. Lajoie-Mazenc, C. Sol, "*Ride-through capability of AC adjustable speed drives in regards to voltage dips on the distribution network*", Proc. of EPE'93, vol. 1, pp. 139-144, 1993.

[7.5] M.J. Sullivan, T. Vardell, M. Johnson, *"Power interruption costs to industrial and commercial consumers of electricity*", IEEE Trans. on Industry Applications, vol. 33, pp. 1448-1457, 1997.

[7.6] G. Yalcinkaya, M.H.J. Bollen, P.A. Crossley, "*Characterisation of voltage sags in industrial distribution systems*", Proc. of IAS Annual Meeting, vol. 3, pp. 2197-2204, 1997.

[7.7] A. von Jouanne, P. Enjeti, B. Banerjee, "*Assessment of ride-through alternatives for adjustable speed drives*", Proc. of IAS Annual Meeting, vol. 2, pp. 1538-1545, 1998.

[7.8] E.M. Sisa, "*Power outages and power dip ride-through*", Proc. of Textile, Fiber and Film Industry Technical Conference, pp. 1-7, 1995.

[7.9] E.R., Jr. Collins, A. Mansoor, "*Effects of voltage sags on AC motor drives*", Proc. of Textile, Fiber, and Film Industry Technical Conference, pp. 1-7, 1997.

[7.10] J. Holtz, W. Lotzkat, *"Controlled AC drives with ride-through capability at power interruption*", Proc. of IAS Annual Meeting, vol. 1, pp. 629-626, 1993.

[7.11] B.J. Siebel, R.J. Kerkman, D. Leggate, "*Inverter control during overload and following power interruption*", IEEE Trans. on Industry Applications, vol. 28, pp. 567-573, 1992.

[7.12] A. David, E. Lajoie-Mazenc, C. Sol, "*Soft restart of an adjustable speed drive after a short disconnection without any mechanical speed sensor*", Proc. of Electrical Machines and Drives, pp. 570-575, 1993

[7.13] A. van Zyl, R. Spee, A. Faveluke, S. Bhowmik, *"Voltage sag ride-through for adjustable speed drives with active rectifiers*", Proc. of IAS Annual Meeting, vol. 1, pp. 486-492, 1997.

[7.14] J.L. Duran-Gomez, P. Enjetti, "*A low cost approach to improve the performance of an adjustable speed drive (ASD) under voltage sags and short-term power interruptions*", Proc. of APEC'98, vol. 2, pp. 587-591, 1998.

[7.15] A. van Zyl, R. Spee, "*Short term energy storage for ASD ride-through*", Proc. of IAS Annual Meeting, vol. 2, pp. 1162-1167, 1998.

[7.16] J.L. Duran-Gomez, P.N. Enjeti, B.O. Woo, "*Effect of voltage sags on adjustable speed drives – A critical evaluation and an approach to improve its performance*", IEEE Trans. on Industry Applications, vol. 35, pp. 1440-1449, 1999.

[7.17] M. Corley, J. Locker, S. Dutton, R. Spee, "*Ultracapacitor-based ride-through system for adjustable speed drives*", Proc. of PESC'99, vol. 1, pp 26 –31, 1999.

[7.18] J.L. Duran-Gomez, P.N. Enjeti, A. von Jouanne, "*An approach to achieve ride-through of an adjustable speed drive with flyback converter modules powered by super capacitors*", Proc. of IAS Annual Meeting, vol. 3, pp. 1623 –1629, 1999.

[7.19] M. James, M.J. Leach, S.J. Mackay, "*Phase-on ride-through control circuit*", US Patent No. 4,459,652, July 1984.

[7.20] D.L. Drinkwater, "*Ride-through energy boost circuit*", US Patent No. 4,818,891, April 1991.

[7.21] P.N. Enjeti, J.L. Duran-Gomez, "*Method and system for ride-through of an adjustable speed drive for voltage sags and short-term power interruption*", US Patent No. 6,005,362, December 1999.

[7.22] R. Langley, A. Mansoor, E.R. Collins, R.L. Morgan, "*Voltage sag ride-through testing of adjustable speed drives using a controllable dynamometer*", Proc. of Harmonics and Quality of Power, vol. 1, pp. 566-571, 1998.

[7.23] "*ACS 600 Single-drive frequency converters for speed and torque control of 2.2 to 3000 kW squirrel cage motors - Technical catalogue*", 3AFY 58059412 R0425 EN, ABB Industry Oy, 1988

[7.24] C.L. Neft, C.D. Shauder, "*Theory and design of a 30-hp matrix converter*", Proc. of IAS Annual Meeting, pp. 248-253, 1998.

[7.25] P. Nielsen, F. Blaabjerg, J.K. Pedersen, "*Novel solution for protection of matrix converter to three phase induction machine*", Proc. of IAS Annual Meeting, vol. 2, pp. 1447-1454, 1997.

Chapter 8

The Matrix Converter-Motor: An Integrated Motor Drive with Bi-directional Power Flow

The trend in electrical drives is to integrate the frequency converter, the electrical motor and even the gear or the pump into a single unit, in order to optimise the electromechanical assembly, to reduce the costs and to increase the overall efficiency and the equipment reliability.
This chapter presents the implementation of an integrated regenerative frequency converter-motor for industry applications, based on a matrix converter topology [8.1]. The low volume, the sinusoidal input current, the bi-directional power flow and the lack of the bulky and limited-lifetime electrolytic capacitors recommend this topology for this application. It is shown how the matrix converter disadvantages - the lack of bi-directional power devices, the lower voltage transfer ratio, the lack of ride-through capability and the overvoltages caused by the input filter during power-up - which have delayed the industrial implementation, have been overcome.
In order to demonstrate the validity of the solution, a 4 kW-Matrix Converter-Motor (MCM) prototype is built using a standard frequency converter-motor enclosure and tested to meet the requirements for an industrial drive.
In Section 8.2, the demands of an industrial drive are analysed with respect to the mechanical characteristic, reliability, harmonics, ride-through capability, in-rush problems and other standards. The main circuit topology of the new matrix converter-motor (MCM) is presented in Section 8.3 and the design procedures for the input filter and the clamp circuit are discussed in Section 8.4. Section 8.5 describes the hardware implementation aspects of the MCM prototype, while Section 8.6 describes the software implementation aspects. Section 8.7 presents experimental results showing voltage and current waveforms during steady state and acceleration tests and measurements on the input side.

8.1 INTRODUCTION

Today, Adjustable Speed Drives (ASDs) constitute a mature technology. Based on IGBT's which can work at 5-20 kHz switching frequency, the ASDs are capable of producing high-resolution waveforms in order to minimise the extra motor losses caused by the current harmonics. Also due to the low losses of the IGBTs, the frequency converter efficiency reaches 0.98 at full load. Furthermore, smart strategies to drive the motor as flux optimisation are able to increase the overall efficiency of the drive [8.2], [8.3].
In the last decade, a new ASD topology - the integrated frequency converter-motor - was developed in order to reduce the production and commissioning costs and to improve the EMC compatibility [8.4]. The application area is limited to the low power range, due to the problems that appear in the high power range such as mechanical vibrations and the difficulties of dissipating a higher amount of heat in dusty environments. The frequency converter employ a classical topology of diode rectifier DC-link Voltage Source Inverter (VSI), is mounted inside an

enclosure placed on the top or on the bottom of the motor and may use the motor fan airflow for cooling. The parts inside the converter must be more reliable due to the environment conditions, which are heavier than for a standard drive. A few frequency converter-motor registered trademarks are presented below:

- ABB Motors, "***Integral Motors***", 0.75 kW – 7.5 kW;
- Alen Bradley, "***Integrated AC Drive & Motor***", 1 HP – 5 HP;
- Brook Hansen, "***Variable Speed Motor***", 0.55 kW – 4 kW;
- Danfoss, "***FCM 300 - VLT DriveMotor***", 0.55 kW – 7.5 kW;
- Grundfos, "***MGE motors***", 1.5 kW – 5.5 kW;
- Siemens, "***Combimaster***", 1.5 kW- 7.5 kW;

In research, efforts are made to replace the traditional limited-lifetime electrolytic capacitors with film capacitors and to improve the line side performance of the drive. Also, new frequency converter topologies are currently being investigated: the VSI with a minimised DC-link capacitance [8.5] the Vienna rectifier [8.6] or the matrix converter (MC) [8.7]-[8.22], which has the advantage of the bi-directional power flow.
In recent years, in order to comply with new IEC directives requiring better interaction with the grid, a new class of frequency converters has been developed and has become commercialised. Based on a back-to-back VSI topology, this regenerative drive allows high-dynamic bi-directional power flow and sinusoidal input currents but requires high-volume input chokes, which increases the volume of the drive. EMC compatibility in the high frequency range is still a problem due to high dU/dt pulses generated by the VSI connected on the input side.
The matrix converter known as a "total silicon solution" has a low-volume reputation and may offer a good alternative by providing the same benefits: bi-directional power flow and sinusoidal input currents. Despite to a low voltage transfer ratio, the matrix converter is recommended in integrated frequency converter-motor applications where the bi-directional power flow is needed. Due to the fact that in the integrated motor-drive application the frequency converter and the motor are designed to fit together, the disadvantage mentioned before could be eliminated by designing the motor to reach the nominal motor voltage at maximum voltage transfer ratio of the matrix converter.
In this chapter is presented the implementation of a matrix converter to a frequency converter-motor prototype for industry application, which uses specially designed power modules with bi-directional switches and a motor matched to the maximum voltage transfer ratio of the matrix converter.

8.2 DEMANDS TO AN INDUSTRIAL DRIVE

The mechanical characteristic of a drive shows the torque-speed dependence, usually in the 1st quadrant, because standard drives without a breaking chopper are able to operate for long term only in quadrant I and III. Due to the fact that the matrix converter allows the bi-directional power flow, the MCM prototype is able to operate in four quadrants, as shown in Fig. 8.1. Until the base speed, the operation area is limited to the nominal torque T_N. In the flux-weakening region ($\Omega_N<\Omega<\Omega_{max}$), the available torque decreases due to the constant power limitation following a hyperbolic dependence. At low-speed, the torque capability decreases due to the ventilation problems. Higher torque is available for short-term and also for long-term only if forced ventilation is used.

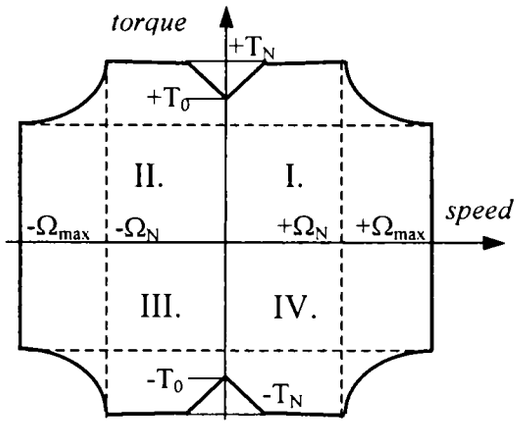

Fig. 8.1: The mechanical characteristic of the MCM prototype

The drive reliability depends on the operating conditions and on the performance of the components, given by the manufacturer. As no moving parts are used in the prototype (fans) and as the film capacitors are able to operate in a wider temperature range, it is expected that the MCM drive to be more reliable than a back-to-back VSI drive. The matrix converter is not able to compete with the classical diode-bridge VSI because the diode-bridge offers the most reliable interaction with the power grid and because it does not require voltage sensors on the grid side.
The input current and voltage harmonics are an important issue in industial drives. The standards demand that the input current THD should be limited. Also, perturbations present in the input voltage should not disturb the drive functionality. It is known that the matrix converter provides sinusoidal input currents and unity displacement power factor. Therefore, a better interaction between the MCM prototype and the power grid is expected, compared to a diode-bridge VSI.
The ride-through capability is a common feature on standard drives and it has been investigated in [8.23], [8.24]. During power-loss, a standard drive decelerates, recovering the necessary energy from the motor and load inertia to feed the control electronics and to magnetize the motor. The main tasks of the ride-through control are to maintain a constant DC-link voltage and when normal power grid conditions are re-established, to accelerate the drive to the reference speed from a nonzero shaft speed. The matrix converter is considered to be a total grid dependent topology, therefore no ride-through capability is normally expected. Using the residual magnetic flux, a short-term ride-through strategy for matrix converters [8.1], [8.25] has been presented in Chapter 7 and may be implemented on the MCM prototype. This may provide the necessary energy to feed the control hardware for hundreds of milliseconds, by forcing the energy to flow from the motor leakage inductance to the clamp circuit capacitor, where the switch-mode power supply (SMPS) is connected. Also it is possible to acquire the necessary information to perform a quick restart of the drive from nonzero shaft speed and residual rotor flux.
Power-up problems are expected to appear, due to the L-C series topology of the input filter. Therefore, a power-up circuit is implemented on the MCM prototype to damp the oscillations and to limit the overvoltage level during power-up.

Other standards: The test specifications for the MCM prototype include:

Immunity and Emission EMC-test:

- Low Frequency on Line supply port
  - Voltage harmonic distortion
  - Commutation notches
  - Voltage dips, voltage interruptions
  - Voltage unbalance
  - Frequency variations
- High Frequency on Line supply port
  - VDE0160 transient
  - Surge
  - Burst

Emission test

- High and Low Frequency on Line supply port
  - RFI
  - Harmonic current

8.3 TECHNICAL SPECIFICATION FOR THE MCM PROTOTYPE

The main circuit diagram of a matrix converter is presented in Fig. 8.2. The 3x3 matrix of bi-directional switches needs a few reactive components to work properly.

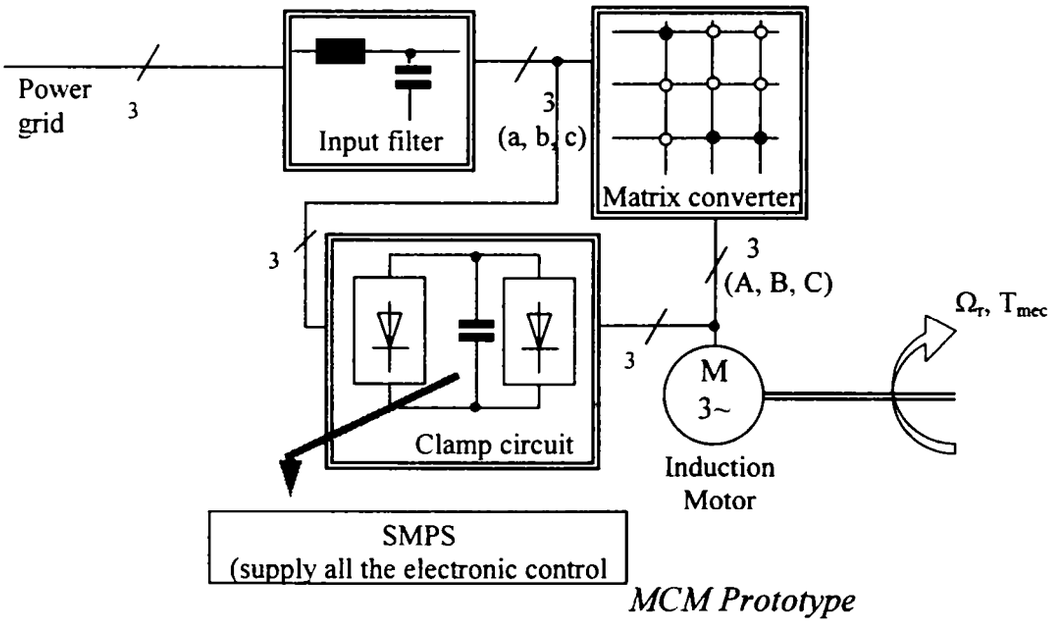

Fig. 8.2. Block scheme of a matrix converter drive

Three AC-chokes and three capacitors which form the input filter are connected into a low-pass filter configuration on the input side to improve the input current waveform by reducing the high frequency current ripple. A clamp capacitor and twelve Fast Recovery Diodes (FRD) form the clamp circuit, which protects the matrix converter against overvoltages on both sides. On the input

side, overvoltages may be caused by line perturbations or by lightning. On the output side, dangerous overvoltages may appear during converter shutdown caused by an overcurrent fault. The energy stored in the motor leakage inductance has to be discharged without any dangerous overvoltage. Therefore, the clamp circuit is considered to be a general overcurrent/overvoltage protection [8.7]. A switch-mode power supply (SMPS) can also be connected to the clamp capacitor to produce the necessary voltage for all the control electronics.
In Fig. 8.3 the main components of the MCM prototype are shown. The matrix converter is assembled inside a metallic box of an industrial a 4kW integrated motor drive (FCM 304 – Danfoss) and mounted on the top of a 4kW/330V induction motor. The control of the MCM prototype is performed from a *Control Panel*, connected with a shielded cable to the MCM prototype. This contains three buttons to give: *STOP/START* command, *DIRECTION* command and *FAST STOP* command and a potentiometer to produce a 0-5V variable voltage which gives the *Reference Frequency*.

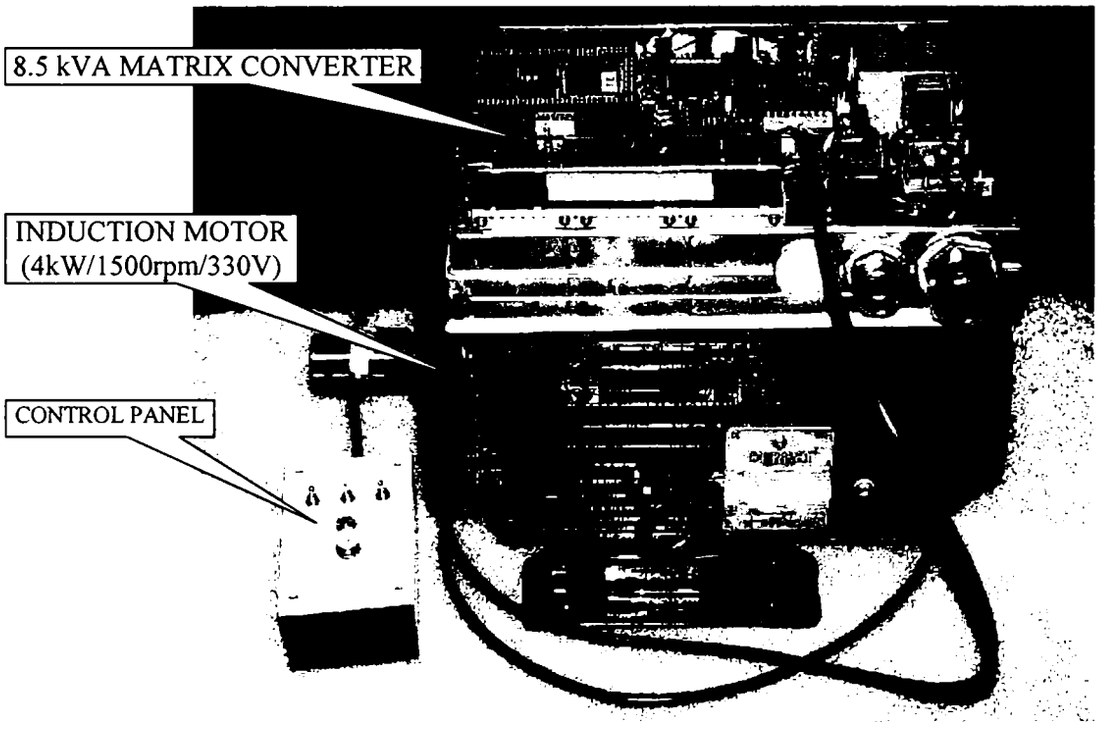

Fig. 8.3: The main components of the MCM prototype

The technical specification of the MCM prototype is presented in Fig. 8.1.

Table 8.1
Technical specification for the MCM prototype

Input terminals:

- Input voltage: 380 V/±10% and 50Hz;
- Voltage unbalance: max. 2%;
- Voltage THD: max. 2%;
- Current THD_{40}: max. 10% at nominal power;
- PF = 0.98;
- cos φ = 1;

Motor rated parameters:
- Nominal motor voltage: 330 V (Y);
- Nominal motor current: 10 A_{rms};
- Nominal motor frequency: 50 Hz;

Motor terminals:
- Motor control strategy: scalar;
- Output voltage: 0-330V;
- Output frequency: 0-100 Hz;
- Switching frequency: 3.5...4.5 kHz;
- Overcurrent protection level: 20 A_{peak};
- Output apparent power: 8.5 kVA;

Motor shaft:
- Speed: 50 rpm – 3000 rpm (1500 rpm base speed)
- Nominal torque: ± 26 Nm;
- Mechanical power: ±4 kW;

Control terminals:
- Digital inputs: 3 (*Start/Stop, Direction, Emergency Stop*);
- Analogue inputs: 1 (*Frequency Reference* 0-5 V);

8.4 MAIN CIRCUIT DESIGN

The input filter design has to reduce the input current ripple with minimum installed energy on the reactive elements. The most used topology is an L-C series circuit. More complex topologies have been recommended in the literature in order to achieve higher attenuation at the switching frequency, but are not practical.
The design of the input filter has:
- to provide a cut-off frequency of the input filter below the switching frequency;
- to maximise the displacement power factor *cos* φ for a given minimum output power P_{min} [8.20];
- to minimise the input filter volume or weight for a given reactive power, by taking into account different energy densities for capacitors and chokes;
- to minimise the voltage drop on the filter inductance at the rated current in order to provide the highest voltage transfer ratio;

Usually, the cut-off frequency of the input filter ω_0 is chosen to provide certain attenuation at the switching frequency. Also, the value of the capacitor or the inductance is chosen based on the previous criteria. The other component has to fulfil equation (8.1):

$$L_{in} \cdot C_{in} = \frac{1}{\omega_0^2} \tag{8.1}$$

The inductance value should verify the maximum voltage drop condition at full load:

$$\frac{\Delta U}{U_n} = 1 - \sqrt{1 - (\omega \cdot L_{in})^2 \cdot \left(\frac{I_n}{U_n}\right)^2} = 1 - \sqrt{1 - l_{in}^2} \tag{8.2}$$

where ω is the grid frequency, C_{in}, L_{in}, are the input filter capacitance and inductance, I_n, U_n are the rated input phase current and voltage, l_{in} is the filter inductance in p.u.

Table 8.2
The characteristics of the MCM input filter

$L_{in}/phase$	1.4mH/13A_{pk} (0.015 p.u.)
$C_{in}/phase$	4.7μF/275V + 3x0.68μF/275V (X2 class)
f_0	1640 Hz
A_{min}	-16.8 dB @ 4 kHz
$cos\ \varphi_{min}$	0.85_{CAP} @ P_{out}=10% P_n (500W input power, 305.6VAr)
$\Delta U_{Lin}/U_n$	0.01% @ 7.5A_{rms}, 50 Hz

The clamp circuit has to provide safe operation of the matrix converter during fault situations [8.7] by limiting the overvoltage level that appears on the grid side or on the motor side (8.3). Also the clamp capacitor has to provide enough energy to feed the control for short momentary power interruptions $t_{p\text{-}loss}$, until the ride-through logic is enabled.

$$\frac{3}{4}\cdot i_{max}{}^2\cdot(L_{\delta S}+L_{\delta R})=\frac{1}{2}\cdot C_{clamp}\cdot\left(U_{max}{}^2-565^2\right) \tag{8.3}$$

where i_{max} is the overcurrent protection level, $L_{\delta S}$+$L_{\delta R}$ is the total motor leakage inductance, C_{clamp} is the value of the clamp capacitor and U_{max} is the maximum admissible overvoltage.

Table 8.3
The characteristics of the MCM clamp circuit

C_{clamp}	25 μF/950 V_{DC}, $(dU/dt)_{max}$=100 V/μs;
$(L_{\delta S}+L_{\delta R})_{max}$	28 mH @ i_{max}=20 A, U_{max}=1000 V
ΔE_{FAULT}	6.8 J @ U_{max}=1000 V, U_n=565 V
$t_{p\text{-}loss}$	0.25 s @ P_{SMPS}=30 W, U_{min}=200 V

The power-up circuit consists of a two-pole (normal closed) relay and two damping resistors (R_1 and R_2), as shown in Fig. 8.4, to reduce the overvoltage level during power-up. As no current flows through the power-up relay during normal operation, the reliability is increased compared to a classical VSI power-up scheme. The value of the damping resistors has to be smaller than the choke reactance considered at the cut-off frequency (ω_0) in order to effectively by-pass the inductors during power-up. Also the clamp diodes should be able to handle the current peak during the power-up.

$$R_{1,2} << \omega_0 \cdot L_{in} \tag{8.4}$$

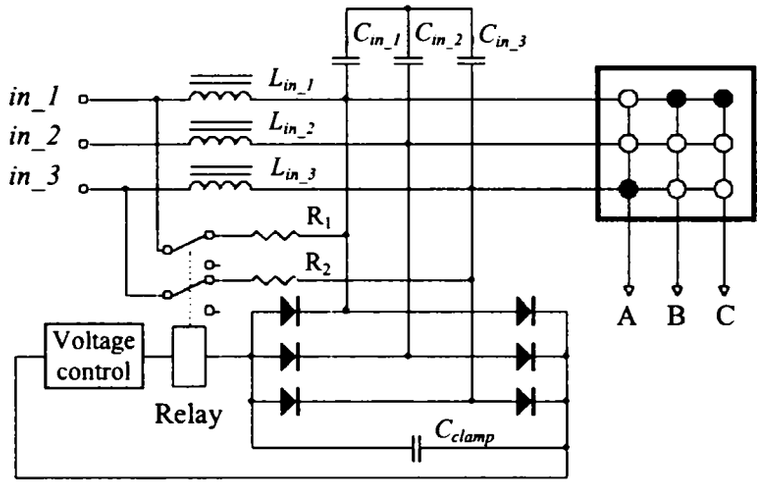

Fig. 8.4: The matrix converter power-up circuit using damping resistors

Simulations of the worst power-up condition show that with no damping (Fig. 8.5), the overvoltage may reach 1050V, but with two damping resistors the overvoltage level is reduced to 853V (Fig. 8.6).

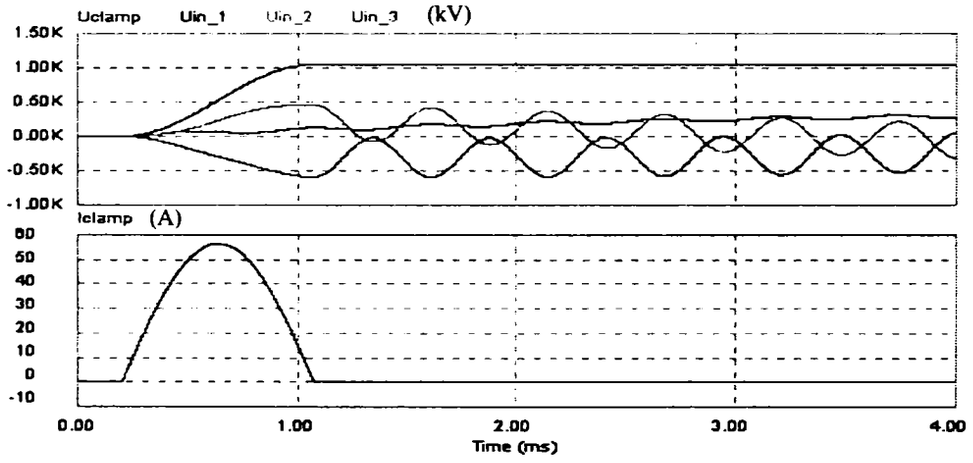

Fig. 8.5: The matrix converter power-up without overvoltage reduction circuits. U_{max}=1050 V

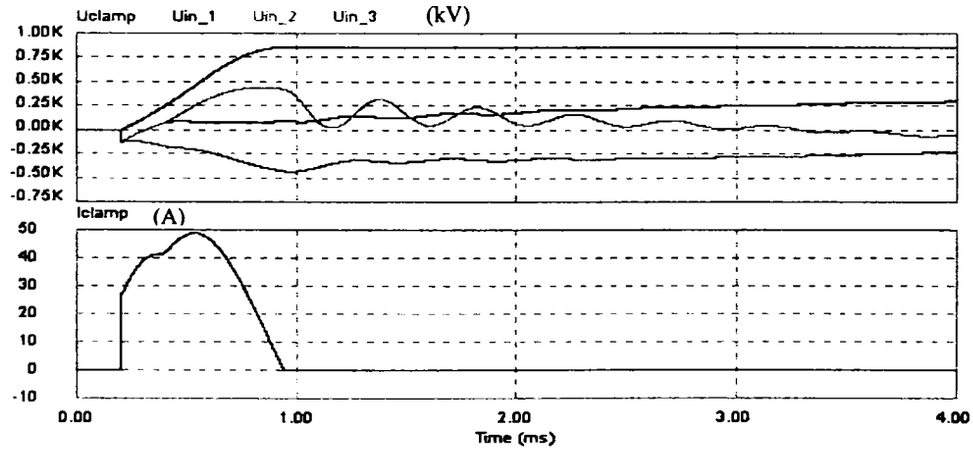

Fig. 8.6: The matrix converter power-up using two by-pass resistors (R_1=R_2=5Ω). U_{max}=853 V

8.5 HARDWARE IMPLEMENTATION

The matrix converter is built using 3-phase/1-phase (3∅/1∅) power modules with bi-directional switches (25A/1200V) in order to minimise the size and the leakage inductance of the main circuit. The 22-pins power module has the physical dimensions of 63x48x12.5 mm and uses bi-directional switches connected in a Common Collector (CC) configuration. The placement of the IGBT's and the FRD's, the connections inside the power module and the pin designation are presented in Fig. 8.7. Unconnected terminals are placed around the power pins (U1, U2, U3, and I1) in order to assure the necessary clearance, required by the standards.

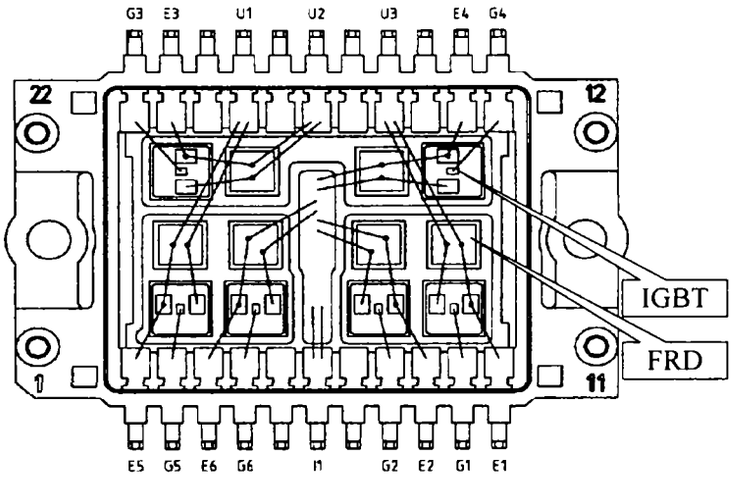

Fig. 8.7: The internal connections of the power module used in the MCM prototype, based on a Common-Collector bi-directional switch topology

In Fig. 8.8 the two generations of power modules built for the matrix converter prototypes which have been developed, are presented for size comparison purpose.

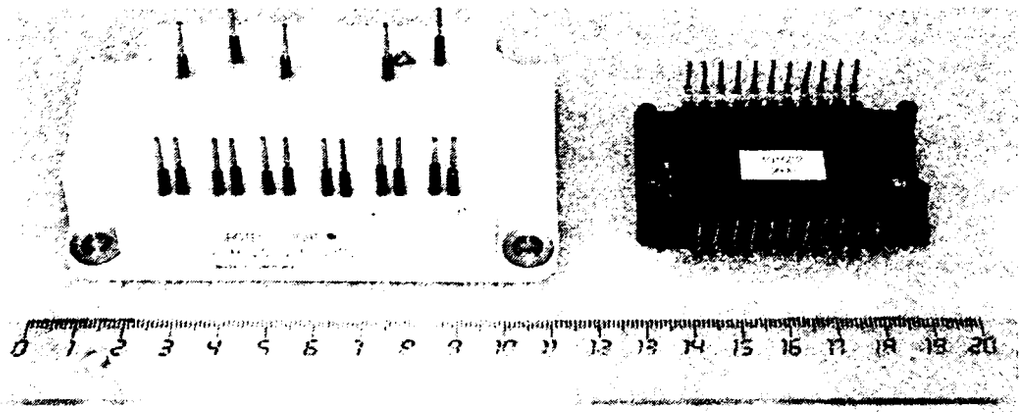

Fig. 8.8: The two generations of three-phase to one-phase power modules for matrix converters: left side - old generation (1994); right side – new generation (1999);

In Fig. 8.9 the block scheme of the MCM prototype is shown, with the boards placed in the same position as in the prototype enclosure.

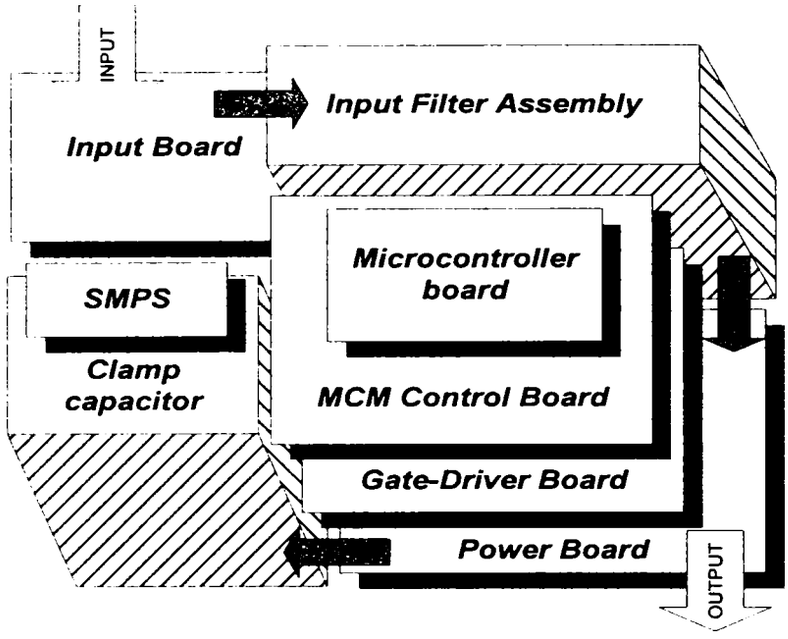

Fig. 8.9: The block diagram of the MCM prototype

The prototype consists of eight parts:

1. the *Input Board* includes a power connector, varistors, a damping circuit for safe power-up and an RFI-filter;
2. the *Input Filter Assembly* includes the AC chokes and star connected film capacitors [8.26];
3. the *Power Board* includes the 3∅/1∅ power modules with bi-directional switches, the clamp diodes, the output current shunts and the motor connector;
4. the *Gate-Driver Board* includes the insulated power supplies, the gate-drivers and the current transducers;
5. the *MCM Control Board* includes a PLD chip (XC95108) [8.27] for commutation control, the current sign detectors and the voltage transducers;
6. the *Microcontroller Board* (miniMODUL 167) with a SAB80C167 microcontroller and 256 kB of flash memory [8.28], [8.29];
7. the *Clamp Capacitor*;
8. the *SMPS Board*, which comes from an industrial converter and provides the necessary galvanic insulation in respect to the safety regulations;

In Fig. 8.10 another block diagram is shown, including the main components and the signal flow. The microcontroller send to the PLD the state of the bi-directional matrix switches, which is 2 bit/4 state encoded, using 6 bits of port P2. Also produces a 400 ns clock signal needed to control the commutation inside the PLD, an ENABLE signal to control the PLD outputs (A, B, C outputs each of 6 bit) and a RESET signal to reset overcurrent state memorised by the PLD and signalised by the ERROR signal.

The current transducers are implemented with HP 788 devices [8.30], which provides galvanic insulation, adapted input for shunt transducer, external analogue reference to establish the maximum output value and built-in overcurrent protection with open drain output allowing for multiple error summing.

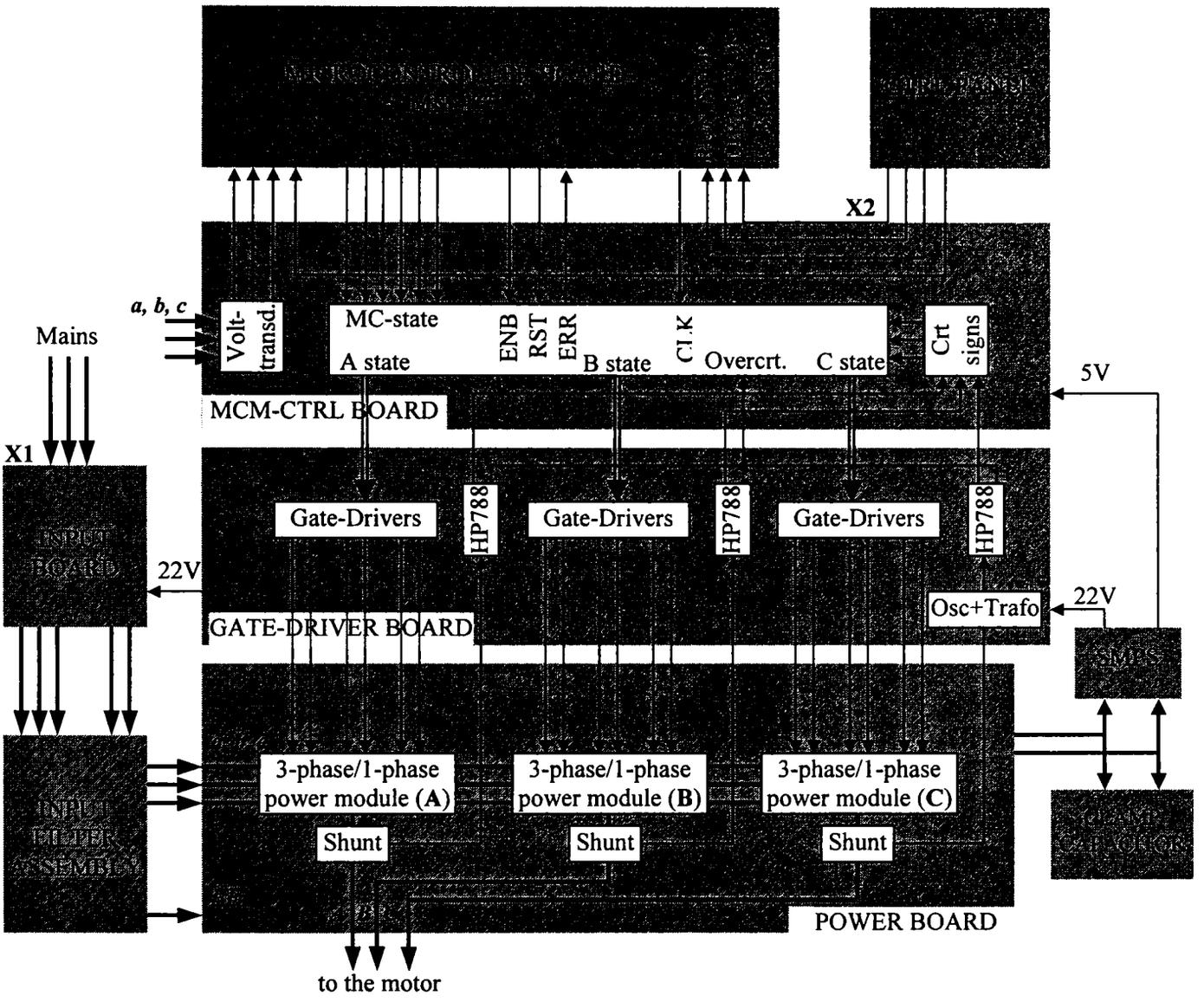

Fig. 8.10: The interconnection diagram in the MCM prototype

The date drivers are implemented with HP 312 devices [8.31] having 2 Amps output capability. The six differential supplies (15 V) to feed the IGBT drivers are implemented with pulse transformers to provide galvanic insulation and are driven by a push-pull output stage (200 kHz). The two supply voltages to feed all the MCM prototype electronics (5 V/0.5A and 22 V/0.3A) are produced by an industrial designed SMPS provided by Danfoss Drives A/S, which is feed from the clamp capacitor DC voltage. This start working when the clamp circuit voltage riches 300 V and stops working when this voltage decreases below 150 V. In this way, by feeding the two-pole normal closed relay from the power-up circuit (*Input Board)* directly to the 22 V supply, provides a safe power-up of the MCM prototype by inserting the 4.7 Ohm resistors in the circuit, as was shown in Section 8.4. After power-up, the relay is energised and the resistors are disconnected from circuit.

The power components (1, 2, 3, 7 and 8) are shown in Fig. 8.11. The connections between them are wired.

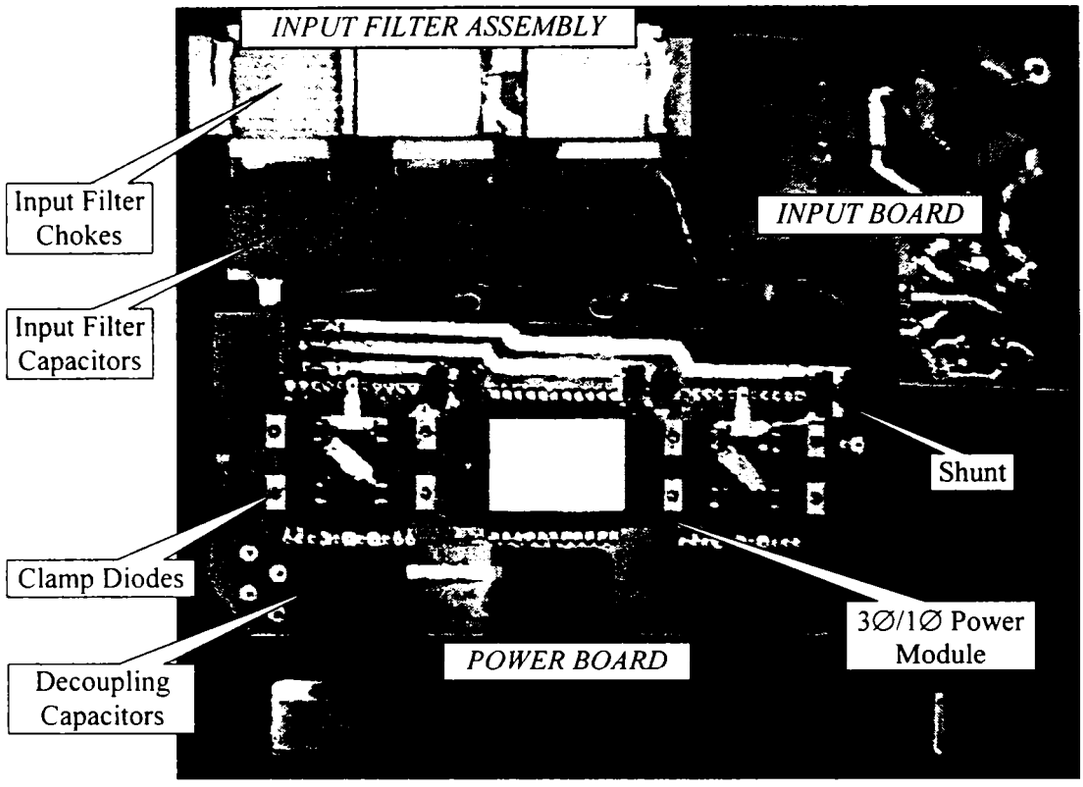

Fig. 8.11: The power components of the MCM prototype

The electronic boards (3, 4, 5 and 6) are designed to fit each other, as it is shown in Fig. 8.12. In this way, the 4 kW-matrix converter is implemented as a Power Electronic Building Block (PEBB), with the necessary protection, bi-directional switch commutation control and motor basic control integrated. The PEBB requires two voltage supplies: 5 V/0.5A and 22 V/0.3A. The connector for the command signals X2 is placed on the *MCM Control Board*. A small adapting board, which has to be plugged in the microcontroller board when needed, allows the user to load the program via an RS-232 interface.

All the matrix converter components presented before are placed inside of a 4 kW standard metallic enclosure (FCM 304 – Danfoss A/S). Minor mechanical changes have been made to allow an optimum placement. This may be seen in Fig. 8.13 where a topside view of the MCM prototype is shown.

In Fig. 8.14 and Fig. 8.15 it is shown the position of the RS-232 interface board on the microcontroler board and the position of the JTAG port and the connection between the JTAG programmer and the MCM Control Board. The RS232 interface board allows a possible developer to upload new versions of the MCM control software "on-board" and to observe the prototype functionality by establishing a full duplex serial communication line, without the need to extract the microcontroller board. The JTAG port also allows a possible developer to upload new versions of the PLD logic scheme "on-board", without the need to extract the 108-pin PLD device.

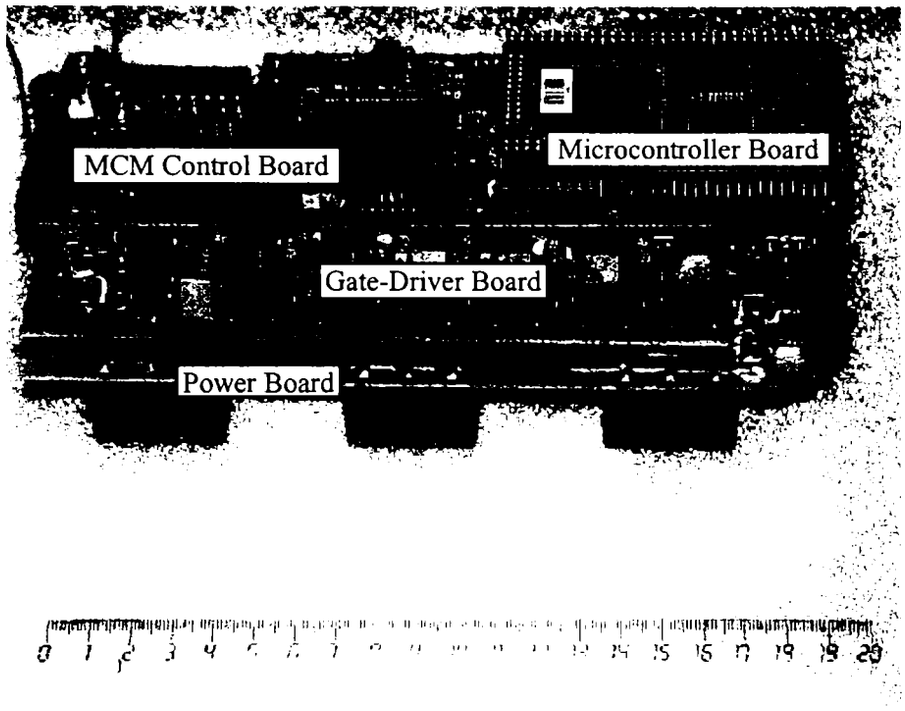

Fig. 8.12. Implementation of the 4kW-matrix converter as a custom designed PEBB for the MCM prototype

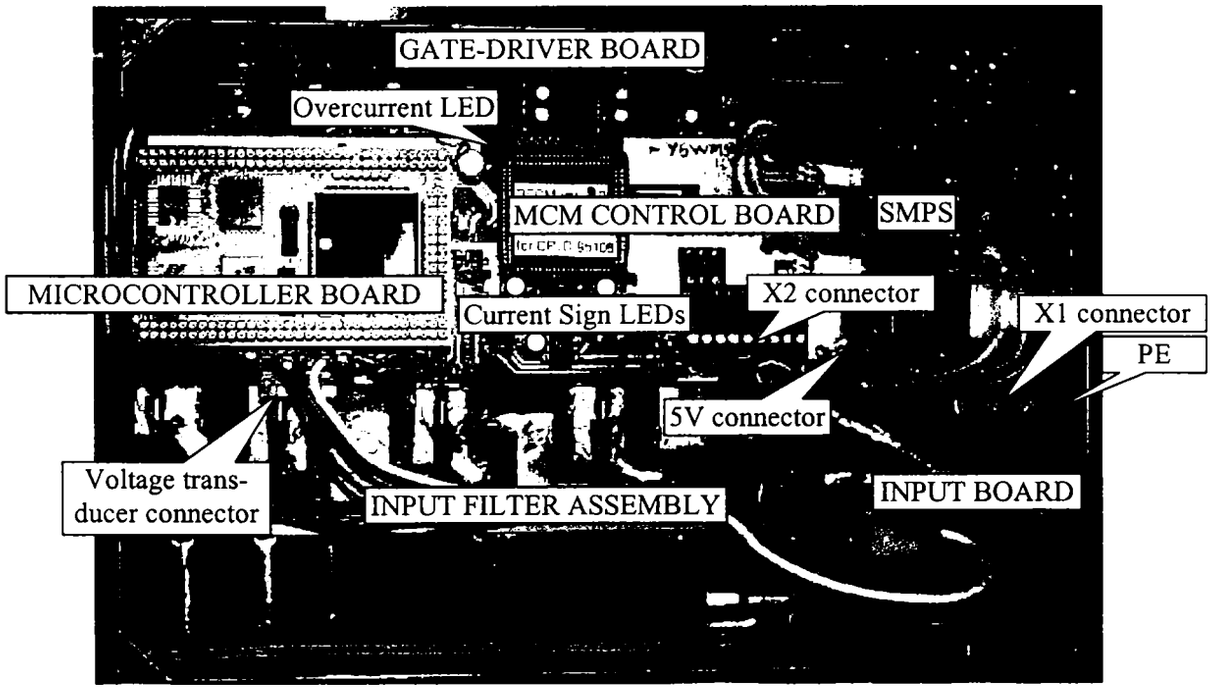

Fig. 8.13: Topside view of the MCM prototype

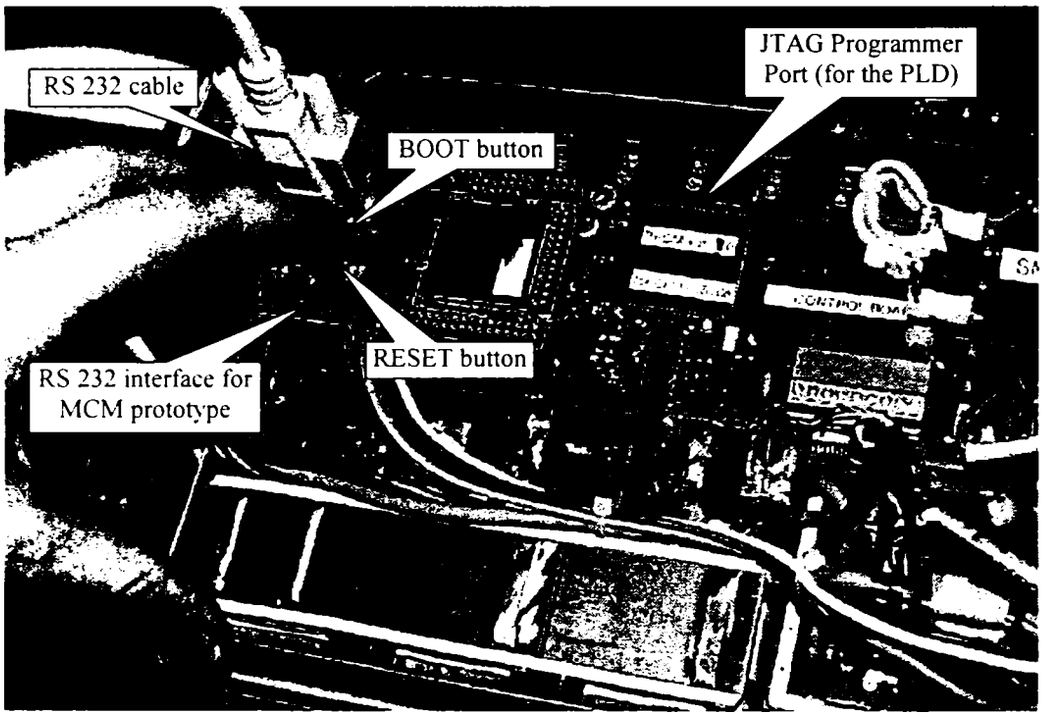

Fig. 8.14: Details of how the RS232-adapter is used to upload the microcontroller program "on board" and the position of the JTAG port used to program the PLD in the MCM prototype

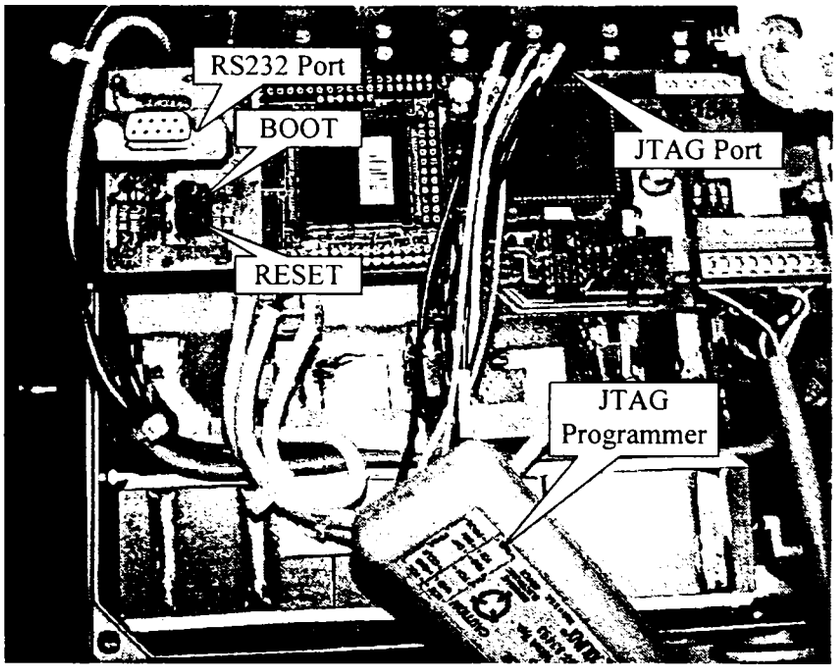

Fig. 8.15: "On-board" programming of the PLD using the JTAG programmer

Table 8.4 and Table 8.5 show the occupied volume with passive components on the FCM304 drive (industrial design) and in the MCM prototype. The situation is favourable for the standard drive, but this may change when the design will be optimised. The measured internal volume of the MCM enclosure is 2275 cm^3. The cylindrical components have been approximated as parallelepipeds.

Table 8.4
The volume of the reactive components in a standard FCM enclosure (Danfoss FCM304 – 4 kW)

DC chokes	60x50x40 mm	2 pcs.	240 cm^3
DC-link capacitors	∅35x47 mm	4 pcs.	230 cm^3
Total: 470 cm^3 (20.7% of the enclosure volume)			

Table 8.5
The volume of reactive components in a MCM enclosure based on a 4 kW matrix converter

AC chokes	60x50x40 mm	3 pcs. (1.4mH)	360 cm^3
Input filter capacitors	21x38x41 mm	3 pcs. (4.7μF)	98 cm^3
De-coupling capacitors	11x20.5x26.5 mm	9 pcs. (0.68μF)	54 cm^3
Clamp capacitor	42.5x46.5x55 mm	1 pcs. (25μF)	109 cm^3
Total: 621 cm^3 (27.3% of the enclosure volume)			

The MCM prototype mounted in the testing system is presented in Fig. 8.16.

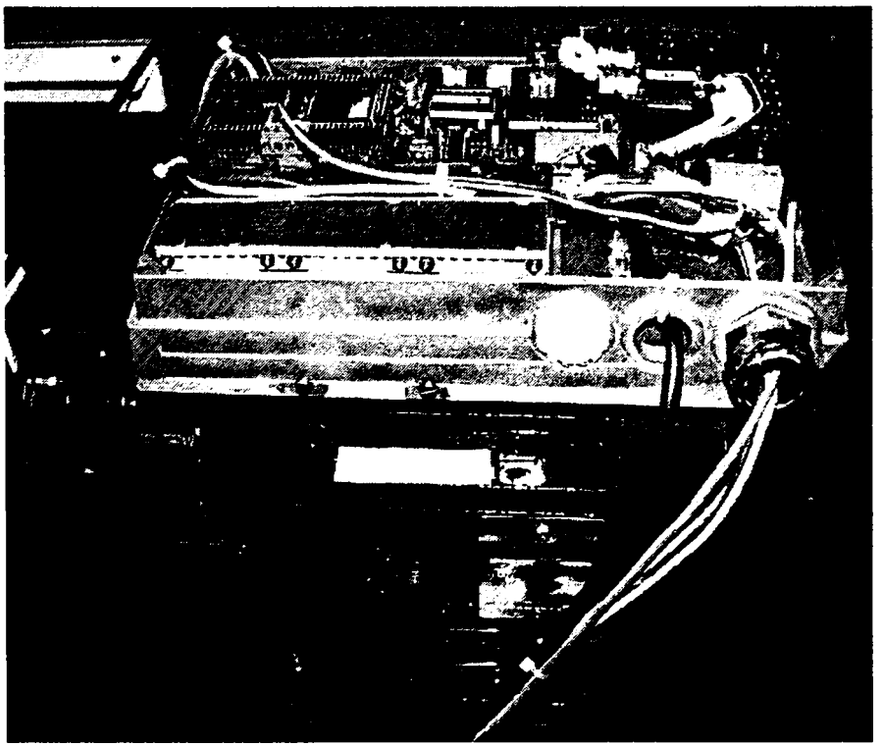

Fig. 8.16: The MCM prototype mounted in the testing system

8.6 SOFTWARE IMPLEMENTATION

The control of the MCM prototype was implemented on a small 16-bit microcontroller card. A few features of the microcontroller board, of interest in the MCM control are presented below:

- 80C167 microcontroller @ 20 MHz clock frequency;
- 256 kByte of RAM (data) and 256 kByte of Flash (program) memory;
- size of microcontroller card 85x54 mm;
- Analog/Digital Converter (ADC) with 8 multiplexed channels (t_{ADC} = 9.7 μs);
- powerful Central Processing Unit (CPU) able to perform a 16-bit by 16 bit multiplication in 0.5 μs and a 32 bit by 16 bit division in 1 μs;
- 16 bit Capture/Compare Unit with a time resolution of 400 ns;
- Peripheral Event Controller (PEC) with 8 PEC channels, able to perform a data transfer from a memory location to a port in 400 ns;
- serial communication port with RS-232 interface;

The motor uses scalar control, implemented into a 16-bit microcontroller (C167), as is shown in Fig. 8.17. An analogue input *REFERENCE FREQUENCY* and three digital inputs *START/STOP, DIRECTION* and *FAST STOP* provide basic control of the motor. The *Ramp Control* block controls the MCM acceleration and deceleration producing the actual frequency. This is used to calculate the motor reference voltage U_{out}, the angle of the output voltage vector θ_{out} and to control the drive stop, depending on the *START/STOP* and on the *Coast Stop Control.*

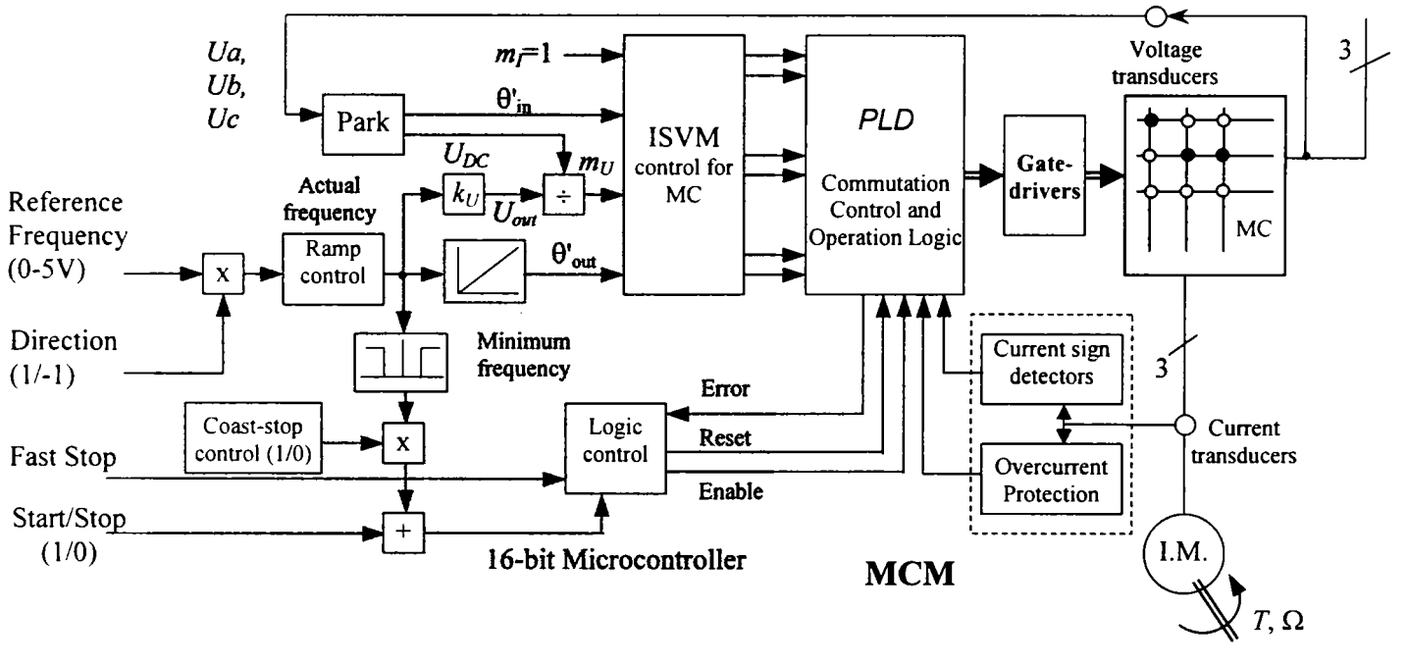

Fig. 8.17: The basic motor control block diagram implemented in the MCM prototype

The three input phase voltages are used to calculate the current angle θ_{in} and the imaginary DC-link voltage used to calculate the voltage modulation index m_U. Inside the ISVM Control Block the duty-cycles of the switching sequence are calculated by using the reference vectors: the current vector given by the angle of the input phase voltage vector and the motor reference voltage vector given by angle and magnitude. Using the optimal switching pattern table described in [8.21], the actual switching pattern is selected during the switching period. The microcontroller capture-

compare unit performs the pulse timing and produces the matrix converter states for the *PLD chip*, which controls the commutation of the bi-directional switches and memorises the overcurrent fault. Based on the output currents, the *Current sign detectors* provide semi-soft commutation and the *Overcurrent protection* provides safe operation of the MCM prototype. The classical double-sided SVM pattern [8.7] has been changed in order to obtain the following benefits:

- only 8 PEC channels needed during the switching period;
- one PEC channels always starts when the timer reloads, this way the number of computations is reduced;
- the switching pattern always starts with a zero vector and provides lower noise in the acquired input voltages, which are measured at the beginning of the switching period.

The generation of the switching pattern uses a Capture/Compare Unit and the Peripheral Event Controller (PEC transfer) provided by the C167 microcontroller and is presented in Fig. 8.18.

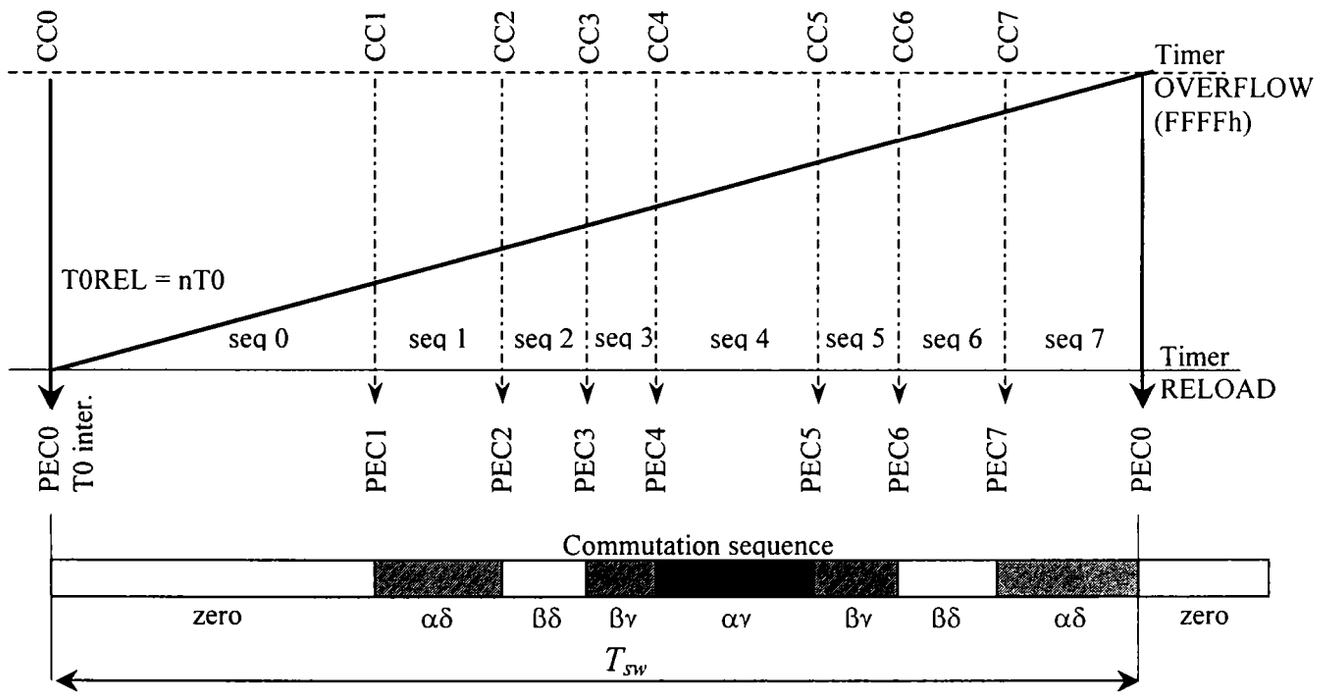

Fig. 8.18: Timing diagram for generation the double-sided ISVM switching pattern

The tasks of the interrupt executed at the beginning of each switching period that provides the control of the MCM prototype:

1. actualise the PEC 5-7 channels with the corresponding new duty-cycles and switch state;
2. starts acquisitions of the three input phase voltages;
3. calculate the actual output frequency from the reference frequency and the acceleration/deceleration ramps;
4. calculate the actual angle of the output voltages, the sector and the angle within the sector used to calculate the duty-cycles;
5. calculate the angle of the input voltages, the sector of the rectifier stage and the reference angle within the sector;
6. calculates the imaginary DC-link voltage;

7. calculates the modulation index, which offers forward compensation for input voltage unbalance and distortion;
8. calculate the duty-cycles of the double-sided ISVM sequence;
9. actualise the PEC 0-4 channels with the corresponding new duty-cycles and switch state for the next switching period;
10. starts acquisition of the REFERENCE FREQUENCY given by potentiometer, to be available for other functions, which are not executed with a fixed sampling period;

The software executes the basic procedures commanded by the MCM Control Panel as follows:

- *Starting the drive:* When the *START/STOP* switch is changed in the *START* position, the drive energises the motor with an initial frequency f_{start}, settable in the microcontroller program, and will accelerate to the reference frequency, as is shown in Fig. 8.19. The acceleration ramp is given by the time needed to accelerate from 0 Hz to 50 Hz, also settable in the program, t_{50_up} (8.5).

$$t_{50\_up} = \frac{50 \quad Hz}{acc\_ramp(Hz/\sec)} \tag{8.5}$$

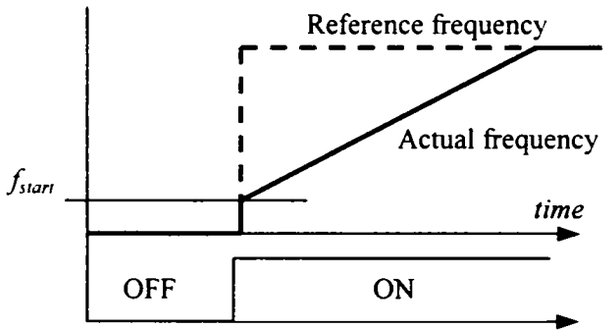

Fig. 8.19: MCM operation when starting the drive

- *Stopping the drive:* When the *START/STOP* switch is changed in the *STOP* position, the drive will decelerate from the actual/reference frequency to a frequency f_{stop}, settable in the microcontroller program, where the motor is coasted, as is shown in Fig. 8.20. The deceleration ramp is given by the time to decelerate from 50 Hz to 0 Hz, also settable in the microcontroller program, t_{50_dwn} (8.6).

$$t_{50\_dwn} = \frac{50 \quad Hz}{decel\_ramp(Hz/\sec)} \tag{8.6}$$

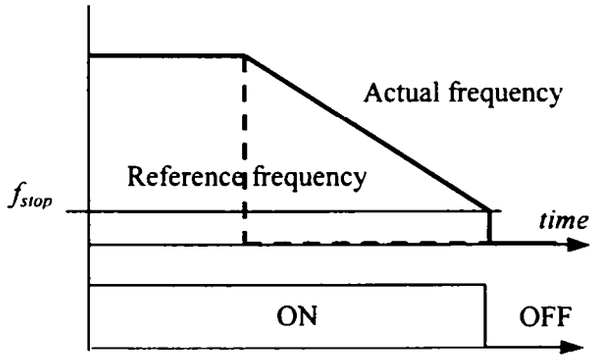

Fig. 8.20: MCM operation when stopping the drive by ramping down

- *Changing the direction of motor (rotation)*: When the position of the *DIRECTION* switch is changed, the drive will decelerate from the actual/reference frequency to a minimum frequency f_{min}, settable in the microcontroller program, where the direction of rotation of the motor voltage vector is changed. After that the motor is immediately accelerated to the reference frequency, as is shown in Fig. 8.21. The deceleration ramp is given by t_{50_dwn} (8.5) and the acceleration ramp is given by t_{50_up} (8.6).

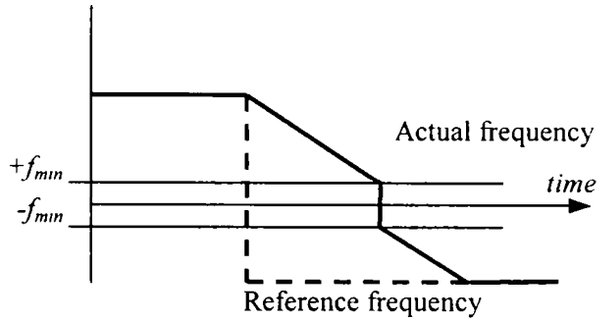

Fig.8.21: MCM operation when the drive is executing a speed reversal

- *Performing a Fast Stop*: By handling the *FAST STOP* switch, a hardware interrupt is triggered and the drive will perform immediately a coast stop.
- *Reset an Overcurrent Fault or/and a Fast Stop*: It is necessary only to turn the *START/STOP* switch from *STOP* position to *START* position, when the microcontroller send a *RESET* signal to the PLD in order to reset a possible overcurrent fault and to perform a software reset, if needed.
- *Changing the REFERENCE FREQUENCY*: This is achieved by handling the *REFERENCE FREQUENCY* potentiometer. The limits of the reference frequency given by the potentiometer rotation angle are both settable in program.

8.7 EXPERIMENTAL EVALUATION

The MCM prototype has been mounted on a laboratory benchmark, as is shown in Fig. 8.22 and includes:

- a DC generator mechanically coupled with the MCM shaft in order to produce a desired load;
- a four channels digital oscilloscope used to acquire the voltage and current waveforms from the MCM transducers;
- a three-phase power analyser mounted on the MCM input side to monitor the line side performance;
- an autotransformer or an AC power source (15kVA from California Instruments) to produce an input voltage system of variable voltage and customised shape in order to test the prototype functionality on a wide range of voltage levels, unbalanced and distorted input voltages;

In Fig. 8.23 it is shown how the MCM prototype coasts when an overcurrent protection fault occurs. This was caused by a short acceleration ramp in order to check the level where the overcurrent protection is triggered. In this case the maximum current reaches 20 Amps, as in the design input data.

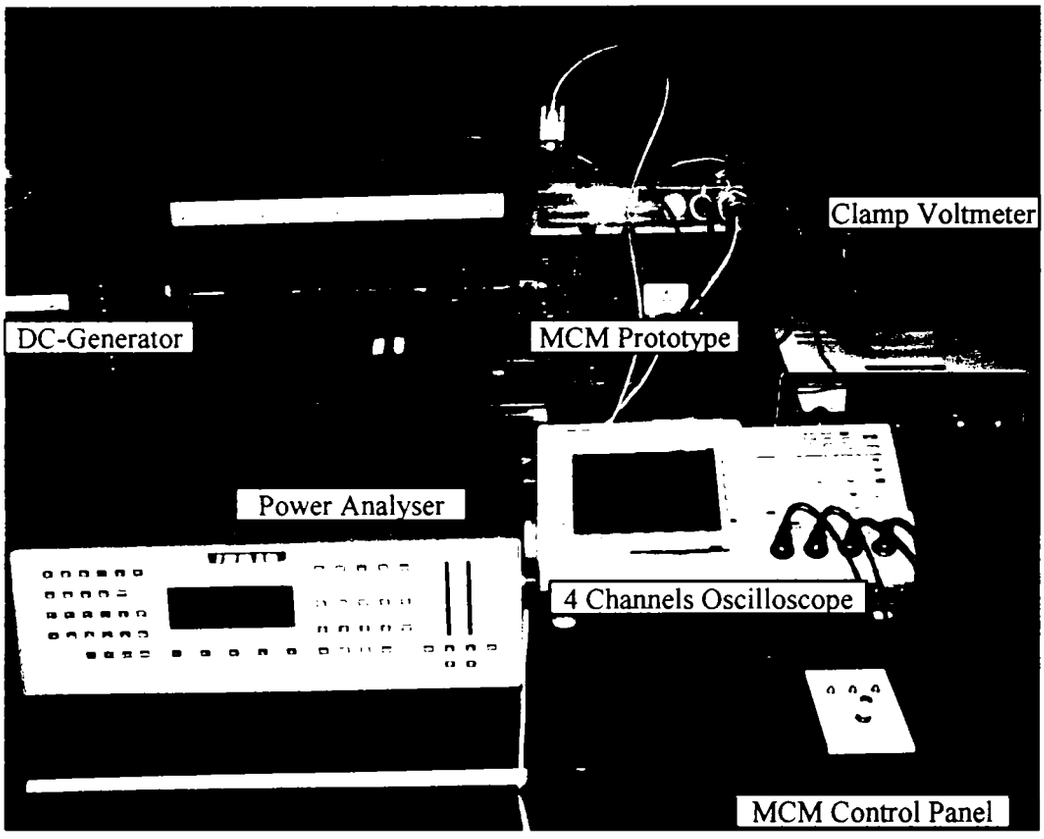

Fig. 8.22: Laboratory benchmark for testing the MCM prototype

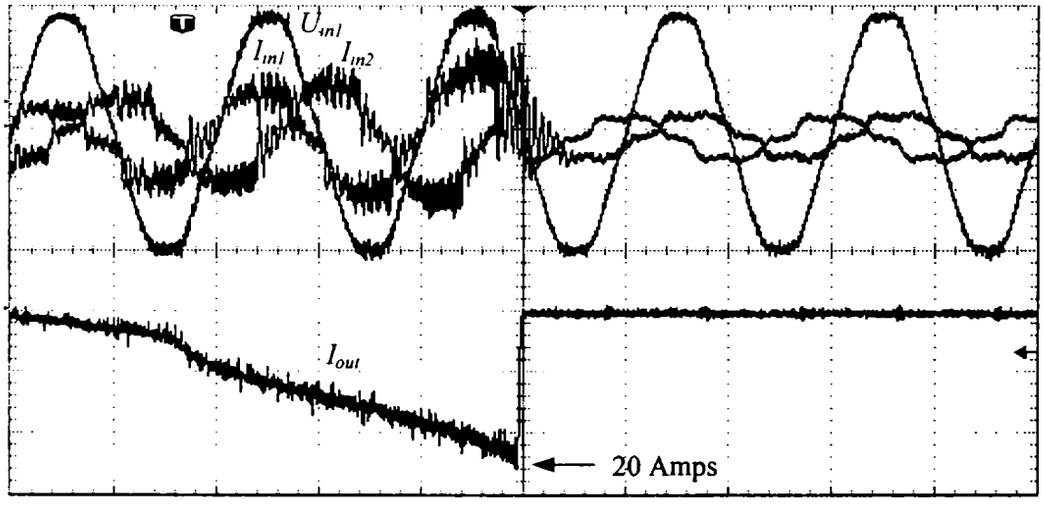

Fig. 8.23: Overcurrent protection fault caused by a higher acceleration ramp: Upper side: input phase voltage (160V/div) and two input currents (3.3 A/div) Lower side: motor current (8A/div); Time scale (4ms/div)

To evaluate the prototype two tests are performed with nominal voltage at the input and 4 kHz switching frequency. The first test consists of running the MCM prototype in steady-state conditions with 30 Hz output frequency and 50% of the nominal MCM torque. In Fig. 8.24 an input phase voltage, input current and the current FFT is shown. In Fig. 8.25 the motor current waveform and FFT is shown. The acquisitions have been performed using a TDS 3014 oscilloscope with built-in FFT (Tektronix). The input voltage measurement and the output current

measurement use the internal MCM prototype transducers. Measurements on the input side have been made with a PM3000A three-phase power analyser (Voltech) in two situations.

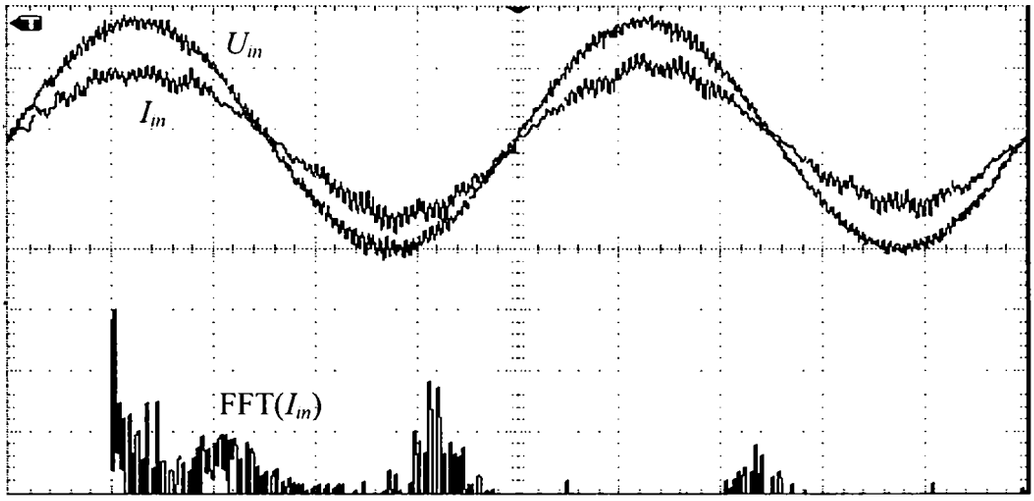

Fig. 8.24: The input phase voltage U_{in} (200 V/div) and current I_{in} (3.3 A/div) vs time (4ms/div) and the FFT of the input current (20 dB/div, 1.25 kHz/div)

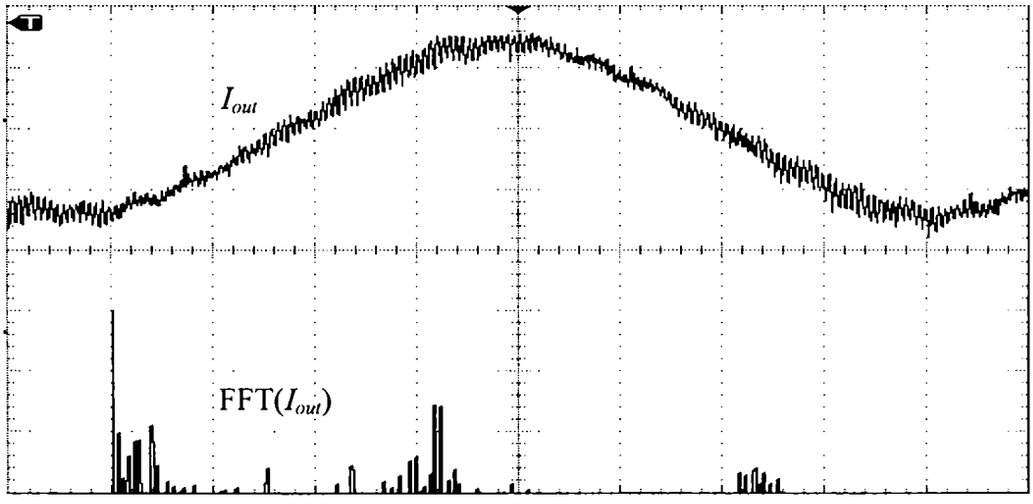

Fig. 8.25: The motor current I_{out} (8 A/div) vs time (4ms/div) and the FFT of the output current (20 dB/div, 1.25 kHz/div)

First situation uses the grid and an auto-transformer as input with a line reactance and real (distorted) voltage. The results are shown in Table 8.6. The other is using an AC Power Source (California Instruments) to generate a custom defined three-phase voltage system, which is a sinusoidal and balanced in this situation. The results are presented in Table VII. The harmonics until 19-th order, which may have an important level in a standard diode-bridge VSI, are also shown. The MCM prototype produces a lower harmonic content than a standard diode-bridge VSI. The current THD is higher due to the switching frequency, because the power analyser takes into account harmonics until 99-th order (4.95 kHz), which includes the switching frequency. This may also be explained because the THD value is similar in Table 8.6 (real distorted voltage) and Table 8.7 (sinusoidal and balanced voltage), but in the second situation, the content in low-order harmonics of the input current is lower.

The second test consists of accelerating the MCM prototype from 5 Hz to 30 Hz. The motor is loaded using a DC-generator, which gives linear speed-torque dependence, with 50% of the MCM nominal torque at 30 Hz. The input phase voltage and current and the motor current are shown in Fig. 8.26. During acceleration, the motor current reaches the nominal value (14 A peak).

Table 8.6
Measurements on the MCM input side feed from the grid with an auto-transformer

Input phase:	*a*	*b*	*c*
U_{phase} [V]	220.4	228	224.4
I_{phase} [A]	2.8	2.8	2.75
P_{phase} [W]	610	635	615
Q_{phase} [Var]	114	112	106
PF	0.983	0.984	0.984
V_{THD} [%]	3.3	2.8	2.8
I_{THD} [%]	17	17.5	17.6
5-th harmonic [%]	3.3	3.4	2.9
7-th harmonic [%]	1.4	1.6	1.6
11-th harmonic [%]	0.25	0.3	0.35
13-th harmonic [%]	0.25	0.2	0.33
17-th harmonic [%]	0.46	0.45	0.68
19-th harmonic [%]	0.46	0.43	0.5

Table 8.7
Measurements on the MCM input side feed from an AC Source (California Instruments)

Input phase:	*a*	*b*	*c*
U_{phase} [V]	214	222	222
I_{phase} [A]	2.76	2.81	2.73
P_{phase} [W]	583	614	600
Q_{phase} [Var]	100	102	100
PF	0.986	0.986	0.985
V_{THD} [%]	0.8	0.9	0.7
I_{THD} [%]	16.2	15.9	16.1
5-th harmonic [%]	0.2	0.4	0.6
7-th harmonic [%]	1.2	1.1	1.0
11-th harmonic [%]	0.16	0.1	0.25
13-th harmonic [%]	0.3	0.2	0.2
17-th harmonic [%]	0.3	0.29	0.38
19-th harmonic [%]	0.42	0.43	0.5

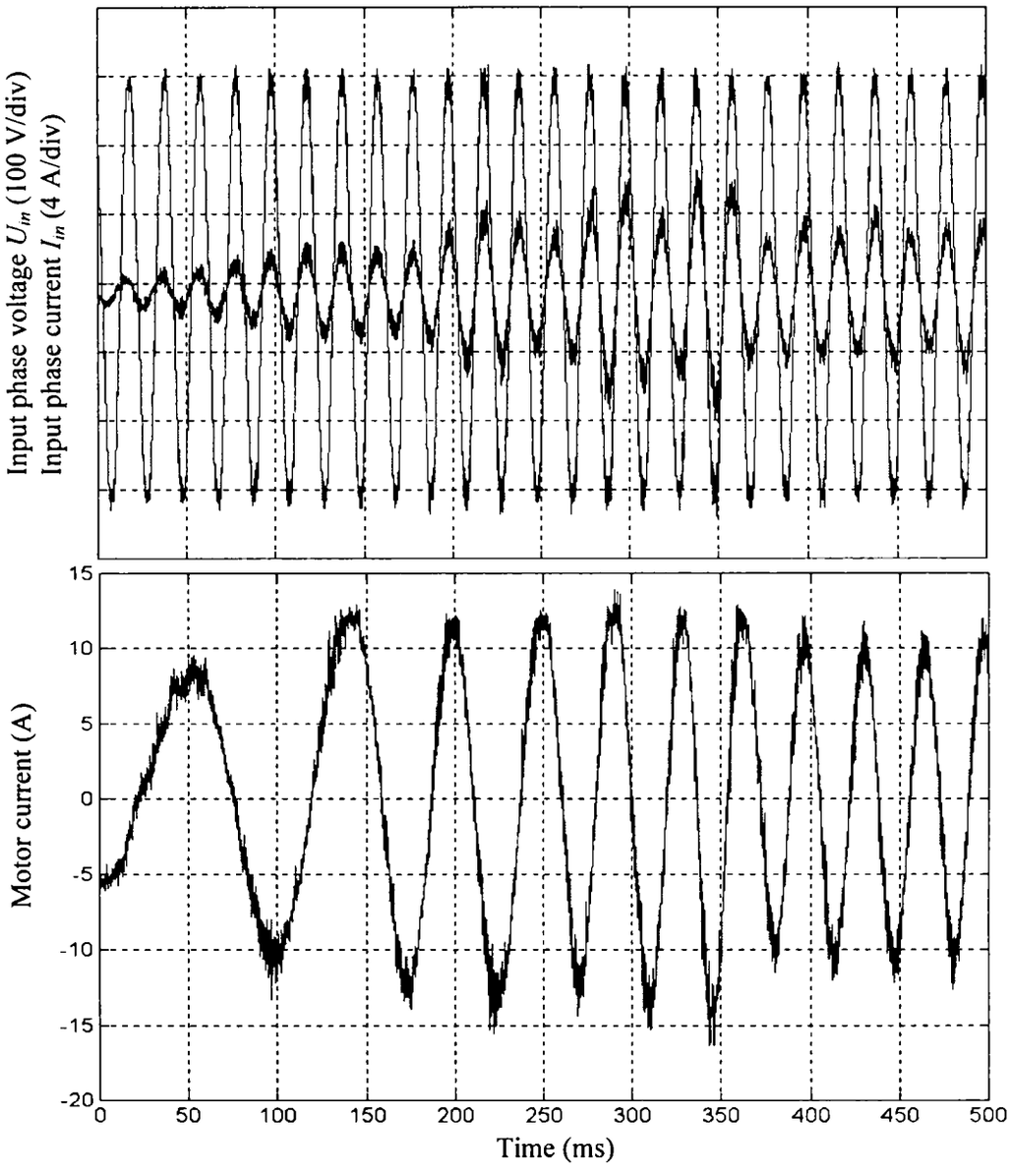

Fig. 8.25: MCM prototype acceleration from 5Hz to 30 Hz
a) the input phase voltage and current; b) the motor current

8.9 SUMMARY

This chapter presents the implementation of a matrix converter-motor (MCM) for industrial application, which leads to a compact regenerative drive solution. In this particular application, redesigning the motor to a lower nominal voltage is a valid solution to overcome the disadvantage of a lower voltage transfer ratio of matrix converters.
The design uses a standard FCM enclosure. Design, control and implementation are explained as well as tests at full voltage are demonstrated. The results show that the MCM-solution can be very compact for industrial drives even though the demonstrated prototype is not completely optimised.

REFERENCES

[8.1] C. Klumpner, P. Nielsen, I. Boldea, F. Blaabjerg, "*A new matrix converter motor (MCM) for industry applications*", Proc. of IAS Annual Meeting, vol. 3, pp. 1394-1402, 2000.

[8.2] R.J. Kerkman, G.L. Skibinski, D.W. Schlegel, "*AC drives: Year 2000 (Y2K) and beyond*", Proc. of APEC'99, vol. 1, pp. 28-39, 1999.

[8.3] P. Thøgersen, P. Nielsen, F. Abrahamsen, "*Impacts on energy savings by variable speed drives from motor and converter technology*", Proc. of PCIM'99, Intelligent Motion, pp. 1-7, 1999.

[8.4] S. Williamson, D.C. Jackson, "*Integrated drives for industrial applications*", Proc. of PCIM'99, Intelligent Motion, pp. 9-13, 1999.

[8.5] J.S. Kim, S.K. Sul, "*New control scheme for AC-DC-AC converter without DC-link electrolytic capacitor*", Proc. of PESC'93, pp. 300-306, 1993.

[8.6] K. Kretschmar, H.-P. Nee, "*Comparison of different converters with sinusoidal line currents suited for a 15 kW permanent magnet integral motor*", Proc. of Nordic Workshop on Power and Industrial Electronics NORPIE'00, pp. 79-83, 2000.

[8.7] P. Nielsen, F. Blaabjerg, J.K. Pedersen, "*Novel solution for protection of matrix converter to three phase induction machine*", Proc. of IAS Annual Meeting, vol. 2, pp. 1447-1454, 1997.

[8.8] J.Chang, D. Braun, "*High-frequency AC-AC converters using 3-in 1 IBPMs and adaptive commutation*", Proc. of PESC'99, pp. 351-357, 1999.

[8.9] C.L. Neft, C.D. Shauder, "*Theory and design of a 30-hp matrix converter*", IEEE Trans. on Industry Applications, vol. 28, no. 3, pp. 546-551, 1992.

[8.10] N. Burany, "*Safe control of 4-quadrant switches*", Proc. of IAS Annual Meeting, pp. 1190-1194, 1989.

[8.11] R. R. Beasant, W.C. Beattie, A. Refsum, "*An approach to realisation of a high-power Venturini converter*", Proc. of PESC'90, pp. 291-297, 1990.

[8.12] P.W. Wheeler, D.A. Grant, "*A low loss matrix converter for AC variable-speed drives*", Proceed. of EPE'93, pp. 27-32, 1993.

[8.13] M. Ziegler, W. Hofmann, "*Semi-natural two steps commutation strategy for matrix converters*", Proc. of PESC'98, pp. 727-731, 1998.

[8.14] A. Schuster, "*A matrix converter without reactive clamp elements for an induction motor drive system*" Proc. of PESC'98, pp. 714-720, 1998.

[8.15] L. Huber, D. Borojevic, "*Space vector modulated three-phase to three-phase matrix converter with input power factor correction*", IEEE Trans. on Industry Applications, vol. 31, no. 6, pp. 1234-1245, 1995.

[8.16] D.G. Holmes, T.A. Lipo, "*Implementation of a controlled rectifier using AC-AC matrix converter theory*", Proc. of PESC'89, pp. 353-359, 1989.

[8.17] J. Oyama, T. Higuchi, E. Yamada, T. Koga, T. Lipo, "*New control strategy for matrix converter*", Proc. of PESC'89, pp. 360-367, vol. 1, 1989.

[8.18] A. Christensson, "*Switch-effective modulation strategy for matrix converters*", Proc. of EPE'97, pp. 4.193-4.198, 1997.

[8.19] E.P. Wiechmann, J.R. Espinoza, L.D. Salazar, J.R. Rodriguez, "*A direct frequency converter controlled by space vectors*", Proc. of PESC'93, pp. 314-317, 1993.

[8.20] D. Casadei, G. Serra, A. Tani, P. Nielsen "*Theoretical and experimental analysis of SVM-controlled matrix converters under unbalanced supply conditions*", Electromotion Journal, no. 4, pp.28-37, 1997.

[8.21] P. Nielsen, F. Blaabjerg, J.K. Pedersen, "*Space vector modulated matrix converter with minimized number of switching and a feedforward compensation of input voltage unbalance*", Proc. of PEDES'96, pp. 833-839, vol. 2, 1996.

[8.22] D. Casadei, G. Serra, A. Tani, "*The use of matrix converter in direct torque control of induction machines*", Proc. of IECON'98, pp. 744-749, 1998.

[8.23] A. von Jouanne, P. Enjeti, B. Banerjee, "*Assessment of ride-through alternatives for adjustable speed drives*", Proc. of IAS Annual Meeting, vol. 2, pp. 1538-1545, 1998.

[8.24] J. Holtz, W. Lotzkat, "*Controlled AC drives with ride-through capability at power interruption*", IEEE Trans. on Industry Applications, vol. 30, no. 5, pp. 1275-1283, 1994.

[8.25] C. Klumpner, I. Boldea, F. Blaabjerg, "*Short term ride through capabilities for direct frequency converters*", Proc. of PESC'00, vol. 1, pp. 235-241, 2000.

[8.26] Evox Rifa, "*Film capacitors 1999-2000*".

[8.27] Xilinx, "*AppLINX CD-ROM*", 1999.

[8.28] Siemens, "*C167 Derivatives - 16 Bit CMOS Single-chip microcontrollers - User' manual 03.93 Version 2.0*", Siemens AG, Munchen, 1996.

[8.29] Phytec, "*miniMODUL-167 Hardware manual*", L-101-05, 1997.

[8.30] Hewlett-Packard, "*HCPL-788 J Isolation amplifier with short circuit and overload detection - Technical data*", 5966-0001E, 1997.

[8.31] Hewlett-Packard, "*HCPL-3120 2.0 Amp output current IGBT gate drive optocoupler – Technical data*", 5965-7875E, 1997.

Chapter 9

Summary and Conclusions

The matrix converter has commanded the attention of many researcher in power electronics frequency converters due to the benefits which accomplish this "all silicon solution": inherent bi-directional power flow, sine-wave in sine-wave out operation, adjustable input current displacement angle and small size of the topology. However, a few major disadvantages accompany this topology. One is the lower voltage transfer ratio, which do not allow the nominal flux in a motor to be reached. The other is generated by the lack of an energy storage element in the main circuit appear, as a higher sensitivity to power grid disturbances and no expectation for ride-through operation during power interruptions. Many scientific papers are dealing with simulations, while this "exotic" converter topology requires a lot of work to build a hardware prototype and to complete the experiments.

9.1. SUMMARY

This thesis starts by presenting the state-of-the art in the bi-directional power-flow converter technology. It is shown that the matrix converter is credited with the highest expectations in the near future, despite of many unresolved application issues, which motivate the research work in matrix converters to contribute to a real technological advance in this field.
Chapter 2 presents an introduction in the matrix converter technology. Basic aspects include practical configuration of the converter hardware, possible implementation of bi-directional switches, specific commutation methods, different modulation strategies to achieve sine wave-in sine wave-out operation and independent displacement power factor control in the input side and other application issues, proposed during the last 20 years in the literature.
Chapter 3 presents details about the 8.5 kVA matrix converter prototype built to perform the experiments. Known design criteria for the reactive elements in the matrix converter input filter and clamp circuit, are presented. Comments on how the volume reduction of the input filter is affected and on determining the real requirements for the clamp capacitor are carried out.
Chapter 4 proposes few hardware improvements for matrix converters. A safe power-up circuit eliminates the risk of overvoltages, caused by transients in L-C circuits. The influence of the size of the reactive elements in the input filter and in the clamp capacitor in order to decrease the overvoltage risk caused by voltage sags or momentary power interruptions is carried out. An analysis of the most convenient bi-directional switch topology, oriented for different power range is carried out, showing that common collector (CC) configuration is recommended in the low power range, while the common emitter (CE) configuration brings more benefits in the high-power range. A new topology of a matrix converter is proposed, using a mixture of both types of bi-directional switch configurations and employing bootstrap supplies. This solution reduces the number of insulated power supplies to a count of three and the number of clamp circuit diodes to a count of six. A new topology of an input filter, which implements physically the filtering in α-β

co-ordinate is proposed and experimentally tested, allowing for the size reduction of the input filter.
Chapter 5 deals with the reduction of the ripple in the filtered input current. Factors, which may influence the ripple, are theoretically investigated. Inserting zero vectors in the switching pattern, while the number of switch commutations does not change, proves to be the solution to reduce the ripple, especially in the low modulation index range. A new SVM modulator able to provide high resolution of pulses and change the switching pattern (single or two-zeros), depending on the modulation index, in order to provide minimum ripple in the input current, is proposed. Experimental results on a 4 kW induction motor validate this idea.
Chapter 6 presents a specific application area for a bi-directional power flow converter, the artificial loading. Requirements from microprocessor controlled power electronic equipments, used in artificial loading are discussed. It is shown that bi-directional power flow converters are the only solution to override the limited braking capability. A comparison shows that the matrix converter is a better alternative to the back-to-back VSI topology, regarding the number of transducers and the reactive elements. This is proven by tests on a 1.1 kW induction motor.
Chapter 7 proposes a new solution to provide a direct frequency converter with limited ride-through capability. This use the residual rotor flux, which decreases slowly due to the rotor flux time constant, during hundreds of milliseconds and the mechanical energy stored in the rotor inertia. The recovered energy is boosted-up in the clamp capacitor to feed the electronic control modules, keeping the converter alive. It is shown that using only the information given by the motor currents, generally accessible in all type of frequency converters, the necessary information for a fast start-up of the drive is accessible. This proposal is proven by tests with a standard frequency converter, which uses only the switching states permitted in a matrix converter.
Chapter 8 proposes the use of a matrix converter in a compact regenerative integrated motor drive: the matrix converter-motor (MCM). Two identical prototypes of a 4 kW matrix converter-motors have been built, with the purpose of evaluating this solution for industrial application. Design and implementation details are presented, including pictures of the prototype, of the test-bench, diagrams of the hardware arrangement and of the software control strategy. Experimental tests are performed, showing very good static and dynamic response.

9.2. CONTRIBUTIONS OF THE THESIS

Chapter 4-8 are based on original material, published previously in scientific papers, which have as first author the author of this PhD thesis. The papers have been presented in international conferences and journals in the year 2000. Main contributions of this thesis in the matrix converter technology are mentioned below:

- © The necessity to employ a safe power-up circuit is proven. Supplementary precautions to design the reactive elements have to be taken into account, to limit the maximum overvoltage level, caused by possible voltage sags or power interruptions (chapter 4).
- © New proposals to reduce the hardware requirements for low-power matrix converters are proposed (chapter 4).
- © Investigation in the reduction of the input current ripple shows that increasing the number of zero vectors decrease the ripple, even though the number of switch commutations remains unchanged, which means lower switching frequency (chapter 5).

© The use of a matrix converter in artificial loading of the induction motors, which is a specific application for a bi-directional power flow converter is investigated. Compared to a back-to-back VSI topology, the matrix converter requires less transducers and energy storage capability in reactive elements. Experimental tests show an excellent dynamic response (chapter 6).

© It is first proposed a new method to provide ride-through capability for matrix converters. Based on the residual rotor flux and on the inertia of the spinning rotor, the proposed strategy extracts energy from the induction motor, while motor circuits are all the time disconnected from the grid. The energy is boosted-up in the clamp circuit to feed the converter electronics control through a switch-mode power supply (chapter 7).

© The first implementation of a matrix converter in an integrated bi-directional power-flow motor drive is reported. A prototype is designed and built, providing a standalone unit, with all electronics and logic control inside the converter enclosure, mounted on the top of the motor, suitable for complete evaluation for industry applications (chapter 8).

9.3 FUTURE WORK

Even though the matrix converter technology shows great perspectives, compliance to standard frequency requirements is difficult. The limited voltage transfer ratio is a real drawback of this technology, to compete directly with DC-link frequency converters. A breakthrough may be the application in integrated motor drives with bi-directional power flow, in the low power range for hoisting applications. Complete evaluation of the MCM prototype for industrial applications has to be performed. However, it is necessary to establish with manufacturers of hoisting equipments, minimal requirements for the drive, in the worst-case conditions, as unbalanced power grid or operation during momentary power interruptions. It has to be established if the matrix converter is able to fulfil these requirements.
In order to further decrease the physical size of the converter, higher switching frequency has to be used, which requires high performance control cards, able to synthesise the specific PWM with a higher resolution. Employing new series of capacitors in the input filter, rated for the real requirement of the reactive components, may be another way to decrease the physical size and to improve the power density.
Finally, a great volume of work has to be carried out, in order to investigate all the possible applications of the matrix converters in various fields and to resolve many application issues. This aim will be possible only by attracting many researchers in this effort, but the first step in order to do that, is to provide them with an accessible matrix converter hardware kit, which is safe to operate and allows for a fast start-up of the research activity.

Complete List of References

[1] ABB, "*ACS600 Multidrive. Commissioning of SAFUT thyristor braking unit*", Student Binder, ABB Industry Oy, Helsinki, Finland, 1997.

[2] ABB, "*ACS 600 Single-drive frequency converters for speed and torque control of 2.2 to 3000 kW squirrel cage motors - Technical catalogue*", 3AFY 58059412 R0425 EN, ABB Industry Oy, 1998

[3] ABB, "*ACS 600 Multi-drive modules. Product catalogue*" 3BFE 64104268 R0125, ABB Industry Oy, Helsinki, Finland, 1999.

[4] J. Adams, "*Boostrap component selection for control IC's*", Design Tip DT 98-2, International Rectifier, http://www.irf.com/technical-info/designtp/dt98-2.pdf, 1998.

[5] L. Aftandilian, V. Mangtani, A. Dubhashi, "*Advances in power semiconductors and packaging lead to a compact integrated power stage for AC drives*", Proc. of Wescon'97, pp. 334-339, 1997.

[6] A. Alesina, M. Venturini, "*Analysis and design of optimum-amplitude nine-switch direct AC-AC converters*", IEEE Trans. on Power Electronics, vol. 4, no. 1, 1989.

[7] Analog Devices, "*ADSP-2106x Sharc User's Manual*", 82-000795-02, USA, 1995.

[8] Analog Devices, "*ADSP-21000 Family. C Runtime library manual*", 31-000007-03, USA, 1995.

[9] R. R. Beasant, W.C. Beattie, A. Refsum, "*An approach to realisation of a high-power Venturini converter*", Proc. of PESC'90, pp. 291-297, 1990.

[10] S. Bernet, T. Matsuo, T.A. Lipo, "*A matrix converter using reverse blocking NPN-IGBT's and optimized pulse patterns*", Proc. of PESC'96, vol. 1, pp. 107-113, 1996.

[11] F. Blaabjerg, J.K. Pedersen, "*An integrated high power factor three-phase AC-DC-AC converter for AC-machines implemented in one microcontroller*", Proc. of PESC'93, vol. 1, pp. 285–292, 1993.

[12] F. Blaabjerg, J.K. Pedersen, "*Optimal design of a complete three-phase PWM-VS Inverter*" IEEE Trans. on Power Electronics, vol. 12, no. 3, pp. 567-577, 1997.

[13] F. Blaabjerg, J.K. Pedersen, U. Jaeger, "*Evaluation of modern IGBT-modules for hard-switched AC/DC/AC converters*", Proc. of IAS Annual Meeting, vol. 2, pp. 997-1005, 1995.

[14] I. Boldea, S.A. Nasar, "*Electric drives*", ISBN 0-8493-2521-8, 411 pages, CRC Press, US, 1999.

[15] B.K. Bose, "*Power Electronics – A technology review*", Proc. of IEEE, vol. 80, no. 8, pp. 1303-1334, 1992.

[16] B.K. Bose (editor), "*Power electronics and variable speed drives. Technology and applications*", ISBN 0-7803-1061-6, 640 pages, IEEE Press, USA, 1997.

[17] M. Bramoulle, "*Electrolytic of film capacitors?*", Proc. of IAS Annual Meeting, paper 25.3, CD-ROM version, 1998.

[18] N. Burany, "*Safe control of 4quadrant switches*", Proc. of IAS Annual Meeting, vol. 2, pp. 1190-1194, 1989.

[19] D. Casadei, G. Serra, A. Tani, P. Nielsen, "*Theoretical and experimental analysis of SVM-controlled matrix converters under unbalanced supply conditions*", Electromotion Journal, vol. 4, no. 1-2, pp 28-37, 1997.

[20] D. Casadei, G. Serra, A. Tani, "*The use of matrix converter in direct torque control of induction machines*", Proc. of IECON'98, pp. 744-749, 1998.

[21] D. Casadei, M. Matteini, G. Serra, A. Tani, C. Klumpner, "*Input power quality in matrix converters: Minimisation of the RMS value of input current disturbances under unbalanced and nonsinusoidal supply voltages*", Proc. of NORpie, pp. 129-133, 2000.

[22] J. Chang, "*Adaptive overlapping commutation control of modular AC-AC converter and integration with device module of multiple AC-AC switches*", US Patent (1997) 5892677, 1999.

[23] J. Chang, D. Braun, "*High-frequency AC-AC converters using 3-in 1 IBPMs and adaptive commutation*", Proc. of PESC'99, pp. 351-357, 1999.

[24] S. Chattopadhyay, T.S. Key, "*Predicting behavior of induction motors during electrical service faults and momentary voltage interruptions*", Proc. of Industrial and Commercial Power Systems Technical Conference, pp. 78-84, 1993.

[25] R. Chokhawala, J. Catt, B. Pelly, "*Gate drive considerations for IGBT module*", Proc. of IAS Annual Meeting, pp. 1186-1195, 1992.

[26] Christensson, "*Switch-effective modulation strategy for matrix converters*", Proc. of EPE'97, pp. 4.193-4.198, 1997.

[27] E.R., Jr. Collins, A. Mansoor, "*Effects of voltage sags on AC motor drives*", Proc. of Textile, Fiber, and Film Industry Technical Conference, pp. 1-7, 1997.

[28] M. Corley, J. Locker, S. Dutton, R. Spee, "*Ultracapacitor-based ride-through system for adjustable speed drives*", Proc. of Power Electronics Specialists Conference PESC'99, vol. 1, pp 26 –31, 1999.

[29] A. David, E. Lajoie-Mazenc, C. Sol, "*Soft restart of an adjustable speed drive after a short disconnection without any mechanical speed sensor*", Proc. of Electrical Machines and Drives, pp. 570-575, 1993

[30] A. David, E. Lajoie-Mazenc, C. Sol, "*Ride-through capability of AC adjustable speed drives in regards to voltage dips on the distribution network*", Proc. of EPE'93, vol. 1, pp. 139-144, 1993.

[31] D.L. Drinkwater, "*Ride-through energy boost circuit*", US Patent No. 4,818,891, April 1991.

[32] W. Drury, D. Grant, "*Variable-speed drives-the future*", Power Engineering Journal, vol. 81, pp. 27 –34, 1994.

[33] G. K. Dubey, "*Power semiconductor controlled drives*", ISBN 0-13-686890-8, 495 pages, Prentice Hall, Englewood Cliffs, New Jersey 07632, USA, 1989.

[34] J.L. Duran-Gomez, P. Enjetti, "*A low cost approach to improve the performance of an adjustable speed drive (ASD) under voltage sags and short-term power interruptions*", Proc. of Applied Power Electronics Conference APEC'98, vol. 2, pp. 587-591, 1998.

[35] J.L. Duran-Gomez, P.N. Enjeti, B.O. Woo, "*Effect of voltage sags on adjustable speed drives – A critical evaluation and an approach to improve its performance*", IEEE Trans. on Industry Applications, vol. 35, pp. 1440-1449, 1999.

[36] J.L. Duran-Gomez, P.N. Enjeti, A. von Jouanne, "*An approach to achieve ride-through of an adjustable speed drive with flyback converter modules powered by super capacitors*", Proc. of IAS Annual Meeting, vol. 3, pp. 1623 –1629, 1999.

[37] L. Empringham, P. Wheeler, J.C. Clare, "*Intelligent commutation of matrix converter bi-directional switch cells using novel gate drive techniques*", Proc. of PESC'98, pp. 707-713.

[38] P.N. Enjeti, J.L. Duran-Gomez, "*Method and system for ride-through of an adjustable speed drive for voltage sags and short-term power interruption*", US Patent No. 6,005,362, December 1999.

[39] Evox Rifa, "*Film capacitors 1999-2000*".

[40] Grantham, "*Full load testing of three phase induction motors without the use of a dynamometer*", Proc. of ICEMA, pp. 147-152, 1993.

[41] Grantham, M. Sheng, E.D. Spooner, "*Synthetic loading of three-phase induction motors using microprocessor controlled power electronics*", IEE Proc. – Electr. Power Appl., vol. 141, no. 2, pp. 101-108, 1994.

[42] Gratham, M. Sheng, "*The synthetic loading of three-phase induction motors using microprocessor controlled power electronics*", Proc. of PEDS'95, vol. 1, pp. 471-476, 1995.

[43] Grantham, H. Tabatabaei-Yazdi, *"A novel machineless dynamometer for load testing three-phase induction motors*", Proc. of Power Electronics and Drive Systems, PEDC'99, pp. 579-584, 1999.

[44] L. Gyugyi, B.R. Pelly, "*Static power frequency changers. Theory, performance and application*", ISBN 0-471-67800-7, 442 pages, John Willey&Sons, USA, 1976.

[45] S. Halasz, I. Schmidt, T. Molnar, "*Matrix converter for induction motor drive*", Proc. of EPE'95, vol. 2, pp. 2-664-2.669, 1995.

[46] S. Halasz, I. Schmidt, T. Molnar, "*Induction motor drive with matrix converter*", Proc. of PEDS'95, vol. 1, pp. 104-109, 1995.

[47] T. Halkosaari, H. Tuusa, "*The comparison of the efficiency in a current and a voltage source inverter supplied from a controlled rectifier*", Proc. of PCIM'99, Intelligent motion, pp. 217-222, 1999.

[48] S. Hansen, P. Nielsen, F. Blaabjerg "*Harmonic cancellation by mixing non-linear single- phase and three-phase loads*", IEEE Trans. on Industry Applications, vol. 36, no. 1, pp. 152-159, 2000.

[49] Hewlett-Packard, "*HCPL-788 J Isolation amplifier with short circuit and overload detection - Technical data*", 5966-0001E, 1997.

[50] Hewlett-Packard, "*HCPL-3120 2.0 Amp output current IGBT gate drive optocoupler – Technical data*", 5965-7875E, 1997.

[51] *Hitachi Inverter - J100 SERIES, Instruction manual*, appendix 5, pp. A-19, Hitachi Ltd., Tokyo, Japan.

[52] D.G. Holmes, T.A. Lipo, "*Implementation of a controlled rectifier using AC-AC matrix converter theory*", Proc. of PESC'89, pp. 353-359, 1989.

[53] J. Holtz, W. Lotzkat, *"Controlled AC drives with ride-through capability at power interruption*", Proc. of IAS Annual Meeting, vol. 1, pp. 629-626, 1993.

[54] J. Holtz, "*Pulsewidth modulation for electronic power conversion*", IEEE Trans. on Industry Applications, vol. 82, no. 8, pp. 1194-1214, 1994.

[55] L. Huber, D. Borojevic, "*Space vector modulator forced commutated cyclo-converters"*, Proc. of PESC'89, pp. 871-8761, 1989.

[56] L. Huber, D. Borojevic, "*Space vector modulated three-phase to three-phase matrix converter with input power factor correction*", IEEE Trans. on Industry Applications, vol. 31, no. 6, pp. 1234-1245, 1995.

[57] IXYS, "IXRH 50N60, IXRH 50N120: *High voltage RBIGBT. Forward and reverse blocking IGBT*", Advanced technical information, http://www.ixys.net/l400.pdf, 2000.

[58] T.M. Jahns, E.L. Owen, "*AC adjustable-speed drives at the millennium: how did we get here?*", Proc. of APEC'00, paper 1.3 (plenary session), CD-ROM version, 2000.

[59] M. James, M.J. Leach, S.J. Mackay, "*Phase-on ride-through control circuit*", US Patent No. 4,459,652, July 1984.

[60] V. John, B.S. Suh, T.A. Lipo, "*High-performance active gate drive for high-power IGBT's*", Proc. of IAS Annual Meeting, vol. 2, pp. 1519-1529, 1998.

[61] von Jouanne, P. Enjeti, B. Banerjee, "*Assessment of ride-through alternatives for adjustable speed drives*", Proc. of IAS Annual Meeting, vol. 2, pp. 1538-1545, 1998.

[62] K.G. Kerris, P.W. Wheeler, F. Clare, L. Empringham, "*Implementation of a matrix converter using P-channel MOS-controlled thyristors*", Proc. of PEVD'00, pp. 35-39, 2000.

[63] R.J. Kerkman, T.M. Rowan, "*Voltage controlled current regulated PWM inverters*", Proc. of IAS Annual Meeting, vol. 1, pp. 381-387, 1988.

[64] R. Kerkman, G.L. Skibinski, D.W. Schengel, "*AC drives: Year 2000 (Y2K) and beyond*", Proc. of APEC'99, vol. 1, pp. 28-39, 1999.

[65] J.S. Kim, S.K. Sul, "*New control scheme for AC-DC-AC converter without DC-link electrolytic capacitor*", Proc. of PESC'93, pp. 300-306, 1993.

[66] C. Klumpner, I. Boldea, F. Blaabjerg, "*The matrix converter: Overvoltages caused by the input filter, bidirectional power flow, and control for artificial loading of induction motors*" Electric Machines and Power Systems Journal, vol. 28, no. 2, pp. 129-142, Taylor & Francis Group, 2000.

[67] C. Klumpner, I. Boldea, F. Blaabjerg, P. Nielsen, "*A new modulator for matrix converters allowing for the reduction of input current ripple*", Proc. of OPTIM, vol. 2, pp. 487-492, 2000.

[68] C. Klumpner, I. Boldea, F. Blaabjerg, "*Short term ride through capabilities for direct frequency converters*", Proc.. of PESC'00, vol. 1, pp. 235-241, 2000.

[69] C. Klumpner, I. Boldea, F. Blaabjerg, "*Artificial loading of the induction motors using a matrix converter*" Proc. of IEE/PEVD, pp. 40-45, 2000.

[70] C. Klumpner, P. Nielsen, I. Boldea, F. Blaabjerg, "*New steps toward a low-cost power electronic building block for matrix converters*", Proc. of IAS Annual Meeting, vol. 3, pp. 1964-1971, 2000.

[71] C. Klumpner, P. Nielsen, I. Boldea, F. Blaabjerg, "*A new matrix converter-motor (MCM) for industry applications*", Proc. of IAS Annual Meeting, vol. 3, pp. 1394-1402, 2000.

[72] K. Kretschmar, H.-P. Nee, "*Comparison of different converters with sinusoidal line currents suited for a 15 kW permanent magnet integral motor*", Proc. of Nordic Workshop on Power and Industrial Electronics NORPIE'00, pp. 79-83, 2000.

[73] R. Langley, A. Mansoor, E.R. Collins, R.L. Morgan, "*Voltage sag ride-through testing of adjustable speed drives using a controllable dynamometer*", Proc. of Harmonics and Quality of Power, vol. 1, pp. 566-571, 1998.

[74] LEM, "*Current transducer LA 25-NP*", 980909/6, LEM Components, 1998.

[75] P. Lesage, M. Alaküla, L. Gertmar, *"The dynamic thermal loading of an induction machine*", Proc. of EPE'97, vol. 2, pp. 520-525, 1997

[76] H-H. P. Li, "*Bidirectional lateral insulated gate bipolar transistor having increased voltage blocking capability*", US Patent (1997) 5977569, 1999.

[77] T.A. Lipo, "*Recent progress in the development in solid-state AC motor drives*", IEEE Trans. on Power Electronics, vol. 32, pp. 105 –117, 1988.

[78] R.D. Lorentz, "*The future of electric drives: where are we headed*?", Proc. of PEVD'00, pp. 1-6, 2000.

[79] G. Mackert, E. Schimanek, "*Comparison of switching off an IGBT with 0V and -8V*", Proc. of PCIM'97, Power Conversion, pp. 383-384, 1997.

[80] M. Malinowski, M.P. Kazmierkowski, S. Hansen, F. Blaabjerg, G. Marques, "*Virtual flux based direct power control of three-phase PWM rectifiers*", Proc. of IAS Annual Meeting, paper 53.6, CD-ROM version, 2000.

[81] V. Manninen, "*Application of direct torque control modulation technology to a line converter*", Proc. of EPE'95, vol. 1, pp. 292-296, 1995.

[82] M. Matteini, D. Casadei, C. Klumpner, F. Blaabjerg, "*Comparison of two current modulation strategies for matrix converters under unbalanced input voltage conditions*", Proc. of ISIE'00, december 2000, in press.

[83] M. Milanovic, B. Dobaj, "*A novel unity power factor correction principle in direct AC to AC matrix converters*", Proc. of PESC'98, pp. 746-752, 1998.

[84] N. Mohan, T.M. Undeland, W.P. Robbins, "*Power electronics. Converters, applications and design*", ISBN 0-471-30576-6, 802 pages, John Wiley&Sons, Inc., USA, 1995.

[85] C.L. Neft, "*AC power supplied static switching apparatus having energy recovery capability*", US Patent (1996) 4697230, 1987.

[86] C.L. Neft, C.D.Shauder, "*Theory and design of a 30-hp matrix converter*", IEEE Trans. on Industry Applications, vol. 28, no. 3, pp. 546-551, 1992.

[87] P. Nielsen, "*The matrix converter for an induction motor drive*", Industrial Ph.D. Fellowship EF 493, ISBN 87-89179-14-5, Aalborg University, Denmark, August 1996.

[88] P. Nielsen, F. Blaabjerg, J.K. Pedersen, "*Space vector modulated matrix converter with minimized number of switchings and feedforward compensation of input voltage unbalance*", Proc. of PEDES'96, vol.2, pp. 833-839, 1996.

[89] P. Nielsen, D. Casadei, G. Serra, A. Tani, "*Evaluation of the input current quality by three different modulation strategies for SVM controlled matrix converters with input voltage unbalance*", Proc. of PEDES'96, vol. 2, pp. 794 –800, 1996.

[90] P. Nielsen, F. Blaabjerg, J.K. Pedersen, "*Novel solution for protection of matrix converter to three phase induction machine*", Proc. of IAS Annual Meeting, vol. 2, pp. 1447-1454, 1997.

[91] T. Noguchi, H. Tomiki, "*Direct power control of PWM converters without power source voltage sensors*", IEEE Trans. on Industry Applications, vol. 34, no. 3, pp. 473-478, 1998.

[92] J. Oyama, T. Higuchi, E. Yamada, T. Koga, T. Lipo, "*New control strategy for matrix Converter*", Proc. of PESC'89, pp. 360-367, vol. 1, 1989.

[93] J. Oyama, X. Xia, T. Higuchi, E. Yamada, T. Koga, "*Effects of the filter on matrix converter characteristics under a new control method*", Proc. of SPEEDAM Symposium, section A5 pp. 7 –14, 1996.

[94] I.G. Park, S. I. Kim, "*A new thyristor phase-controlled voltage source converter with bidirectional power flow capability*", Proc. of IAS Annual Meeting, vol. 2, pp. 1368-1375, 1997.

[95] K. Phillips, "*Power electronics: Will our current technical vision take us to the next level of AC drive product performance*?", Proc. of IAS Annual Meeting, paper 1.1 (plenary session), CD-ROM version, 2000.

[96] Phytec, "*miniMODUL-167 Hardware Manual*", L-101-05, 1997.

[97] P. Poure, S. Saadate, B. Davat, "*Double fed rotor controlled machine used for dynamic compensation of mains harmonics*", Proc. of E.M&D'96, IEEE London, pp. 84-89, 1996.

[98] M.F. Rahman, L. Zhong, S.Y. Hui, "*A single-phase, regenerative, variable speed induction motor drive with sinusoidal input current*", Proc. of EPE'95, vol. 3, pp. 3.777-3.780, 1995.

[99] D. Rendusara, P. Enjeti, "*A method to reduce common mode & differential mode dv/dt at the motor terminals in PWM rectifiers/PWM inverter type adjustable speed drive system*", Proc. of APEC'98, paper 22.2 , CD-ROM version, 1998.

[100] J. Rodriguez, J. Pontt, A. Weinstein, "*Regenerative drives in the megawatt range for high performance downhill belt conveyors*", Proc. of IAS Annual Meeting, paper 50.2, CD-ROM version, 2000.

[101] G. Roy, G.E. April, "*Cycloconverter operation under a new scalar control algorithm*", Proc. of PESC'89, vol. 1, pp. 368-375, 1989.

[102] C.D. Schauder, "*Matrix converter circuit and commutation method*", US Patent (1994) 5594636, 1997.

[103] A. Schuster, "*A matrix converter without reactive clamp elements for an induction motor drive system*" Proc. of PESC'98, pp. 714-720, 1998.

[104] M. Sheng, C. Grantham, "*Synthetic loading of three-phase induction motors by magnetic field magnitude modulation*", IEE Proc. – Electr. Power Appl., vol. 141, no. 2, pp. 95-100, 1994.

[105] B.J. Siebel, R.J. Kerkman, D. Leggate, "*Inverter control during overload and following power interruption*", IEEE Trans. on Industry Applications, vol. 28, pp. 567-573, 1992.

[106] Siemens, "*C167 Derivatives - 16 Bit CMOS Single-chip microcontrollers - User' manual 03.93 Version 2.0*", Siemens AG, Munchen, 1996.

[107] Siemens Matsushita Components, "*Technical product information. Passive components. Databook library*", Ordering no. B465-P6580-X-X-7400, Germany, 1997.

[108] SGS-Thomson Microelectronics, "*BYPT 12PI-1000 Fast recovery rectifier diode*", Datasheet, Italy, 1994.

[109] E.M. Sisa, "*Power outages and power dip ride-through*", Proceed. of Textile, Fiber and Film Industry Technical Conference, pp. 1-7, 1995.

[110] M.J. Sullivan, T. Vardell, M. Johnson, *"Power interruption costs to industrial and commercial consumers of electricity*", IEEE Trans. on Industry Applications, vol. 33, pp. 1448-1457, 1997.

[111] S. Sunter, H. Altun, "*A method for calculating semiconductor losses in the matrix converter*", Proc. of MELECON'98, vol. 2, pp. 1260 –1264, 1998.

[112] P. Templin, M. Alaküla, L. Gertmar, *"Dynamic thermal loading of inverter fed induction machine*", Stockholm Power Tech, pp. 241-244, 1995

[113] P. Thoegersen, P. Nielsen, F. Abrahamsen, "*Impact on energy savings by variable speed drives from motor and converter technology*", Proc. of PCIM'99, Intelligent motion, pp. 1-7, 1999.

[114] P. Thoegersen, F. Blaabjerg, "*Adjustable speed drives in the next decade. The next step in industry and academia*", Proc. of PCIM'00, Intelligent motion, pp.95-104, 2000.

[115] S. Tnani, S. Diop, S.R. Jones, A. Berthon, "*Novel control strategy of doubly-fed induction machines*", Proc. of EPE'95, vol. 1, pp. 1.553-1.558, 1995.

[116] Toshiba, "*TLP-250 IGBT Gate drive",* Technical data, 1996-4-8.

[117] L. Tutelea, I. Boldea, E. Ritchie, P. Sandholdt, F. Blaabjerg, *"Thermal testing for inverter-fed induction machines using mixed frequency method*", Proc. of ICEM'98, vol. 1, pp. 248-253, 1998.

[118] "*Vacon starts new era for frequency converters. Active input bridge enhances performance of Vacon frequency converters*", http://www.vacon.com/what/newera.html, april 2000.

[119] M. Venturini, "*A new sine wave in, sine wave out conversion technique eliminates reactive elements*", Proc. of Powercon7, E3_1-E3-15, 1980.

[120] M. Venturini, A. Alesina, "*The generalised transformer: a new bi-directional sinusoidal waveform frequency converter with continuously adjustable input power factor*", Proc. of PESC'80, pp. 242-252, 1980.

[121] M. Venturini, A. Alesina, "*Analysis and design of optimum-amplitude nine-switch direct AC-AC converters*", IEEE Trans. on Power Electronics, vol. 4, no. 1, pp 101-112, 1989.

[122] J.D. van Wyk, F.C. Lee, "*Power electronics technology at the dawn of the new millennium – status and future*", Proc. of PESC'99, paper 1.1 (plenary session), CD-ROM version, 1999.

[123] P.W. Wheeler, D.A. Grant, "*A low loss matrix converter for AC variable-speed drives*", Proc. of EPE'93, pp. 27-32, 1993.

[124] P. Wheeler, D. Grant, "*Optimized input filter design and low-loss switching techniques for a practical matrix converter*", IEE Proc.-Electr. Power Appl., vol. 144, no. 1, pp. 53-60, 1997.

[125] E.P. Wiechmann, J.R. Espinoza, L.D. Salazar, J.R. Rodriguez, "*A direct frequency converter controlled by space vectors*", Proc. of PESC'93, pp. 314-317, 1993.

[126] S. Williamson, D.C. Jackson, "*Integrated drives for industrial applications*", Proc. of PCIM'99, Intelligent motion, pp. 9-13, 1999.

[127] Wu, G.R. Slemon, S.B. Dewan, "*PWM-CSI induction motor drive with phase angle control*", Proc. of IAS Annual Meeting, vol. 1, pp. 675-679, 1989.

[128] Xilinx, "*AppLINX CD-ROM*", 1999.

[129] L. Xu, W. Cheng, "*Torque and reactive power control of a doubly fed induction machine by position sensorless scheme*", IEEE Trans. on Industry Applications, vol. 31, no. 3, pp. 636-642, 1995.

[130] G. Yalcinkaya, M.H.J. Bollen, P.A. Crossley, "*Characterization of voltage sags in industrial distribution systems*", Proc. of IAS Annual Meeting, vol. 3, pp. 2197-2204, 1997.

[131] J.H. Youm, B.-H. Kwon, "*Switching technique for current-controlled AC-to-AC converters*", IEEE Trans. on Industrial Electronics, vol. 46, no. 2; pp. 309-318, 1999.

[132] A. Ytteberg, "*Ny method for fullbelassting av electrisca maschiner utan drivmotor eler avlastningsmaskin*", Tekmisktidskrift, pp. S42-44, 1921.

[133] M. Ziegler, W. Hofmann, "*Semi natural two steps commutation strategy for matrix converters*", Proc. of PESC'98, pp. 727-731, 1998.

[134] L. Zhang, C. Watthanasarn, W. Shepherd, "*Analysis and comparison of control techniques for AC-AC matrix converters*", IEE Proc.-Electr. Power App., vol. 145, no. 4, pp. 284-294, 1998.

[135] L. Zhang, C. Watthanasarn, "*A matrix converter excited doubly-fed induction machine as a wind power generator*", Proc. of PEVD'98, pp. 532-537, 1998.

[136] A. van Zyl,. R. Spee, A. Faveluke, S. Bhowmik, "*Voltage sag ride-through for adjustable speed drives with active rectifiers*", Proc. of IAS Annual Meeting, vol. 1, pp. 486-492, 1997.

[137] A. van Zyl, R. Spee, "*Short term energy storage for ASD ride-through*", Proc. of IAS Annual Meeting,vol. 2, pp. 1162-1167, 1998.